EUROPEAN COOPERATION

ECSS

FOR SPACE STANDARDIZATION

Space engineering

Thermal design handbook - Part 7: Insulations

Foreword

This Handbook is one document of the series of ECSS Documents intended to be used as supporting material for ECSS Standards in space projects and applications. ECSS is a cooperative effort of the European Space Agency, national space agencies and European industry associations for the purpose of developing and maintaining common standards.

The material in this Handbook is a collection of data gathered from many projects and technical journals which provides the reader with description and recommendation on subjects to be considered when performing the work of Thermal design.

The material for the subjects has been collated from research spanning many years, therefore a subject may have been revisited or updated by science and industry.

The material is provided as good background on the subjects of thermal design, the reader is recommended to research whether a subject has been updated further, since the publication of the material contained herein.

This handbook has been prepared by ESA TEC-MT/QR division, reviewed by the ECSS Executive Secretariat and approved by the ECSS Technical Authority.

Disclaimer

ECSS does not provide any warranty whatsoever, whether expressed, implied, or statutory, including, but not limited to, any warranty of merchantability or fitness for a particular purpose or any warranty that the contents of the item are error-free. In no respect shall ECSS incur any liability for any damages, including, but not limited to, direct, indirect, special, or consequential damages arising out of, resulting from, or in any way connected to the use of this document, whether or not based upon warranty, business agreement, tort, or otherwise; whether or not injury was sustained by persons or property or otherwise; and whether or not loss was sustained from, or arose out of, the results of, the item, or any services that may be provided by ECSS.

Table of contents

Figures

Tables

1
Scope

There are 3 main categories of insulators used in spacecrafts:

(a) foams: organic and inorganic;

(b) fibrous insulations: for internal and external insulation and for high temperature environments

(c) multilayer insulations (MLI): layers of radiation reflecting shields.

Properties, thermal behaviour and application areas of the insulation materials used in spacecrafts are detailed in this Part 7.

The Thermal design handbook is published in 16 Parts

ECSS-E-HB-31-01 Part 1	Thermal design handbook – Part 1: View factors
ECSS-E-HB-31-01 Part 2	Thermal design handbook – Part 2: Holes, Grooves and Cavities
ECSS-E-HB-31-01 Part 3	Thermal design handbook – Part 3: Spacecraft Surface Temperature
ECSS-E-HB-31-01 Part 4	Thermal design handbook – Part 4: Conductive Heat Transfer
ECSS-E-HB-31-01 Part 5	Thermal design handbook – Part 5: Structural Materials: Metallic and Composite
ECSS-E-HB-31-01 Part 6	Thermal design handbook – Part 6: Thermal Control Surfaces
ECSS-E-HB-31-01 Part 7	Thermal design handbook – Part 7: Insulations
ECSS-E-HB-31-01 Part 8	Thermal design handbook – Part 8: Heat Pipes
ECSS-E-HB-31-01 Part 9	Thermal design handbook – Part 9: Radiators
ECSS-E-HB-31-01 Part 10	Thermal design handbook – Part 10: Phase – Change Capacitors
ECSS-E-HB-31-01 Part 11	Thermal design handbook – Part 11: Electrical Heating
ECSS-E-HB-31-01 Part 12	Thermal design handbook – Part 12: Louvers
ECSS-E-HB-31-01 Part 13	Thermal design handbook – Part 13: Fluid Loops
ECSS-E-HB-31-01 Part 14	Thermal design handbook – Part 14: Cryogenic Cooling
ECSS-E-HB-31-01 Part 15	Thermal design handbook – Part 15: Existing Satellites
ECSS-E-HB-31-01 Part 16	Thermal design handbook – Part 16: Thermal Protection System

2
References

ECSS-S-ST-00-01   ECSS System - Glossary of terms

All other references made to publications in this Part are listed, alphabetically, in the **Bibliography**.

3
Terms, definitions and symbols

3.1 Terms and definitions

For the purpose of this Standard, the terms and definitions given in ECSS-S-ST-00-01 apply.

3.2 Abbreviated terms

The following abbreviated terms are defined and used within this Standard.

F	flammable
NF	non-flammable
LS	linear shrinkage, percent
MLI	multilayer insulation
SE	self-extinguishing
TWL	total weight loss, percent
VCM	volatile condensable materials, percent by weight
gpd	grams per denier

3.3 Symbols

A	area, [m]
C	coefficient for the degradation due to a joint, [m]
D	dissipation factor
D_K	knudsen diffusion coefficient, [m.s^{-1}]
E	modulus of elasticity, [Pa]
E_c	compressive modulus of elasticity, [Pa]
E_f	flexural modulus of elasticity, [Pa]

F	propagating tear strength in a foil, [N]
F$_{HC}$	View factor, fraction of the total radiation which arrives at C coming from H
K$_0$	constant dependent on the interaction between gas and porous medium, [m]
L	length, [m]
L*	equivalent length for the degradation because of a joint, [m]
M	gas molecular mass, [kg.mol^{-1}]
N	Clause 5: factor relating the radiative contribution to the effective thermal conductivity of a foam to the warm boundary temperature
	Clause 7: number of shields in an MLI, number of patch layers in an MLI
N$_A$	Avogadro constant, $N_A = 6{,}02252 \times 10^{23}$ mol^{-1}
P	applied compressive load, [Pa]
Q	heat flow through the insulation, [W]
	outgassing rate, [Pa.m.s^{-1}]
R	electrical resistance of a foil, [Ω per Square]
	boltzmann constant, $R = 1{,}38054 \times 10^{-23}$ J.K^{-1}
R(2π,β')	reflectance factor, irradiation over a complete hemisphere
S	steric factor accounting for the distortion of the heat flow path due to foam expansion
T	temperature, [K]
T$_m$	arithmetic mean temperature, [K]
V	gas volume flow rate per unit area of the insulation, [m.s^{-1}]
a	absorption coefficient, [m^{-1}]
c	specific heat, [J.kg^{-1}.K^{-1}]
c$_P$	gas specific heat at constant pressure, [J.kg^{-1}.K^{-1}]
$\bar{c}$	average molecular speed, [m.s^{-1}], $\bar{c} = (8RT/\pi m)^{1/2}$
d	diameter, [m]

f	frequency, [Hz]
h	thermal conductance, [W.m^{-2}.K^{-1}]
k	thermal conductivity, [W.m^{-1}.K^{-1}]
k$_g$	gas thermal conductivity, [W.m^{-1}.K^{-1}]
k$_{rad}$	radiative contribution to the effective thermal conductivity, [W.m^{-1}.K^{-1}]
m	mass of one molecule, [kg]
m	mass flow rate per unit cross-sectional area, [kg.m^{-2}.s]
m$_{h'}$	mass flow rate per unit cross-sectional area of an isolated hole, [kg.m^{-2}.s]
n,	refractive index
n$_s$	number of space layers per shield
p	gas pressure, [Pa]
	Clause 7: fraction of the electrons suffering specular reflection at the surface of a metallic film
p$_o$	ambient pressure, [Pa]
s	scattering coefficient, [m^{-1}]
t	insulation thickness, [m]
t'	spacer thickness, [m]
t$_c$	coating thickness, [m]
t$_{c\Omega}$	coating thickness as measured by the electrical resistance method, [m]
t$_u$	uncompressed insulation thickness, [m]
t	time, [s] or [min]
w	width, [m]
x	geometrical coordinate
ΔL/L	linear thermal expansion
α	Clause 6: sound absorption coefficient.
	Clause 7: absorptance, thermal diffusivity
α_s	normal solar absorptance

α'_λ		directional spectral absorptance
β		Clauses 5 and 7: linear thermal expansion coefficient
		Clause 7: angle between surface normal and direction of incident flux, [angular degrees]
β'		angle between surface normal and direction of reflected, emitted or transmitted flux, [angular degrees]
δ		strain
ε		hemispherical total emittance
ε_a		apparent emittance of a groove
ε_r		dielectric constant
ε'		directional total emittance
θ		groove angle, [angular degrees]
κ		permeability of a porous medium, [m^2]
λ		wavelength of the incident radiation, [m]
		mean free path, [m]
μ		dynamic viscosity, [Pa.s]
π		pressure differential, [Pa]
ρ		density, [$kg.m^{-3}$]
		Clauses 5 and 7: reflectance
		Clause 7: bulk electrical resistivity, [$\Omega.m$]
σ		Clauses 5 and 7: Stefen-Boltzmann constant, $\sigma = 5{,}6697 \times 10^{-8}$ W.m^{-2}.K^{-4}
		Clause 5: strength, either tensile, compressive or flexural, [Pa]
σ_0		yield strength, [Pa]
τ		Clause 5: shear strength, [Pa]
		Clause 7: fractional area of perforations or transmittance of a perforated shield
τ_0		shear yield strength, [Pa]

Subscripts

C	cold boundary
H	hor boundary
e	concerns MLI evacuation by edge-controlled pumping
eff	effective
eff(nor)	normal effective ((nor) is omitted except when normal and lateral heat transfer appear simultaneously)
eff(lat)	lateral effective (same comment as for (nor))
h	concerns MLI evacuation by hole-controlled pumping
i	concerns the ith Layer or the ith joint of an MLI
ult	concerns ultimate strength

Superscripts

j	concerns species *j*

4
Foams

4.1 General

Foams are commonly used as insulating materials in building, storage vessels, sports equipment, spacecraft, and others. They can be also used for potting and encapsulation of shock-sensitive components and for packaging. Because they have many advantages for cryogenic and space applications, efforts have been made to develop suitable foams; establish their physical, chemical and structural properties, and integrate foams with thermal insulation systems.

Because of their cellular structure of discrete or interconnected voids, a large percentage of the foam volume is air, or whatever gas used as the expanding agent, thence foams are light-weight and very low thermal conductivity, that could be decreased further by evacuation. In most cryogenic applications the insulation efficiency is achieved by condensation of the gases contained in the cellular structure of the plastic material (cryopumping).

The main shortcomings of the foams are that they are not gas-tight, that their mechanical properties are relatively poor, and that thermal stresses induce cracks which require the use of constrictive wraps to maintain the insulation integrity.

According to their chemical composition foams may be classified in inorganic and organic.

Inorganic foams have been used at elevated temperatures. These foams are difficult to produce and have inferior physical properties than organic foams at low densities (16 to 80 kg.m^{-3}).

Organic foams, on the other hand, can be readily manufactured in low densities. These foams are used, in the range of cryogenic temperatures, either as a single insulation or combined with other materials to form an integrated system.

Three basic problems should be considered regarding the application of organic foams as thermal insulators, namely: thermal conductivity, thermal expansion and contraction, and flammability and explosion hazards.

1. Thermal Conductivity. Thermal conduction through a foam combines solid conduction, gas conduction and radiation. Although an effective thermal conductivity, in the Fourier law sense, can be measured with relative ease, analytical models are available for predicting the thermal conductivity and the net heat flow through candidate foam materials to be used as thermal insulators.

The solid thermal conductivity of most foams varies with temperature in an almost linear manner as with many other materials. When the density decreases, the solid conductivity will be reduced, not only because the decreasing of the solid cross section, but also by the influence of a steric factor since, even assuming that the shape of the cells is independent of the density, expansion elongates the paths through which heat flow. As an illustration Figure 4-1 shows the calculated variation of the thermal conductivity of a polyurethane resin as a function of foam density.
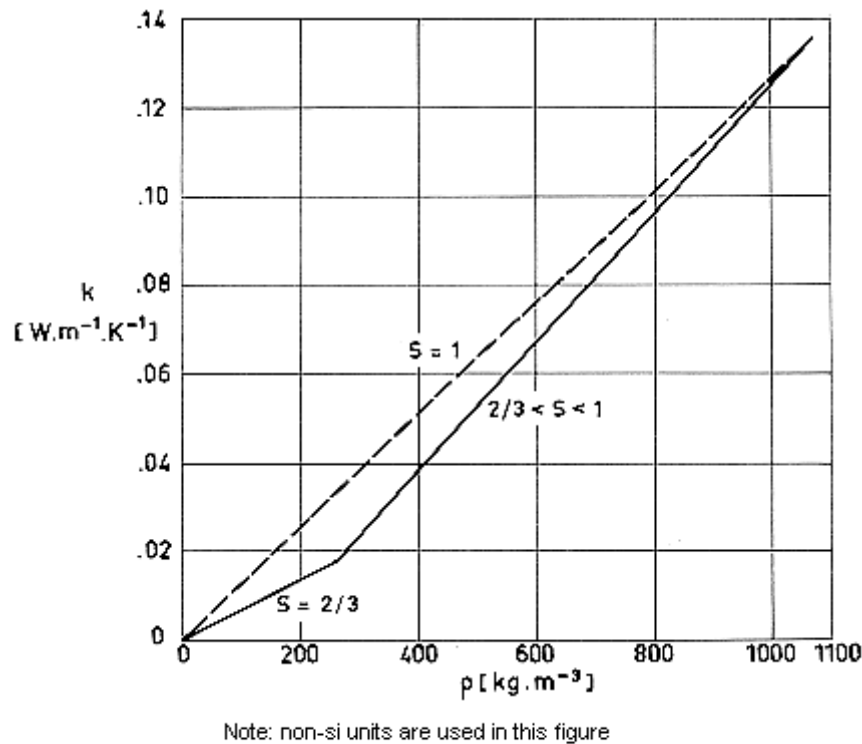
Figure 4-1: Resin thermal conductivity

k, as a function of foamed resin density, ρ. *S* is the steric factor which takes into account the distortion of the heat flow paths because expansion of the foam. Polyurethane resin. From Hammond (1969) [28].

The second mode of heat transfer of heat is heat conduction. In the case of closed-cell foams the gas thermal conductivity is a function of the concentration of both the foaming agent and the air which may diffuse into the foam outside. Since condensation can take place the thermal conductivities of both gases will depend not only on temperature but also on pressure. Figure 4-2 gives the gas thermal conductivity for mixtures of Freon 11, a typical foaming agent, and air, at atmospheric pressure, as function of temperature.
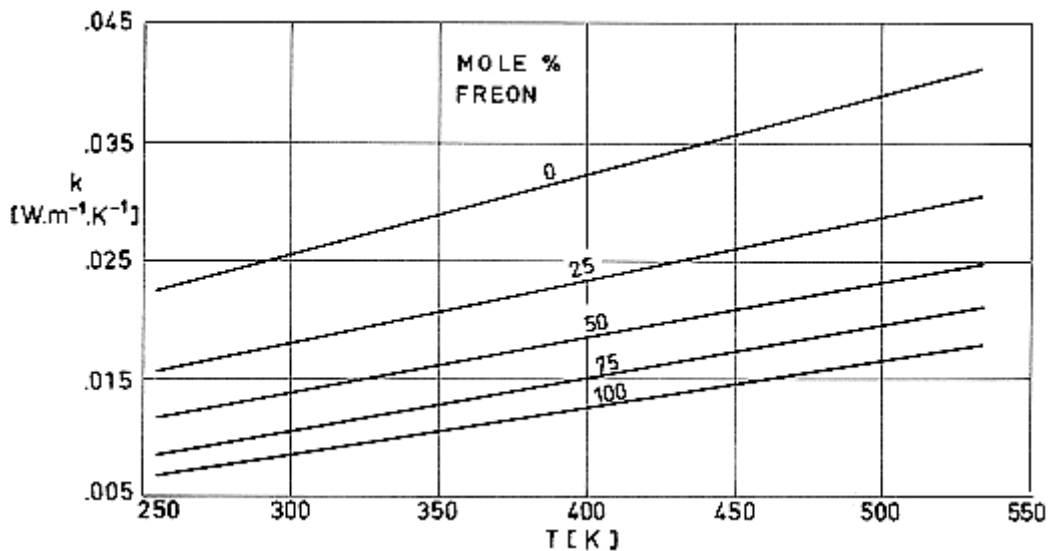
Note: non-si units are used in this figure

Figure 4-2 : Gas thermal conductivity

k, for mixtures of Freon 11 and air as a function of temperature, *T*, for different concentrations of Freon 11. From Hammond (1969) [28].

In most spacecraft applications the foam is outgassed, so that the gas conductivity is kept small enough to be neglected as compared with the other thermal conductivities. However, in the case of foams sprayed on cryogenic tanks for insulating purposes, the air has enough time to diffuse into the foam, possibly degrading the insulation characteristics in an amount which can be estimated. For example: in a typical case (Schroeder (1973)b [61]) a total cure of 72 hours is required, after spraying the foam, before the cryogenic exposure of the tank wall.

The radiative transfer of heat within the foam involves simultaneous transmission, absorption and scattering. According to Hammond (1969) [28] the radiative contribution to thermal conductivity of the foam can be written as

$$k_{rad} = N\sigma \frac{T_H^4 - T_C^4}{a(T_H - T_C)} = 4N\sigma \frac{T_H^3}{a} \qquad [4\text{-}1]$$

where: *N* is a constant factor which lies between 0,5 (for low temperatures) and 2 (for high temperatures).
T_C, T_H are the cold and warm boundary temperatures, respectively. [K].

a is the foam absorption coefficient. [m^{-1}].

σ is the Stefan-Boltzmann Constant. [W.m^{-2}.K^{-4}].

Values of the radiation thermal conductivity are given in Figure 4-3 versus mean temperature, T_m. It can be deduced from this figure that radiation becomes significant above 350 K.
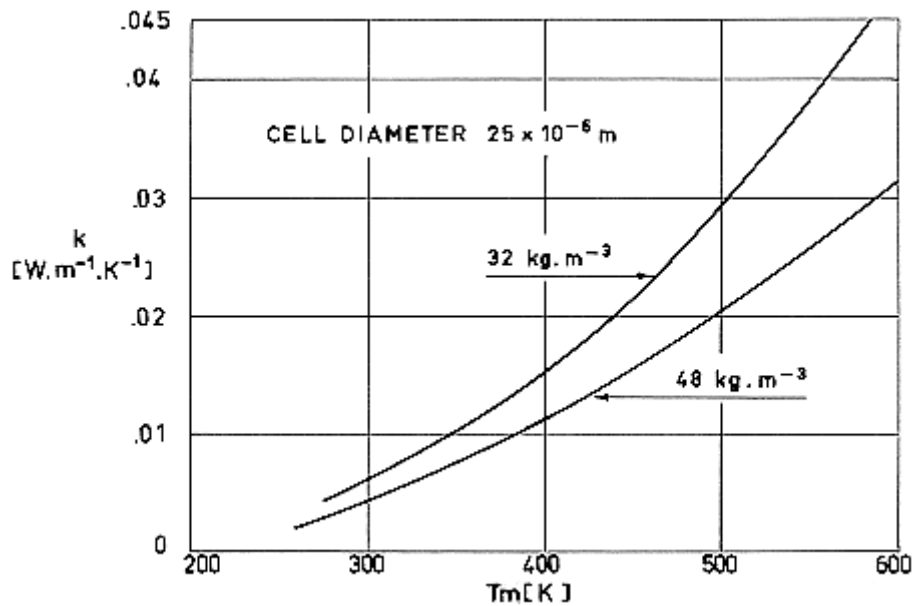
Figure 4-3: Radiation thermal conductivity

k_{rad}, as a function of mean temperature, T_m, for two polyurethane foams. From Hammond (1969) [28].

2. Thermal Expansion and Contraction. Broadly speaking, the thermal expansion coefficient of polyurethane foams is 2 to 5 times that of aluminium and 4 to 10 times that of steel. Because of this large difference in thermal expansions, the foam cannot be foamed in place against the metal or bonded directly to it, since during chilldown from ambient temperature to cryogenic temperatures high stresses are created in the foam, and it fail either in shear along the tank surface or in tension in direction normal to it.

Various techniques for overcoming the effects of thermal contraction have been developed. For example, Glaser et al. (1967) [23], report that the addition of 10 percent (based on the weight of foam) of chopped glass fibers, 6,35x10⁻³ to 12,7x10⁻³ m long, to a low-viscosity one-shot foam eliminated cracking of the foam when exposed to liquid nitrogen. The same authors indicate that in work on the Saturn S-IV stage, where an internal insulation system was developed for the liquid-hydrogen propellant tank, urethane foam was reinforced with threads in order to prevent foam failure.

3. Fire and Explosion Hazards. The fire hazard of plastic materials has been demonstrated in the most dramatic fashion many times. Depending upon anticipated use, some polymeric materials are required to pass various flammability tests. The passing of these tests is assured by the addition of fire retardants.

When external foam insulation is used in spacecraft tankage, the possibility of ignition can be enhanced by the diffusion of air into foam. Because of the low temperatures the air condenses, and this oxygen rich condensed air, in conjunction with an oxidizable organic foam, can create an explosion hazard.

Flame-retardant coatings can be applied to the exterior of the insulation, once it has been cured, to enhanced its self-extinguishing characteristics. When this precaution has been taken, the possibility of ignition or explosion in a well-designed foam insulation system is remote.

A further hazard associated with burning of foams is the toxicity of their combustion products, which can be ascribed to the fire-retardant additives. Petajan et al. (1975) [51] report that the physiological and toxicological effects of the combustion products of a laboratory-formulated fire-retarded rigid-polyurethane foam, proved fatal to rats in a matter of minutes, while the same rigid-polyurethane

foam, without fire retardant, produced only minor signs of toxicity. The fire-retardant used in these experiments, a reactive phosphate, is not uncommon in the commercial formulations.

4.2 Inorganic foams

Porous ceramic foams have been developed to be used as high temperatures insulators, for space applications. These foams provide the high strength required in many instances. Nevertheless, their use is somewhat limited because of their high density and relatively high thermal conductivity.

Table 4-1 gives the relevant properties of several ceramics foams.

The influence of temperature on thermal conductivity and linear thermal expansion of the same types of foam is shown in Figure 4-4 and Figure 4-5 respectively.

Table 4-1: Relevant Properties of Ceramic Foams

	Alumina	Silica	Silicon Carbide	Zircon
Maximum Recommended Service Temperature [K]	2090	1920	2200	2470
Porosity [percent]	88	84	90	86
Density, ρx10^{-3} [kg.m^{-3}]	0,51	0,32	0,32	0,74
Thermal Conductivity, k, [W.m^{-1}.K^{-1}]	0,605	0,158	0,821	0,137
Compressive Strength, σ_{ult}x10^{-6} [Pa]	6,41	5,31	1,38	1,65

NOTE   From Glaser et al. (1967) [23].
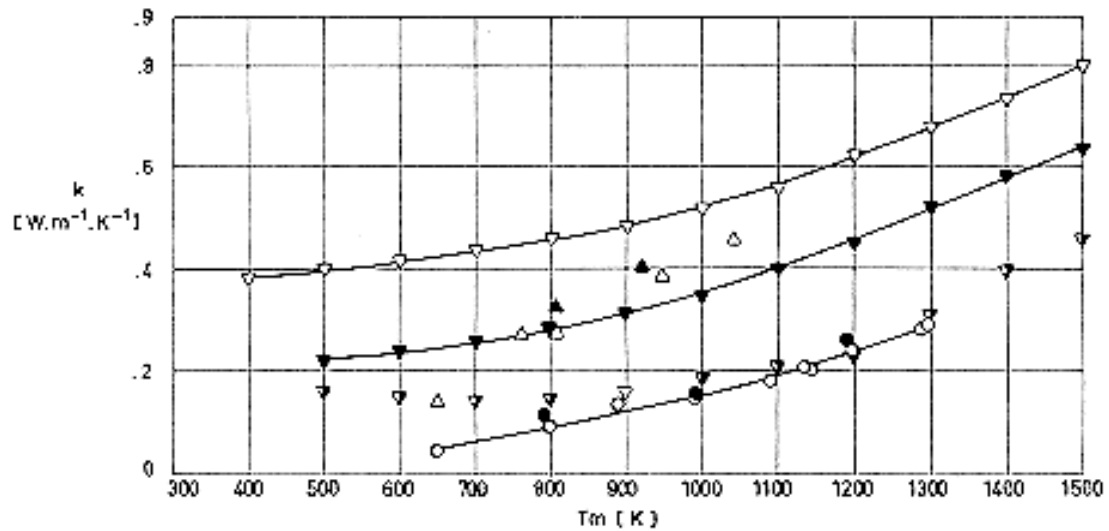
Note: non-si units are used in this figure

Figure 4-4: Thermal conductivity, *k*, of several ceramic foams as a function of arithmetic mean temperature, T_m.

Explanation

Key	Description	Comments	References
○	Alumina. Density, $\rho = 470$ kg.m⁻³.	Measured in 5,33x10⁻⁵ to 2,66x10⁻² Pa pressure range.	Touloukian (1967)a [72].
●	Same as above.	Measured when cooled.	
△	Silicon Carbide. Density, $\rho = 460$ kg.m⁻³.	Measured in 5,33x10⁻⁵ to 4x10⁻² Pa pressure range.	Touloukian (1967)b [73].
▲	Same as above.	Measured when cooled.	
▽	Zircon. Density, $\rho = 960$ kg.m⁻³.	Data extracted from smooth curve.	Glaser et al. (1967) [23].
▼	Zircon Z-90. Density, $\rho = 940$ kg.m⁻³.		
▽	Zircon Z-67. Density, $\rho = 830$ kg.m⁻³.		
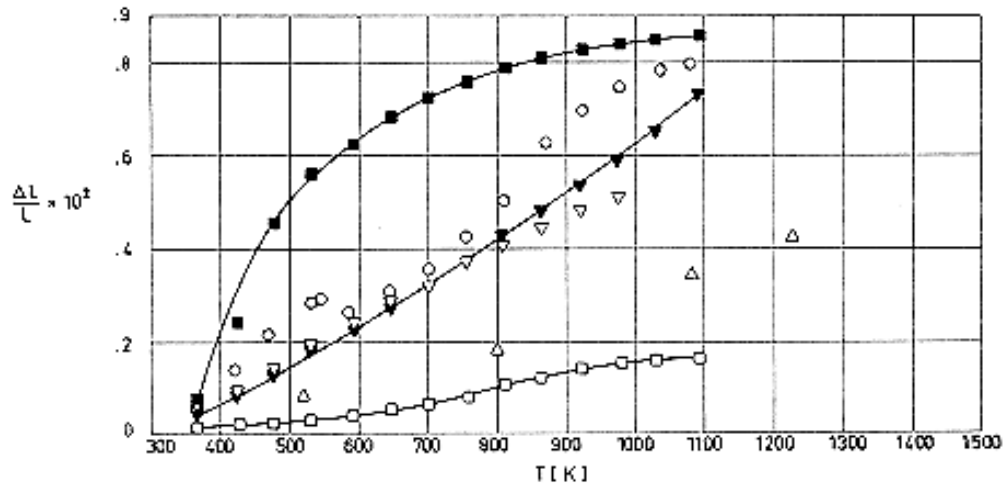
Note: non-si units are used in this figure

Figure 4-5: Linear thermal expansion, *ΔL/L*, of several ceramic foams as a function of temperature, *T*.

Explanation

Key	Description	Comments	References
○	Alumina. 35-40 alumina hidrate, 25-30 Al_2O_3, 22-27 H_3PO_4 (85%), 8-12 H_2O, 1-1,5 carbon powder, and 0,05-0,1 Al powder. Density, $\rho = 930$ kg.m^{-3}. Dimensions, $5,08 \times 10^{-2}$ m long by $6,35 \times 10^{-3}$ m square.	Cured at 366 K; temperature raised continuously to 588,5 K during a 20 h period and then held at this temperature for 12 h. Reference temperature not given, assumed to be 293 K.	Touloukian (1967)a [72].
□	Silica. 50-55 Glasrock Slip, 30-35 Ludox (colloidal SiO_2), 5-7 SiO_2 400 mesh, 3-6 Al powder, 3-6 carbon powder, and 2-3 microballons. Density, $\rho = 640$ kg.m^{-3}. Dimensions, $5,08 \times 10^{-2}$ m long by $6,35 \times 10^{-3}$ m square.	Cured at 366 K; temperature raised continuously to 588,5 K during a 24 h period and then held at this temperature for 8 h. Reference temperature not given, assumed to be 293 K.	
■	Same as above.	Second run.	
△	Silicon Carbide. Carborundum Company. Density, $\rho = 610$ kg.m^{-3}. Dimensions, $7,62 \times 10^{-2}$ m long by $1,27 \times 10^{-2}$ m diameter.	Measured in vacuum of $1,7 \times 10^3$ Pa up to 1200 K and with a slight purge of argon above 1200 K.	Touloukian (1967)b [73].

▽	Zircon. 30-35 ZrO_2 100 mesh, 20-25 ZrO_2 325 mesh, 20-25 of 90 rare-earth oxide, 10-12 H_3PO_4, 10-12 H_2O, 1-2 carbon powder, and 0,05-0,1 Al powder. Density, $\rho = 1600$ kg.m^{-3}. Dimensions, $5,08 \times 10^{-2}$ m long by $6,35 \times 10^{-3}$ m square.	Cured at 366 K; temperature raised continuously to 588,5 K during a 20 h period and then held at this temperature for 24 h. Reference temperature not given, assumed to be 293 K.	Touloukian (1967)c[74] .
▼	Same as above.	Second run.	

Zircon foams that can be cast and later cured in place at temperatures below 390 K have been developed. These foams have excellent insulating and structural properties and are suitable for use in rigid heat shields. Figure 4-6 shows the temperature evolution of the hot face, T_H, and back face, T_C, of several pieces of zircon foam which are heated by a heat flux of $4,5 \times 10^5$ W.m^{-2}. To perform the tests the foams were placed in contact with a stainless-steel honeycomb panel exposed to the heat flux.
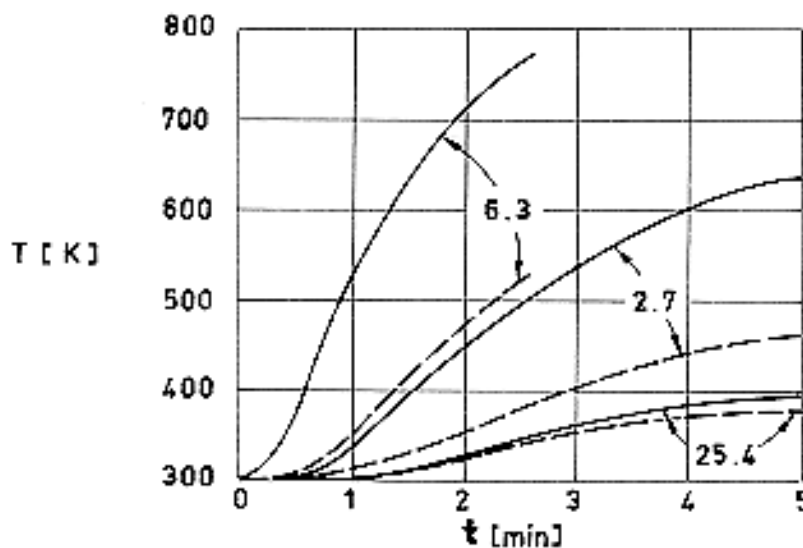
Note: non-si units are used in this figure

Figure 4-6: Temperature evolution of the hot and cold faces of several pieces of Zircon foam. Solid line: T_H, hot face. Dashed line: T_C, cold face.

The numbers in the figure indicate the foam thickness in mm. From Glaser et al (1967) [23].

Impregnated porous ceramics may also be used as insulating materials (Glaser et al, (1967) [23]). These foams consist of a refractory porous base uniformly impregnated with a solid substance which sublimes or decomposes at elevated temperatures. Phenolics, and thermoplastics such as nylon, polyethylene, and polypropylene, have been used as the impregnating material. The composite is very similar to ablative substances used in reentry heat shields; although it presents the advantage that no changes in the shape of the surface occur.

Thermal switches formed by ceramic foams impregnated with metals such as silver or copper can be used to protect radioisotope capsules from reentry heating (Bustard, Princiotta & Barr (1970) [9]). These composites are thermal conductors ($k \cong 9$ W.m^{-1}.K^{-1}) below the melting point of the metal

impregnate and switch to insulators ($k \cong 0,2$ W.m^{-1}.K^{-1}) above its melting point. In this manner, the thermal conductance during normal power system operation is relatively high, facilitating the transfer of heat from the fuel capsule to the hot side of the energy conversion device, without excessive capsule and/or radioisotope temperatures. During reentry into the earth's atmosphere the capsule is protected against the aero thermodynamic heating by the unimpregnated ceramic foam.

Table 4-2, which has been borrowed from Bustard et al. (1970) [9], gives additional properties of several ceramic foams.

Table 4-2: Properties of Ceramic Foams

Description	Alumina Ipsen 3300	Alumina Ipsen 3400	Alumina Astro Met 200	Alumina Insalute	Fused Silica Glassrock 25
Chemical Formula	Al_2O_3	Al_2O_3	Al_2O_3	Al_2O_3	SiO_2
Thermal Conductivity, k, at 1350 K, [W.m^{-1}.K^{-1}]	0,64	0,52	0,69	0,40	0,28
Specific Heat, cx10^{-3} at 1350 K, [J.kg^{-1}.K^{-1}]	1,34	1,34	1,34	1,34	1,46
Melting Point [K]	2320	2320	2320	2320	2000
Density, ρx10^{-3} [kg.m^{-3}]	0,92	0,56	0,39	0,85	0,42
Pore Structure	Coarse pore-bubble structure	Coarse pore-bubble structure	Open pore-lacey structure	Irregular pore	Fine pore-bubble structure
Thermal Shock Resistance	Good-bairline cracks developed	Fair to poor-spalling	Very poor-severe cracking	Fair to poor-cracking and spalling	Excellent-no structural damage
Compressive Strength, σ_{ult}x10^{-6} [Pa]	6,20	4,83	0,34	2,31	3,10
Shear Strength, τ_{ult}x10^{-6} [Pa]	3,59	3,03	0,69	1,24	1,72
Machinability	Fair	Good	Very poor	Fair	Excellent

Description	Fused Silica Thermo Matls. 50	Fused Silica Thermo Matls. HP50	Zircon Ipsen 4400	Zircon Ipsen 4300
Chemical Formula	SiO_2	SiO_2	ZrO_2 [a]	ZrO_2 [b]
Thermal Conductivity, k, at 1350 K, $[W.m^{-1}.K^{-1}]$	0,38	0,38	0,40	0,40
Specific Heat, $c \times 10^{-3}$ at 1350 K, $[J.kg^{-1}.K^{-1}]$	1,46	1,46	0,75	0,75
Melting Point [K]	2000	2000	2960	2960
Density, $\rho \times 10^{-3}$ $[kg.m^{-3}]$	0,80	0,80	1,45	1,10
Pore Structure	Fine pore-bubble structure	Fine pore-bubble structure	Coarse pore-bubble structure	Coarse pore-bubble structure
Thermal Shock Resistance	Excellent-no structural damage	Excellent-no structural damage	Good-no structural damage	Poor-severe cracking
Compressive Strength, $\sigma_{ult} \times 10^{-6}$ [Pa]	12,1	22,4	6,14	5,51
Shear Strength, $\tau_{ult} \times 10^{-6}$ [Pa]	3,45	5,38	3,72	3,79
Machinability	Excellent	Excellent	Fair	Good

[a]   Partially stabilized to cubic structure.

[b]   Fully stabilized to cubic structure.

NOTE   From Bustard, Princiotta & Barr (1970) [9].

4.3   Organic foams

Low density organic foams are used for cryogenic insulation because they offer the following advantages:

1.   Ease of fabrication,

2.   Relatively low cost, and

3.   Self-supporting structure.

Like plastics, organic polymer foams can be divided into two basic groups: thermoplastic foams and thermosetting foams.

Thermoplastic foams soften at temperatures of 340 to 390 K and, in most cases, tend to become brittle at cryogenic temperatures. These foams can be made from such polymers as cellulose acetate, polystyrene, styrene-acrylonitrile copolymer, polyvinylchloride, polyethylene, and polypropylene. Among these foams polystyrene and polyvinyl-chloride are the most commonly used. Polystyrene foams are rigid and polyvinyl chloride are flexible, although rigid PVC foams have been developed recently which are competitive with other rigid foams.

Thermosetting foams are commonly made with phenolic, urea-formaldehyde, epoxy, and polyurethane resins. Flexible polyurethane foams dominate the market; these foams exhibit very good properties at cryogenic temperatures with a minimum tendency to become brittle. Urea-formaldehyde foams are brittle and do not show good structural properties at low densities. Low density phenolic resin foams tend to be brittle and friable at room temperature and are difficult to manufacture. Epoxy foams have met only with limited use because of difficulties in controlling satisfactorily the foaming.

Tetrafluoroethylene foam (TFE) is an intermediate material between a thermosetting and a thermoplastic foam. It melts at very high temperature, has very good physical properties at cryogenic temperatures and, because of its extreme chemical inertness, resists the effects of liquid oxygen, hydrazine, and other chemically reactive rocket fuels.

4.3.2   Thermal properties of organic foams

Figure 4-7 summarizes the available information on the thermal conductivity of polyurethane foams in a wide range of temperatures, and for different foam densities and preconditioning. Data for polystyrene foams are given in Figure 4-8.
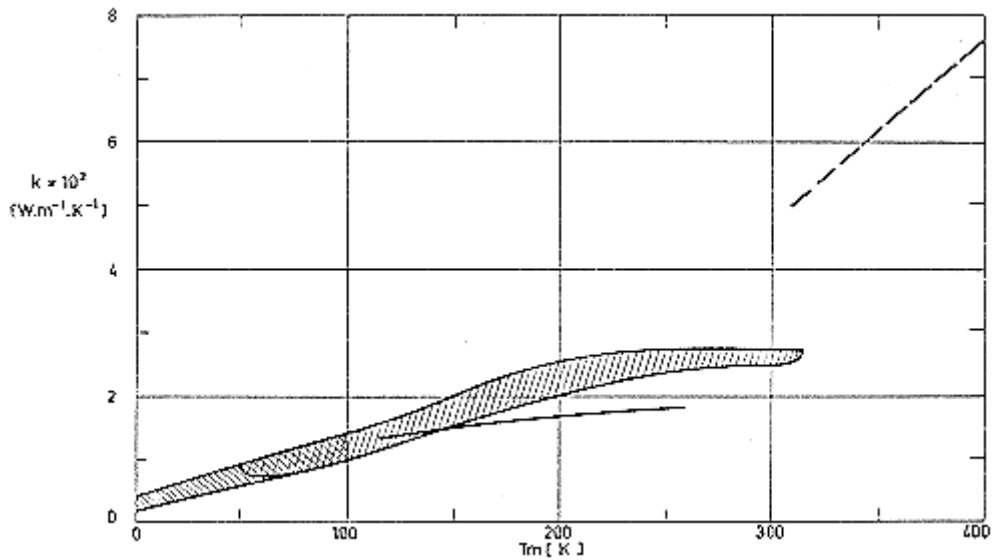
Figure 4-7: Thermal conductivity k, of polyurethane foams vs. arithmetic mean temperature, T_m.

Left-oriented shadowed area: 64 kg.m^{-3} > ρ > 32 kg.m^{-3}; cryopumped; from Coston (1967).
Right-oriented shadowed area: From Rosato (1968) [56].
Solid line: CO_2 blown, ρ = 32 kg.m^{-3}; evacuated; from Schroeder (1973)b [61].
Dashed line: The same foam at ambient pressure in air; from Schroeder (1973)b [61].
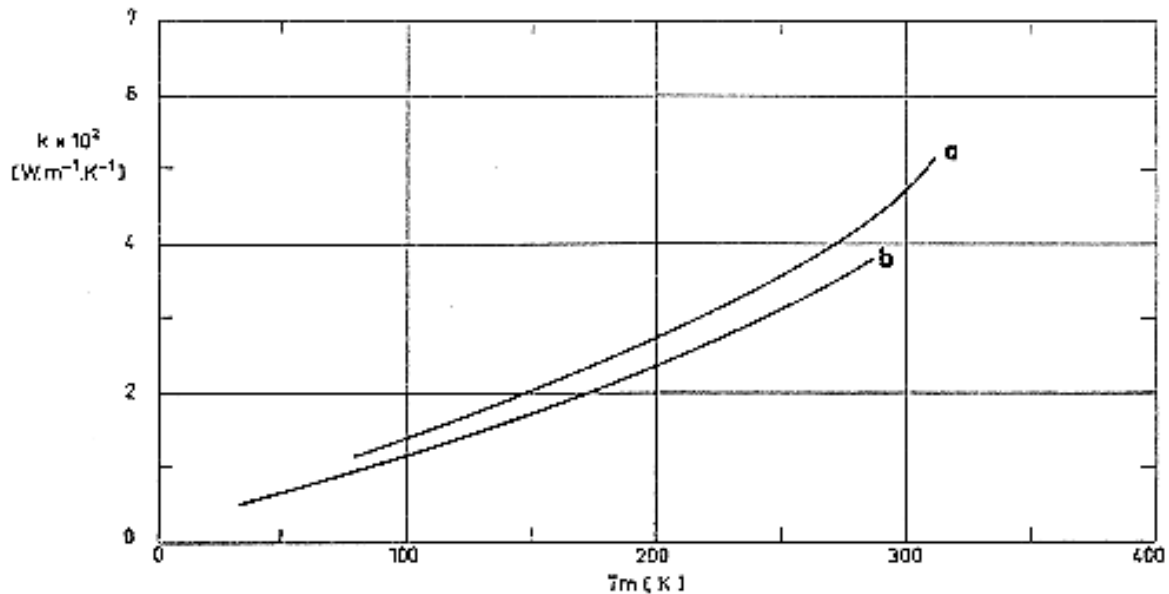
Figure 4-8: Thermal conductivity, *k*, of cryopumped polystyrene foams.

a: Styrofoam, ρ = 33 kg.m⁻³. *b*: Styrofoam, ρ = 22 kg.m⁻³. Styrofoam is a registered trade name of Dow Chemical Co. From Rosato (1968) [56].

As has been already said, the thermal conductivity of foams can be reduced further by evacuation.

Evacuation by vacuum pumps is used when foams are employed as spacers of multilayer insulations. However, for insulating relatively large cryogenic tanks pump evacuation is normally impractical, nevertheless, in that case the gas contained in the cellular structure condenses because of the prevailing low temperature level, thus leaving the void space evacuated (cryopumping).

A close examination of the thermal conductivity-temperature curve in the proximity of the condensation temperature of the filling gas reveals the typical S-curve behavior shown in Figure 4-9. This particular curve corresponds to a Freon 11-air filled foam. At atmospheric pressure Freon 11 condenses between 260 and 290 K. At temperatures below 260 K air controls the gas conduction contribution to the foam thermal conductivity. This contribution decreases when the temperature decreases, reaching very low levels when the air condenses. In the temperature range above the Freon condensing temperature the gas conduction depends on the concentration of Freon in the binary Freon-air system, and on temperature, increasing when the temperature increases, as occurs with single-phase gaseous systems. In the intermediate temperature range, when Freon starts boiling, the conductivity of the gaseous system decreases since the thermal conductivity of Freon is about a fourth of that of air.
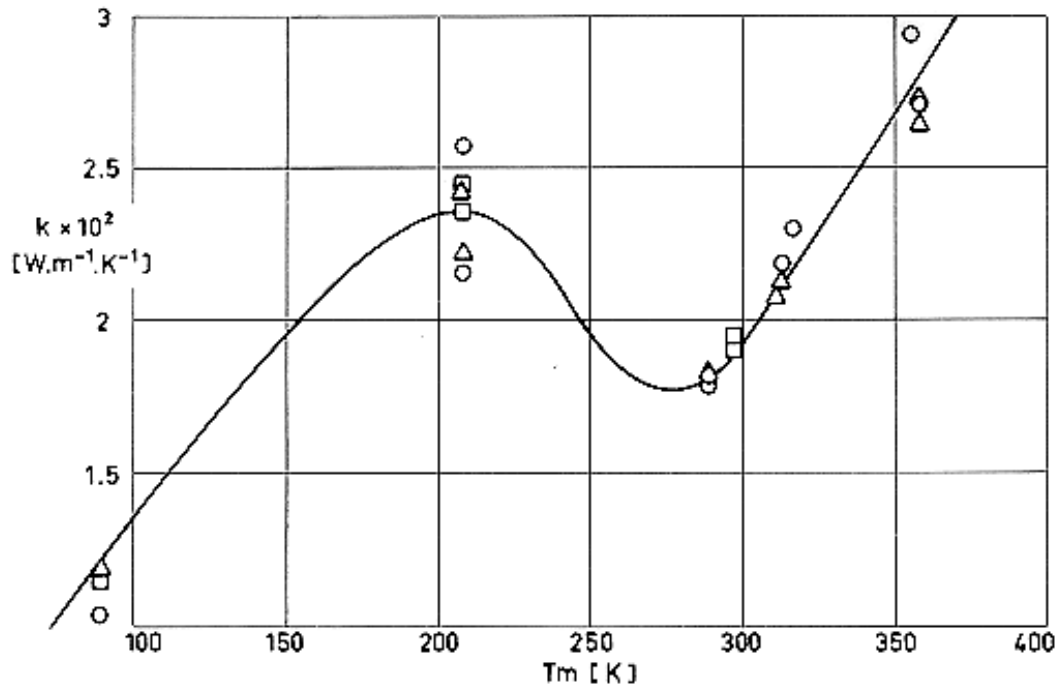
Note: non-si units are used in this figure

Figure 4-9: Thermal conductivity, *k*, vs. arithmetic mean temperature, T_m, of a polyurethane foam in the proximity of the condensation temperature of the filling gas.

The temperature gradient is parallel to the foam rise direction. Foam: Nopcofoam BX-250, two-component, flame retardant, spray foam. Filling gas: Freon 11.
○: ρ = 30,6 kg.m⁻³.
□: ρ = 32,7 kg.m⁻³.
△: ρ = 37,5 kg.m⁻³.
From Schroeder (1973)b [61].

Linear thermal expansion of relevant foams is shown in Figure 4-10. It can be seen that Epoxy foams have the lowest thermal expansion. For a given foam, the thermal expansion increases when the temperature increases. Especially significant is the fact that in the cryogenic range all the foams have thermal expansion characteristics which can be reasonably considered as linear functions of temperature, the nonlinearities becoming apparent at room temperature.
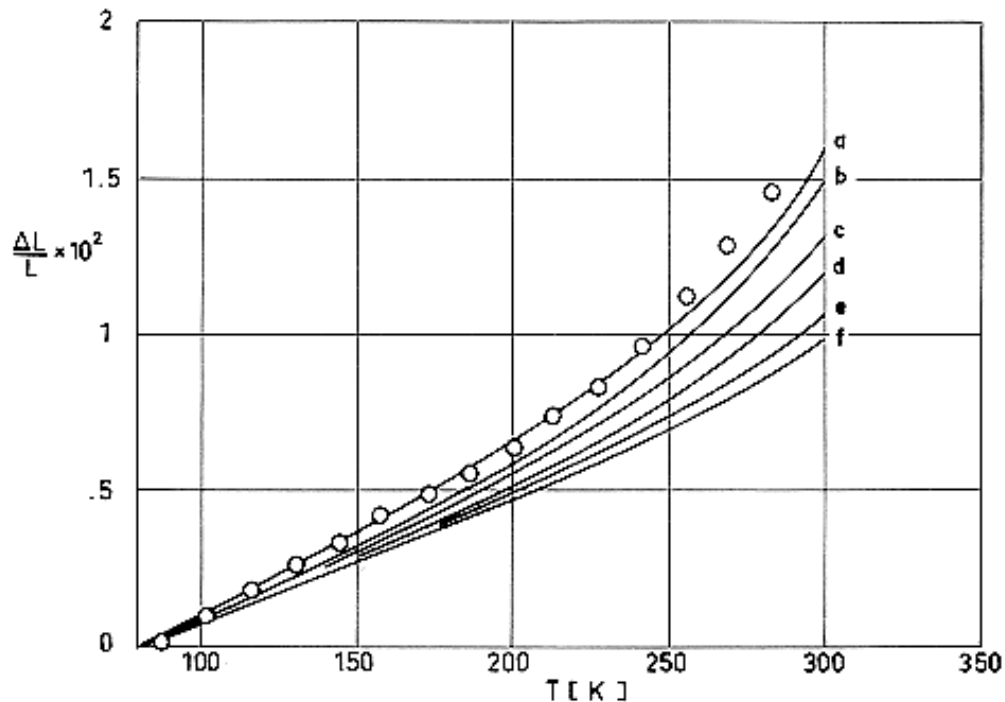
Note: non-si units are used in this figure

Figure 4-10: Linear thermal expansion, *ΔL/L*, of several organic foams as a function of temperature, *T*.

$\bigcirc$: Polyurethane foam. $\rho = 50$ kg.m^{-3}. From Schroeder (1973)b [61].

a Urethane foam. $\rho = 80$ kg.m^{-3}.

b Urethane joint filler.

c Syntactic foam. Urethane filler with hollow silica spheres.

d Semiflexible Urethane.

e Epoxy.

f Epoxy.

Curves *a* to *f* are from Glasser et al. (1967) [23].

4.3.3   Mechanical properties of organic foams

In general, the main function of an insulation system is to provide thermal protection; it is not intended to be a primary load-carrying structure. However, since the insulation system is normally bonded or mechanically attached to the primary structure, it should match the strains and deflections of that structure, and therefore significant stresses could be introduced in it.

Low temperature mechanical property data of foams are extremely scarce, notwithstanding the fact that they are required for efficient design of foam-based insulations. Because of these reasons it seems advisable to collect these data in the present item.

The tensile strengths of a number of foams at temperatures ranging from 400 K down to 20 K are shown in Figure 4-11. At 20 K both the semirigid polyurethane and the epoxy foams have tensile strengths of the order of 4x10^5 Pa. At room temperature the rigid polyurethane foam has the highest tensile strength, closely followed by the semirigid polyurethane foam. At room temperatures of the order of 400 K the tensile strength of all the organic foams practically vanishes.
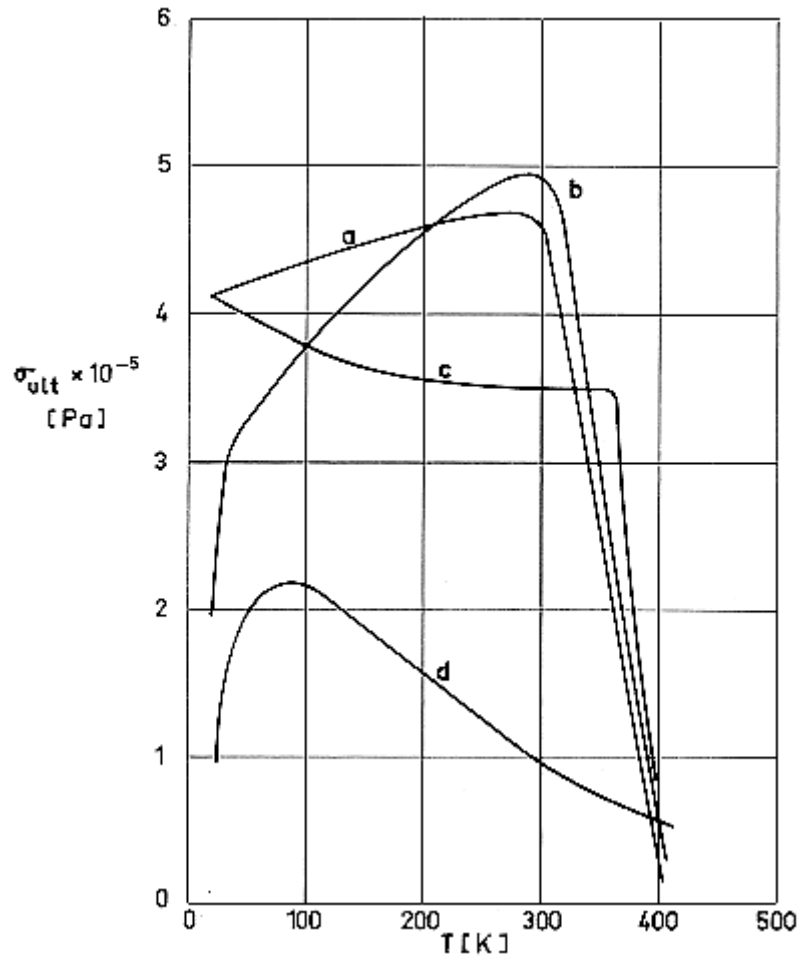
Figure 4-11: Ultimate tensile strength, of several foams as a function of temperature, *T*.

a: Barret semirigid polyurethane.
b: Hexcel 1414-2 polyester polyurethane rigid.
c: Magnolia 7015 epoxy.
d: Baron S-39 flexible polyester.
From Rosato (1968) [56].

The results of shear strength tests are summarized in Figure 4-12. All the foams tested exhibit minimum shear strengths at the two extreme temperatures. Again the rigid polyurethane foam has the highest shear strength among all of them.
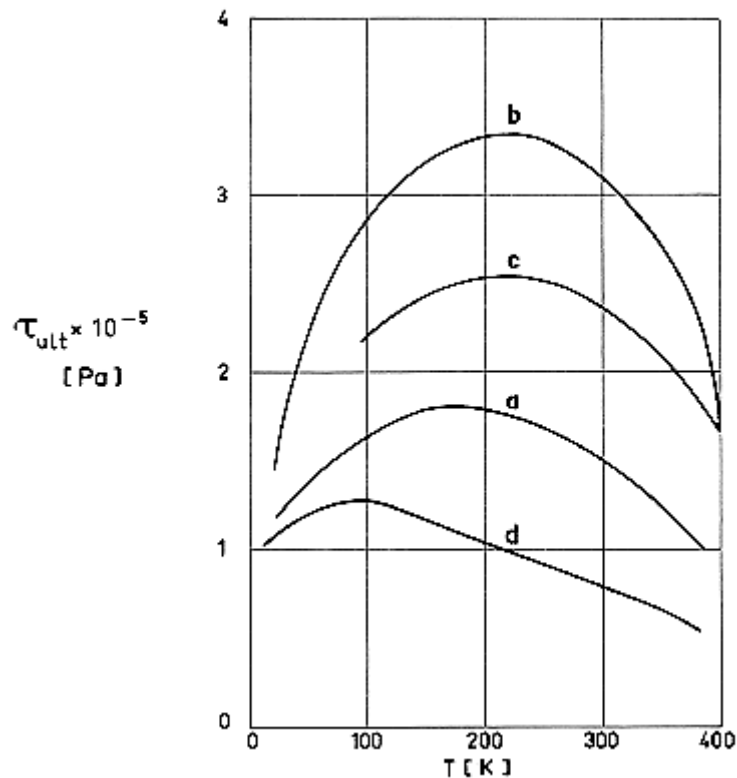
Figure 4-12: Ultimate shear strength, τ_{ult}, of several foams as a function of temperature, *T*.

a: Barret semirigid polyurethane.
b: Hexcel 1414-2 polyester polyurethane rigid.
c: Magnolia 7015 epoxy.
d: Baron S-39 flexible polyester.
From Rosato (1968) [56].

The above or similar figures could give some order of magnitude idea useful for comparison purposes, however, the available information indicates that mechanical properties of foams are very sensitive to foam density, direction of cell-rise versus direction of loading, and test method.

All organic materials tested to date behave in a viscoelastic manner. Strictly speaking the thermal stresses caused on these materials by differential expansions or contractions cannot be expressed in terms of the standard modulus of elasticity and the free contraction constant.

Test methods have been devised to measure the thermal stress-thermal strain ratio (thermoelastic modulus) and the thermoelastic contraction as a function of temperature (Schroeder (1973) [60]). The main objection of such type of data is that because of the nonlinearity of the phenomenon it is not easy to superpose thermally induced and mechanically induced stresses. For example, tests reveal that the thermoelastic strain of a loaded specimen is not the same as that corresponding to the unloaded or free shrink specimen.

One way to circumvent these difficulties and still generate data which would be useful for engineering purposes, is to neglect non-linear effects, which at low temperatures seems to be justified, as was mentioned in connection with Figure 4-10 and is confirmed later, and to obtain mechanical property data using normal widely used test techniques, with the obvious additions to reproduce the required low temperature environment and to minimize thermally induced stresses.

A collection of data generated by US National Bureau of Standards is presented in Table 4-3 to Table 4-8 and Figure 4-13 to Figure 4-18 below. These data concern both tensile and compressive strengths. The main results of these tests can be summarized as follows:

1. The Modulus of Elasticity, yield strength, and ultimate strength increase with decreasing temperature, while the elongation decreases, Table 4-4 and Table 4-8 below.

2. The Modulus of Elasticity is twice as great in tension compared to compression, but the difference diminishes at lower temperatures. Compare Figure 4-14 and Figure 4-17 below.

3. Most foams become brittle at low temperatures, whereas the ductility is considerable at 195 K and above (Figure 4-13 and Figure 4-16 below). On the average, polystyrene foams are more ductile than polyurethanefoams at 76 K (Figure 4-16 below).

4. The Modulus of Elasticity and the strength, both tensile and compressive, are approximately linearly dependent on density. At low temperatures the density dependence is greater (Figure 4-14, Figure 4-15, and Figure 4-17, Figure 4-18 below). In the compressive case there is a minimum density below which the rigid foam cannot withstand any applied compressive force at low temperatures; by extrapolation of the straight lines corresponding to circle and inverted triangle data points in Figure 4-17 below, one obtains a zero value of E at finite density.

5. Specimens loaded along the rise are stronger than those loaded transversally to rise (Figure 4-13 and Figure 4-16 below). In the compressive case this is not necessarily true; notice, for instance, the foam YR-1 in Figure 4-16 below.

6. At most densities there is considerable data spread which can be attributed to foam components, manufacturing process, and blowing agent.

Table 4-3: Characterization of Foams Whose Properties Will Be Given Later

	Sample [a]	Type [b]	Density, ρ [kg.m^{-3}]	Polyol Component	Isocyanate Component [c]	Blowing Agent	Flame Retardant
Flexible	AF-1	PU	34,8	Polyether	TDI	All CO$_2$	No
	BF-4	PU	125	Polyether	PAPI/TDI		No
	BF-5	PU	123	Polyether	PAPI/TDI		No
	BF-6	PU	116	Polyether	PAPI/TDI		No
	CF-7	PU	33,8	Polyester	TDI		No
	CF-8	PU	32,7	Polyester	TDI		No
	CF-9	PU	33,5	Polyester	TDI		No
	DF-1	PU	110	Polyester	TDI		No
	DF-2	PU	111	Polyester	TDI		No
	DF-3	PU	105	Polyester	TDI		No
Rigid	JR-1	PU	66,2	Polyether	PAPI Prepol	CO$_2$ and	Yes
	KR-1	PU	30,6	Polyether	PAPI Prepol	Freon 11	Yes
	LR-3	PU	42,4	Polyether	TDI Prepol	CO$_2$ and	No
	MR-1	PU	68,4	Polyether	TDI Prepol	Freon 11	No
	NR-1	PU	95,6	Polyether	TDI Prepol	CO$_2$	No
	OR-1	PU	47,6	Polyester	TDI Prepol	CO$_2$	No
	OR-2	PU	47,7	Polyester	TDI Prepol	CO$_2$	No
	PR-1	PU	48,1	Polyether	PAPI	Freon 11	No

	Sample [a]	Type [b]	Density, ρ [kg.m⁻³]	Polyol Component	Isocyanate Component [c]	Blowing Agent	Flame Retardant
	SR-2	PU	47,7	Polyether	PAPI	Freon 11	Yes
	TR-2	PU	32,4	Polyester	TDI Prepol	Freon 11	No
	UR-2	PU	43,6	Polyester	TDI Prepol	Freon 11	No
	VR-2	PU	61,0	Polyester	TDI Prepol	CO_2	No
	WR-2	PU	87,8	Polyester	TDI Prepol	CO_2	No
	XR-3	PU	48,2	Polyether	TDI Prepol	CO_2	No
	XR-4	PU	47,6	Polyether	TDI Prepol	CO_2	No
	YR-1	PS	52,2	Polystyrene	-	CO_2 Pentane	No
	ZR-1	PS	100	Polystyrene	-	CO_2 Pentane	No

[a] Material source: AF-1 to SR-2: CPR Division, Upjohn Company; TR-2 to Zr-1: Bendix Corporation

[b] PU: Polyurethane foam; PS: Polystyrene foam.

[c] TDI: Tolylene diisocyanate; PAPI: Polymethylene polyphenylisocyanate, registered trade name of Upjohn Co.; Prepol: Prepolymerized.

NOTE   From Reed, Arvidson & Durcholz (1972) [52].

Table 4-4: Average Tensile Data of Polyurethane and Polystyrene Foams

Data at T = 76 K	Table 4-5
Data at T = 195 K	Table 4-6
Data at T = 300 K	Table 4-7

NOTE   From Reed, Arvidson & Durcholz (1972) [52].

Table 4-5: Average Tensile Data of Polyurethane and Polystyrene Foams at T = 76 K T: Transverse; L: Longitudinal

Foam	Density, ρ [kg.m^{-3}]	Type [a]	Modulus of Elasticity, Ex10^{-6} [Pa]		Proportional limit σx10^{-5} [Pa]		Yield [b] strength, σ_0x10^{-5} [Pa]		Compressive strength, σx10^{-5} [Pa]		Elongation % Plastic		Total	
			T	L	T	L	T	L	T	L	T	L	T	L
KR-1	30,6	PUR	12,5	-	3,2	-	-	-	3,7	-	0,06	-	3,05	-
KR-1	29,5	PUR	-	18,2	-	1,4	-	-	-	4,6	-	0,03	-	1,81
TR-2	32,4	PUR	20,4	-	3,0	-	-	-	3,6	-	0,03	-	1,80	-
LR-3	42,4	PUR	38,5	-	6,8	-	-	-	8,3	-	0,04	-	1,86	-
UR-2	43,6	PUR	33,4	-	4,7	-	-	-	6,0	-	0,01	-	1,88	-
UR-2	44,5	PUR	-	27,1	-	4,1	-	-	-	6,1	-	0,07	-	2,40
XR-4	47,6	PUR	31,7	-	-	-	-	-	5,6	-	0,00	-	1,77	-
OR-1	47,7	PUR	37,0	-	-	-	-	-	10,1	-	0,00	-	2,72	-
OR-1	46,3	PUR	-	45,0	-	-	-	-	-	6,3	-	0,00	-	2,03
SR-2	47,7	PUR	38,7	-	-	-	-	-	6,6	-	0,00	-	1,67	-
PR-1	47,7	PUR	32,8	-	5,0	-	-	-	5,4	-	0,02	-	1,70	-
VR-2	61,0	PUR	51,0	-	6,3	-	-	-	9,2	-	0,02	-	1,62	-
JR-1	64,6	PUR	40,4	-	-	-	-	-	7,9	-	0,00	-	1,93	-
MR-1	68,2	PUR	44,5	-	6,5	-	-	-	9,4	-	0,05	-	2,17	-
WR-2	87,8	PUR	63,0	-	11,0	-	-	-	14,4	-	0,05	-	2,22	-
NR-1	95,6	PUR	95,8	-	14,4	-	-	-	18,5	-	0,04	-	1,98	-
NR-1	94,8	PUR	-	85,4	-	13,2	-	-	-	15,7	-	0,06	-	2,21
CF-7	33,8	PUF	16,5	-	1,9	-	2,7	-	4,4	-	1,79	-	4,63	-
CF-7	32,5	PUF	-	17,6	-	2,6	-	3,7	-	4,9	-	0,83	-	3,54
AF-1	34,8	PUF	15,4	-	2,0	-	2,8	-	4,2	-	2,40	-	5,35	-
DF-1	108	PUF	102,7	-	6,6	-	12,3	-	26,3	-	3,27	-	5,90	-
BF-4	124	PUF	120,1	-	7,8	-	-	-	10,4	-	0,08	-	0,73	-
YR-1	52,2	PSR	57,4	-	7,2	-	9,9	-	11,2	-	0,72	-	2,02	-
YR-1	51,3	PSR	-	50,4	-	6,5	-	9,4	-	10,9	-	0,83	-	2,95
ZR-1	101	PSR	108,2	-	11,8	-	19,2	-	22,5	-	0,76	-	2,18	-

[a] PUR: polyurethane rigid; PUF: polyurethane flexible; PSR: polystyrene rigid.

[b] At 0,2% offset.

NOTE   COMMENTS: 1) The rigid foam samples were cylindrical, 2,866x10^{-2} m in diameter and 7,62x10^{-2} m long. Specimens having a reduced middle subclause 6.21x10^{-2} m in diameter and 2,54x10^{-2} m long m in side and 7,62x10^{-2} m long. The specimens were epoxied to polycarbonate grips. Polycarbonate was chosen because its thermal expansion matched that of the adhesive at low temperature.

2) The rate of head movement of the testing machine was 5×10^{-4} m.min^{-1}.

3) Each value represents the average of about four tests. Strength data variation from the reported average were ± 10%. Suggested inaccuracies of the reported average strength data are ± 5%. Average elongation data are supposed to be inaccurate to ± 5%, and data variations from the reported averages are ± 10%. For a given test individual strength and elongation measurements are thought to be accurate to ± 1%.

NOTE   From Reed, Arvidson & Durcholz (1972) [52].

Table 4-6: Average Tensile Data of Polyurethane and Polystyrene Foams at *T* = 195 K T: Transverse; L: Longitudinal

Foam	Density, ρ [kg.m^{-3}]	Type [a]	Modulus of Elasticity, $E \times 10^{-6}$ [Pa]		Proportional limit $\sigma \times 10^{-5}$ [Pa]		Yield [b] strength, $\sigma \times 10^{-5}$ [Pa]		Compressive strength, $\sigma \times 10^{-5}$ [Pa]		Elongation %			
											Plastic		Total	
			T	L	T	L	T	L	T	L	T	L	T	L
KR-1	30,6	PUR	10,1	-	2,2	-	2,6	-	3,2	-	0,88	-	4,01	-
KR-1	30,6	PUR	-	11,2	-	1,04	-	2,1	-	4,0	-	1,98	-	5,69
UR-2	39,2	PUR	11,9	-	2,6	-	4,1	-	6,1	-	0,96	-	6,10	-
UR-2	42,0	PUR	-	15,9	-	4,6	-	6,1	-	6,8	-	0,12	-	4,40
OR-1	47,1	PUR	14,5	-	3,8	-	7,5	-	8,1	-	0,16	-	5,70	-
NR-1	95,8	PUR	38,7	-	6,2	-	10,5	-	17,1	-	1,15	-	5,57	-
NR-1	94,3	PUR	-	45,2	-	6,3	-	11,4	-	17,4	-	1,14	-	4,03
CF-7	32,2	PUF	3,7	-	0,74	-	1,2	-	3,2	-	34,30	-	45,55	-
CF-7	33,6	PUF	-	6,9	-	1,1	-	1,7	-	3,7	-	23,7	-	28,9
YR-1	51,7	PSR	35,0	-	4,5	-	6,8	-	8,8	-	2,81	-	4,91	-
YR-1	50,6	PSR	-	30,2	-	3,2	-	6,4	-	8,7	-	1,83	-	3,92

[a] PUR: polyurethane rigid; PUF: polyurethane flexible; PSR: polystyrene rigid.

[b] At 0,2% offset.

NOTE   COMMENTS: 1) The rigid foam samples were cylindrical, $2,866 \times 10^{-2}$ m in diameter and $7,62 \times 10^{-2}$ m long. Specimens having a reduced middle subclause 6.21×10^{-2} m in diameter and $2,54 \times 10^{-2}$ m long m in side and $7,62 \times 10^{-2}$ m long. The specimens were epoxied to polycarbonate grips. Polycarbonate was chosen because its thermal expansion matched that of the adhesive at low temperature.

2) The rate of head movement of the testing machine was 5×10^{-4} m.min^{-1}.

3) Each value represents the average of about four tests. Strength data variation from the reported average were ± 10%. Suggested inaccuracies of the reported average strength data are ± 5%. Average elongation data are supposed to be inaccurate to ± 5%, and data variations from the reported averages are ± 10%. For a given test individual strength and elongation measurements are thought to be accurate to ± 1%.

NOTE   From Reed, Arvidson & Durcholz (1972) [52].

Table 4-7: Average Tensile Data of Polyurethane and Polystyrene Foams at T = 300 KT: Transverse; L: Longitudinal

Foam	Density, ρ [kg.m⁻³]	Type [a]	Modulus of Elasticity, Ex10⁻⁶ [Pa]		Proportional limit σx10⁻⁵ [Pa]		Yield [b] strength, σ_bx10⁻⁵ [Pa]		Compressive strength, σx10⁻⁵ [Pa]		Elongation %			
											Plastic		Total	
			T	L	T	L	T	L	T	L	T	L	T	L
KR-1	30,8	PUR	5,6	-	1,03	-	1,3	-	2,9	-	4,84	-	9,96	-
UR-2	40,0	PUR	16,1	-	1,0	-	2,4	-	5,0	-	2,86	-	5,89	-
UR-2	41,2	PUR	-	13,7	-	1,5	-	2,6	-	4,9	-	2,42	-	6,02
OR-1	47,3	PUR	17,2	-	2,4	-	3,7	-	5,4	-	1,57	-	4,35	-
NR-1	94,7	PUR	26,4	-	3,7	-	6,1	-	10,8	-	3,09	-	7,05	-
NR-1	94,7	PUR	-	31,0	-	3,4	-	6,3	-	10,4	-	2,00	-	5,68
CF-7	33,0	PUF	0,12	-	0,20	-	0,28	-	0,73	-	37,25	-	96,27	-
CF-7	33,2	PUF	-	0,19	-	1,6	-	0,28	-	0,85	-	35,33	-	82,03
YR-1	50,8	PSR	36,1	-	3,0	-	6,2	-	8,2	-	2,84	-	5,24	-
YR-1	50,9	PSR	-	38,7	-	3,9	-	6,3	-	8,3	-	2,10	-	4,20

[a] PUR: polyurethane rigid; PUF: polyurethane flexible; PSR: polystyrene rigid.

[b] At 0,2% offset.

NOTE   COMMENTS: 1) The rigid foam samples were cylindrical, 2,866x10⁻² m in diameter and 7,62x10⁻² m long. Specimens having a reduced middle subclause 6.21x10⁻² m in diameter and 2,54x10⁻² m long m in side and 7,62x10⁻² m long. The specimens were epoxied to polycarbonate grips. Polycarbonate was chosen because its thermal expansion matched that of the adhesive at low temperature.
2) The rate of head movement of the testing machine was 5x10⁻⁴ m.min⁻¹.
3) Each value represents the average of about four tests. Strength data variation from the reported average were ± 10%. Suggested inaccuracies of the reported average strength data are ± 5%. Average elongation data are supposed to be inaccurate to ± 5%, and data variations from the reported averages are ± 10%. For a given test individual strength and elongation measurements are thought to be accurate to ± 1%.

NOTE   From Reed, Arvidson & Durcholz (1972) [52].

Table 4-8: Average Compressive Data of Polyurethane and Polystyrene Foams

Data at T = 76 K	Table 4-9
Data at T = 195 K	Table 4-10
Data at T = 300 K	Table 4-11

NOTE   Individual strength and elongation measurements are accurate to ± 1%. Reported strength and elongation measurements are thought to be accurate to ± 7%, with the principal contributor to test inaccuracy being material inconsistency.

NOTE   From Arvidson, Durcholz & Reed (1972) [4].

Table 4-9: Average Compressive Data of Polyurethane and Polystyrene Foams at T = 76 K T: Transverse; L: Longitudinal

Foam	Density, ρ [kg.m⁻³]	Type [a]	Modulus of Elasticity, Ex10⁻⁶ [Pa]		Proportional limit σx10⁻⁵ [Pa]		Yield [b] strength, σ_0x10⁻⁵ [Pa]		Compressive Strength [c], σx10⁻⁵ [Pa]		Elongation %			
											Plastic		Total	
			T	L	T	L	T	L	T	L	T	L	T	L
UR-2	47,6	PUR	29,4	-	4,0	-	5,1	-	6,3	-	0,41	-	2,58	-
PR-1	46,8	PUR	-	36,1	-	5,4	-	-	-	6,5	-	0,11	-	1,92
NR-1	48,4	PUR	13,6	-	2,3	-	3,8	-	6,2	-	2,69	-	7,32	-
CF-7	47,4	PUF	-	23,0	-	3,5	-	5,8	-	7,0	-	0,72	-	3,75
YR-1	94,8	PSR	67,8	-	11,3	-	-	-	14,8	-	0,04	-	2,39	-
ZR-1	95,6	PSR	-	81,7	-	10,8	-	-	-	14,2	-	0,13	-	1,87
	34,1		12,0	-	2,1	-	2,8	-	3,0	-	0,35	-	2,88	-
	31,7		-	10,9	-	2,2	-	3,2	-	3,4	-	0,45	-	3,55
	51,6		31,6	-	3,7	-	5,0	-	5,4	-	3,28	-	5,02	-
	51,3		-	32,4	-	3,7	-	4,6	-	5,1	-	4,65	-	6,28
	99,5		73,8	-	9,3	-	13,7	-	15,1	-	0,58	-	2,32	-
	99,2		-	74,8	-	9,4	-	13,2	-	14,5	-	0,95	-	2,93

[a] PUR: polyurethane rigid; PUF: polyurethane flexible; PSR: polystyrene rigid.

[b] At 0,2% offset.

[c] Tests in which the stress continued to increase as the test progressed (i.e., the material did not exhibit an ultimate) were concluded at 10% total elongation. The corresponding values are in parentheses.

NOTE   COMMENTS: 1) The rigid foam samples were cylindrical, 2,866x10⁻² m in diameter and 2,54x10⁻² m long. Flexible specimens were machined into a cube geometry with the length of each side equal to 2,54x10⁻² m.
2) The rate of head movement of the testing machine was 5x10⁻⁴ m.min⁻¹.
3) Each value represents the average of at least three tests. The average strength deviations for a given type and loading direction were ± 9%, while the average elongation deviations were ± 8%. Individual strength and elongation measurements are accurate to ± 1%. Reported strength and elongation measurements are thought to be accurate to ± 7%, with the principal contributor to test inaccuracy being material inconsistency.

NOTE   From Arvidson, Durcholz & Reed (1972) [4].

Table 4-10: Average Compressive Data of Polyurethane and Polystyrene Foams at
T = 195 K T: Transverse; L: Longitudinal

Foam	Density, ρ [kg.m⁻³]	Type [a]	Modulus of Elasticity, Ex10⁻⁶ [Pa]		Proportional limit σx10⁻⁵ [Pa]		Yield [b] strength, σ_0x10⁻⁵ [Pa]		Compressive Strength [c], σx10⁻⁵ [Pa]		Elongation %			
											Plastic		Total	
			T	L	T	L	T	L	T	L	T	L	T	L
UR-2	43,9	PUR	12,6	-	1,7	-	2,6	-	3,8	-	1,84	-	4,91	-
NR-1	41,3	PUR	-	11,2	-	1,7	-	2,3	-	3,4	-	2,35	-	5,59
CF-7	94,2	PUF	40,4	-	4,1	-	7,0	-	(11.6)	-	7,10	-	10,00	-
YR-1	94,5	PSR	-	51,4	-	4,6	-	7,3	-	(11.7)	-	7,68	-	10,00-
	33,3		2,0	-	0,33	-	0,57	-	(0.84)	-	5,96	-	10,00	5,43
	32,0		-	3,5	-	0,72	-	0,99	-	1,19	-	1,87	-	-
	51,3		23,6	-	3,2	-	4,1	-	(5.2)	-	7,80	-	10,00	10,00
	51,4		-	21,5	-	3,0	-	3,8	-	(4.8)	-	7,70	-	-

[a] PUR: polyurethane rigid; PUF: polyurethane flexible; PSR: polystyrene rigid.

[b] At 0,2% offset.

[c] Tests in which the stress continued to increase as the test progressed (i.e., the material did not exhibit an ultimate) were concluded at 10% total elongation. The corresponding values are in parentheses.

NOTE   COMMENTS: 1) The rigid foam samples were cylindrical, 2,866x10⁻² m in diameter and 2,54x10⁻² m long. Flexible specimens were machined into a cube geometry with the length of each side equal to 2,54x10⁻² m.
2) The rate of head movement of the testing machine was 5x10⁻⁴ m.min⁻¹.
3) Each value represents the average of at least three tests. The average strength deviations for a given type and loading direction were ± 9%, while the average elongation deviations were ± 8%. Individual strength and elongation measurements are accurate to ± 1%. Reported strength and elongation measurements are thought to be accurate to ± 7%, with the principal contributor to test inaccuracy being material inconsistency.

NOTE   From Arvidson, Durcholz & Reed (1972) [4].

**Table 4-11: Average Compressive Data of Polyurethane and Polystyrene Foams at
T = 300 K T: Transverse; L: Longitudinal**

Foam	Density, ρ [kg.m⁻³]	Type [a]	Modulus of Elasticity, Ex10⁻⁶ [Pa]		Proportional limit σx10⁻⁵ [Pa]		Yield [b] strength, σ_0x10⁻⁵ [Pa]		Compressive strength [c], σx10⁻⁵ [Pa]		Elongation % Plastic		Elongation % Total	
			T	L	T	L	T	L	T	L	T	L	T	L
UR-2	46,3	PUR	7,0	-	1,3	-	1,9	-	3,0	-	3,26	-	7,62	-
NR-1	40,8	PUR	-	7,2	-	1,4	-	2,2	-	3,0	-	2,04	-	6,34
CF-7	95,1	PUF	17,2	-	3,5	-	5,2	-	8,0	-	3,27	-	7,93	-
YR-1	93,2	PSR	-	20,2	-	4,3	-	5,9	-	8,1	-	3,27	-	7,38
	33,3		0,06	-	0,021	-	0,024	-	(0.035)	-	4,13	-	10,00	-
	33,3		-	0,20	-	0,014	-	0,021	-	(0.04)	-	7,31	-	10,00
	51,9		19,8	-	3,4	-	3,7	-	(4.0)	-	7,94	-	10,00	-
	51,1		-	19,1	-	2,3	-	3,2	-	3,4	-	0,68	-	2,46

[a] PUR: polyurethane rigid; PUF: polyurethane flexible; PSR: polystyrene rigid.

[b] At 0,2% offset.

[c] Tests in which the stress continued to increase as the test progressed (i.e., the material did not exhibit an ultimate) were concluded at 10% total elongation. The corresponding values are in parentheses.

NOTE   COMMENTS: 1) The rigid foam samples were cylindrical, 2,866x10⁻² m in diameter and 2,54x10⁻² m long. Flexible specimens were machined into a cube geometry with the length of each side equal to 2,54x10⁻² m.
2) The rate of head movement of the testing machine was 5x10⁻⁴ m.min⁻¹.
3) Each value represents the average of at least three tests. The average strength deviations for a given type and loading direction were ± 9%, while the average elongation deviations were ± 8%. Individual strength and elongation measurements are accurate to ± 1%. Reported strength and elongation measurements are thought to be accurate to ± 7%, with the principal contributor to test inaccuracy being material inconsistency.

NOTE   From Arvidson, Durcholz & Reed (1972) [4].

Figure 4-13: Tensile stress, σ, vs. strain, δ, for several polyurethane foams at 76, 195 and 300 K.

From Reed, Arvidson & Durcholz (1972) [52].
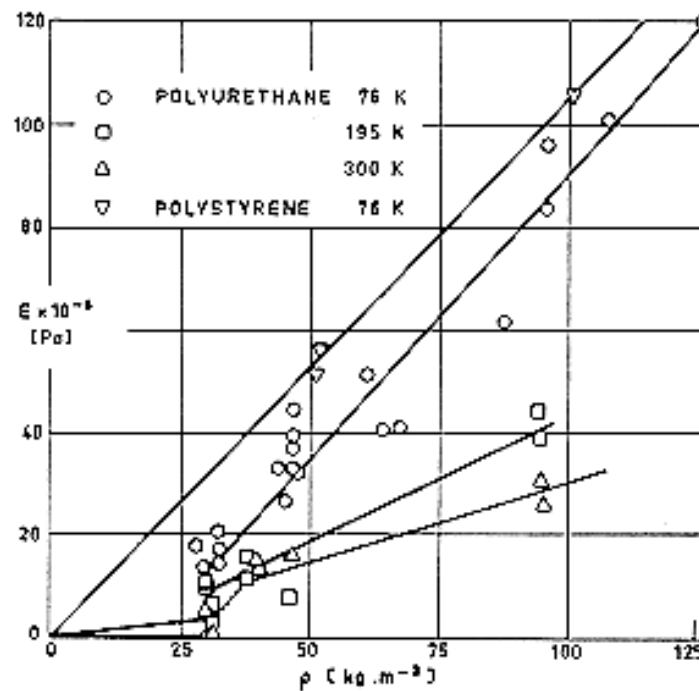
Figure 4-14: Modulus of Elasticity-tensile-E, as a function of density, ρ, for several organic foams.

Solid lines show the estimated dependence of E on foam density; dashed lines indicate transition between rigid foams (large E) and flexible foams (small E). From Reed et al. (1972) [52].
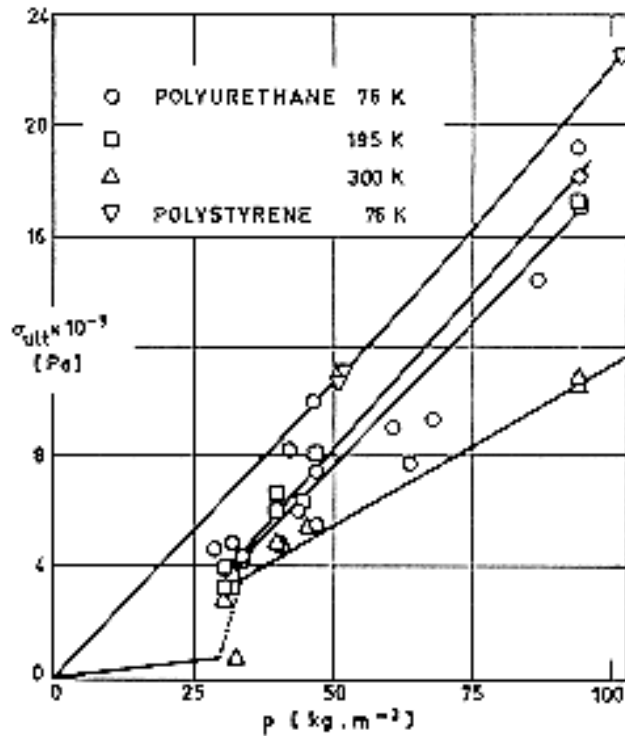
Figure 4-15: Ultimate tensile strength, σ_{ult}, as a function of density, ρ, for several organic foams.

Solid and dashed lines have the same meaning as in Figure 4-8. From Reed et al. (1972) [52].

Note: non-si units are used in this figure
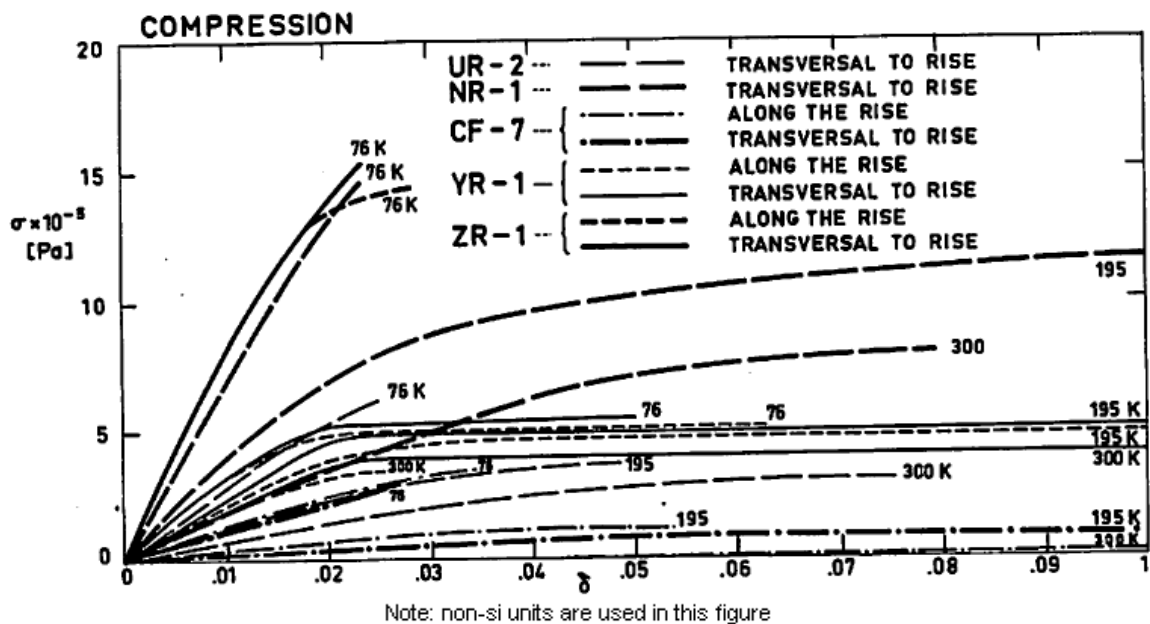
Figure 4-16: Compressive stress, s, vs, strain, d, for several organic foams at 76, 195 and 300 K.

From Arvidson, Durcholz & Reed (1972) [4].
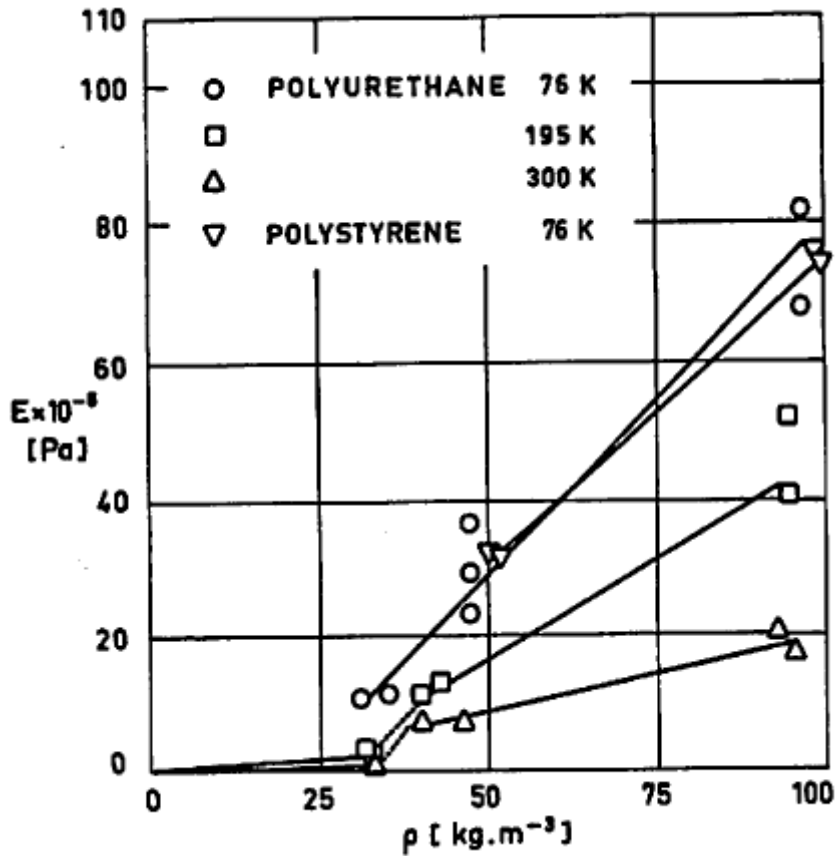
Figure 4-17: Modulus of Elasticity-tensile-*E*, as a function of density, ρ, for several organic foams.

Solid lines show the estimated dependence of *E* on foam density; dashed lines indicate transition between rigid foams (large *E*) and flexible foams (small *E*). From Arvidson et al. (1972) [4].
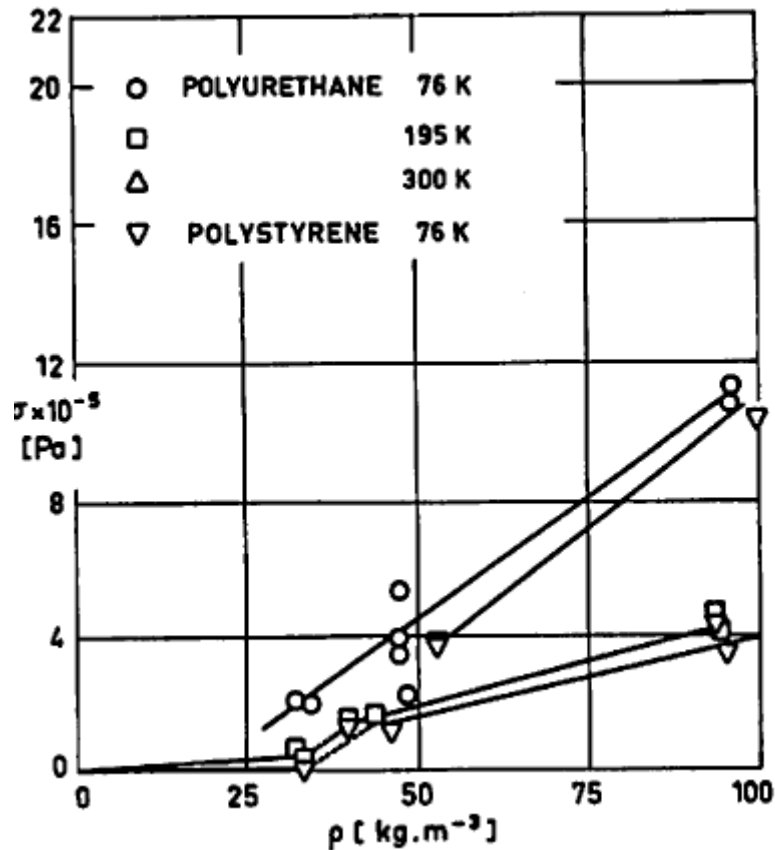
Figure 4-18: Proportional limit-compressive-σ, as a function of density, ρ, for several organic foams.

Solid lines show the estimated dependence of E on foam density; dashed lines indicate transition between rigid foams (large E) and flexible foams (small E). From Arvidson et al. (1972) [4].

A second set of data - this one from North American Rockwell - is presented in Figure 4-19 to Figure 4-22. Basically these data confirm the general trends mentioned above. Additional information concerning the influence of different loading directions on the compressive strength is shown in Figure 4-21.

Shear strength data are given in Figure 4-22. Regarding these data, it should be said that mechanically and thermally induced stresses are strongly coupled, since in this particular test, which was performed using the ASTM C-273 standard method, the loading plates are bonded to the facings of the foam along their whole length. Thence, these results should be considered as merely qualitative.
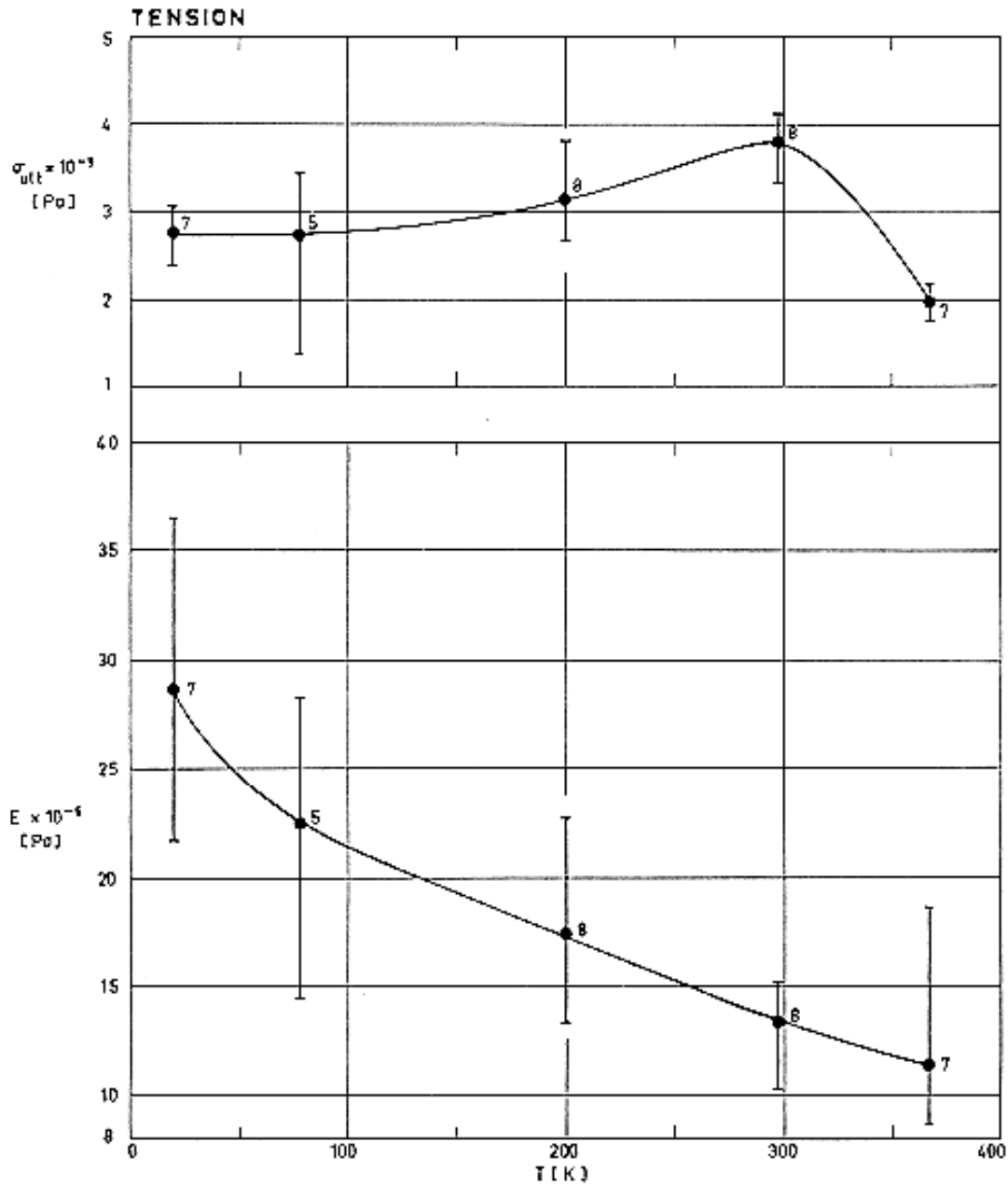
Figure 4-19: Ultimate tensile strength, σ_{ult}, and Modulus of Elasticity-tensile-E, as functions of temperature, T.

Polyurethane spray foam, ρ = 32 kg.m⁻³. Tested per ASTM D-1623; transversal to the rise. Numbers indicate how many tests were performed in each case. From Schroeder (1973)b [61].
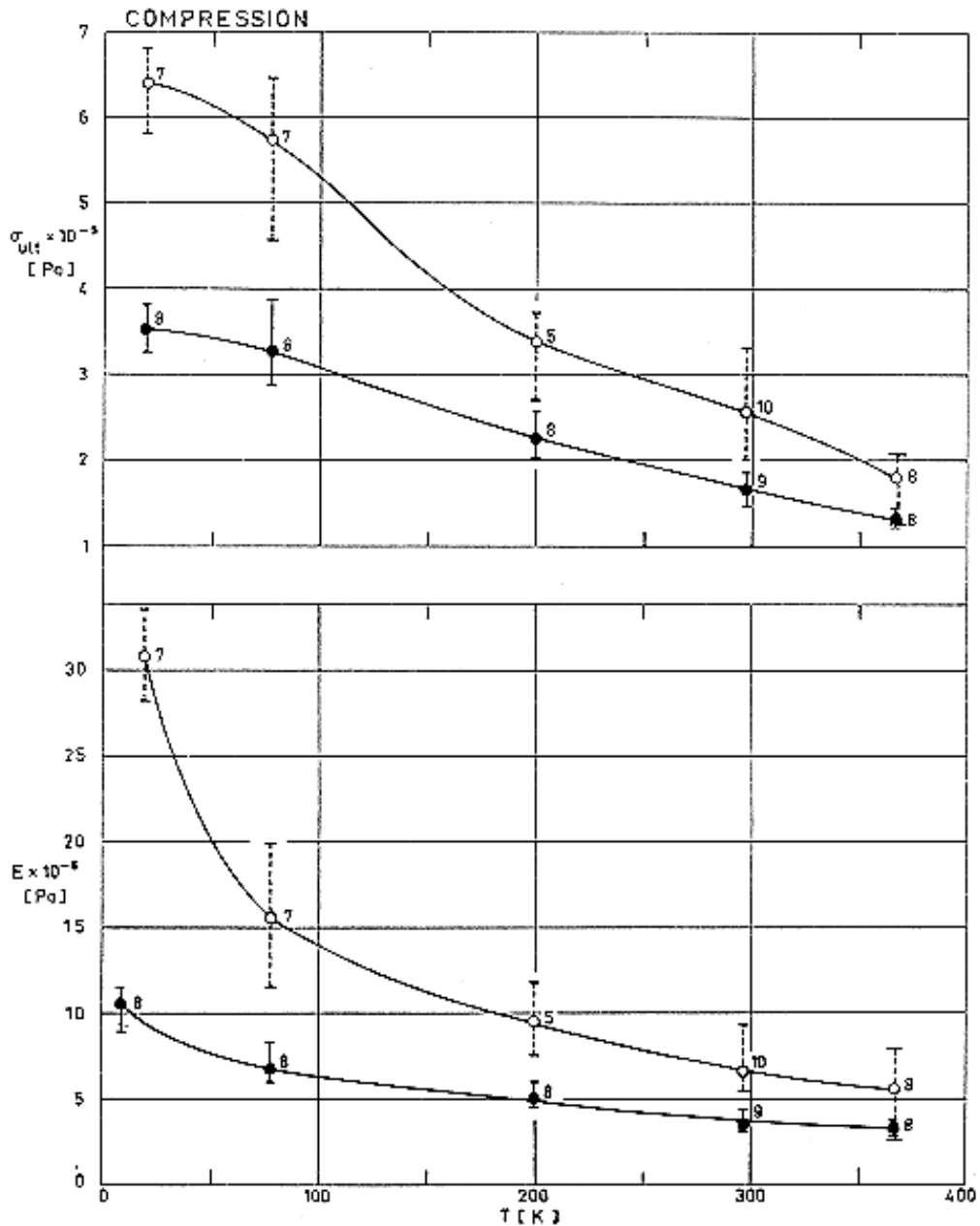
Figure 4-20: Ultimate compressive strength, σ_{ult}, and Modulus of Elasticity-compressive-E, as functions of temperature, T.

Polyurethane spray foam, ρ = 32 kg.m^{-3}. Tested per ASTM D-1621; White circle: along the rise, black circle transversal to the rise. Numbers indicate how many tests were performed in each case. From Schroeder (1973) [60].
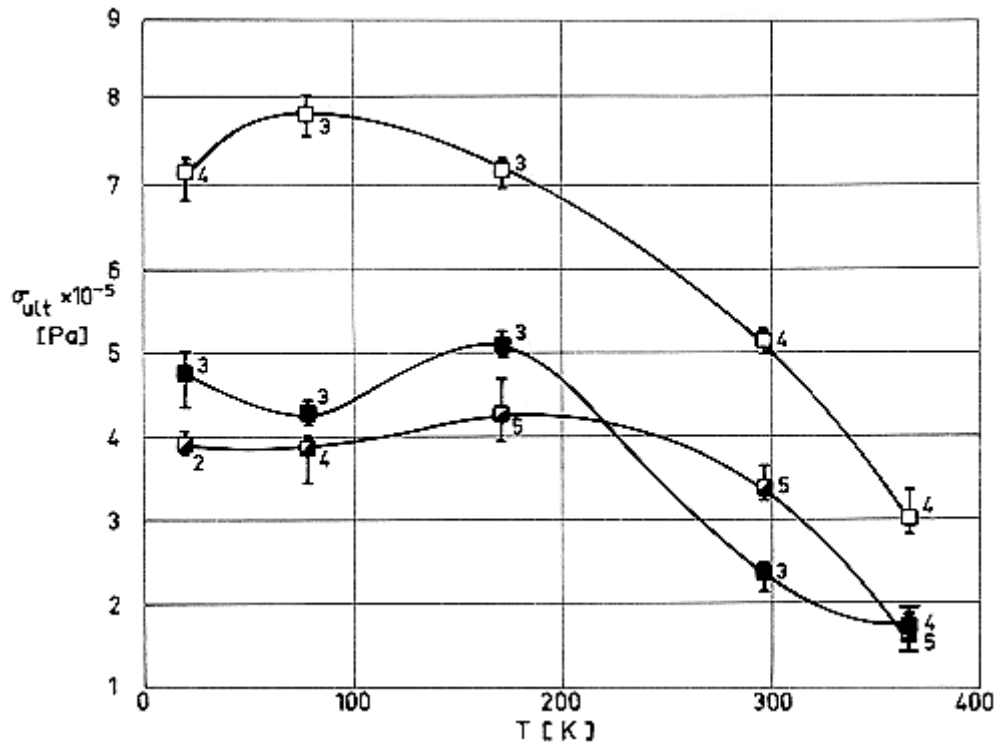
Figure 4-21: Ultimate compressive strength, σ_{ult}, as a function of temperature, T.

Polyurethane spray foam, $\rho = 45$ kg.m^{-3}. Tested per ASTM D-1621; White square: along the rise, Black square: transversal to the rise, Half black square: 45 degrees to the rise. Numbers indicate how many tests were performed in each case. From Schroeder (1973) [60].
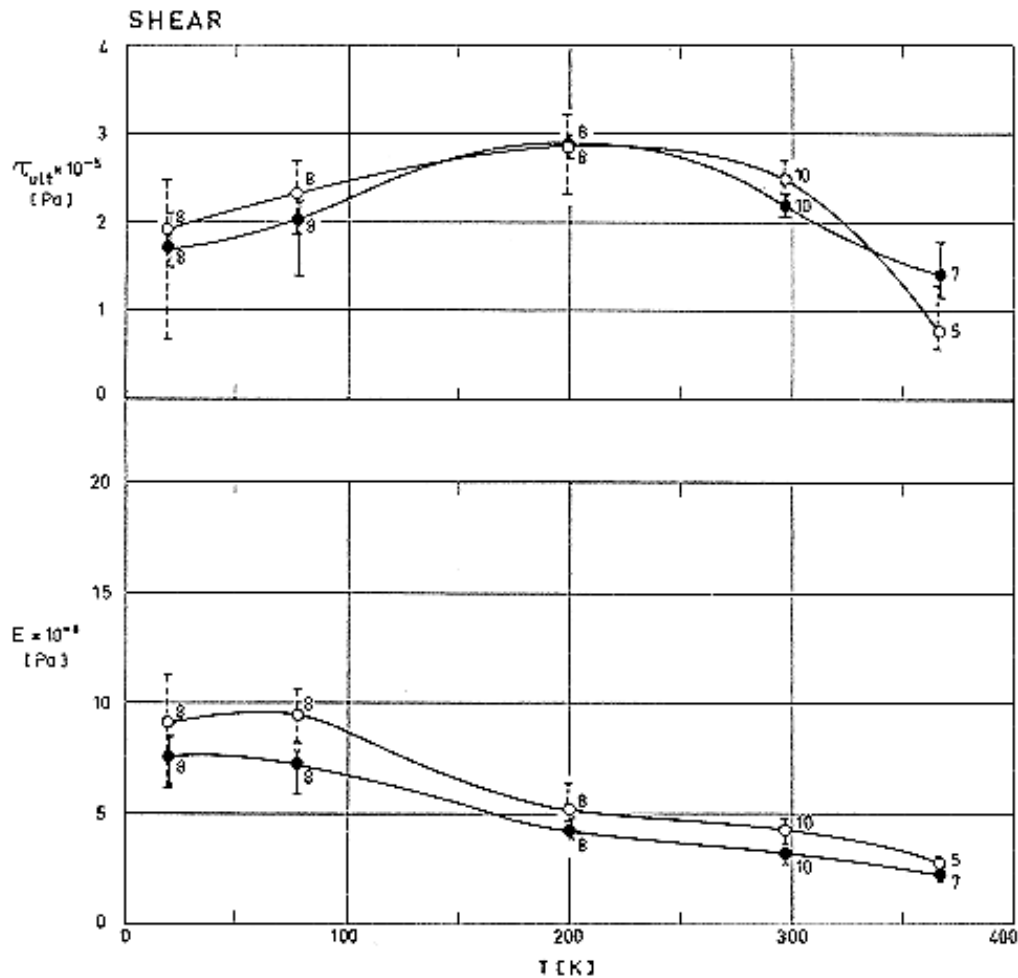
Figure 4-22: Ultimate block shear strength, τ_{ult}, and Modulus of Elasticity-shear block-E, as functions of temperature, T.

Polyurethane spray foam, ρ = 32 kg.m⁻³. Tested per ASTM C-273; White circle: along the rise, Black circle: transversal to the rise. Numbers indicate how many tests were performed in each case. From Schroeder (1973) [60].

4.3.4   Data on commercially available foams

The physical characteristics, availability and information which concerns the processing of several organic foams are given in the pages of this item.

The number of commercially available foams is very large and no attempt has been made to present an exhaustive list of all of them; rather it is hoped that the information presented is representative enough and could be used in a large number of cases.

MANUFACTURER	DOW CORNING	EMERSON & CUMING, INC						
TRADE NAME	SILASTIC S-5370	ECCOFOAM FPH			ECCOFOAM SH			ECCOBOND SF-40
NATURE	SILICONE	POLYURETHANE			POLYURETHANE			EPOXY
DESCRIPTION	Resilient rubbery foam, for molding and foaming in place	High temperature resistant foam in place			Sheets made from Eccofoam FPH			Syntactic foam epoxy adhesive and rigid filler
PHYSICAL PROPERTIES								
Color	Tan	Pink			Pink			White
Cell Type	10% Closed	Closed			Closed			
Density, ρ [kg.m^{-3}]	154	32	128	224	32	128	224	641
OPERATING TEMP.								
Max. Temperature [K]	470	408	408	408	408	408	408	422
THERMAL PROPERTIES								
Thermal Conductivity, k [W.m^{-1}.K^{-1}]	0,045	0,021	0,043	0,062	0,017	0,034	0,034	1,44
Linear Coefficient of Thermal Expansion, βx10^{-5} [K^{-1}]		2,5	4	5				3,78
MECHANICAL PROP.								
Tensile Strength, σx10^{-6} [Pa]		0,28	1,38	3,10				
Compressive Modulus, Ex10^{-9} [Pa]								
Compressive		0,21	1,72	4,14	0,21	1,72	4,14	68,94

MANUFACTURER	DOW CORNING		EMERSON & CUMING, INC						
Strength, σx10^{-6} [Pa]									
Flexural Modulus, Ex10^{-6} [Pa]			4,45	48,26	137,8				
Flexural Strength, σx10^{-6} [Pa]			0,17	1,55	5,51				
Shear Strength, τx10^{-6} [Pa]			0,24	0,96	2,07				10,34 [a]
ELECTRIC PROPERTIES									
Dielectric Strength x10^{-6} [V.m^{-1}]	3,15		1,57	1,57	1,57				13,8
Volume Resistivity [Ω.m]	10^{17}								10^{10}
Dielectric Constant, ε_r	1,42 (at 10^5 Hz)		1,04	1,12	1,25	1,04	1,12	1,25	2,5 (at 10^6 Hz)
			(from 10^4 to 10^{10} Hz)			(from 60 to 10^{10} Hz)			
Dissipation Factor Dx10^3	1 (at 10^5 Hz)		1	2	5	0,5	1	3	20 (at 10^6 Hz)
			(at 10^{10} Hz)			(from 60 to 10^{10} Hz)			
WATER ABSORPTION									
% gain in 24 h			3	1,5	1	0,8	0,2	0,1	0,4
OUTGASSING [b]									
Cure Time [h]	72	16	16				0		48
Cure Temperature [K]	423	477	328				0		298
Atmosphere	E-4	Air	Air				0		Air
% TWL	0,592	0,315	1,182				1,030		0,238
% VCM	0,096	0,120	0,040				0,010		0,043
AVAILABILITY	S-5370, foam					Available in			

MANUFACTURER	DOW CORNING	EMERSON & CUMING, INC		
	base with catalyst, is supplied in 0,45 kg and 4,5 kg containers		maximum sheet size of 0,3 m x 0,61 m. Thickness: available from $25,4 \times 10^{-3}$ m to $101,6 \times 10^{-3}$ m	
PROCESSING	Table 4-12	Table 4-12		Table 4-12
APPLICATIONS	SILASTIC S-5370 RTV foam is a general purpose material used for vibration or thermal insulation, cushioning, foam rubber parts, etc. ECCOFOAM FPH is used for electronic embedments, radome cores, void filling, etc. this foam was used for encapsulation of electronic modules in Telstar, Sidewinder missile and Concorde SST aircraft. ECCOFOAM SH sheets are used for high temperature structural members and thermal barriers. ECCOBOND SF-40: edge filler on honeycomb papel fabrication, fillet development, etc.			

[a]   Sample placed between two aluminium plates.

[b]   Outgassing characteristics have been borrowed from Campbell, Marriott & Park (1973) [10].
TWL: Total Weight Loss.
VCM: Volatile Condensable Materials (by weight).
A zero indicates that cure conditions are unknown.
E-4: Chamber pressure 10^{-4} torr = 0,013 Pa.

NOTE   From manufacturer's bulletins.

MANUFACTURER	EMERSON & CUMING	FIBERFIL DIVISION, DART INDUSTRIES INC.			MOSITES
TRADE NAME	STYCAST 1090	F-1200/20 ABSAFIL	F-60/20 PROFIL	F-30/20 STYRAFIL	FLUOREL 1062
NATURE	EPOXY	ABS [a]	POLY-PROPYLENE	POLY-STYRENE	FLUOREL [b]
DESCRIPTION	Low weight epoxide casting	Fiberglass reinforced foams for molding			Sponge sheets
PHYSICAL PROPERTIES					
Color	Black				
Cell Type					Closed
Density, ρ [kg.m^{-3}]	880	840	730	840	240-480
OPERATING					

MANUFACTURER	EMERSON & CUMING	FIBERFIL DIVISION, DART INDUSTRIES INC.			MOSITES
TEMP.					
Max. Temperature [K]	477 (200 min.)				480 (240 min.)
THERMAL PROPERTIES					
Thermal Conductivity, k [W.m^{-1}.K^{-1}]	0,187				
Linear Coefficient of Thermal Expansion, βx10^{-5} [K^{-1}]	4				
MECHANICAL PROP.					
Tensile Strength, σx10^{-6} [Pa]		48,26	20,68	34,47	
Compressive Modulus, Ex10^{-9} [Pa]	2,41	See Figure 4-23: Deformation vs. Compressive load		See Figure 4-23: Deformation vs. Compressive load	
Compressive Strength, σx10^{-6} [Pa]					
Flexural Modulus, Ex10^{-6} [Pa]		5170	2760	5170	
Flexural Strength, σx10^{-6} [Pa]	28,96	82,74	41,37	58,60	
Shear Strength, τx10^{-6} [Pa]					
ELECTRIC PROPERTIES					
Dielectric Strength x10^{-6} [V.m^{-1}]	14,8				
Volume Resistivity [Ω.m]	10^{10}				

MANUFACTURER	EMERSON & CUMING			FIBERFIL DIVISION, DART INDUSTRIES INC.			MOSITES
Dielectric Constant, ε_r	Figure 4-24						
Dissipation Factor Dx10^3	Figure 4-24						
WATER ABSORPTION							
% gain in 24 h	0,4						non-absorbent
OUTGASSING [c]							
Cure Time [h]	16 [d]	24 [e]	24 [e]	0	0	0	0
Cure Temperature [K]	323	373	394	0	0	0	0
Atmosphere	Air	Air	Air	0	0	0	0
% TWL	0,310	0,130	0,040	0,339	0,169	0,269	0,380
% VCM	0,070	0,130	0,040	0,010	0,044	0,022	0,030
AVAILABILITY							Sheets up to 0,61 mx1,22 m with thicknesses from 3,18x10^{-3} m to 12,7x10^{-3} m [f]
PROCESSING	Table 4-6			Table 4-7			
APPLICATIONS	STYCAST 1090: Airbone embedment applications. FIBERFIL PRODUCTS are used in fornitures, appliance cabinets, housings, automotive products, etc. FLUOREL 1090: Low pressure fluid and gas sealing, thermal insulation shock absorbing, padding, joint filling and flotation.						

a   Acrylonitrile-Styrene-Butadiene.

b   Fluorel is a trade name given to a series of compounds made from hexafluoropropene and vinylidene fluoride.

c   Outgassing characteristics have been borrowed from Campbell, Marriott & Park (1973) [10].
     TWL: Total Weight Loss.
     VCM: Volatile Condensable Materials (by weight).
     A zero indicates that cure conditions are unknown.

d   These outgassing data concern STYCAST 1090 obtained using Catalyst 9.

e   These outgassing data concern STYCAST 1090 obtained using Catalyst 11 (See also Table 4-12).

f   Thickness tolerances are ± ¼ of nominal thickness.

NOTE   From manufacturer's bulletins.

Table 4-12: Information Concerning Processing

PRODUCT	SILASTIC S-5370	ECCOFOAM FPH	ECCOBOND SF-40	STYCAST 1090
COM-PONENTS	SILASTIC S-5370 foam base SILASTIC S-5370 Catalyst	Resin component and Catalysts 12-2H, 12-4H, 12-6H and 12-10H	Part A and Part B	STYCAST 1090, and either Catalyst 9 or Catalyst 11
PROCESS	Catalize 100 parts by weight of foam base with 6 parts of catalyst mixing by stirring for about 30 seconds. The mixture should be poured in place within 60 seconds of the catalyst addition.	Mix thoroughly liquid resin components (preferably heated to about 305 K) with an appropriate Catalyst (which may be at room temperature), and pour the mixture into a mold. The catalyst should be selected according to table below. [a]	Mix 100 parts by weight of Part A with 9 parts of Part B and apply the material with a suitable tool (towel, spatula,...). Pot life of the blended material is 30 min.	Weight out the quantity required and add the percent by weight of the chosen catalyst as indicated below, blending thoroughly. Catalyst 9: 9%. Catalyst 11: 12%. Pour the blend into a mold. Pot life is 30 min, when Catalyst 9 is used and 4 h when using Catalyst 11.
CURE CONDITIONS	Cures at room temperature, reaching optimum strength after 24 h.	Cures at room temperature. For optimum dimensional stability a post cure for 3 h at 395 K is suggested.	Cure time is 48 h for optimum strength.	Cure time is 24 h at room temperature when Catalyst 9 is used. When using Catalyst 11, cure time is 2 h at 366 K-377 K for casting up to 0,2 kg and at lower temperatures for larger castings.
STORAGE	Base products should be stored at temperature below 305 K.		Base products should be stored at room temperature in unopened	Stored uncatalyzed in well sealed, unopened containers at temperatures

PRODUCT	SILASTIC S-5370	ECCOFOAM FPH	ECCOBOND SF-40	STYCAST 1090
			containers.	not above 298 K.
SHELF LIFE	Six months from date of shipment.		Six months at least when stored under the above mentioned conditions.	Six months when stored under the above mentioned conditions.
WARNINGS	STYCAST S-5370 contains stannous octoate and may cause skin and eye irritation. During the expansion period a small quantity of hydrogen is outgassed.	ECCOFOAM FPH contains tolylene diisocyanate, and obnoxious and hazardous material which is an irritant to the skin and mucous membranes, specially eyes and upper respiratory tract.		Avoid breathing vapors and protect skin and eyes.
Desired Bulk Density [kg.m^{-3}] Catalyst Designation Parts of Catalyst per 100 parts of Resin	32 to 48 12-2H 65	64 to 80 12-4H 75	96 to 160 12-6H 75	160 to 224 12-10H 85

[a]   ECCOFOAM FPH can be produced at any bulk density from 32 kg.m^{-3} to 224 kg.m^{-3} using a confined mold and the appropriate catalyst as indicated below. The resin component is the same in any case.
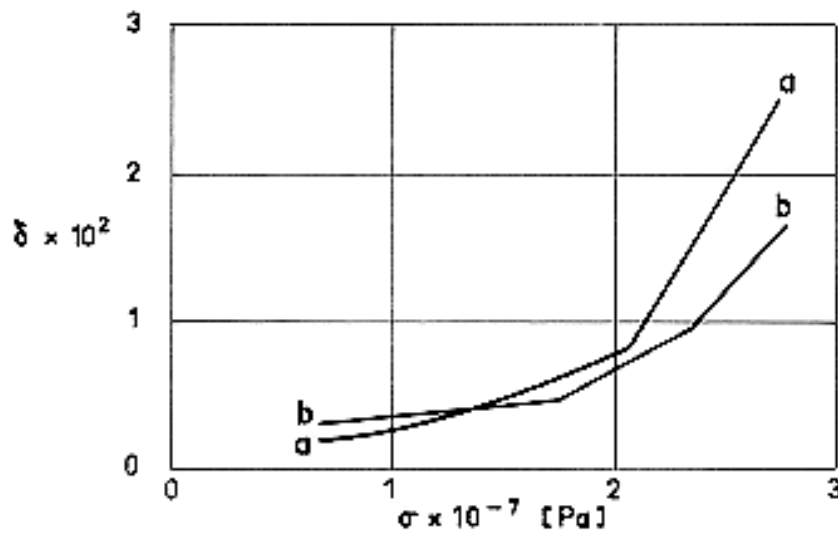
Figure 4-23: Strain, δ, vs. compressive stress, σ, of Fiberfill Structural Foams.

a: F-1200/20 Absafil.
b: F-30/20 Styrafil.
Specimen: 12,7x10⁻³ m x 12,7x10⁻³ m x 12,7x10⁻³ m.
Test temperature: 323 K.
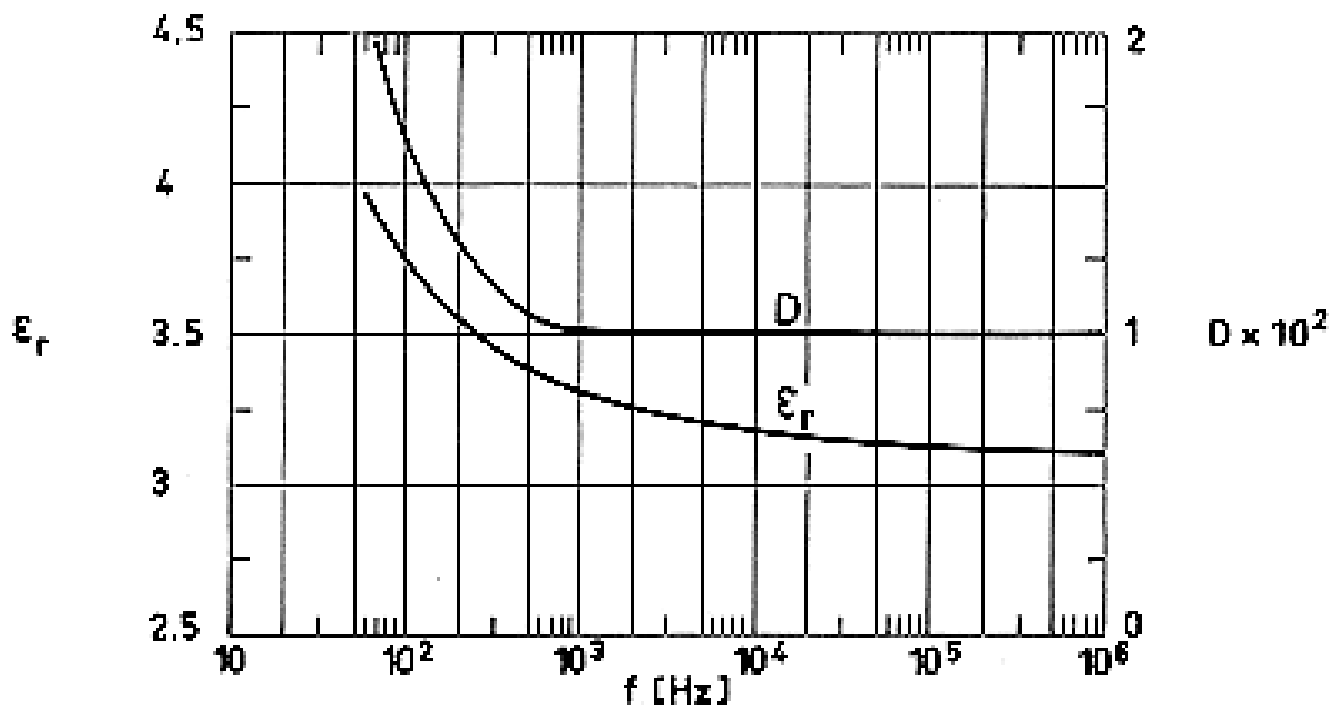
Note: non-si units are used in this figure

Figure 4-24: Dielectric constant, ε_r, and dissipation factor, D, vs. frequency, f. Stycast 1090.

Table 4-13: Information Concerning Processing of Fiberfil Products Recommendations for Molding

		STYRAFIL F-30	PROFIL F-60	ABSAFIL F-1200
Drying of material		Not necessary		
Preferred Melting Temperature [K]		477,5	450	477,5
Cylinder Temperatures [K]	Rear	444,5-455,5	416,5-427,5	444,5-455,5
	Center	461-472	433-444,5	461-472
	Front	483-505,5	455,5-477,5	483-505,5
	Mold	483-505,5	455,5-477,5	483-505,5
When large voids appear in several parts		The stock temperature has been too high		

5
Fibrous insulations

5.1 General

Fibrous materials are used both as internal and external insulations for many spacecraft applications.

The main advantages of these materials are:

Low thermal conductivity.

Low density.

Structural integrity.

Ease of integration into thermal protection system.

Flexibility to conform to shapes and contours of the structural components.

Availability and relatively reduced cost.

Most of these materials have been developed for furnace insulations, ovens, and high-temperature processing. Their use in spacecraft, however, has been reported several times. In addition, the refractory fibers are used in composites as matrices for ablative materials, as localized insulators, and as spacers for multilayer insulations.

The use of fibrous materials for internal insulation is somewhat hampered by the extreme scarcity of data concerning outgassing. When binders are used to improve the dimensional stability of these materials, outgassing can be significant. In addition, there may be several other sources of gaseous products added in order to make easier the manufacturing process; these additives pose one of the major flammability threats to fibrous material that, being based on inorganic substances, are otherwise non-flammable.

A summary of thermal conductivity values for several fibrous insulations is shown in Figure 5-1. Detailed engineering and procurement data, as reported by the manufacturers, are given in the subsequent tables and figures.
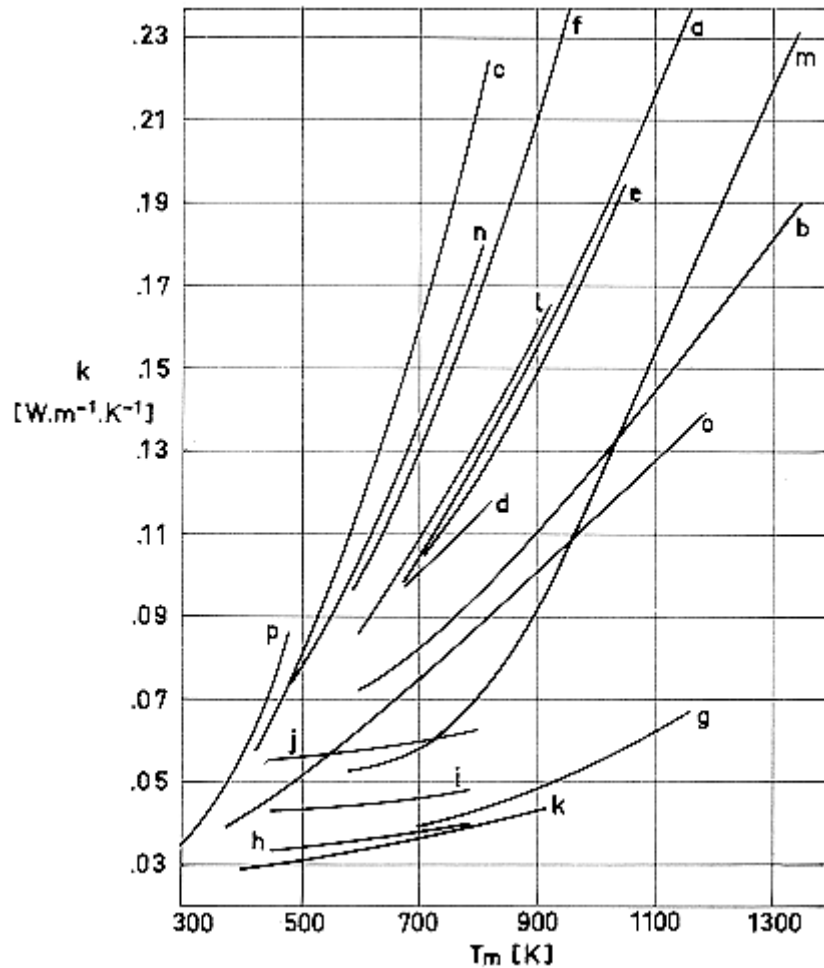
Note: non-si units are used in this figure

Figure 5-1: Thermal conductivity, *k*, vs. mean temperature, *T_m*, for several fibrous insulations. From Glasser et al. (1967) [23].

Explanation

Key	Insulation	ρ [kg.m⁻³]	Key	Insulation	ρ [kg.m⁻³]	Key	Insulation	ρ [kg.m⁻³]
a	Fiberfrax Lo-Con	96	g	Min-K 2000	320	l	Micro-Quartz	48
b	Fiberfrax Paper	192	h	Min-K 2000	400	m	Dyna-Quartz	155
c	Kaowool bulk	48	i	Min-K 2000	480	n	Thermoflex	48
d	Kaowool bulk	160	j	Min-K 2000	561	O	Thermoflex	384
e	Refrasil Batt A-100	56	k	Min-K 1301	320	P	Microlite AA	24
f	Refrasil Batt B-100	48						

5.2 Bulks

MANUFACTURER	BABCOCK & WILCOX. Trade name KAOWOOL				
NATURE	ALUMINA-SILICA				
FIBER FORM	High Purity Low percentages of iron oxide and titania	Bulk-A Lubricated	Bulk-B Unlubricated	Bulk-C Unlubricated Short fiber	Chopped Unlubricated Shorter fiber
PHYSICAL PROPERTIES					
Color	White			White	
Fiber Diameter, d [m]	$2,8x10^{-6}$ Average			$2,8x10^{-6}$ Average	
Fiber Length, [m]	Up to 0,254 (0,102 Average)			Shorts to 0,013	
Fiber Density, ρ [kg.m^{-3}]	$2,56x10^3$			$2,56x10^3$	
Shipping Density, [kg.m^{-3}]					
Surface Area [m^2.kg^{-1}]					
OPERATING TEMP. Continuous [K]	up to 1533				
MELTING POINT [K]	2033				
THERMAL PROPERTIES Specific Heat, c [J.kg^{-1}.K^{-1}]	1067 a				
Thermal Conductivity, k [W.m$^{-1.K^{-1}}$]	Figure 5-2				
Temperature Differential [K]					
MECHANICAL PROP. Fiber Modulus of Elasticity [Pa]	$1,15x10^{11}$				

MANUFACTURER	BABCOCK & WILCOX. Trade name KAOWOOL				
NATURE	**ALUMINA-SILICA**				
FIBER FORM	High Purity Low percentages of iron oxide and titania	Bulk-A Lubricated	Bulk-B Unlubricated	Bulk-C Unlubricated Short fiber	Chopped Unlubricated Shorter fiber
Bulk Modulus of Elasticity [Pa]					
Tensile Strength. Fiber [Pa]	$1,3 \times 10^9$				
CHEMICAL COMPOSITION %					
Al_2O_3	47,0	45,1			
SiO_2	52,9	51,9			
ZrO_2					
Fe_2O_3	0,05 (0,1 max)	1,3			
P_2O_5					
TiO_2	0,07 (0,15 max)	1,7			
B_2O_3		0,08			
Na_2O		0,2			
CaO		0,1			
MgO		trace			
Trace inorganics	trace				
		Leachable element on surface of fiber <165 PPM.			
CHEMICAL DEGRADATION	Excellent resistance to chemical attack. Exceptions are hydrofluoric and phosphoric acids and strong alkalies. Unaffected by oil. Thermal and physical properties are restored after drying. The lubricant in Bulk-A should be burned out at 811 K prior to use in proximity of liquid oxygen. Bulk-B, C and Chopped do not require this treatment.				

MANUFACTURER	BABCOCK & WILCOX. Trade name KAOWOOL				
NATURE	ALUMINA-SILICA				
FIBER FORM	High Purity Low percentages of iron oxide and titania	Bulk-A Lubricated	Bulk-B Unlubricated	Bulk-C Unlubricated Short fiber	Chopped Unlubricated Shorter fiber
MOISTURE ABSORPTION	Unaffected by water				
OUTGASSING					
AVAILABILITY					
APPROXIMATE COST	2,2 US \$.kg⁻¹ F.O.B.				
APPLICATIONS	INSULATION: Kiln car tops, walls and crowns of annealing, brazing, heat treating and holding furnaces. Fill for roofs and walls of furnaces and kilns. PACKING: Expansion joints, emergency repair and patching. SECONDARY PRODUCTS PROCESSING: Paper, block, spray mix, vacuum formed shapes, monolithics, etc. REINFORCED FOR COMPOSITE STRUCTURES: Plastics, resins, etc.				

ª   At 1255 K Mean Temperature.

NOTE   From manufacturer's bulletins.

MANUFACTURER	CARBORUNDUM. Trade name FIBERBRAX				
NATURE	ALUMINA-SILICA				
FIBER FORM	Bulk Fiber	Washed Low content of unfiberized particles	HI-FI Washed Lower content of unfiberized particles	Chopped Short fiber	Milled Shorter fiber
PHYSICAL PROPERTIES					
Color	White	White	White	White	White
Fiber Diameter, d [m]	$2\text{-}3\times10^{-6}$	$2\text{-}3\times10^{-6}$	$1,6\times10^{-6}$	$2\text{-}3\times10^{-6}$	$2\text{-}3\times10^{-6}$
Fiber Length, [m]	0,1		up to 0,05	3×10^{-4}	14×10^{-6}
Fiber Density, ρ [kg.m^{-3}]	$2,53\times10^{3}$	$2,53\times10^{3}$	$2,53\times10^{3}$	$2,53\times10^{3}$	$2,53\times10^{3}$
Shipping Density, [kg.m^{-3}]	96	64-96		112-192	176
Surface Area [m^2.kg^{-1}]	500	500			
OPERATING TEMP. Continuous [K]	1533				
MELTING POINT [K]	2066,5				
THERMAL PROPERTIES Specific Heat, c [J.kg^{-1}.K^{-1}]	1130 [b]	1130 [b]	1130 [b]	1130 [b]	1130 [b]
Thermal Conductivity, k [W.m^{-1}.K^{-1}]	Figure 5-3	Figure 5-3	Same as Washed	0,144 [a]	0,187 [a]
Temperature Differential [K]	Figure 5-3 to Figure 5-6	Figure 5-7			
MECHANICAL PROP. Fiber Modulus of Elasticity [Pa]	$1,09\times10^{11}$				
Bulk Modulus of	$2,74\times10^{9}$	$2,74\times10^{9}$	$2,74\times10^{9}$		

MANUFACTURER	CARBORUNDUM. Trade name FIBERBRAX				
NATURE	ALUMINA-SILICA				
FIBER FORM	Bulk Fiber	Washed Low content of unfiberized particles	HI-FI Washed Lower content of unfiberized particles	Chopped Short fiber	Milled Shorter fiber
Elasticity [Pa]					
Tensile Strength. Fiber [Pa]					
CHEMICAL COMPOSITION %					
Al_2O_3	51,7				
SiO_2	47,6				
ZrO_2					
Fe_2O_3	0,02				
P_2O_5					
TiO_2					
B_2O_3	0,15				
Na_2O	0,3				
CaO					
MgO					
Trace inorganics	0,2				
	Leachable chlorides <50 PPM.				
CHEMICAL DEGRADATION	Excellent chemical stability, resisting attack from most corrosive agents. Exception are hydrofluoric and phosphoric acids and concentrated alkalies. Fiberfrax also resists oxidation and reduction. If wet by steam or oil, thermal and physical properties are restored upon drying.				
MOISTURE ABSORPTION	Unaffected by water.				
OUTGASSING					

MANUFACTURER	CARBORUNDUM. Trade name FIBERBRAX				
NATURE	ALUMINA-SILICA				
FIBER FORM	Bulk Fiber	Washed Low content of unfiberized particles	HI-FI Washed Lower content of unfiberized particles	Chopped Short fiber	Milled Shorter fiber
AVAILABILITY	11,3 kg bags 18,2 kg bags for shipments over 906 kg.	Standard: 13,6 and 22,65 kg. Trial: 0,453 and 4,53 kg cartons		Standard: 6,79 kg cartons. Trial: 0,453 and 4,53 kg cartons	Standard: 90,6 kg drums. Trial: 0,453 and 4,53 kg cartons
APPROXIMATE COST	For amount below 11,3 kg: 7 US $.kg^{-1} For amount above 45,3 kg: 5 US $.kg^{-1}				
APPLICATIONS	BULK: Expansion joints, burner openings, glass feeder bowls, fire boxes, furnace repairs, furnace base seals, kiln insulation. Bulk fiber is also used for the secondary processing of other Fiberfrax product forms: Blanket, felt, paper, etc. WASHED: Manufacture of high temperature papers, as an aditive for ablative compositions, insulation of aerospace vehicles and components, reinforcing additives to plastics and resins, resilient packing material. CHOPPED AND MILLED: Compact filler insulation.				

[a]   At 811 K Mean Temperature.

[b]   At 1366,5 K Mean Temperature.

NOTE   From manufacturer's bulletins.

MANUFACTURER	CARBORUNDUM. Trade name FIBERFRAX		
NATURE	**ALUMINA-SILICA**		
FIBER FORM	Long Staple Fine Extra Long Fiber	Long Staple Coarse Extra Long Fiber	H Bulk
PHYSICAL PROPERTIES			
Color	White	White	White
Fiber Diameter, d [m]	8×10^{-6}	18×10^{-6}	$2\text{-}4 \times 10^{-6}$
Fiber Length, [m]	up to 0,25	up to 0,25	up to 0,25
Fiber Density, ρ [kg.m^{-3}]	2,62	2,62	2,6
Shipping Density, [kg.m^{-3}]	48	48	
Surface Area [m^2.kg^{-1}]			
OPERATING TEMP. Continuous [K]	1533		1700
MELTING POINT [K]	2066,5		2200
THERMAL PROPERTIES Specific Heat, c [J.kg^{-1}.K^{-1}][l]			
Thermal Conductivity, k [W.m^{-1}.K^{-1}][l]			Same as bulk
Temperature Differential [K]			
MECHANICAL PROP. Fiber Modulus of Elasticity [Pa]			
Bulk Modulus of Elasticity [Pa]			
Tensile Strength. Fiber [Pa]			
CHEMICAL COMPOSITION %			
Al$_2$O$_3$	43,9		62
SiO$_2$	50,1		38
ZrO$_2$	5,1		

MANUFACTURER	CARBORUNDUM. Trade name FIBERFRAX		
NATURE	ALUMINA-SILICA		
FIBER FORM	Long Staple Fine Extra Long Fiber	Long Staple Coarse Extra Long Fiber	H Bulk
Fe_2O_3			
P_2O_5			
TiO_2			
B_2O_3	0,15		
Na_2O			
CaO			
MgO			
Trace inorganics	0,75		
CHEMICAL DEGRADATION	Same characteristics as other Fiberfrax fibers		
MOISTURE ABSORPTION	Unaffected by water		
OUTGASSING			
AVAILABILITY	Standard Quantity: 11,32 kg cartons Trial Quantities: 0,453 and 4,53 kg cartons		
APPROXIMATE COST			
APPLICATIONS	LONG STAPLE & COARSE: Catalyst recovery filter in nitric acid production, diffusion medium for fluidized beds, high temperature acoustical insulations, filtration and catalyst carrier medium for radioactive particles and hot exhaust gases, raw material for the manufacture of textiles, rope and square braid.		

NOTE   From manufacturer's bulletins.
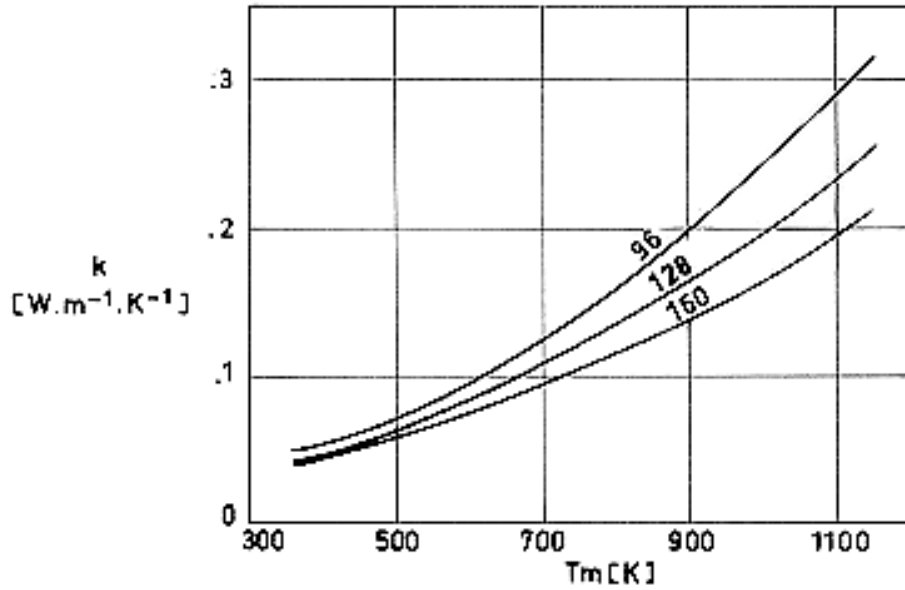
Note: non-si units are used in this figure

Figure 5-2: Thermal conductivity, *k*, of B & W Kaowool bulk vs. mean temperature, *Tm*.

Numbers on curves indicate the density in kg.m⁻³.
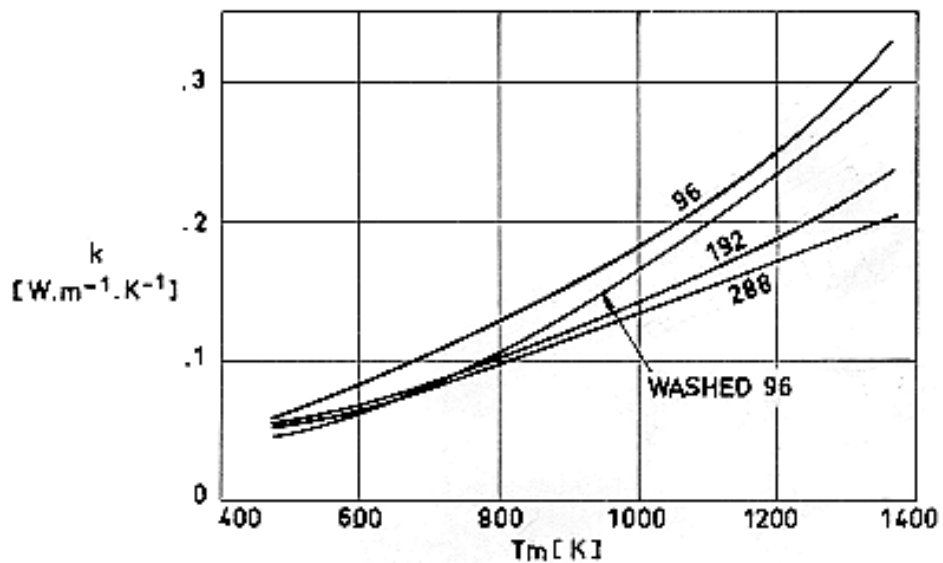
Note: non-si units are used in this figure

Figure 5-3: Thermal conductivity, *k*, of Carborundum Fiberfrax bulk and washed fibers vs. mean temperature, *Tm*.

Numbers on curves indicate the density in kg.m⁻³.

Note: non-si units are used in this figure
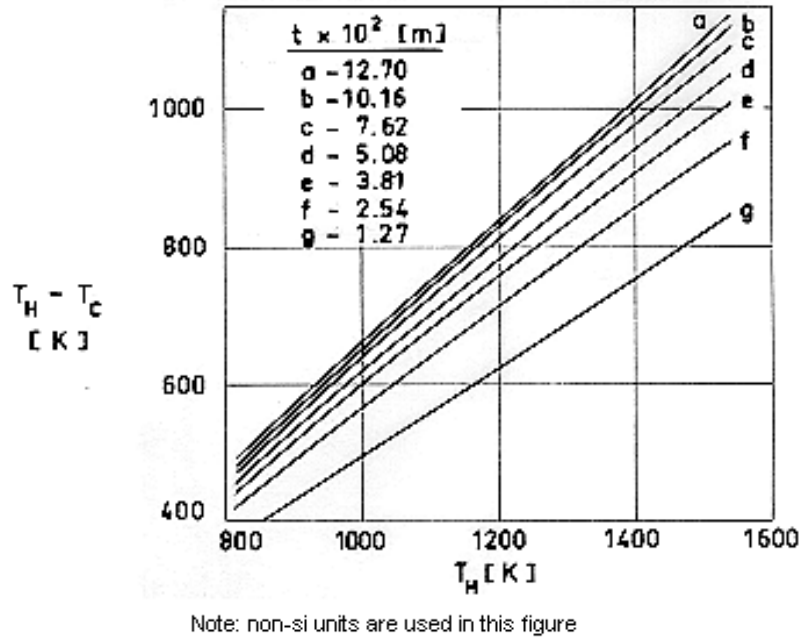
Figure 5-4: Temperature differential, T_H–T_C, vs. mean temperature of the hot face, T_H,

for different values of the insulation thickness, t. Fiberfrax bulk, $\rho = 96$ kg.m^{-3}.

Note: non-si units are used in this figure
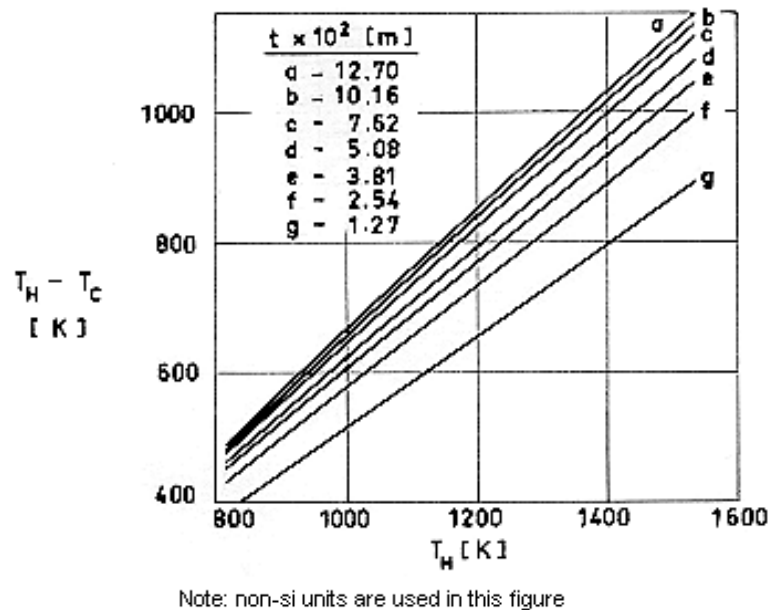
Figure 5-5: Temperature differential, T_H–T_C, vs. mean temperature of the hot face, T_H,

for different values of the insulation thickness, t. Fiberfrax bulk, $\rho = 192$ kg.m^{-3}.
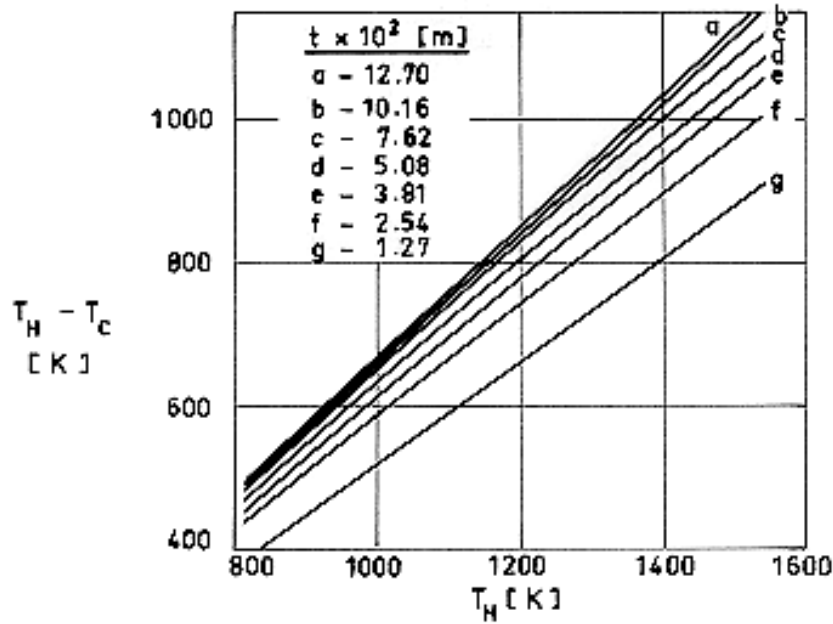
Note: non-si units are used in this figure

Figure 5-6: Temperature differential, T_H–T_C, vs. mean temperature of the hot face, T_H,

for different values of the insulation thickness, t. Fiberfrax bulk, $\rho = 288$ kg.m^{-3}.
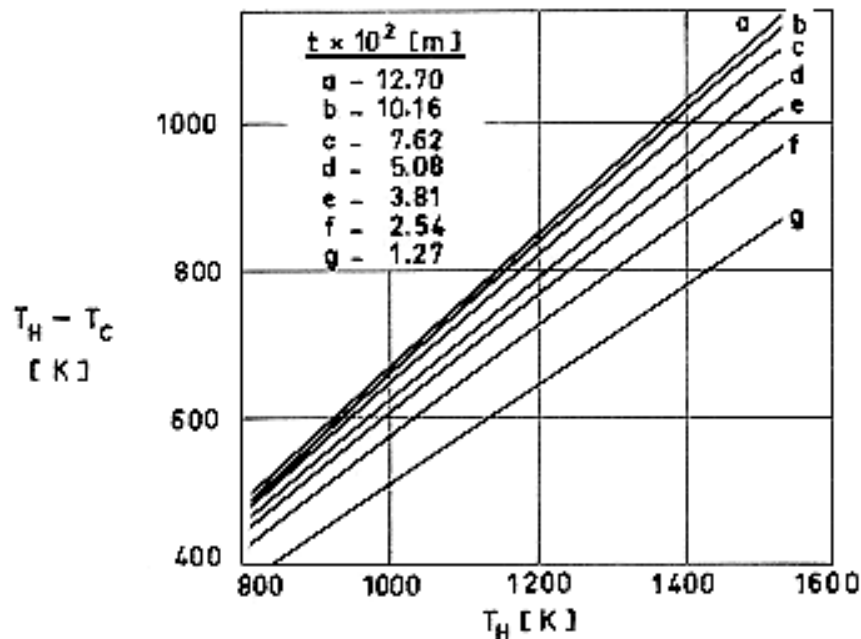
Note: non-si units are used in this figure

Figure 5-7: Temperature differential, T_H–T_C, vs. mean temperature of the hot face, T_H for different values of the insulation thickness, t. Fiberfrax washed fiber, $\rho = 96$ kg.m^{-3}.

5.3   Blankets and felts

MANUFACTURER	BABCOCK & WILCOX		CARBORUNDUM		
TRADE NAME	**KAOWOOL**		**FIBERFRAX**		
NATURE	**ALUMINA-SILICA**		**ALUMINA-SILICA**		
FORM	Blanket, made from B&W Kaowool Ceramic Fibers	High Purity Blanket, made from B&W Kaowool High Purity Fibers	Lo-Con Blanket and Felt, made from Fiberfrax Bulk Ceramic Fibers	PH Blanket, made from Fiberfrax Long Staple Fine or Long Staple Coarse Fibers.	H Blanket and Felt, made from Fiberfrax H Bulk
PHYSICAL PROPERTIES	Table 4-10Table 4-11				
Color	White		White	Tan	White (Felt Tan)
Sound Absorption Coefficient	Figure 5-8		Figure 5-9	Figure 5-9	
Binder Content	No		Small in Felt	3-5%	up to 3% in Felt
Air Permeability	Figure 5-10		Figure 5-11	Figure 5-11	
Dielectric Strength [V.m^{-1}]			$3{,}3 \times 10^{6}$		
OPERATING TEMP. Continuous [K]	1533		1533	1533	1700
MELTING POINT [K]	2033		2066,5	2066,5	2200

THERMAL PROPERTIES Specific Heat, c [J.kg^{-1}.K^{-1}]	1067 [a]		1130 [b]		
Thermal Conductivity, k [W.m^{-1}.K^{-1}]	Figure 5-12		Figure 5-13		Figure 5-13
Temperature Differential [K]			Figure 5-14, Figure 5-15		
MECHANICAL PROP. Compression Resistance					
Linear Shrinkage vs. Temp.					
CHEMICAL COMPOSITION	Same as B&W Kaowool Ceramic Fiber	Same as B&W Kaowool High Purity Fiber	Same as Fiberfrax Bulk Ceramic Fiber	Same as Fiberfrax Long Staple Fiber	Same as Fiberfrax H Bulk
CHEMICAL DEGRADATION	Excellent resistance to chemical attack. Exceptions are phosphoric and Hydrofluoric acids and strong alkalies. Unaffected by oil. Thermal and physical properties are restored after drying.		These blankets and felts resists attack from most corrosive agents. Exceptions are hydrofluoric and phosphoric acids and concentrated alkalies. Also resist oxidation and reduction. If wet by steam or oil, thermal and physical properties are restored upon drying. No water of combination is present.		
MOISTURE ABSORPTION	Unaffected by water		Unaffected by water		
OUTGASSING					
AVAILABILITY	Available in nominal densities of 48, 64, 96 and 128 kg.m^{-3} Roll sizes: Width: 0,61 and 1,22 m		See Table 5-2	Roll sizes Thickness tx10^{2}m: 1,27 and 0,635 Width: 1,22 m	Roll sizes Thickness tx10^{2}m: 2,54, 1,27 and 0,635 Width: 0,3, 0,61 and

			Length: 15,24 and 7,62 m Density: 96 kg.m^{-3}	1,22 m Length: 7,62 m Density: 96 kg.m^{-3}
	Length: 7,31 m For thickness see Table 5-1			
APPROXIMATE COST	6,5 US $.kg^{-1}F.O.B.			
APPLICATIONS	High temperature insulation: Furnace linings. Gas turbines. Fans. Boiler combustion chambers and heat exchangers, oil fired. Catalytic mufflers and automotive afterburners. Laboratory ovens. Steam valves of headers and steam separators. Thin walls kilns-back up. Water and steam tubes-back up. Acoustical service for missiles and jet aircraft. Cryogenic vessel fire protection. High temperature filters. Superheater seals. Etc.	LO-CON Blanket: Furnace insulation, firewall protection, insulation for stress relieving welds, skid rail insulation, ingot cover insulation, titanium and beryllium hot forming insulation, heating element support bases, refractory back-up insulation, catalytic combustion surfaces, furnace base seals and high temperature filtration media. LO-CON Felts: Furnace, kiln and boiler linings, gas turbine silencer and muffler insulation, thermal reactor insulation, high temperature gaskets and expansion joint seals, etc. PH Blanket: Insulation for gas turbine and jet engines, high temperature acoustical insulation, diffusion medium for fluidized beds, etc.		

[a]   At 1255,5 K Mean Temperature.

[b]   At 1366,5 K Mean Temperature.

NOTE   From manufacturer's bulletins

MANUFACTURER	JOHNS-MANVILLE				
TRADE NAME	THERMOFLEX	MICRO-QUARTZ	DYNA-QUARTZ	MICROLITE AA & B	MICROLITE AA & B
NATURE	ALUMINA-SILICA	SILICA	SILICA	BOROSILICATE	
FORM	Felt	Felt, made from 98,5% pure silica fibers. Also in bulk form	Lightweight, semi-rigid tiles. Specially heat treated Micro-Quartz	Standard Blanket and Felt bonded with a phenolic resin.	Silicone Binder Blanket and Felt bonded with a high temperature silicone binder.
PHYSICAL PROPERTIES					
Color					
Sound Absorption Coefficient				Figure 5-16	
Binder Content	Small	No	No	Yes (Details not given)	
Air Permeability					
Dielectric Strength [V.m^{-1}]					
OPERATING TEMP. Continuous [K]	1366,5	1366,5	1783	477	677

MELTING POINT [K]				
THERMAL PROPERTIES Specific Heat, c [J.kg^{-1}.K^{-1}]	Figure 5-23	Figure 5-23	Figure 5-17	
Thermal Conductivity, k [W.m^{-1}.K^{-1}]	Table 5-3	Figure 5-18	Figure 5-19	Figure 5-20
Temperature Differential [K]				
MECHANICAL PROP. Compression Resistance			Figure 5-21	
Linear Shrinkage vs. Temp.			Less than 1% [a]	
CHEMICAL COMPOSITION		SiO$_2$ 98,50 minimum B 0,01 maximum Fe 0,06 maximum Al$_2$O$_3$ 0,50 maximum CaO 0,35 maximum MgO 0,35 maximum Na$_2$O 0,15 maximum		
CHEMICAL DEGRADATION	Non-alkaline, contains no sulphur.	Incombustible and resistant to most acids.		Incombustible and non-corrosive (has no effect on aluminium or steel). Non cellular and non-hygroscopic.

	Thermoflex will not cause nor accelerate corrosion.	Micro-Quartz will not cause nor accelerate corrosion.					
MOISTURE ABSORPTION		Unaffected by moisture		Absorbs less than 3% by weight after exposure to 95% RH at 333 K for 96 hours.			
OUTGASSING		Figure 5-22					
AVAILABILITY	Width: 1,06 m Length (sheets) 1,22 and 2,44 m Length (rolls) 7,31 m Thickness and Density: Table 5-4	Sheet width: 0,914 m Sheet length: 1,52 and 3,04 m Thickness and Density: Table 5-5	Width: 0,304 m Length: 0,354 m Thickness: tx10^2 [m]: 0,63, 1,27, 2,54, 3,81, 5,08, 6,35 and 7,62 Density: 67, 99 and 128 kg.m^{-3}	Width: 0,61, 0,91 and 1,82 m Roll length: 30,48 m			

Thickness tx10^2 [m]	Density kg.m^{-3}	
	Type "AA"	Type"B"
0,95 1,27 2,54	24 9,6, 16 9,6	9,6, 16 8, 16

APPROXIMATE COST	
APPLICATIONS	THERMOFLEX: Aircraft jet engine insulations. High flexibility and compressibility make Thermoflex an ideal insulation filler in complicated metallic enclosures fabricated from heat-resistant alloys. MICRO-QUARTZ: Thermal insulation for aircraft, missiles, spacecraft and special industrial applications. It is also designed to provide reinforcement for high-temperature plastic such as exhaust nozzles, nose cones and aerodynamically heated surfaces. MICROLITE: Thermal and acoustical insulation for aircraft. "AA" is used for applications requiring an insulation with superior thermal and acoustical properties. "B" is for less critical applications permitting the use of a more economical insulation.

[a] After 24 h soak at 1783 K.

NOTE   From manufacturer's bulletins

MANUFACTURER	JOHNS-MANVILLE			
TRADE NAME	**MIN-K 1301**	**MIN-K 2000**	**UNBONDED B-FIBER**	**MICRO-FIBER "E"**
NATURE	SILICA		BOROSILACATE	
FORM	Standard Type Blanket of Min-K faced on both sides with No. 116 glass fabric.	High Temperature Blanket on Min-K faced on both sides with high silica fabric.	Batt or Blanket consists of flame-blown glass fibers loosely felted.	Felt, made by water disposition of fine glass fibers.
PHYSICAL PROPERTIES				
Color				
Sound Absorption Coefficient				
Binder Content				No
Air Permeability				
Dielectric Strength [V.m^{-1}]				
OPERATING TEMP. Continuous [K]	1255		728	922
MELTING POINT [K]				
THERMAL PROPERTIES	Figure 5-23	Figure 5-23		

Specific Heat, c [J.kg^{-1}.K^{-1}]				
Thermal Conductivity, k [W.m^{-1}.K^{-1}]	Figure 5-24 to Figure 5-26	Figure 5-27 to Figure 5-29	Figure 5-30	Figure 5-31
Temperature Differential [K]				
MECHANICAL PROP. Compression Resistance	Figure 5-32	Figure 5-33		
Linear Shrinkage vs. Temp.				
CHEMICAL COMPOSITION				
CHEMICAL DEGRADATION			Under normal use Unbonded B-Fiber will not cause nor accelerate corrosion	Under normal use Micro-Fiber "E" will not cause nor accelerate corrosion
MOISTURE ABSORPTION				
OUTGASSING				
AVAILABILITY	Table 5-6	Table 5-7	Roll sizes: Length: 30,48 m Width: 0,914 m	Sheet Length: 1,52 and 3,05 m Width: 0,914 m Thickness: 4,7x10^{-3} and

			Thickness: $6,35 \times 10^{-3}$ m Density: 24 and 48 kg.m^{-3}	$12,7 \times 10^{-3}$ m Density: 64 and 80 kg.m^{-3}
APPROXIMATE COST				
APPLICATIONS	MIN-K: Insulation for operational missiles, aircraft and spacecraft. Flexible Min-K blankets lend themselves to bonding, lamination with plastics, service coatings, and as insulation system components. Gemini spacecraft walls were insulated with Min-K. UNBONDED B-FIBER: Used by manufacturers as a source of basic glass fibers for other products and processes. It may be used as a back-up or cold face insulation as in thermal fabrications for jet aircraft engines. MICRO-FIBER: Thermal insulation, and air and gas filtration in the medium temperature range.			

NOTE   From manufacturer's bulletins.
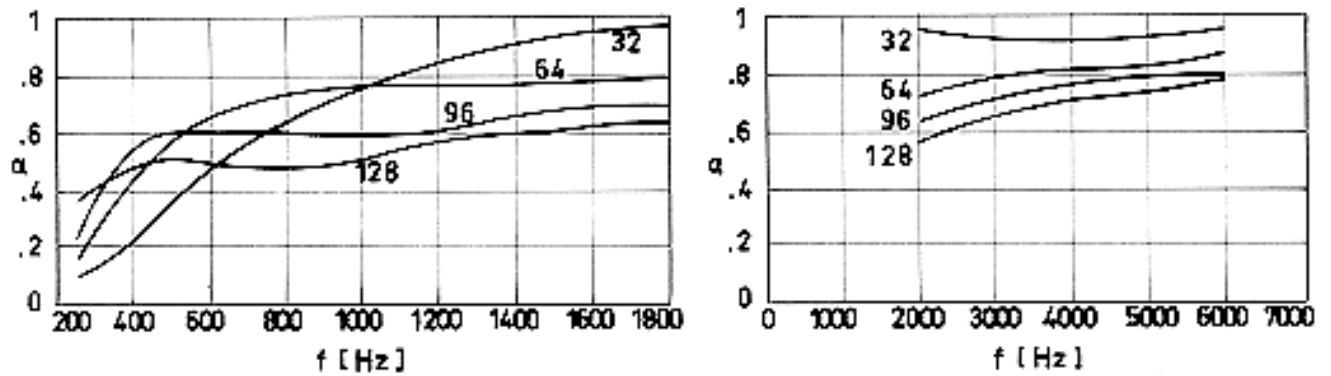
Note: non-si units are used in this figure

Figure 5-8: Sound absorption coefficient, α, as a function of frequency, f, for B & W Kaowool blanket 2,54x10⁻² m thick.

Numbers on curves indicate blanket densities in kg.m⁻³.
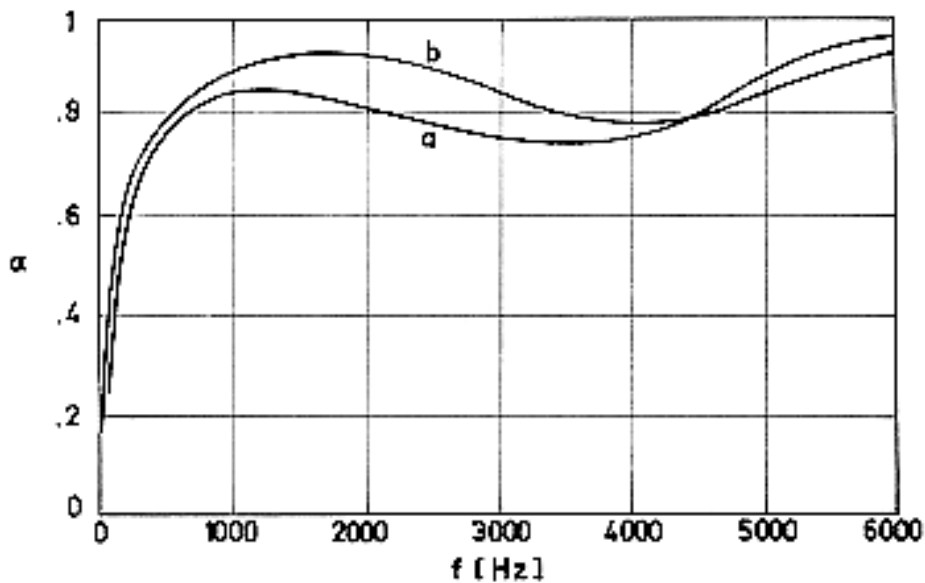
Note: non-si units are used in this figure

Figure 5-9: Sound absorption coefficient, α, as a function of frequency, f, for the following Fiberfrax products:

a Lo-Con blanket and felt. t = 2,54x10⁻² m. ρ = 96 kg.m⁻³.
b PH Fine blanket. t = 2,54x10⁻² m. ρ = 96 kg.m⁻³.
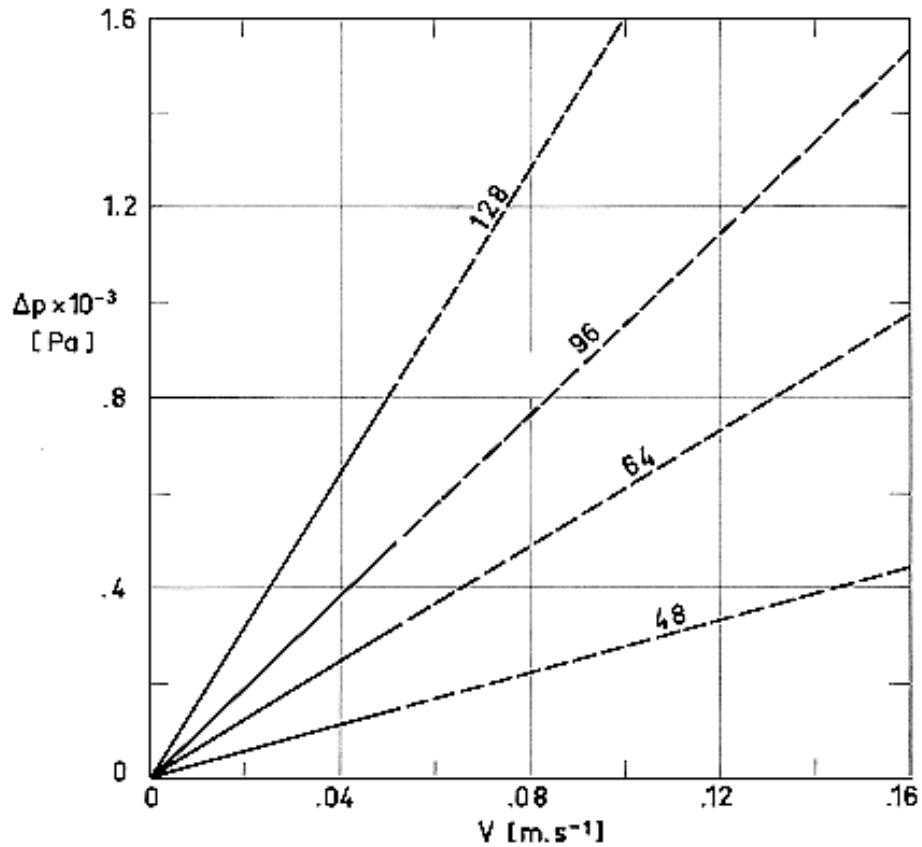
Figure 5-10: Air permeability across B & W Kaowool blankets

Expressed as the variation of pressure drop, Δp, with the volume flow rate per unit area, V. Tests made under standard conditions and temperature. Numbers on curves indicate blanket densities in $kg.m^{-3}$.

Note: non-si units are used in this figure
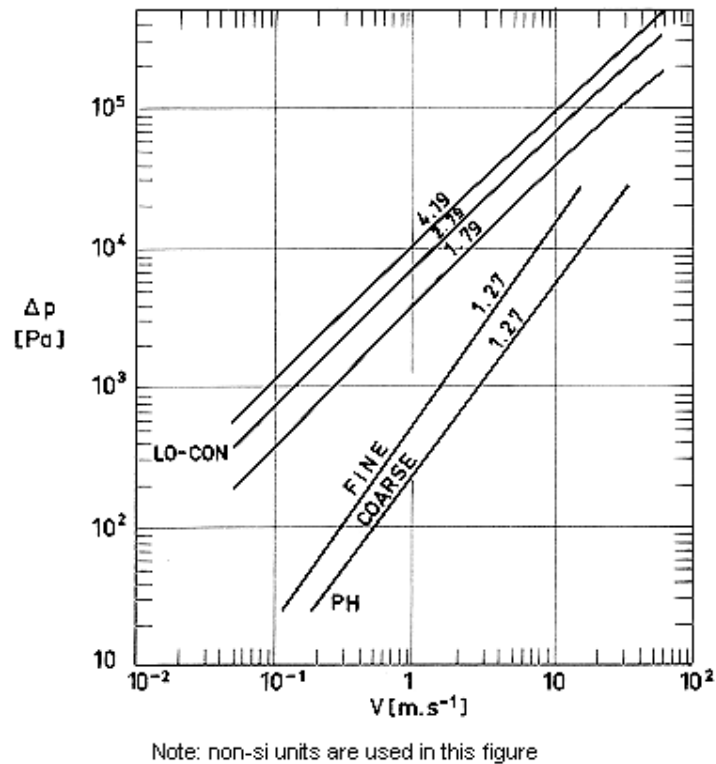
Figure 5-11: Air permeability across Carborundum Fiberfrax blankets

Expressed as the variation of pressure drop, Δp, with the volume flow rate per unit area, V. Tests made under standard conditions and temperature. The density of the blankets is, in any case, $\rho = 96$ kg.m^{-3}. Numbers on curves give the thickness, $t\times10^2$, measured in m.

Note: non-si units are used in this figure
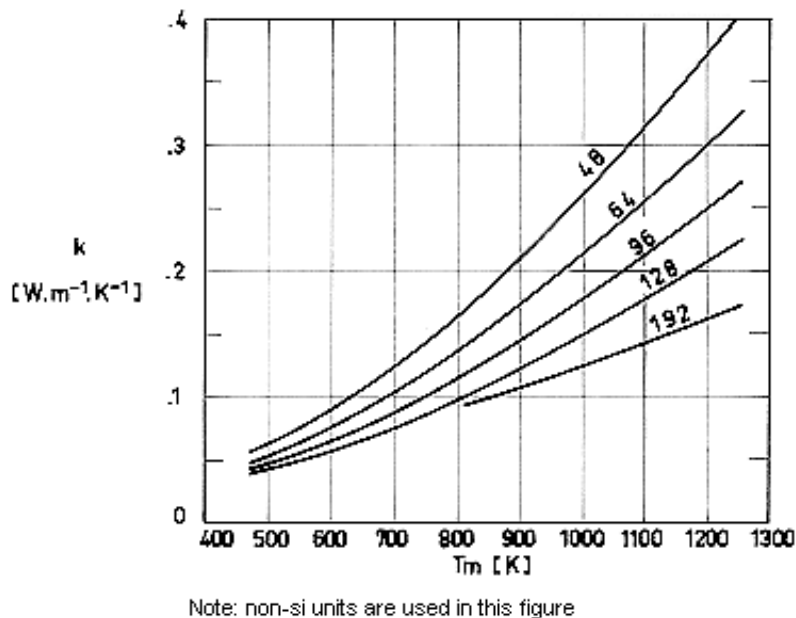
Figure 5-12: Thermal conductivity, k, of B & Kaowool blankets vs. mean temperature, T_m.

Numbers on curves indicate blanket densities in kg.m^{-3}.
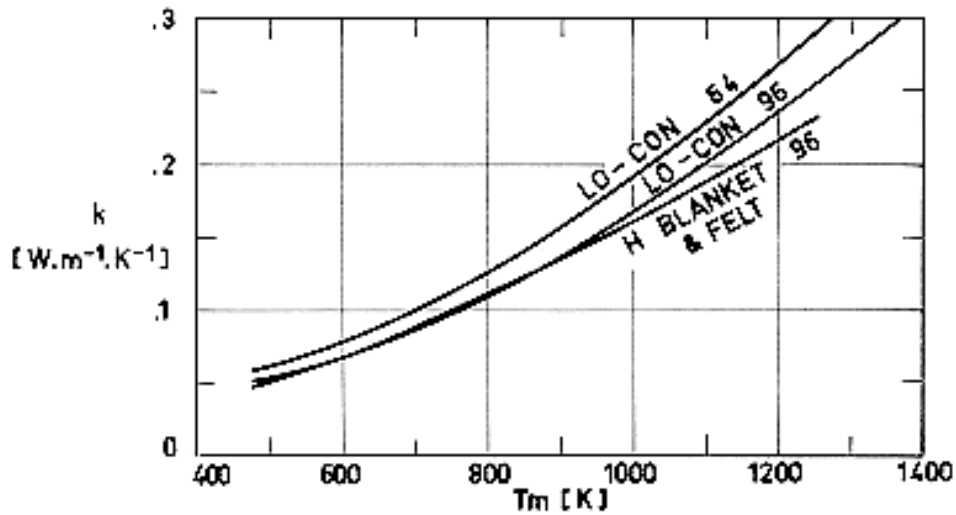
Note: non-si units are used in this figure

Figure 5-13: Thermal conductivity, *k*, of Fiberfrax blankets vs. mean temperature, *Tₘ*.

Numbers on curves indicate blanket densities in kg.m⁻³.
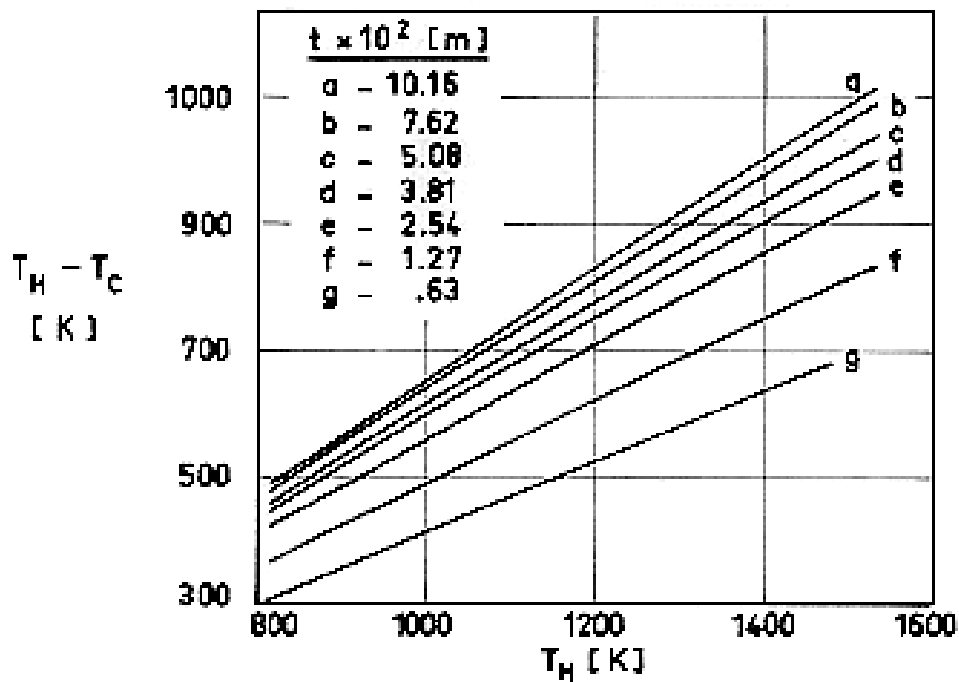
Note: non-si units are used in this figure

Figure 5-14: Temperature differential, *Tₕ–Tᴄ*, vs. temperature of the hot face *Tₕ* for different values of the blanket thickness, *t*. Fiberfrax Lo-Con Blanket & felt, $\rho = 64$ kg.m⁻³.
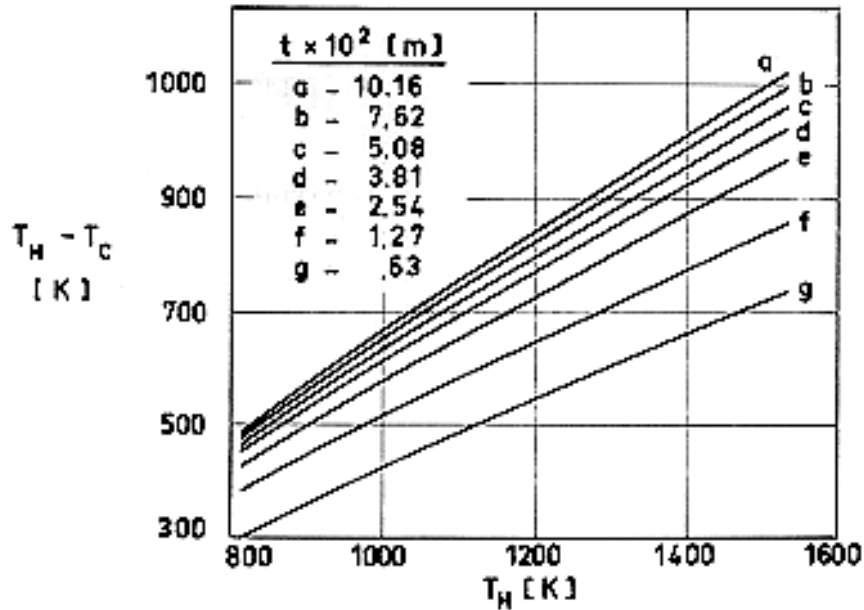
Note: non-si units are used in this figure

Figure 5-15: Temperature differential, T_H–T_C, vs. temperature of the hot face, T_H,

for different values of the blanket thickness, t. Fiberfrax Lo-Con Blanket & felt, $\rho = 96$ kg.m^{-3}.

Table 5-1: Available Densities, ρ, and Thicknesses, t, of B & W Kaowool Blanket. X denotes available.

ρ [kg.m^{-3}]				tx10^3 [m]
48	**64**	**96**	**128**	
-	-	X	X	6,35
X	X	X	X	12,70
X	X	X	X	25,40
X	X	X	X	38,10
X	X	-	-	50,80

Table 5-2: Available Thicknesses, *t*, and Lengths, *L*, of Fiberfrax Lo-Con Blanket and Felt for densities of64 kg.m⁻³ and 96 kg.m⁻³ and roll widths 0,3 m, 0,61 m, and 1,22 m.

tx10³ [m]	6,35	9,56	12,70	19,12	25,40	31,75	38,10
L [m]	15,24	7,62	7,62	3,81	3,81	1,83	1,83

Note: non-si units are used in this figure

Figure 5-16: Sound absorption coefficient, α, as a function of frequency, f, for J-M Microlite Standard and Silicone Binder.

Numbers on curves indicate the blanket thickness, tx10², measured in m.

Note: non-si units are used in this figure

Figure 5-17: Calculated specific heat, *c*, as a function of temperature, *T*, for J.M Dyna-Quartz

Table 5-3: Thermal Conductivity, k, [W.m⁻¹.K⁻¹], of J-M Thermoflex Felt for different values of Density, ρ, [kg.m⁻³], and Mean Temperature, T_m, [K].

ρ / T_m	48	64	96	128	160	192	224	256	288	320	352	384
422	0,058	0,055	0,052	0,049	0,048	0,050	0,052	0,053	0,055	0,056	0,056	0,056
477,5	0,069	0,063	0,059	0,056	0,055	0,055	0,056	0,056	0,058	0,059	0,059	0,061
533	0,082	0,075	0,068	0,065	0,062	0,061	0,061	0,061	0,061	0,062	0,063	0,065
588,5	0,098	0,088	0,078	0,073	0,071	0,066	0,066	0,065	0,065	0,066	0,066	0,069
644,5	0,115	0,102	0,089	0,082	0,079	0,071	0,071	0,071	0,071	0,071	0,072	0,073
700	0,134	0,118	0,100	0,092	0,088	0,078	0,076	0,076	0,076	0,076	0,076	0,078
755,5	0,156	0,135	0,114	0,104	0,098	0,085	0,082	0,082	0,081	0,081	0,082	0,082
811	0,180	0,154	0,128	0,117	0,109	0,094	0,091	0,089	0,088	0,088	0,088	0,088
866,5	-	-	0,146	0,130	0,121	0,102	0,099	0,097	0,095	0,095	0,094	0,094
922	-	-	0,164	0,146	0,134	0,112	0,108	0,105	0,104	0,102	0,100	0,100
977,5	-	-	-	-	-	0,123	0,117	0,114	0,111	0,109	0,108	0,108
1033	-	-	-	-	-	0,134	0,128	0,124	0,121	0,118	0,117	0,115
1088,5	-	-	-	-	-	0,146	0,138	0,133	0,128	0,125	0,124	0,123
1144,5	-	-	-	-	-	0,159	0,151	0,144	0,138	0,135	0,133	0,131
1200	-	-	-	-	-	0,174	0,163	0,156	0,148	0,144	0,141	0,140
1255,5	-	-	-	-	-	0,190	0,177	0,167	0,159	0,154	0,151	0,148

Accuracy: ± 6% based on the precision of measurement and the variability of thickness.

Temperatures: T_H = T_m+366,5; T_C = T_m−366,5.
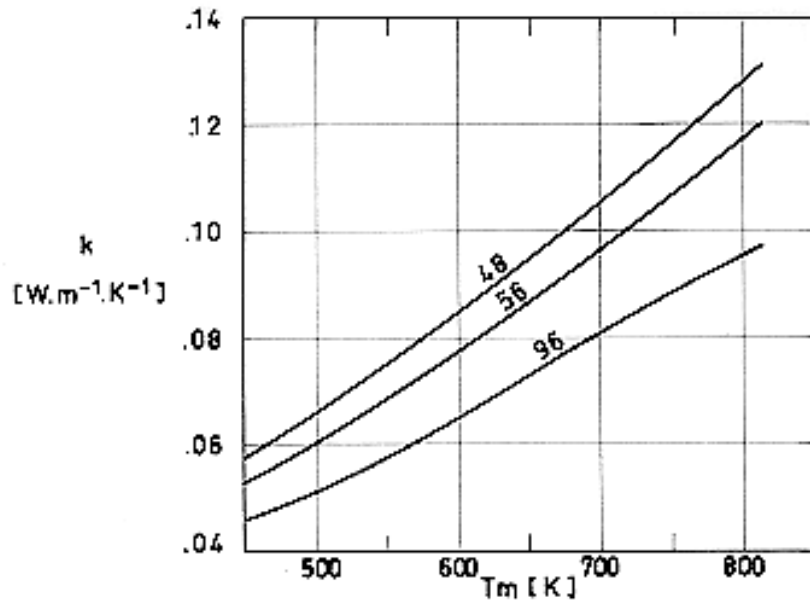
Note: non-si units are used in this figure

Figure 5-18: Thermal conductivity, *k*, of J-M Micro-Quartz felt vs. mean temperature, *Tm*.

Numbers on curves indicate the density in kg.m⁻³.
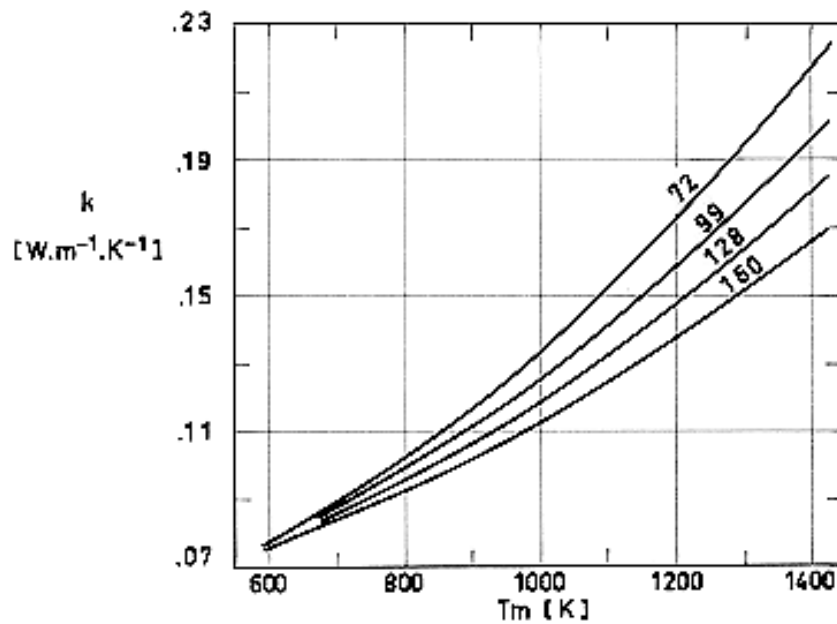
Note: non-si units are used in this figure

Figure 5-19: Thermal conductivity, *k*, of J-M Dyna-Quartz vs. mean temperature, *Tm*.

Numbers on curves indicate the density in kg.m⁻³.
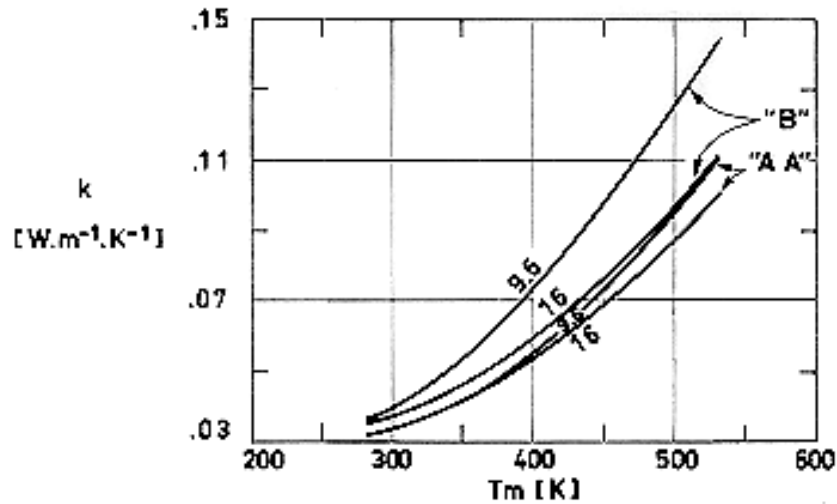
Note: non-si units are used in this figure

Figure 5-20: Thermal conductivity, *k*, of J-M Microlite "AA" and "B" vs. mean temperature, *T*$_m$.

Numbers on curves indicate the density in kg.m^{-3}.
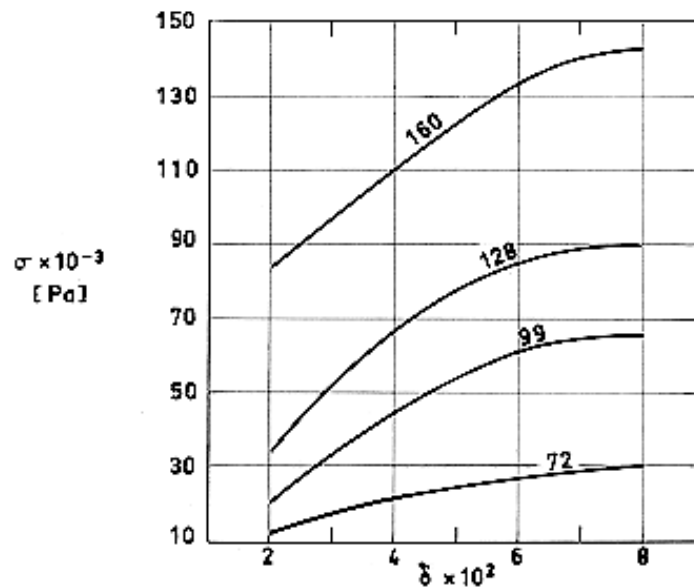
Figure 5-21: Compressive stress, σ, vs. compressive strain, δ, for J-M Dyna-Quartz.

Numbers on curves indicate the density in kg.m^{-3}.
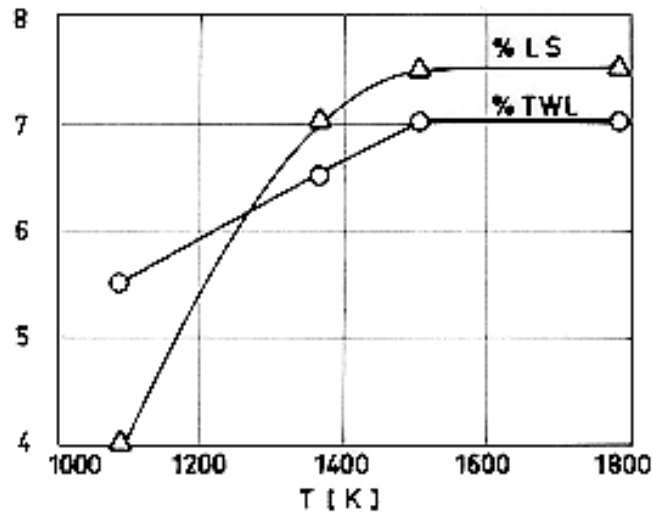
Figure 5-22: Linear Shrinkage, *LS*, and Total Weight Loss, *TWL*, of J-M Micro-Quartz Felt as a function of temperature, *T*.

Table 5-4: Available Densities, ρ, [kg.m^{-3}], and Thicknesses, tx10^3 [m], of J-M Thermoflex.

tx10$_3$ ρ	3,18	4,76	6,35	9,54	12,70	10,05	25,40	38,10	50,80
48	-	-	-	A	A	A	A	B	B
64	-	-	A	A	A	A	A	B	-
96	-	-	A	A	A	A	B	B	-
128	B	B	A	A	A	A	B	-	-
160	B	B	B	B	B	B	B	-	-
192	B	B	B	B	B	B	B	-	-
224	B	B	B	B	B	B	-	-	-
288	B	B	B	B	B	-	-	-	-
384	B	B	B	B	B	-	-	-	-

NOTE A   Sheets 1,22 m and 2,44 m length, or rolls 7,31 m length. Oven cured; can be recognized by the color and the imprint of the oven screen or conveyor flights on the surface.

NOTE B   Sheets 1,22 m and 2,44 m length. Hot press cured; can be recognized by the gray-green color and the smooth surface resulting from the press platens.
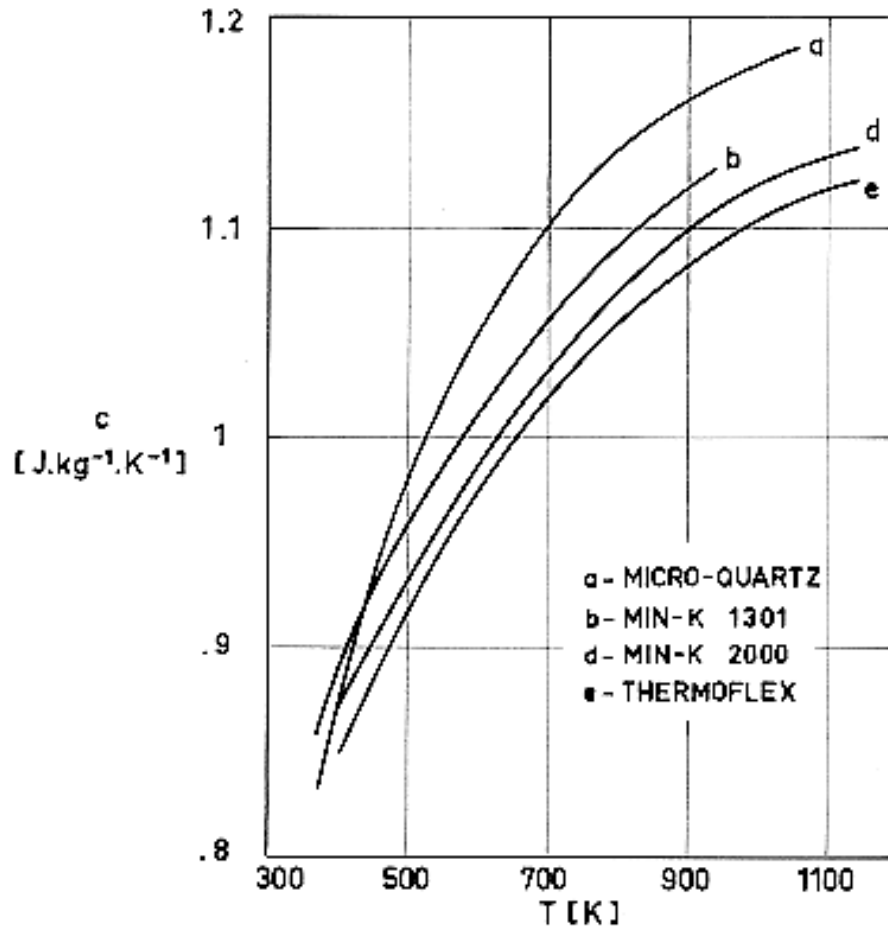
Note: non-si units are used in this figure

Figure 5-23: Calculated specific heat, *c*, as a function of temperature, *T*, for several J-M insulations.

Table 5-5: Available Densities, ρ, and Thicknesses, *t*, of J-M Micro-Quartz

ρ [kg.m⁻³]	tx10³ [m]
48	4,76
56	12,70
96	4,76
96	12,70
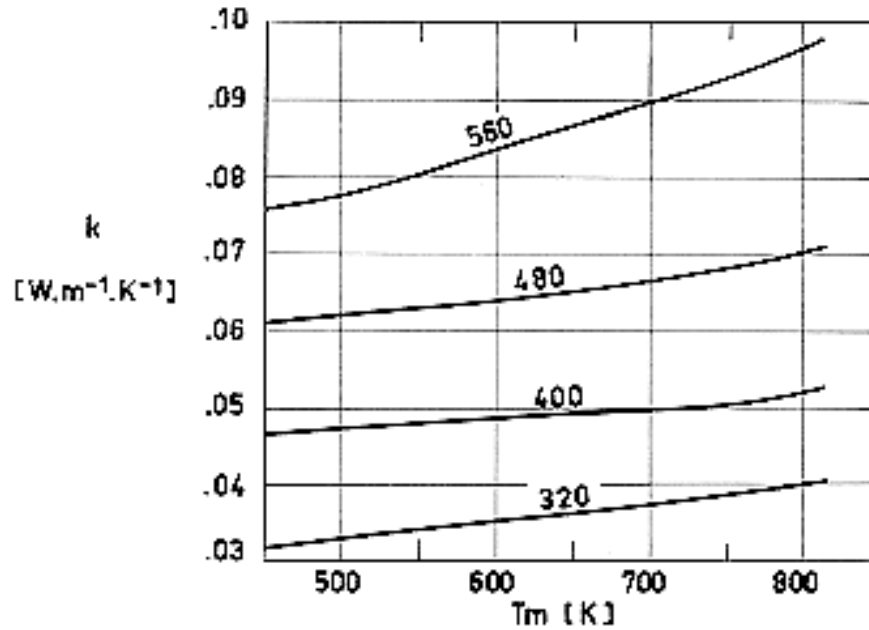
Figure 5-24: Thermal conductivity, *k*, of J-M Min-K 1301 vs. mean temperature, T_m. Numbers on curves indicate the density in kg.m⁻³.
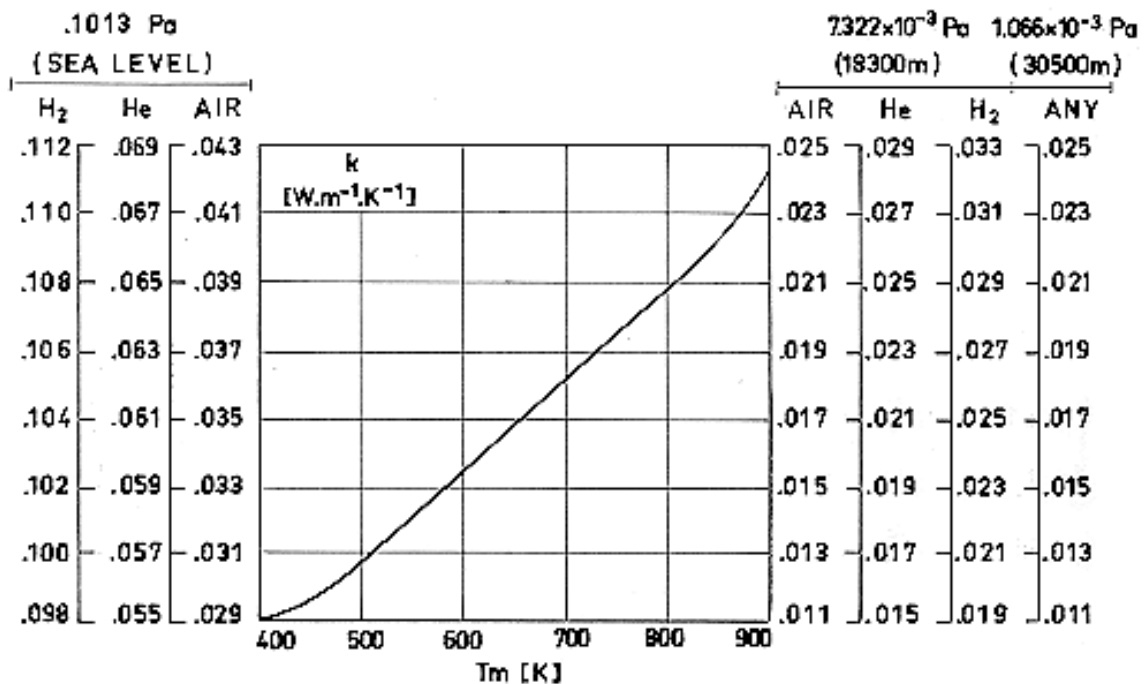
Figure 5-25: Influence of ambient pressure on the variation of thermal conductivity, *k*, of J-M Min-K 1301 vs. mean temperature, T_m, for several filling gases.
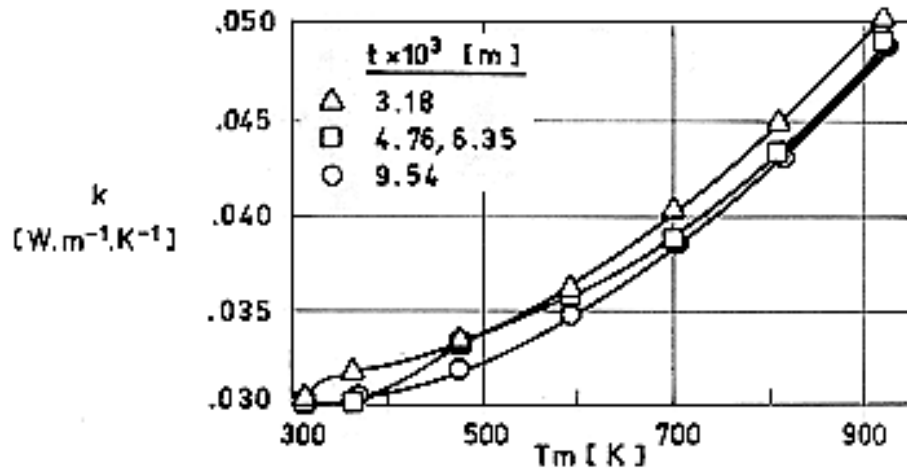
Note: non-si units are used in this figure

Figure 5-26: Thermal conductivity, *k*, of J-M Min-K 1301 vs. mean temperature, T_m, for different values of thickness, *t*.
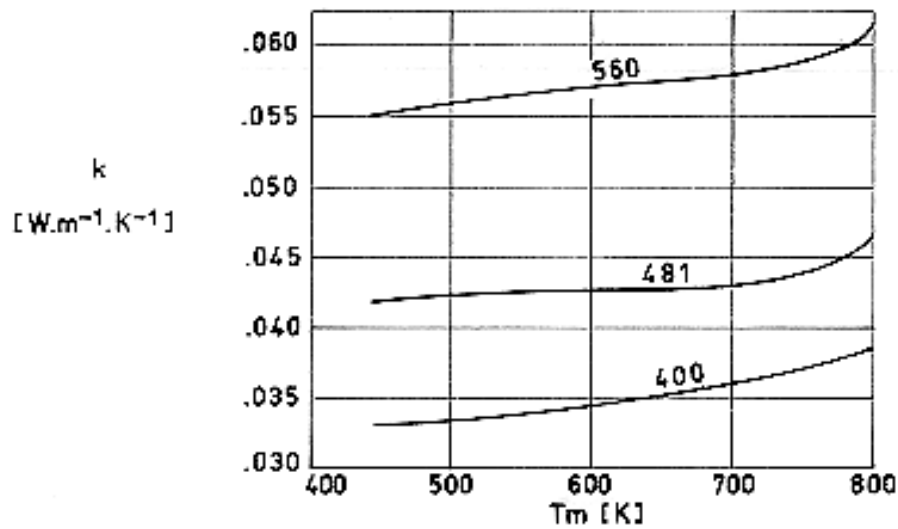
Note: non-si units are used in this figure

Figure 5-27: Thermal conductivity, *k*, of J-M Min-K 2000 vs. mean temperature, T_m.
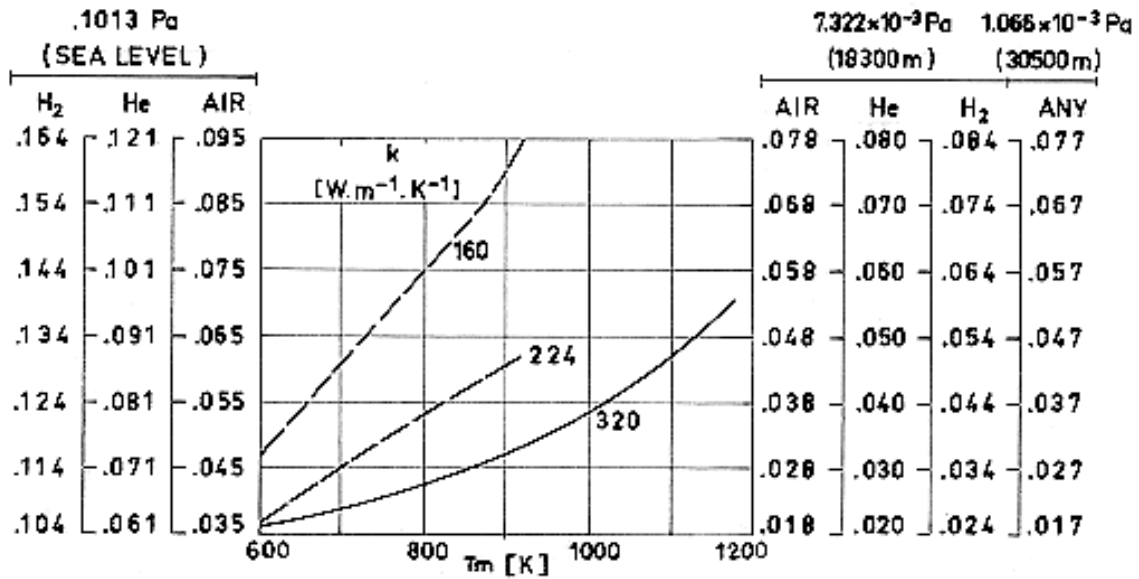
Numbers on curves indicate the density in kg.m^{-3}.

Figure 5-28: Influence of ambient pressure on the variation of thermal conductivity, *k*, of J-M Min-K 2000 vs. mean temperature, T_m, for several filling gases.

Numbers on curves indicate the density in kg.m^{-3}.
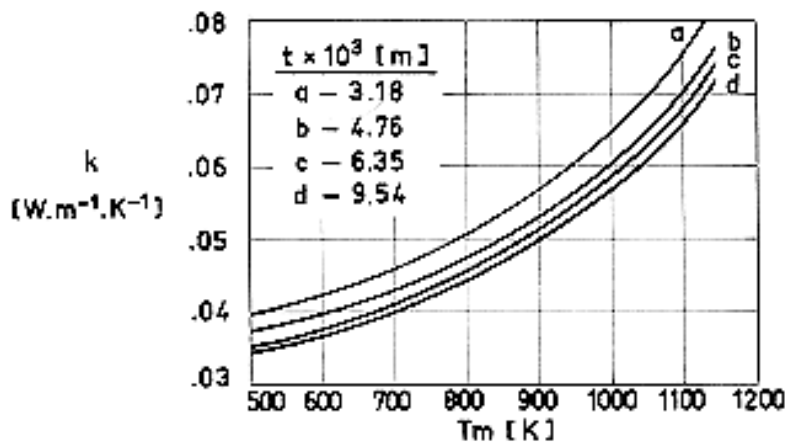
Figure 5-29: Thermal conductivity, *k*, of J-M Min-K 2000 vs. mean temperature, T_m, for different values of thickness, *t*.

The thermal conductivities are average for the composite insulation.
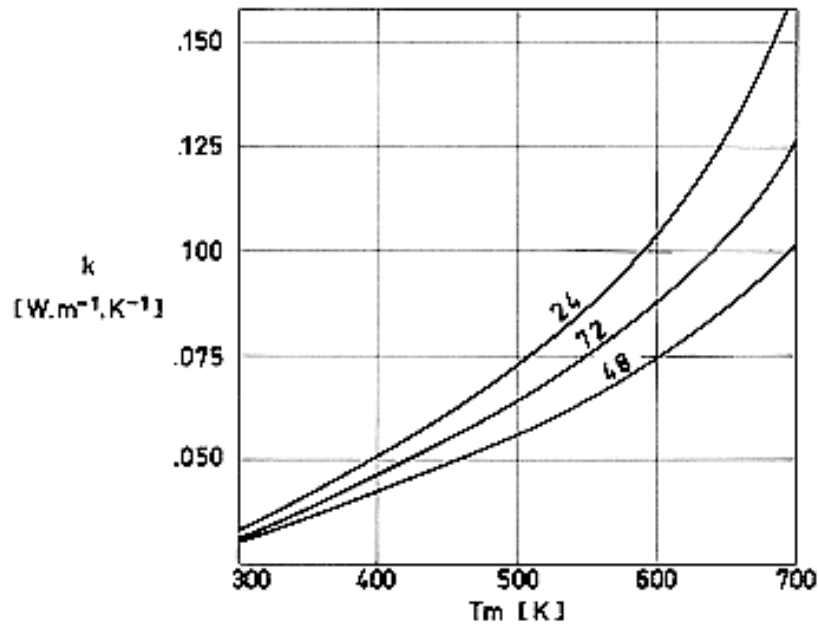
Note: non-si units are used in this figure

Figure 5-30: Thermal conductivity, *k*, of J-M unbounded B-Fiber batt vs. mean temperature, *Tm*.

Numbers on curves indicate the density in kg.m^{-3}.
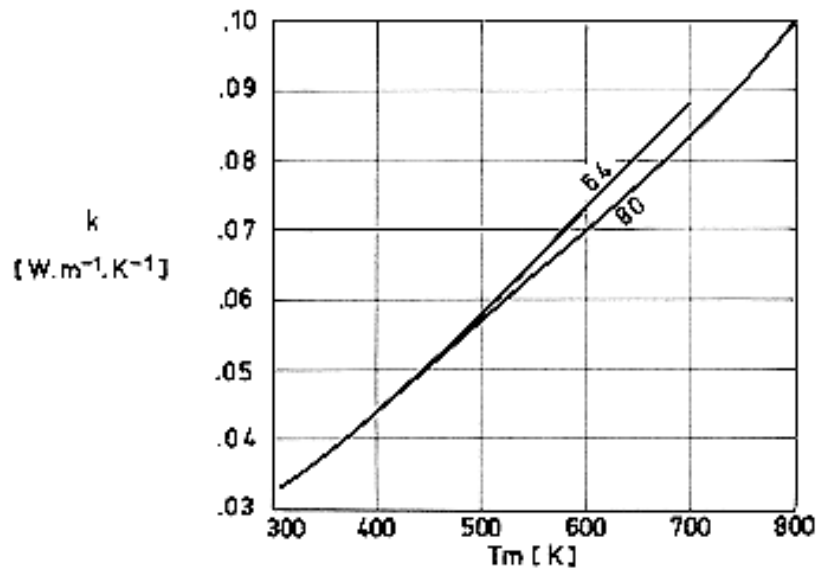
Note: non-si units are used in this figure

Figure 5-31: Thermal conductivity, *k*, of J-M Micro-Fibers felt Type "E" vs. mean temperature, *Tm*.

Numbers on curves indicate the density in kg.m^{-3}.
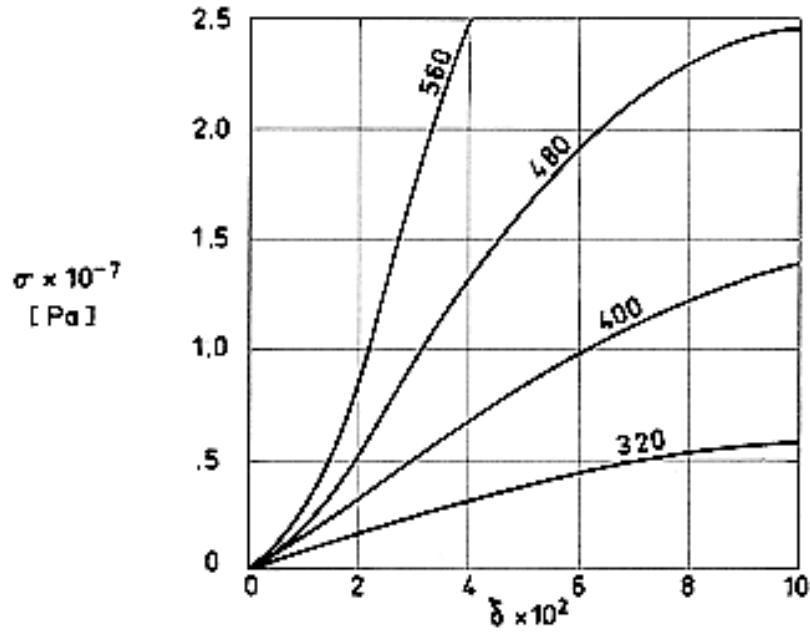
Note: non-si units are used in this figure

Figure 5-32: Compressive stress, σ, vs. compressive strain, δ, for J-M Min-K 1301. Numbers on curves indicate the density in kg.m^{-3}.
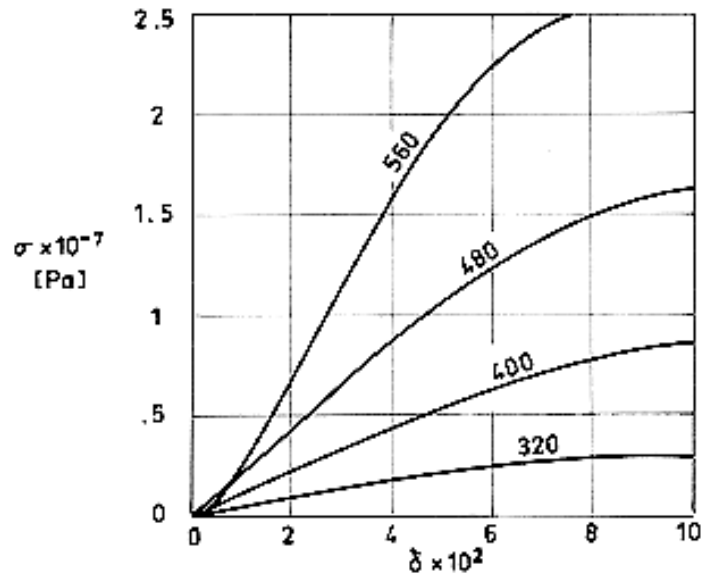
Note: non-si units are used in this figure

Figure 5-33: Compressive stress, σ, vs. compressive strain, δ, for J-M Min-K 2000.

Numbers on curves indicate the density in kg.m^{-3}.

Table 5-6: Available Forms of J-M Min-K 1301

Type	Width [m]	Length [m]	tx10^3 [m]	Mass/Area [kg.m^{-2}]
SS	0,914	0,914	3,18	1,02
SS	0,914	0,914	4,76	1,42
SS	0,914	0,914	6,35	1,85
SS	0,914	0,914	9,54	2,64
SP	0,914	1,828	4,76	1,42
SP	0,914	1,828	6,35	1,81
SP	0,914	1,828	9,54	2,64

Table 5-7: Available Forms of J-M Min-K 2000

Type	Width [m]	Length [m]	tx10^3 [m]	Mass/Area [kg.m^{-2}]
SS	0,762	0,762	3,18	1,61
SS	0,762	0,762	4,76	2,05
SS	0,762	0,762	6,35	2,44
SS	0,762	0,762	9,54	3,27
SP	0,762	1,828	4,76	2,00
SP	0,762	1,828	6,35	2,39
SP	0,762	1,828	9,54	3,22

NOTE   SS: Stitched in 2,54x10^{-2} m square.
SP: Stitched in 2,54x10^{-2} m parallel patterns.

5.4   Papers

MANUFACTURER	BABCOCK & WILCOX	CARBORUNDUM			
TRADE NAME	KAOWOOL PAPER	FIBERFRAX PAPER			
NATURE	ALUMINA-SILICA	ALUMINA-SILICA			
FORM	Paper, made from B&W Kaowool Ceramic Fibers	970 Paper, made from Fiberfrax Washed Fibers	H880 Paper, made from Fiberfrax H Washed Fibers	Hi-Fi 660 Paper made from Fiberfrax Hi-Fi Fibers	550 Paper
PHYSICAL PROPERTIES					

Color	White	White	White	White	Light Blue [a]
Binder Content	Amount not given	Table 5-9		Table 5-11	5% approx.
Density, ρ [kg.m^{-3}]	192-208	160-192	192	192	192-224
OPERATING TEMP. Continuous [K]	Up to 1533	1533	1700	1533	1533
MELTING POINT [K]	Above 1972	2066,5	Above 2200	Above 2033	2033
THERMAL PROPERTIES Specific Heat, c [J.kg^{-1}.K^{-1}]					
Thermal Conductivity, k [W.m^{-1}.K^{-1}]	Figure 5-34	Figure 5-34	Same as 970 Paper	Figure 5-34	20% higher than 970 Paper
Temperature Differential [K]		Figure 5-35		Figure 5-36	
Thermal Reflectance, ρ		Figure 5-37			
MECHANICAL PROP.					
CHEMICAL COMPOSITION	Same as B&W Kaowool Ceramic Fibers	Same as Fiberfrax Washed Fibers	Al_2O_3 62% SiO_2 38%	Same as Fiberfrax Washed Fibers	Al_2O_3 51,7% SiO_2 47,6%
CHEMICAL DEGRADATION	Papers exhibit good chemical stability with resistance to most chemicals, with the exception of hydrofluoric and phosphoric acids and strong alkalies. No water of combination.				
MOISTURE ABSORPTION	Unaffected by water				
OUTGASSING					

MANUFACTURER	BABCOCK & WILCOX		CARBORUNDUM	
TRADE NAME	**KAOWOOL PAPER**		**FIBERFRAX PAPER**	
NATURE	**ALUMINA-SILICA**		**ALUMINA-SILICA**	
FORM	Paper, made from B&W Kaowool Ceramic Fibers	970 Paper, made from Fiberfrax Washed Fibers	H880 Paper, made from Fiberfrax H Washed Fibers	Hi-Fi 660 Paper made from Fiberfrax Hi-Fi Fibers	550 Paper
AVAILABILITY	Table 5-8	Table 5-9, Table 5-10	Width: 0,305 and 0,61 m. Roll weight: 4,53 and 11,34 kg. Thickness: Table 5-11	Width: 0,305 and 0,61 m. Roll weight: 4,53 and 11,34 kg. Thickness: Table 5-11	Width: 0,305 and 0,6 and 1,22 m. Roll weight: 4,53 and 11,34 kg. Thickness: Table 5-11
APPROXIMATE COST					
APPLICATIONS	KAOWOOL PAPER: Aluminium & zinc launder and trough linings. Gasketing between aluminium & zinc trough sections. Aluminium furnace tap-out plug cover and parting agent. Aluminium distributor pan linings. Super Alloy Ingot mold and hot tops. FIBERFRAX 970 PAPER: High temperature gaskets. Thermal and electrical insulation. Combustion chamber liners. Back-up linings for metal troughs. Hot top linings. Tape hole plug covers. Ingot mold linings for high purity metals and glass. Etc. FIBERFRAX HI-FI 660 PAPER: Finer filtration and thermal insulation. FIBERFRAX 550 PAPER: For applications were high temperature protection is more critical than specific heat retention. Typical applications are: Industrial gasketing. Liquid metal back-up insulation. Brazing furnace insulation.				

[a] White upon firing to approximately 811 K.

NOTE   From manufacturer's bulletins.

Table 5-8: Available Thicknesses of B&W Kaowool Paper

Code	20 Mil	40 Mil	80 Mil
Rated thickness, $t \times 10^3$ [m] [a]	0,508	1,016	2,032
Uncompressed thickness, $t_u \times 10^3$ [m]	0,795	1,59	3,18

[a] Thickness measured at 54800 Pa compression, per Tappi Method T-411m44.

Table 5-9: Available Thicknesses of Fiberfrax 970 Paper

Code [a]	970-A	970-AH	970-F	970-FH	970-J	970-JH
Rated thickness, tx10^3 [m] [b]	0,508	0,508	1,016	1,016	2,032	2,032
Uncompressed thickness, t_ux10^3 [m]	0,795	0,795	1,59	1,59	3,18	3,18
Mass/Area [kg.m^{-2}]	0,155	0,155	0,259	0,244	0,512	0,488

[a] Series 970 may contain up to 5% organic binder. H indicates completely inorganic paper.

[b] Thickness measured at 54800 Pa compression, per Tappi Method T-411m44.

Table 5-10: Available Roll Sizes of Fiberfrax 970 Paper

	Length [m]								
Width [m]	0,305			0,610			1,22		
Weight [kg] Thick. tx10^3 [m]	1,13	4,53	11,32	1,13	4,53	11,32	1,13	4,53	11,32
0,508	24,40	97,60	244,0	12,20	48,80	122,0	6,10	24,40	61,0
1,016	15,25	61,00	152,5	7,62	30,50	76,2	3,66	15,25	38,1
2,032	7,62	30,50	76,2	3,66	15,25	38,1	1,83	7,62	18,3

Each roll has indicated length; however, may vary slightly. Also available in sheet sized 0,305 m x 0,305 m, 0,61 m x 0,61 m, and 0,61 m x 1,22 m. "H" Series (no binder) is not available in 1,22 m width.

Table 5-11: Available Thicknesses and Corresponding Mass/Area of Fiberfrax Paper H880; Hi-Fi 660, and 550.

	H 880			Hi-Fi 660			550	
Code [a]				C	A, AH	F, FH	F	J
Compressed thickness tx10^3 [m]	0,508	1,016	2,032					
Uncompressed thickness t_ux10^3 [m]	0,795	1,59	3,18	0,387	0,795	1,59	1,59	3,18
Mass/Area [kg.m^{-2}]	0,155	0,259	0,517	0,057	0,155	0,259	0,327	0,610

[a] Series 660 may contain up to 5% organic binder. H indicates completely inorganic paper.
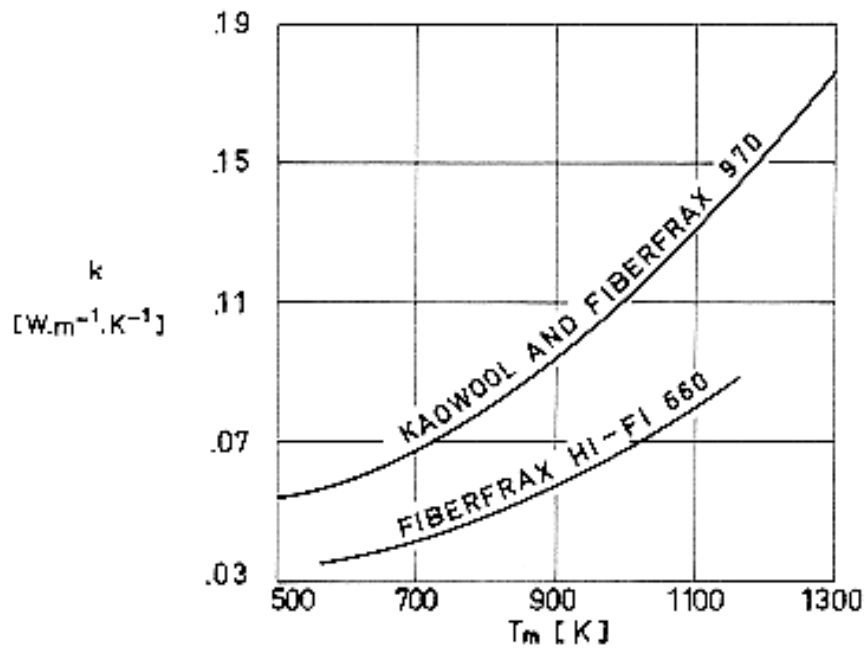
Figure 5-34: Thermal conductivity, *k*, of B & W Kaowool, Carborundum Fiberfrax 970 paper, and Fiberfrax Hi-Fi 660 paper vs. mean temperature, *Tm*.
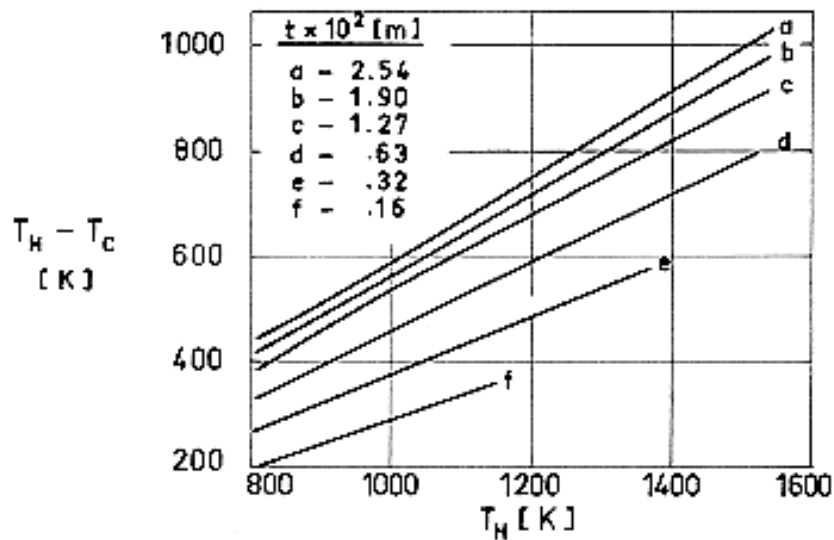
Figure 5-35: Temperature differential, *TH–TC*, vs. temperature of the hot face, *TH*, for different values of the paper thickness, *t*. Fiberfrax 970 paper, ρ = 160 kg.m⁻³.
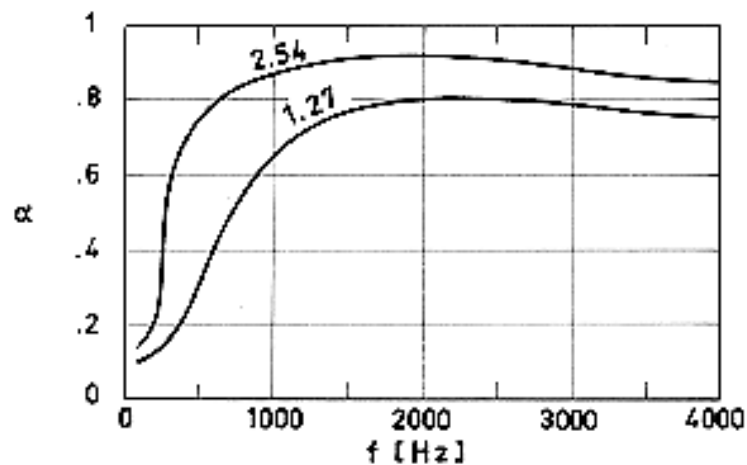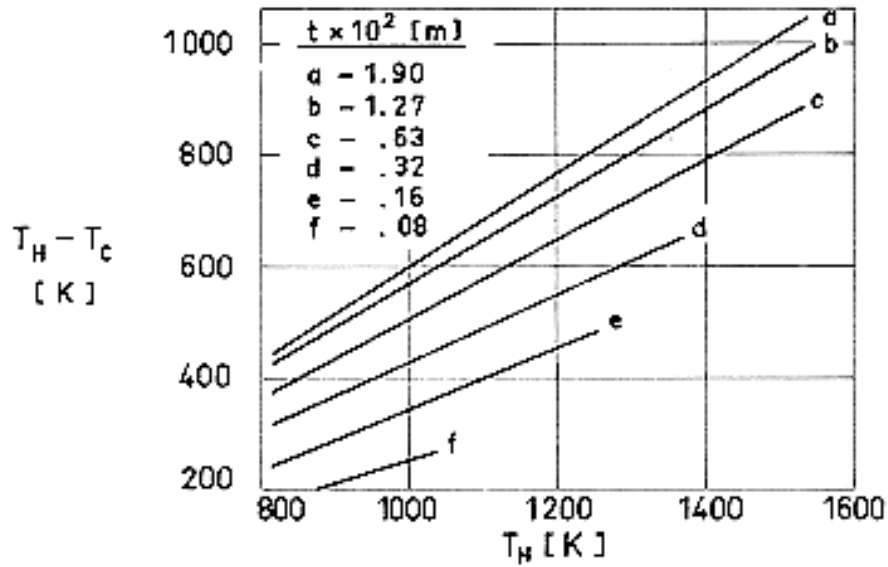
Note: non-si units are used in this figure

Figure 5-36: Temperature differential, T_H–T_C, vs. temperature of the hot face, T_H, for different values of the paper thickness, t. Fiberfrax Hi-Fi 660 paper.
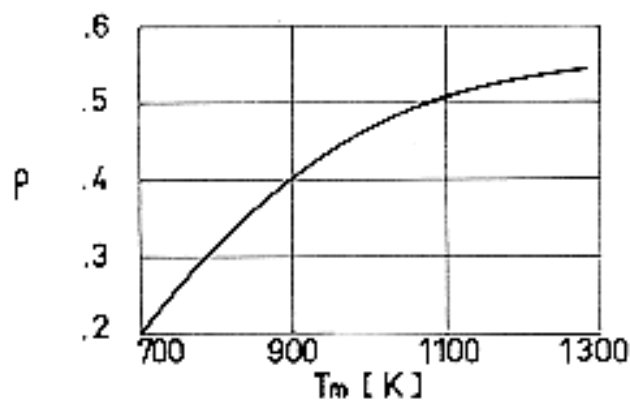
Note: non-si units are used in this figure

Figure 5-37: Thermal reflectance, ρ, of Fiberfrax 970-J paper vs. mean temperature, T_m.

6
Multilayer insulations

6.1 General

A multilayer insulation (MLI) consists of several layers of closely spaced radiation-reflecting shields which are placed perpendicular to the heat flow direction. These radiation shields aim at reflecting a large percentage of the radiation the layer receives from a warmer surface.

To avoid direct contact between shields, low-conductivity spacers may be used. Sometimes embossing or crinkling the shields produces small contact areas whose thermal joint conductance is low enough to keep conductive heat transfer between shields substantially below radiative heat transfer.

The space between shields is evacuated to decrease gas conduction. For space applications, proper venting of the insulation inner space should be provided to avoid undue pressure loads on the shields during ascent flight, to achieve an effective repressurization during re-entry, and to deliver outgassing from the insulation materials when long-term on-orbit missions are contemplated.

One-dimensional heat transfer testing has shown (Figure 6-1) that an evacuated MLI provides, for a given mass, insulation which is orders of magnitude greater than that furnished by more conventional materials such as foams and fiber-glass batting.
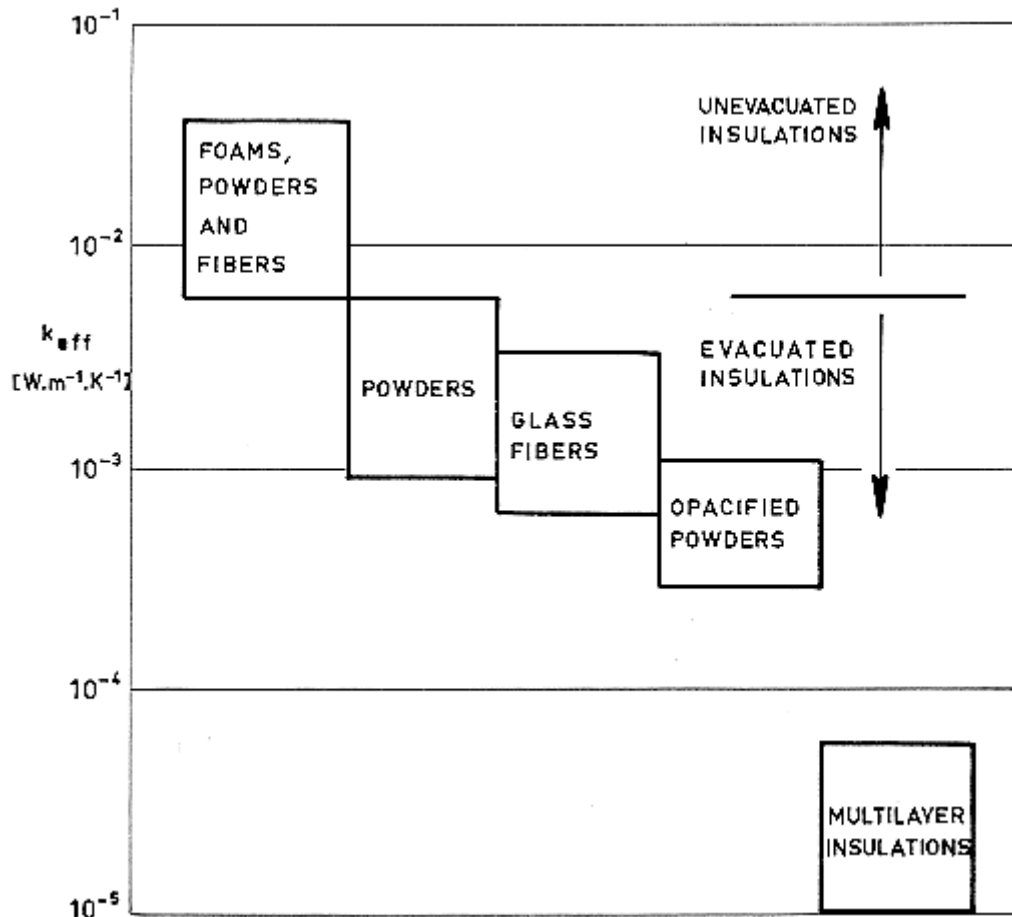
Figure 6-1: Effective thermal conductivity, k_{eff}, of multilayer insulations as compared with other insulation materials. From Glaser et al. (1967) [23].

Recent developments, see clause 6.17.3, seem to indicate that even smaller values of the effective thermal conductivity, k_{eff}, are at reach.

The thermal performance of evacuated multilayer insulation systems for use on liquid gas transportation and thermal conditioning of space borne subsystems and components has been extensively studied in the 1960's. The new impetus mainly comes from the applications to large superconducting magnet systems, which are usually radiation-shielded by surfaces at 50 K to 80 K insulated with MLIs. The evacuation of the relatively small diameter (~ 0,3 m) long (several hundred meters) vacuum space on superconducting accelerator magnet sections can be very time consuming for typical insulation layer densities. The vacuum pumping characteristics should be improved by reducing the number of layers. This requirement sets a new constraint in the optimization of the MLI systems, which places the emphasis on new aspects of the problem which were disregarded until recently.

6.1.1   Fundamental concepts concerning MLI performance

The prediction of the thermal performance of multilayer insulations is difficult because their properties are anisotropic, discontinuous and subject to variations due to manufacture, handling and use. The variables which should be taken into account in an actual system are the following:

Number of shields, N, and total thickness, t.

Temperatures of the cold and warm boundaries, T_C and T_H , respectively.

Thermo-optical properties of the cold boundary.

Applied compressive load, P.

Gas filling the insulation and its pressure, P.

Size and number of perforations to permit evacuation.

Most of the available data concerning heat transfer through multilayer insulations are based on a Fourier-Law type "effective conductivity", k_{eff}, namely

$$\frac{Q}{A} = k_{eff} \frac{T_H - T_C}{t} \qquad\qquad [6\text{-}1]$$

where:

A is the area normal to the temperature gradient [m^2].

Q is the heat flow through the insulation [W].

T_C is the cold boundary temperature.[K].

T_H is the warm boundary temperature. [K].

k_{eff} is the effective thermal conductivity [W.m^{-1}.K^{-1}].

t is the insulation thickness [m].

It should be indicated that k_{eff} can be used only when comparing the qualities of various insulators, and should not be considered as an average property of the materials constituting the insulation.

Sometimes the performance of MLI systems is given in terms of a "heat transfer coefficient" or "effective thermal conductance", h_{eff}, defined as

$h_{eff} = k_{eff}/t$.

The use of the effective thermal conductance, h_{eff}, could be recommended in those cases where the thickness, t, cannot be measured with enough accuracy.

An alternative comparison between several MLI may be made on the basis of an "effective emittance", ε_{eff}.

$$\frac{Q}{A} = \sigma \varepsilon_{eff} \left(T_H^4 - T_C^4 \right) \qquad\qquad [6\text{-}2]$$

where

ε_{eff} is the effective emittance.

σ is the Stefan-Boltzmann Constant [W.m^{-2}.K^{-4}].

The following relations between the abovementioned magnitudes result:

$k_{eff} = h_{eff}t = \sigma\varepsilon_{eff}t4T^3$,

where T is the characteristic temperature of the insulation, given by the expression:

$$T = \sqrt[3]{\frac{T_H^4 - T_C^4}{4(T_H - T_C)}} \qquad\qquad [6\text{-}3]$$

The effective thermal conductivity of a multilayer insulation is, loosely speaking, inversely proportional to the number of radiation shields per unit thickness, N/t, while the effective emittance is inversely proportional to N. The reason is that for an ideal system without radiation-absorbing spacers the radiative heat transfer decreases as $1/N$. The measurements indicate that the real behavior of most MLIs deviates from the ideal one when N/t increases, due to increased thermal conduction between adjacent layers.

Most of the heat transfer data presented in this compilation are based on k_{eff}, with the only exception of data giving the effect of surface perturbations on the characteristics of the MLI (such as overlaps, stitches, buttons, ...), which are based on ε_{eff}.

6.1.2   Failure modes

Failure of a multilayer insulation system can only occur by physical removal from the guarded surface. Performance can be degraded by compression, exposure to moisture and elevated temperatures, or improper handling techniques.

Blankets should be manufactured and manipulated in clean rooms, with a humidity range of 40-60% and a temperature range between 288 and 300 K. Persons handling the blankets and associated material should wear normal clear room clothing and flint-free gloves. For transportation purposes, the blankets should be welded in plastic bags containing silica gel packages.

The shielding of aluminium foil or aluminized Mylar ignite both in oxygen and air atmospheres. The inflammability and explosiveness of packs of multilayer insulation with glass-fiber spacing can be reduced by lowering the content of organic additives in the spacer.

6.1.3   Heat transfer through an MLI

Heat is transferred from the hot to the cold face of an MLI by the three usual mechanisms, namely:

(a)   radiation,

(b)   solid conduction; and

(c)   gas conduction.

Gas convection is quite negligible.

Let us discuss briefly how the three heat transfer mechanisms contribute to the heat balance and how they are reduced, whenever possible.

6.1.3.2   Radiation

The heat transfer rate between two infinite parallel gray planes, 1 and 2, separated by a non-absorbing medium can be expressed (McAdams (1954) [47]) as:

$$Q = \sigma A(T_2^4 - T_1^4)\frac{1}{\dfrac{1}{s_1} + \dfrac{1}{s_2} - 1} \qquad\qquad [6\text{-}4]$$

where:

A is the surface area. [m].

Q is the heat flow between both surfaces, through area A. [W].

T_i is the temperature of surface i. [K]. i = 1,2.

ε_i is the emittance of surface i.

σ is the Stefan-Boltzmann Constant. [W.m^{-2}.K^{-4}].

If N parallel shields are inserted between two boundaries C and H, the above expression, particularized to shields i and $i+1$, can be written as follows:

$$\frac{1}{s_{i,1}} + \frac{1}{s_{i+1,2}} - 1 = \frac{\sigma A\left(T_{i+1}^4 - T_i^4\right)}{Q} \qquad [6\text{-}5]$$

The second subscript, either 1 or 2, is introduced to take into account the fact that when single-metallized plastic films are used, the emittance of both faces of a given shield are unequal.

Summing the $N+1$ equations which give the heat transfer rate between the consecutive couples of parallel plates, one can express the heat transfer rate between the boundaries H and C in terms of the boundary temperatures and the emittance of the shields. The resulting expression is:

$$Q = \sigma A\left(T_H^4 - T_C^4\right)\frac{1}{\dfrac{1}{s_C} + \dfrac{1}{s_H} + \sum_{i=1}^{N}\left(\dfrac{1}{s_{i,1}} + \dfrac{1}{s_{i,2}}\right) - \left(N+1\right)} \qquad [6\text{-}6]$$

Assuming that all the shields are made from exactly the same material, and neglecting the dependence of ε on temperature, so that $\varepsilon_{i,1} = \varepsilon_1$, $\varepsilon_{i,2} = \varepsilon_2$, the above equation becomes:

$$Q = \sigma A\left(T_H^4 - T_C^4\right)\frac{1}{\dfrac{1}{s_C} + \dfrac{1}{s_H} + N\left(\dfrac{1}{s_1} + \dfrac{1}{s_2}\right) - \left(N+1\right)} \qquad [6\text{-}7]$$

In most space simulation tests, where a tank calorimeter is used, the boundary emittance, ε_C and ε_H, approach unity.

In other cases the cold and warm plates are the two shields bounding the MLI. If the total number of shields is N (intermediate shields) plus the two bounding shields, which are assumed to be of the same material, Eq. [6-7] becomes:

$$Q = \sigma A\left(T_H^4 - T_C^4\right)\frac{1}{\left(N+1\right)\left(\dfrac{1}{s_1} + \dfrac{1}{s_2} - 1\right)} \qquad [6\text{-}8]$$

Several authors quote expressions where N or N-1 appear instead of $N+1$ depending on the assumed thermal coupling of heat source and sink through the MLI.

The effective thermal conductivity, k_{eff}, of the whole assembly will be given by:

$$k_{eff} = \frac{(Q/A)t}{T_H - T_C} = \frac{\sigma t}{(N+1)\left(\dfrac{1}{s_1} + \dfrac{1}{s_2} - 1\right)} \frac{T_H^4 - T_C^4}{T_H - T_C}$$ [6-9]

where t is the thickness of the MLI.

Equation [6-8] gives the lower limit to the effective thermal conductivity of an ideal MLI.

Typical values of k_{eff} vs. the characteristic temperature, T (see Eq. [6-3]) for $\varepsilon_1 = \varepsilon_2 = 0,02$, $N = 22$, $t = 2,92$ x 10^{-2} m are represented in Figure 6-2, clause 6.1.3.3.

Data concerning the hemispherical total emittance of metallic foils and metallized plastic films are given in clauses 6.2 and 6.3.

Even leaving aside the conductive heat transfer, the effective thermal conductivity of a practical MLI will be larger than that in Eq. [6-7] dueto three purely radiative effects which is considered in the following.

6.1.3.2.1   Absorptance of the shields

Shield absorptance has not been mentioned yet since it has been assumed to be equal to emittance. This assumption is only valid when the radiative source and the receiver are approximately at the same temperature, as is the case with neighbouring shields of an MLI system. However, when metallic foils are used to shield a cryogenic surface from an outer source, such as the Sun, the above assumption can be no longer valid.

The net rate of heat absorption for a surface, C, exposed in a vacuum environment to direct and reflected thermal radiation from an adjacent surface, H, may be written, according to Smolak, Knoll and Wallner (1962) [68], as:

$$Q = \sigma A \left[\frac{s_H F_{HC} \alpha_C T_H^4}{1 - F_{HC} F_{CH}(1-\alpha_H)(1-\alpha_C)} + \frac{s_C F_{HC} F_{CH}(1-\alpha_H)\alpha_C T_C^4}{1 - F_{HC} F_{CH}(1-\alpha_H)(1-\alpha_C)} - s_H T_C^4 \right]$$ [6-10]

where F_{HC} is the view factor giving the fraction of the total radiation that arrives at C coming from H; $F_{HC} = F_{CH} = 1$ for closely spaced parallel foils of the same surface area. α is the absorptance, while the other symbols have been used previously.

When N parallel closely spaced shields are placed between surfaces H and C, the net rate of heat absorption for surface C is given (Smolak et al. (1962) [68]) by:

$$Q = \sigma A \frac{s}{\alpha} \frac{\left[\left(\frac{\alpha}{s}\right)_C \left(\frac{s}{\alpha}\right)_H\right]^{N+1} T_H^4 - T_C^4}{\left(\frac{1}{\alpha_C} + \frac{1}{\alpha_H} - 1\right)\left[\frac{1 - \left[\left(\frac{\alpha}{s}\right)_C \left(\frac{s}{\alpha}\right)_H\right]^{N+1}}{1 - \left(\frac{\alpha}{s}\right)_C \left(\frac{s}{\alpha}\right)_H}\right]} \qquad [6\text{-}11]$$

Notice that when $T_H = T_C$ and $(\alpha/\varepsilon)_C(\varepsilon/\alpha)_H = 1$, Q becomes zero, as it should be.

To obtain the above expression it has been assumed that all the shields have the same thermal radiation properties, namely: α_H and ε_H for the face looking to the cold surface and α_C and ε_C for the opposed face.

The effective thermal conductivity, keff, now deduced from Eq. [6-11], becomes:

$$k_{eff} = \sigma t \left(\frac{s}{\alpha}\right)_C \frac{\left[\left(\frac{\alpha}{s}\right)_C \left(\frac{s}{\alpha}\right)_H\right]^{N+1} T_H^4 - T_C^4}{\left(\frac{1}{\alpha_C} + \frac{1}{\alpha_H} - 1\right)\left[\frac{1 - \left[\left(\frac{\alpha}{s}\right)_C \left(\frac{s}{\alpha}\right)_H\right]^{N+1}}{1 - \left(\frac{\alpha}{s}\right)_C \left(\frac{s}{\alpha}\right)_H}\right]\left(T_H - T_C\right)} \qquad [6\text{-}12]$$

When $(\alpha/\varepsilon)_C(\varepsilon/\alpha)_H = 1$ the denominator in Eq. [6-12] becomes equal to $(N+1)[(1/\alpha_C)+(1/\alpha_H)-1](T_H-T_C)$. If, in addition, it is assumed that $\alpha_C = \varepsilon_X = \varepsilon_1$ and $\alpha_H = \varepsilon_2$, one obtains again Eq. [6-9]. See Figure 6-2, clause 6.1.3.3.

Data concerning spectral absorptance, α'_λ, and solar absorptance, α_s, of metallic foils are given in clause 6.5.

6.1.3.2.2   Small spacing effects

When the distance between two adjacent radiation shields is of the same order of magnitude as the wavelength, λ, of the radiation, the classical Stefan-Boltzmann radiation law is inadequate to describe the net energy transfer.

The wavelength, λ, is related to temperature, T, by the Wien's displacement law (Siegel & Howell (1968) [66]):

$\lambda_{max}T = 2{,}9 \times 10^{-3}\,\text{m.K}$,

where λ_{max} is the wavelength in vacuum at maximum black body emissive power from a surface at sink temperature T.

Two wave electromagnetic effects appear for small spacing between shields (Cravalho, Tien & Caren (1967) [15]).

The first effect is due to wave interference. An electromagnetic wave (of known amplitude and phase) transmitted into the vacuum gap between the two dielectric shields is reflected back and forth in the gap. As a result of these multiple reflections, wave interference occurs which can be either constructive or destructive in nature. In the limit of zero distance between shields no phase lag exists

and the interference is entirely constructive which results in maximum transmissivity. As the distance increases, a phase difference between waves arises and thus the amplitudes of the different waves differ and although constructive interference exists, it is not so strong.

The second effect is radiation tunneling. Under normal conditions, when vacuum with refractive index n_o = 1 is placed between the two dielectric shields (n_1 and n_2, both larger than 1), some of the radiation in 1 travelling to 2 can undergo total internal reflection when the incidence angle is larger than $\sin^{-1}(1/n_1)$. When the vacuum region is sufficiently thin, however, even a ray at a larger incidence could not suffer total internal reflection and pass from 1 to 2. The energy has been "tunneled" through vacuum from 1 to 2.

The actual magnitude of these effects is a complicated function of the spacing between shields, the refractive indexes and temperatures of these, ... It can be as large as an order of magnitude larger, but disappears at a shield spacing of approximately $3\lambda_{max}$.

6.1.3.3 Solid conduction

In most practical instances, spacers of fiber material or powder are introduced between radiation shields with the two fold aim of 1) avoiding radiation tunneling and 2) decreasing the solid thermal conductance between contacting metallic or metallized shields.

The thermal conductance across each point of contact depends on the contact area, pressure generated by the winding tension and whether the Inter-fiber contact is wet or dry.

Spacers are introduced in clause 6.8. They are so varied in characteristics and performance that it is difficult to introduce a single expression for predicting its influence on the heat balance.

The following empirical expression has been given by Keller, Cunnington & Glassford (1974) [35] and is used here for illustrative purposes, see Figure 6-2..

$$\frac{Q}{A} = C_1 \frac{(N/f)^{2,56}}{N-1}\left(T_H^2 - T_C^2\right) + C_2 \frac{\varepsilon}{N-1}\left(T_H^{4,67} - T_C^{4,67}\right) \qquad [6\text{-}13]$$

Note: non-si units are used in this figure

where

C_1 = 6,79 x 10^{-13} W.m^{0,56}.K^{-2}

C_2 = 5,39 x 10^{-10} W.m^{-2}.K$^{-4,67}$

According to the authors, this equation accounts for the temperature dependence of solid thermal conduction.

Equation [6-13] has been obtained by best fit to experimental data obtained with unperforated double-aluminized Mylar shields with Tissuglas (see Table 6-10) or silk net spacers at T_H temperatures between 250 K and 286 K, and T_C close to 96 K; and at pressures below 1,3 x 10^{-5} Pa so that gas thermal conduction can be neglected.

The effective thermal conductivity, keff, can be deduced from Eq. [6-13], after introduction of Eq. [6-1]. Values of k_{eff} as a function of the characteristic temperature, T, for T_H = 300 K are given in Figure 6-2.

The figure indicates that increases in k_{eff} because of solid conduction are not too large provided that suitable optimized spacers are used. This is not always the case, as can be seen in the same figure, where the values of k_{eff} corresponding to a practical system can be an order of magnitude larger than those corresponding to a theoretical minimum, given by Eq. [6-9].
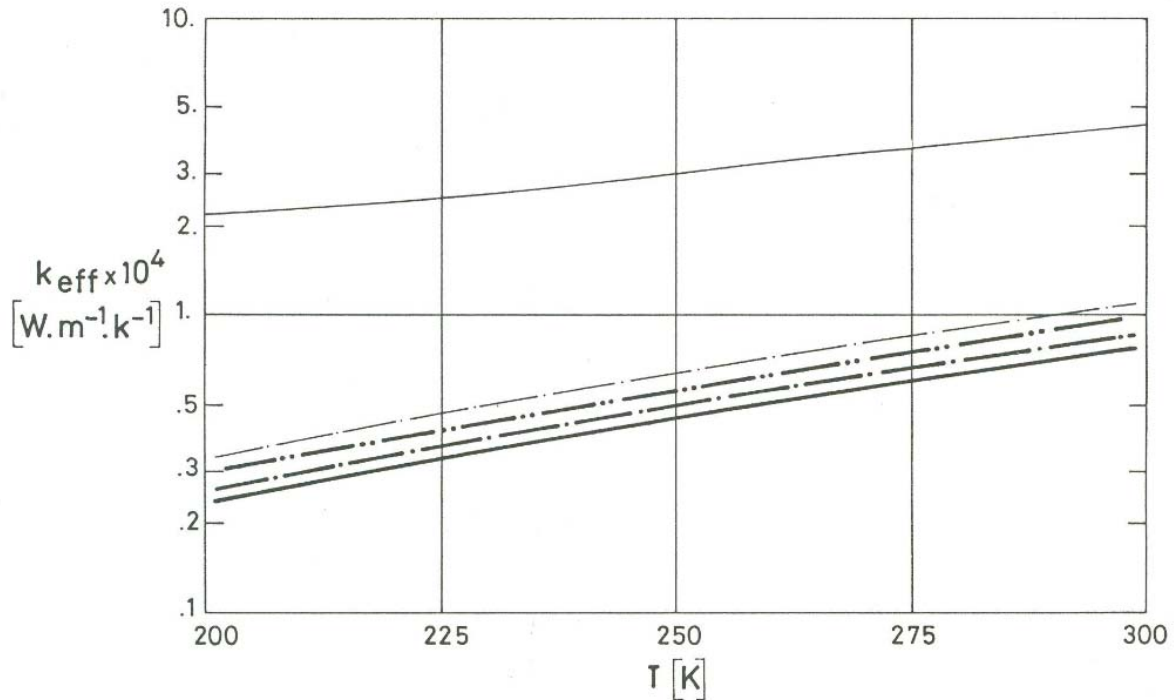
Note: non-si units are used in this figure

Figure 6-2: Effective thermal conductivity, keff, of several multilayer insulation systems as a function of the characteristic temperature, T. Calculated by the compiler.

Explanation

Key	Eq.	N	$t \times 10^2$ [m]	Other	Highlights
────	[6-9]	22	2,92	$\varepsilon_1 = \varepsilon_2 = 0,02$	ε Effects
──·──	[6-12]			$\varepsilon_C = \varepsilon_H = 0,02$ $\alpha_C = \alpha_H = 0,2$	α/ε Effects
──·──				$\varepsilon_C = \varepsilon_H = 0,02$ $\alpha_C = \alpha_H = 0,6$	
──··──	[6-13]			$\varepsilon = 0,02$, $T_H = 300$ K $C_1 = 6,79 \times 10^{-13}$ $C_2 = 5,39 \times 10^{-10}$	Solid Conduction Effects
────	Figure 6-63, clause 6.11			Mylar Single-Aluminized Dimpled $p < 0,5 \times 10^{-3}$ Pa	Practical System

6.1.3.4 Gas conduction

The contribution to the heat transfer through an MLI of the interstitial gas conduction is hard to estimate and to measure.

At pressures lower than 10^{-2} Pa gas conduction is a free molecular flow process with an upper k_{eff} value of around 10^{-5} $W.m^{-1}.K^{-1}$, which varies linearly with pressure. This topic is discussed extensively in clause 6.16.

Gas pressure within the insulation is surely higher than that observed by a vacuum gage externally connected to it. Despite pumping at elevated temperatures, residual degassing will continue to take place for long times.

Several methods have been suggested for self-degassing MLI systems (see, in addition, clause 6.17).

In the self-evacuating principle, SEMI (Perkins, Dengler, Niendorf & Nies (1968) [50], Nies & Niendorf (1971) [49]), a vacuum-tight flexible casing encloses the multilayers, forming panels that are bounded to the cryogenic tank walls in an overlapping single arrangement. The panel-bags are filled with CO_2 gas which cryopumps to provide the required vacuum when the tank is loaded with the cryogen.

The idea is not completely new, having been used in industrial gas processing, space simulation chambers and rarefied flow aerodynamic facilities. Any gas which is condensable at the required temperature can be used. Helium is normally used in terrestrial facilities, but it is highly thermal conductive and will result in a high heat transfer through the insulation during ground hold.

The configuration for large space borne cryogenic storage tanks results to be complicated and, although it was suggested for using on Space Shuttle cryogenic tanks (Nies & Niendorf (1971) [49]), apparently it has never been implemented.

Self pumping has been considered by Scurlock & Saull (1976) [63]. The idea is to incorporate a getter material (activated carbon) into the spacers of the MLI. Although spectacular reductions in the heat transfer through the MLI of an order of magnitude were reported, results on the contrary also exist (Halaczek & Rafalowicz (1986) [25]). It seems that the rise in the heat transfer observed by the last authors can be attributed to conductive interaction with the getter material.

The early promising results have not been confirmed yet in large scale applications (Barth & Lehmann (1988) [8]). Nevertheless self-pumping seems to be a very promising idea worth of being considered more extensively. It has been introduced and discussed in clause 6.17.

6.1.4   Cost

Information on comparative costs of MLI systems is fairly scanty.

According to Knopf & Murray (1970) [39], the material cost for a multilayer of 30 crinkled or embossed shields of single-aluminized Mylar is about 30 US $.m^{-2}. The combined cost of 22 Mylar shields and Tissuglass spacers is about 130 US $.m^{-2}.

Klippel & Langer (1974) [37], performing a selection among available European products, quoted the following prices:

1. Shields

    Single (or double)-aluminized Hostaphan (Polyester) 6×10^{-6}, 12×10^{-6}, 25×10^{-6} m thick: 0,60 to 1,50 DM.m^{-2}.

    Single (or double)-aluminized Melinex (Polyester) 12×10^{-6} to 25×10^{-2} m thick: 1 to 2 DM.m^{-2}.

2. Spacers

    Fibrex-Polyesterplies Type H 3002

    4×10^{-5} to 5×10^{-5} m thick: 0,50 DM.m^{-2}.

    Polyester-Bobinet Tüll (Net) 1946: 2,50 DM.m-2.

It has been estimated (Kropschot et al. (1960) [41]) that the material cost of an MLI is 10 to 20 times the cost of perlite, installation cost excluded.

In any case, the material cost is small relative to the cost of fabricating the total system, and special attention should be devoted to the improvement of the manufacturing processes involved such as crinkling, cutting, sewing, hole-drilling and the like. For example, Maccalous (1968) [44] reports that a reduction in cost of approximately 80% may be achieved in the cutting process by using appropriate techniques as compared with single layer cutting.

In order to give an order of magnitude idea of the cost of an MLI system it should be mentioned that Hale (1969) [27] evaluates in US $ 400 per insulation the cost of preparation of multilayer specimens, of fairly simple shape, used to measure k_{eff} with a cylindrical calorimeter, 0,76 m in diameter, 1 m in length.

6.2   Radiation shields

Radiation shields are low emittance foils used to attenuate the incoming radiation. Aluminium, gold and silver are the most commonly used materials either for coatings or to form thin metallic foils.

6.2.1   Aluminium foils and aluminium coated plastic films

These materials are frequently used as radiation shields owing to the following reasons:

1. Aluminium is inexpensive and readily available in various thicknesses of foil and as a coating on a variety of metallic and non-metallic surfaces.

    Aluminium vaporizes at a lower temperature than gold, making the aluminium deposition process easier to control. In addition, plastic films with an aluminium deposit have been used for decorative purposes for many years. As a result aluminium-coated films are less expensive and of better average quality than gold or silver-coated films.

2. The emittance of aluminium is only slightly higher than that of clear silver, but, whereas silver tarnishes in air, aluminium forms a very thin layer of oxide which prevents further degradation of the surface.

On the opposite side, moisture has a pernicious effect on aluminized plastic, as has been observed several times when Mylar and Kapton coated films have been used (ADL (1964) [1], Leonhard & Hyde (1971) [42]). Aluminium films tend to discolor and separate from the substrate.

For some applications, such as Space Suit Systems, abrasion resistance may be of concern. As it has been indicated by Richardson, Ruccia & French (1970) [54], the abrasion resistance of aluminized radiation shields can be substantially improved, without degrading the low emittance surfaces, by overcoating with a 5×10^{-8} m thick layer of vapor deposited germanium.

For comparable MLI systems, the aluminized polyester film is less effective than the aluminium shields by a factor of 1 to 2,5 based on the measured heat flux (Kropschot et al. (1960) [41]). In applications where lightness is important, 6×10^{-6} to 12×10^{-6} m thick aluminium foils can be used for radiation shields even though these foils have very little tensile strength and are difficult to handle. Heavier foils (25×10^{-6} to 125×10^{-6} m thick) find only limited application where the weight is of secondary importance. According to Glaser et al. (1967) [23], the main advantages of these thicker foils are the following:

1. Ease of handling.

2. Stiffness. They do not exhibit a tendency to bridge between the supports and maintain a given structural shape.

Plastic films are approximately one-half the weight of aluminium foils of equivalent thickness. In addition a $6,35 \times 10^{-6}$ m thick Mylar film offers a tear strength much larger than that of an $1,27 \times 10^{-5}$ m thick aluminium foil (Glaser et al. (1967) [23]).

6.2.2 Gold foils and gold coated plastic films

The use of gold foils has been suggested several times. The cost of such systems would be several orders of magnitude higher than that of systems based on more conventional materials. In addition gold foils are only available in narrow widths and short lengths which would make the installation of such systems impractical.

Vapor-deposited gold appears more attractive for reusable vehicle radiation shields because of the lower emittance and no degradation effects after exposure to moisture.

Although gold-coated surfaces exhibit excellent thermal properties, their use is not so widely extended owing to problems of cost and manufacturing process control. The increased cost is due to the manufacture and not to the cost of the metal itself, which is deposited in very thin layers.

6.2.3 Silver coated plastic films

Since silver tarnishes in air, it is normally overcoated with SiOx. Although silver-coated plastic films with SiO$_x$ overcoating are commercially available, they are very sensitive to structural changes and are expensive owing to problems presented by some evaporation techniques.

6.2.4　　Operating temperature ranges

The use of most polyester films is limited to operating temperatures below 420 K, the point at which the film begins to deteriorate. Kapton polyimide retains 70 % of its room temperature strength up to 480 K (Leonhard & Hyde (1971) [42]).

Larger operating temperatures can be achieved using metallic foils. Aluminium foils can be used for temperatures up to 800 K, copper foils for temperatures between 720 and 1250 K, and nickel foils for temperatures up to 1470 K (Kaganer (1969) [33]).

Emittances of copper and nickel are very sensitive to the degree of surface oxidation. There is the possibility of using gold to replace copper, and platinum to replace nickel, but the cost of such systems would be fairly large.

For some specific applications, when a refractory metal is necessary to prevent long term evaporation and metallurgical changes, molybdenum foil can be used (Dixon & Musgrove (1973) [18]). Molybdenum has a particularly low emittance and is readily available commercially.

6.2.5　　Normally used plastic films

Although Mylar polyester film is currently used in most MLI shields, many candidate film materials exist such as Melinex and Hostaphan (polyesters), Kinfol and Lexan (polycarbonates), and Kapton H (polyimide).

The polycarbonates, although not very widely used, are attractive primarily due to their comparatively low density, and Kinfol is available in thicknesses down to 2×10^{-6} m. Kapton, while slightly heavier and thicker than Mylar, and much more expensive, has the same room temperature tensile strength, higher maximum operating temperature and is non-flammable. Although Kapton has a higher moisture regain than the other materials, surface coating minimizes the importance of this factor.

In addition to Kapton H film, there is a commercially available Type F film which is coated with Teflon to impart heat sealability and enhance chemical resistance.

A significant advantage of most plastic films is the fact that the plastic itself has a low thermal conductivity, which enables the film to be used without spacers between the shields. In this case the film is coated on one side only, and is crinkled or embossed in order to reduce the area of contact between sheets. Since the emittance of an uncoated side is higher than that of a coated side, more radiation shields are required to reduce the heat transfer to the level that can be achieved by coating both sides.

Embossment of Kapton is fairly troublesome. As a general rule long cycles are required to produce molded shapes from this high temperature polymer. Schroeder (1973) [60] reports some difficulties connected with the fact that embossment of Kapton is not permanent, and suggests that more development effort should be spent in the near future on this problem.

In addition to the advantages mentioned above, metallized plastic films have a low thermal conductivity in a direction parallel to the film. This is so because the metal layer (the highly thermal conducting component of the system) is extremely thin (approximately 5×10^{-8} m). The longitudinal conductivity of aluminized films is several hundred times lower than that of aluminium foils. This may be useful to increase the net efficiency of the insulation, whose ideally one-dimensional behavior is hampered by the end effects which are normally due to multidimensional heat transfer.

In instances where electromagnetic radiation has to pass through the shield, uncoated plastic films can be used. Obviously, the insulating characteristics of the MLI are grossly degraded.

6.3 Emittance of metallic foils

Data regarding the hemispherical total emittance of metallic foils are presented in Figure 6-3 to Figure 6-15. These data have been arranged as is indicated in the following table.

Metal	Total Emittance Modifier	Variable	Fig.	Comments
Aluminium	Hemispherical	T	Figure 6-3	Summary of available data
Copper	Hemispherical	T	Figure 6-4	Summary of available data
Copper	Hemispherical	T	Figure 6-5	Surface lapped, oxidated
Copper	Hemispherical	T	Figure 6-6	Surface grinded, oxidated
Gold	Hemispherical	T	Figure 6-7	
Molybdenum	Hemispherical	T	Figure 6-8	
Nickel	Hemispherical	T	Figure 6-9	
Nickel	Hemispherical	T	Figure 6-10	Influence of oxygen on the
Nickel	Normal	T	Figure 6-11	surface.
Ni Alloy (Incoel)	Normal	T	Figure 6-12	
Ni Alloy (Incoel X)	Normal	T	Figure 6-13	
Platinum	Hemispherical	T	Figure 6-14	
Silver	Hemispherical	T	Figure 6-15	

NOTE   Emittance of Aluminium.
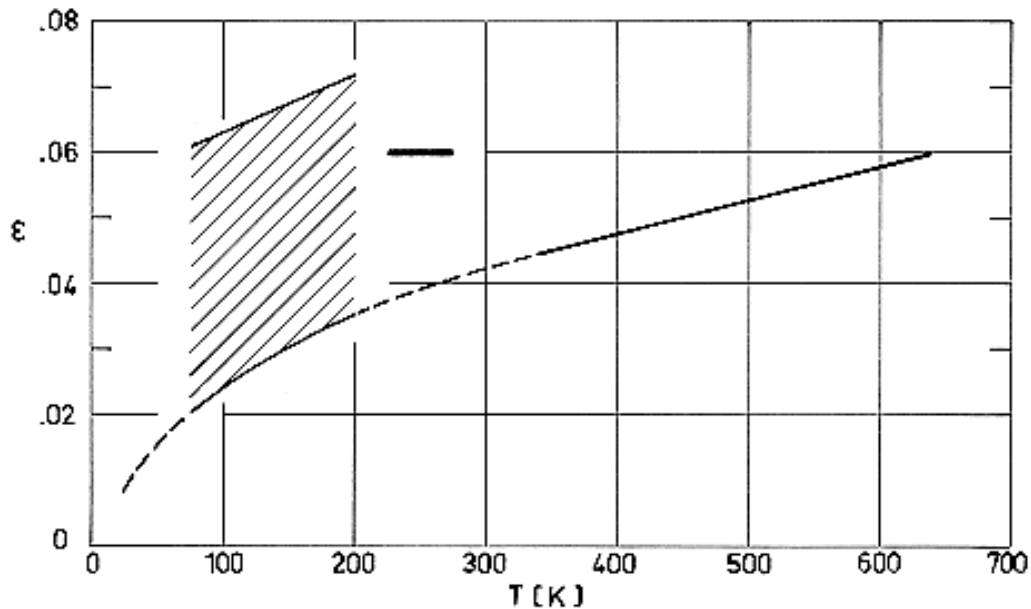
Note: non-si units are used in this figure

Figure 6-3: Summary of data concerning hemispherical total emittance, ε, of Aluminium foils and thin sheets as a function of temperature, T.

From Touloukian & DeWitt (1970) [74].

Explanation

Key	Description	Test Method	Comments
	Foils, Sheets.		Measured in vacuum (<2,7x10⁻² Pa)
	Plate, 5,08x10⁻³ m thick. Hand polished.		Measured in vacuum (1,33x10⁻² Pa). Reported error ± 3%.
	Hollow sphere; polished to approx. 5x10⁻⁶ m, then rinsed with distilled water and alcohol, dried in a stream of nitrogen.		Measured in vacuum. Data from smooth curve. Reported error ± 5%.

NOTE   Emittance of Copper.
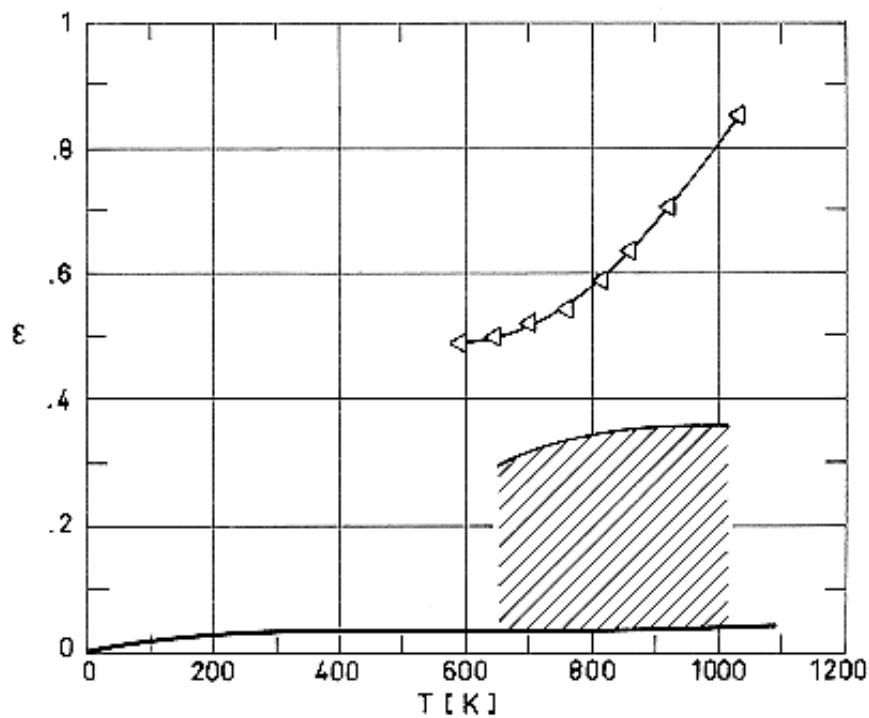
Note: non-si units are used in this figure

Figure 6-4: Summary of data concerning hemispherical total emittance, ε, of Copper as a function of temperature, T.

Curves are from Touloukian & DeWitt (1970) [74], while the shadowed zone is from Reid & Coon (1971) [53].

Explanation

Key	Description	Test Method	Comments
——	Polished or electropolished.		Average of data from several sources.
△	Stably oxidized at 1033 K in quiescent air.	From normal total emittance.	Reported error <2%.
▨	Electrolytic tough pitch Copper. 99,9% pure. Oxidized.	Calorimetric. T measured with thermocouples.	Measured in vacuum (<4x10⁻² Pa). Additional details in Figure 6-5 and Figure 6-6.
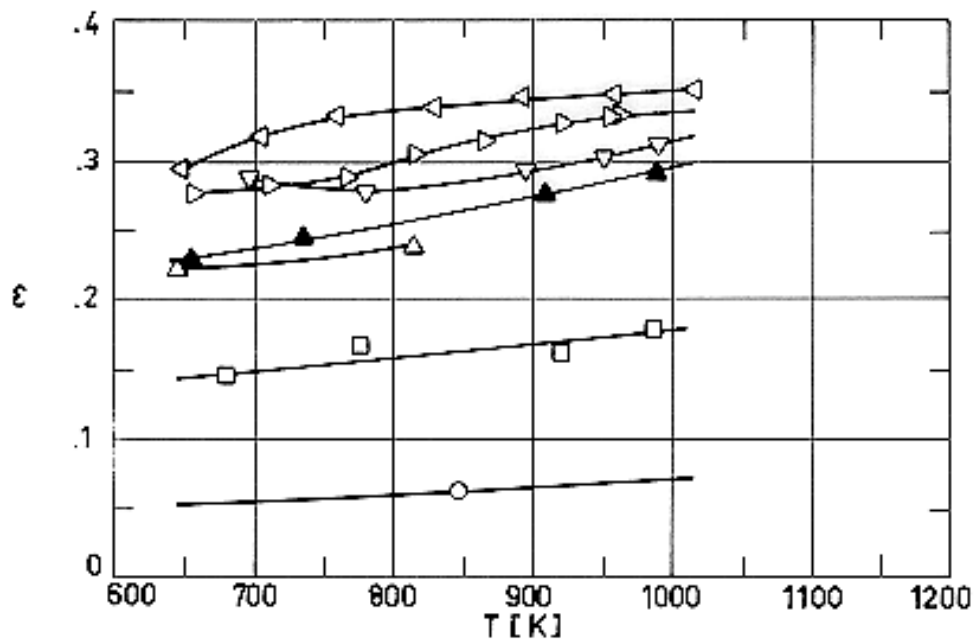
Note: non-si units are used in this figure

Figure 6-5: Hemispherical total emittance, ε, of Copper as a function of temperature, T.

From Reid & Coon (1971) [53].

Explanation

Key	Description	Test Method	Comments
○	Electrolytic tough pitch Copper 99,9% pure. Lapped, wiped lightly just before use, unoxidized.	Calorimetric. T measured with thermocouples.	Measured in vacuum (<4x10⁻² Pa).

Key	Description	Test Method	Comments
□	Oxidized, 15 min at 529 K.	Electrical heater into the box-like specimen.	
△	Oxidized, 3,3 h at 531,4 K.		
▲	Oxidized, 3,2 h at 532,5 K.		
▽	Oxidized, 47,2 h at 530 K.		
▷	Oxidized, 15,6 h at 527,5 K.		
◁	Oxidized, 13,25 h at 533 K.		
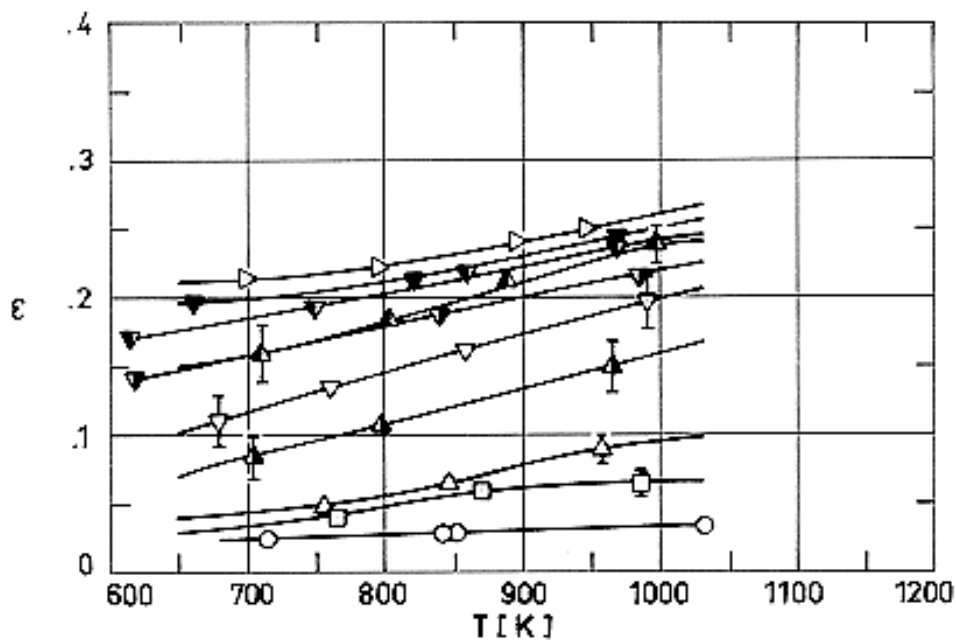
Note: non-si units are used in this figure

Figure 6-6: Hemispherical total emittance, ε, of Copper as a function of temperature, T.

From Reid & Coon (1971) [53].

Explanation

Key	Description	Test Method	Comments
○	Electrolytic tough pitch Copper 99,9% pure. Surface grinded, wiped lightly just before use, unoxidized.	Calorimetric. T measured with	Measured in vacuum (<4x10^{-2} Pa).

Key	Description	Test Method	Comments
□	Oxidized, 19 h at 417,8 K.	thermocouples. Electrical heater into the box-like specimen.	
△	Oxidized, 45 min at 480,3 K.		
◮	Oxidized, 4,42 h at 477,2 K.		
◭	Oxidized, 17,5 h at 475,7 K.		
▽	Oxidized, 15 min at 539,2 K.		
▼	Oxidized, 15 min at 550,6 K.		
▽	Oxidized, 43 min at 532,8 K.		
▼	Oxidized, 3,03 h at 534,4 K.		
▷	Oxidized, 8,38 h at 535,3 K.		

NOTE   Emittance of Gold.
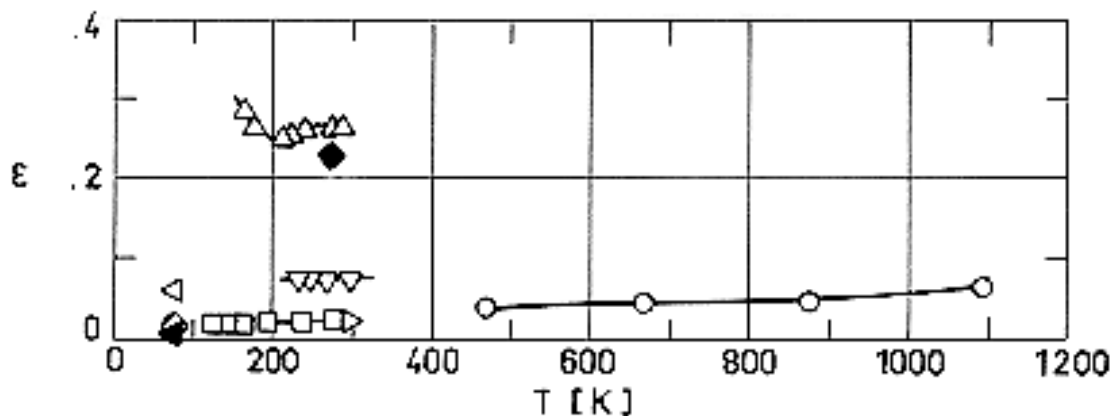
Note: non-si units are used in this figure

Figure 6-7: Hemispherical total emittance, ε, of Gold vs. temperature, T.

From Touloukian & DeWitt (1970) [74].

Explanation

Key	Description	Test Method	Comments
○	Ground with 600 grit Carborundum and polished on a wet cloth lap.		Measured in vacuum (1,33x10^{-3} Pa). Reported error ≤ 10%.
□	Polished.		Measured in vacuum (6,67x10^{-3} Pa). Reported error ± 10%.

Key	Description	Test Method	Comments
△	Foil 3,81x10⁻⁵ m thick.		Measured in vacuum (1,33x10⁻⁴ Pa). Contaminated? Reported error <5%.
▽	Commercial foil 2,54x10⁻⁴ m thick cleaned in both sodium dichromate and dilute nitric acid solutions, buffed, cleaned with carbon tetrachloride and acetone.		Measured in vacuum (1,33x10⁻⁴ Pa). Data from smooth curve. Reported error 3%.
▷	Gold plating 7,62x10⁻⁶ m thick. Polished, kerosene buff.		Measured in vacuum (4x10⁻⁴ Pa). Reported error ± 20%.
◁	Leaf 2,54x10⁻⁷ m thick.	Calorimetric absorptance. Source: 300 K blackbody. Absorbed heat related to boil-off rate of LN_2. Authors assumed $\alpha = \varepsilon$.	Measured in vacuum (1,33x10⁻⁴ to 1,33x10⁻⁵ Pa). Reported error 5%.
◀	Foil 1,27x10⁻⁵ m thick. Solvent cleaned.		
◇	Foil 1,02x10⁻⁶ m thick. Solvent cleaned.		
◆	Bright foil. Typical of adhesive backed metal		Reported error 10%.

NOTE   Emittance of Molybdenum.

Note: non-si units are used in this figure
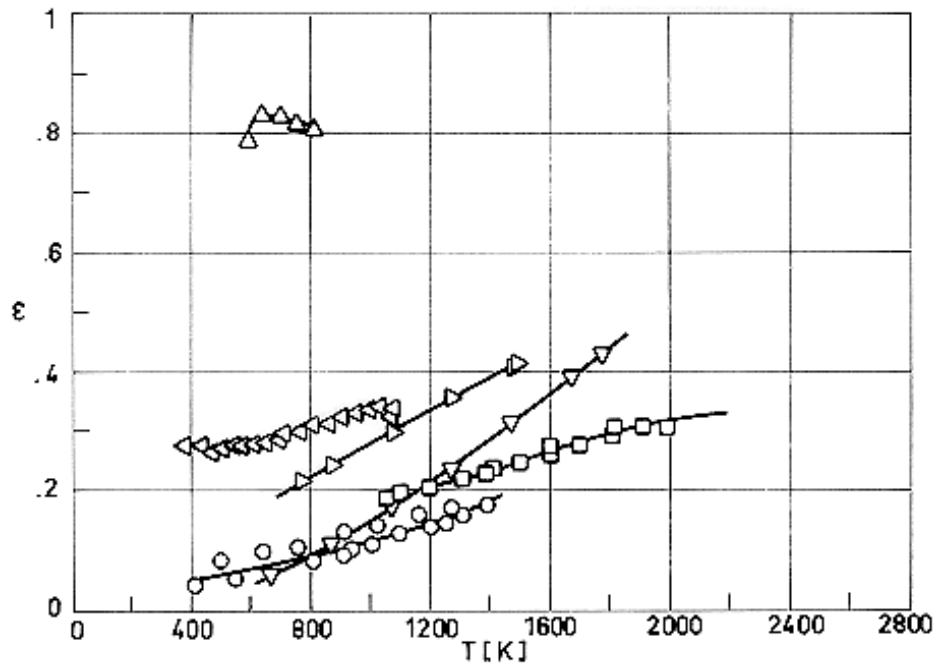
Figure 6-8: Hemispherical total emittance, ε, of Molybdenum vs. temperature, T.

From Touloukian & DeWitt (1970) [74].

Explanation

Key	Description	Test Method	Comments
◯	Vapor-blasted with Techline Liquabrasive, PCM-3067, grit No. 325.		Measured in vacuum (<6,7x10⁻⁴ Pa). Reported error ± 2,7%.
☐	Degreased with acetone, cleaned with a rubber eraser, wiped with acetone.		Measured in vacuum (1,33x10⁻² to 1,33x10⁻⁴ Pa). Reported error ± 4%.
△	Stably oxidized at 811 K in quiescent air.		Reported error <2%.
▽	Lightly etched and flashed in vacuum at 2073 K for 10 min.		Measured in vacuum (<6,7x10⁻⁴ Pa). Data from smooth curve. Reported error ± 2,5%.
▷	Shot-blasted and picled in hydrochloric acid.		
◁	Grit blasted with aluminium oxide No. 90 (PCM-3043A).		Measured in vacuum(<3,9x10⁻⁴ Pa). Data from smooth curve. Reported error ± 2,7%.

NOTE   Emittance of Nickel.
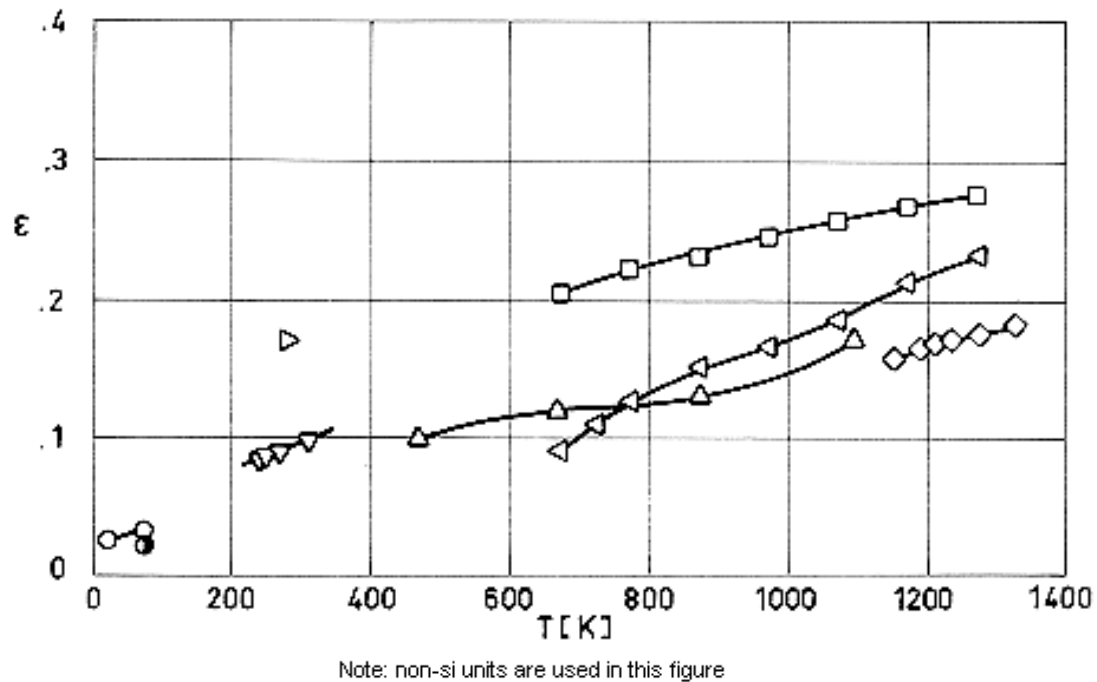
Figure 6-9: Hemispherical total emittance, ε, of Nickel vs. temperature, *T*.

Data from Touloukian & DeWitt (1970) [74], except ○ , which are from Wood, Deem & Lucks (1961) [76].

Explanation

Key	Description	Test Method	Comments
○	Commercially pure. As received, cleaned.	Calorimetric absorptance. Source: 300 K blackbody. Absorbed heat related to boil-off rate of LN2. Authors assumed $\alpha = \varepsilon$.	Measured in vacuum ($1,33 \times 10^{-4}$ to $1,33 \times 10^{-5}$ Pa). Reported error 5%.
◑	Foil $1,02 \times 10^{-4}$ m thick. solvent cleaned.		
□	Sandblasted.		Measured in vacuum ($<6,65 \times 10^{-4}$ Pa). Reported error ± 2,5%.
△	Commercially pure. Ground with 600 grit carborundum, polished.		Measured in vacuum ($1,33 \times 10^{-3}$ Pa). Reported error <10%.
▽	Commercial sheet. Cleaned, buffed, cleaned.		Measured in vacuum ($1,33 \times 10^{-4}$ Pa). Reported error 3%.
▷	Electroless nickel.		Reported error ± 10%.

Key	Description	Test Method	Comments
◁	Commercially pure. Vacuum heated at 1473 K for 15 min.		Measured in vacuum (<6,65x10⁻⁴ Pa). Reported error ± 2,5%.
◇	99,95 Ni.		
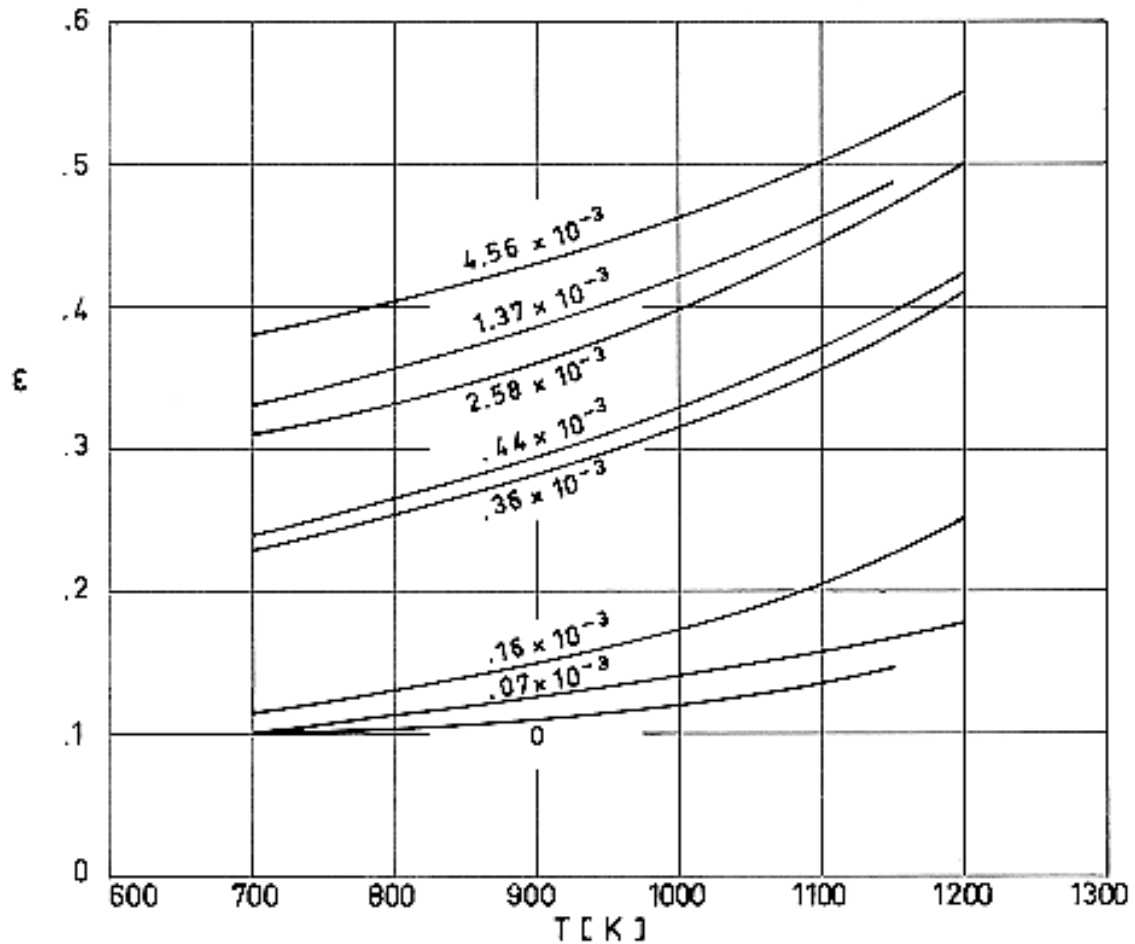
Note: non-si units are used in this figure

Figure 6-10: Hemispherical total emittance, ε, of oxidized Nickel as a function of temperature, *T*.

Numbers near curves give the amount of oxygen on the surface in $kg.m^{-2}$. The emittance has been measured calorimetrically by the filamentin-vacuum method. The amount of oxygen has been deduced from the weight loss on reduction in hydrogen. Chamber pressure $1,33x10^{-5}$ Pa. From Shelton & Akers (1961) [64].
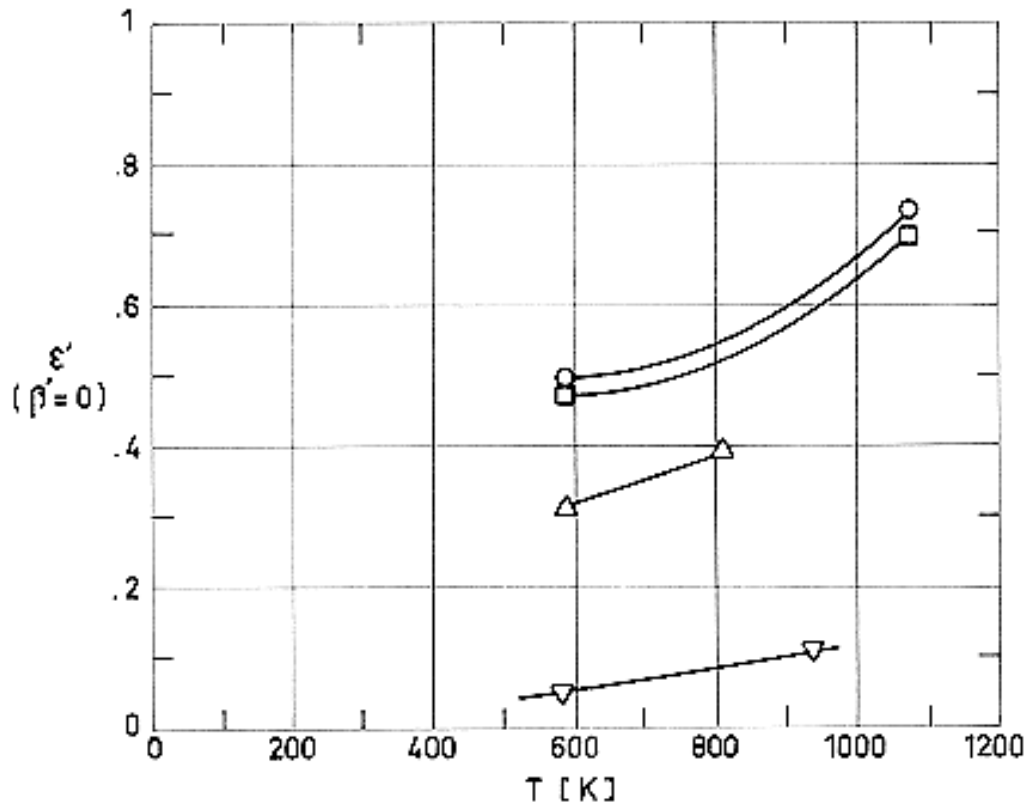
Note: non-si units are used in this figure

Figure 6-11: Normal total emittance, ε', of Nickel as a function of temperature, T.

From Wood, Deem & Lucks (1961) [76].

Explanation

Key	Description	Test Method	Comments
○	Oxidized at 1015 K, shot blasted.	Thermopile detector.	Measured in air.
□	Oxidized, buffed.	Comparison blackbody.	
△	Unoxidized, shot blasted.	T measured with thermocouples.	Data from smooth curves.
▽	Unoxidized, buffed.	Self-resistance-heat specimen.	

NOTE   Emittance of Nickel Alloys (INCOEL).

131
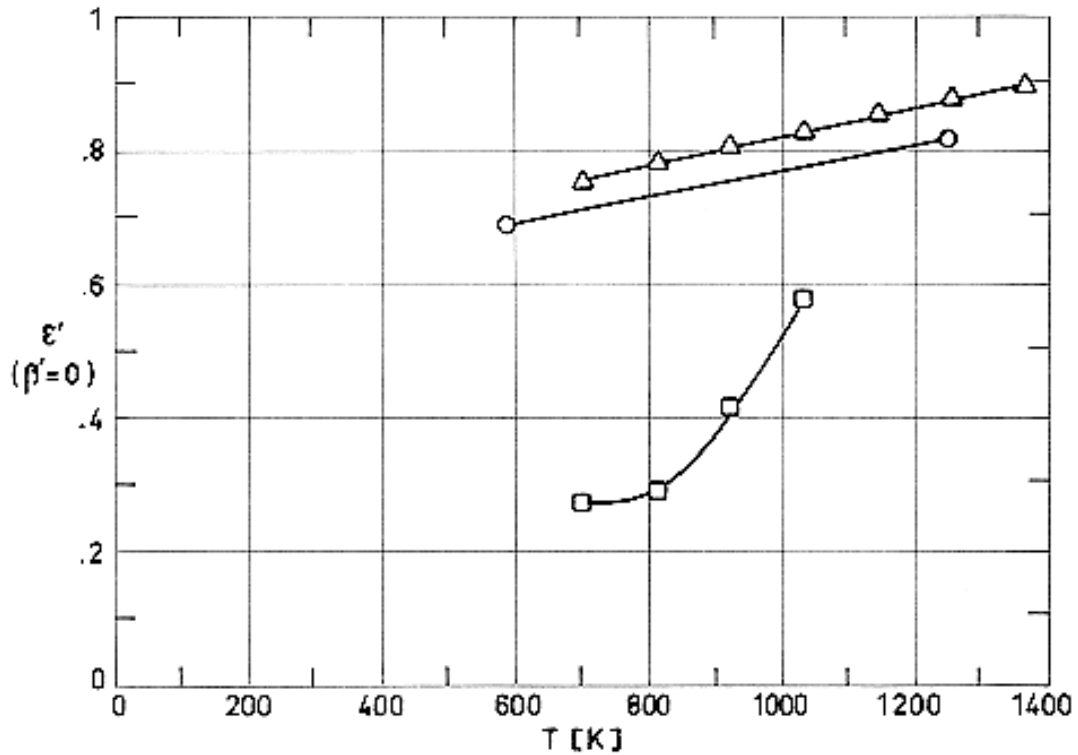
Note: non-si units are used in this figure

Figure 6-12: Normal total emittance, ε', of Inconel as a function of temperature, *T*.

From Wood, Deem & Lucks (1961) [76].

Explanation

Key	Description	Test Method	Comments
○	Stably oxidized at 1370 K.	Thermopile detector. Comparison blackbody. T measured with thermocouples. Resistance-heated specimens.	Measured in air. Data from smooth curves.
□	As rolled.		
△	Heated in air for 15 min at 1420 K.		

NOTE   Emittance of Nickel Alloys (INCONEL X).
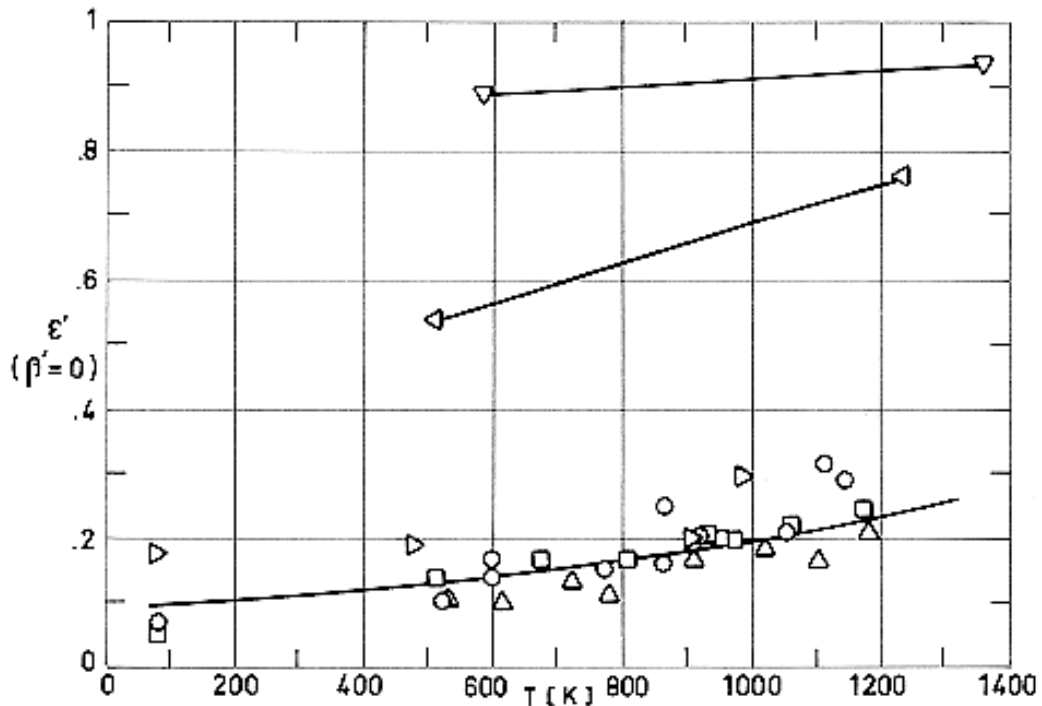
Note: non-si units are used in this figure

Figure 6-13: Normal total emittance, ε′, of Inconel X as a function of temperature, *T*.

From Wood, Deem & Lucks (1961) [76].

Explanation

Key	Description	Test Method	Comments
○	Oxidized.	Resistance-heated specimens. Thermistor-bolometer detector. Comparison blackbody. T measured with thermocouples.	Measured in vacuum. Data from smooth curves.
□	As received or wiped clean.		
△	Polished.		
▽	Stably oxidized at 1370 K.	Thermopile detector. Comparison blackbody. T measured with thermocouples.	Measured in air. Data from smooth curves.
▷	Polished.	Total-radiation detector. Comparison blackbody. T measured with thermocouples.	Measured in helium at 1,33x10⁻³ Pa.
◁	After prolonged heating and cycling above 1370 K. (Some oxide indicated).		

NOTE   Emittance of Platinum.
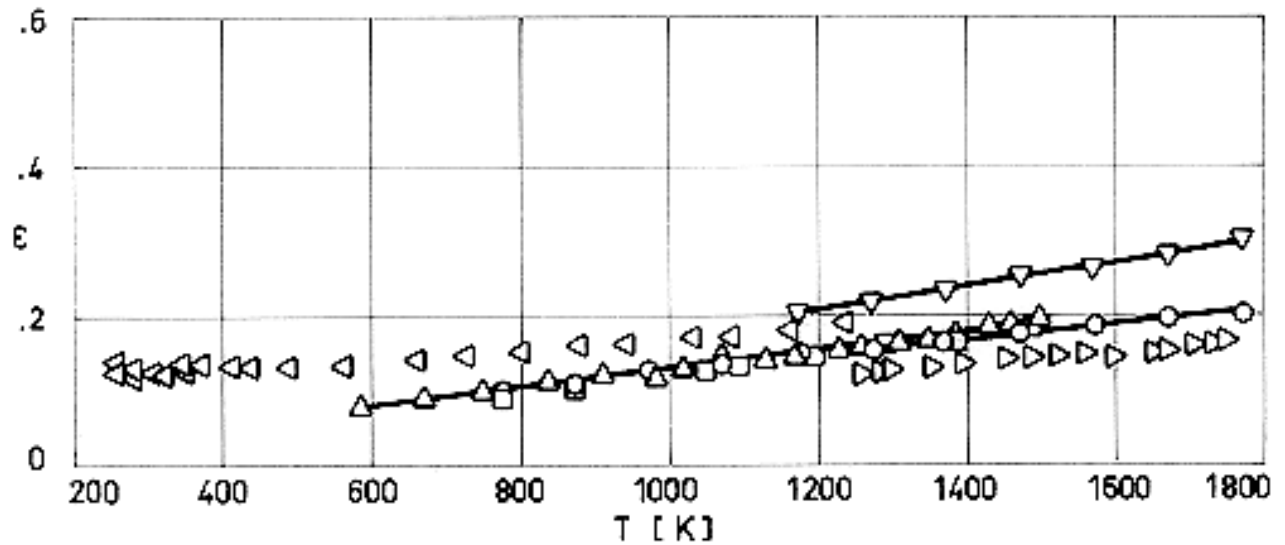
Note: non-si units are used in this figure

Figure 6-14: Hemispherical total emittance, ε, of Platinum as a function of temperature, T.

From Touloukian & DeWitt (1970) [74].

Explanation

Key	Description	Test Method	Comments
○	Clean polished surface.		Measured in vacuum (1,33x10⁻² to 1,33x10⁻⁴ Pa). Reported error ± 4%.
□	Clean rolled.		
△			Measured in vacuum.
▽	Flashed in vacuum at 2023 K.		Measured in vacuum (<6,6x10⁻⁴ Pa). Data from smooth curve. Reported error ± 2,5%.
▷	Thin strip.		Reported error <8%.
◁	Disc. Polished on a cloth lap saturated with water and alumina.		Measured in vacuum (6,65x10⁻³ Pa).

NOTE   Emittance of Silver.

Note: non-si units are used in this figure
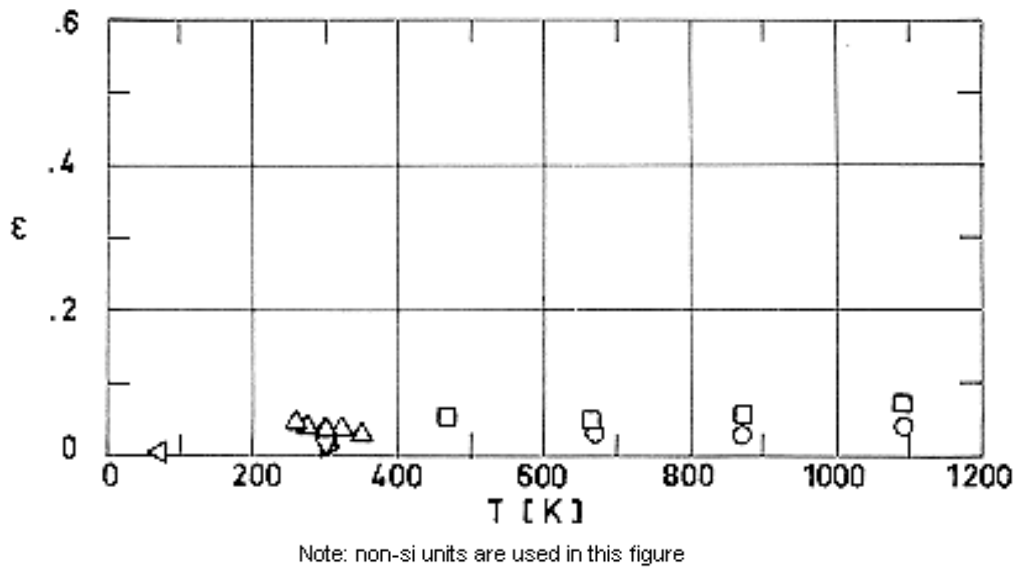
Figure 6-15: Hemispherical total emittance, ε, of Silver as a function of temperature, T.

From Touloukian & DeWitt (1970) [74].

Explanation

Key	Description	Test Method	Comments
○	Commercial rolled plate, 99,9 pure. Ground with 600 grit carborundum and polished on a wet cloth lap with unlevigated jewellers rouge.		Measured in vacuum ($1,33 \times 10^{-3}$ Pa). Reported error <10%.
□	Same as ○ after thermal etching.		
△	Commercial sheet. Cleaned with sodium dichromate and dilute nitric acid solutions. Buffed on a felt wheel, cleaned with carbon tetrachloride and acetone.		Measured in vacuum ($1,33 \times 10^{-4}$ Pa). Data from smooth curve. Reported error 3%.
▽	Silver plating ($7,62 \times 10^{-6}$ m thick). Matte surface.		Measured in vacuum ($< 4 \times 10^{-4}$ Pa). Reported error $\pm$ 20%.
▷	Same as ▽ except lume surface.		
◁	Solvent cleaned.	Calorimetric absorptance. From 300 K blackbody. LN$_2$ boil-off rate measured. Authors assumed $\alpha = \varepsilon$.	Measured in vacuum ($1,33 \times 10^{-4}$ to $1,33 \times 10^{-5}$ Pa). Reported error 5%.

6.4 Emittance of metallized films

Data regarding the hemispherical total emittance of metallized plastic films are presented in Figure 6-16 to Figure 6-26. These data have been arranged as is indicated in the following table.

Metallized Plastic Film		Total Emittance Modifier	Variable	Fig	Comments
Metal	**Plastic**				
Aluminium	Mylar	Hemispherical	t_c [a]	Figure 6-16	T = 307 K.
Copper	Mylar	Hemispherical	t_c		T = 307 K.
Gold	Mylar	Hemispherical	t_c	Figure 6-17	T = 307 K.
Gold-Aluminium	Mylar	Hemispherical	t_c		T = 307 K.
Silver	Mylar	Hemispherical	t_c	Figure 6-18	T = 307 K.
SiO-Silver	Mylar	Hemispherical	t_c	Figure 6-19	T = 307 K.
Aluminium	Kapton	Hemispherical	T		For several values of t_c.
Aluminium	Kapton	Hemispherical	t_c	Figure 6-20	T = 300 K.
Aluminium	Kapton	Hemispherical	t_c		T = 400 K.
Gold	Kapton	Hemispherical	T	Figure 6-21	For several values of t_c.
Silver	Kapton	Hemispherical	T		For several values of t_c.
				Figure 6-22	
				Figure 6-23	
				Figure 6-24	
				Figure 6-25	
				Figure 6-26	

[a] t_c is the metallic coating thickness.

NOTE   Emittance of Aluminium Coated Mylar.
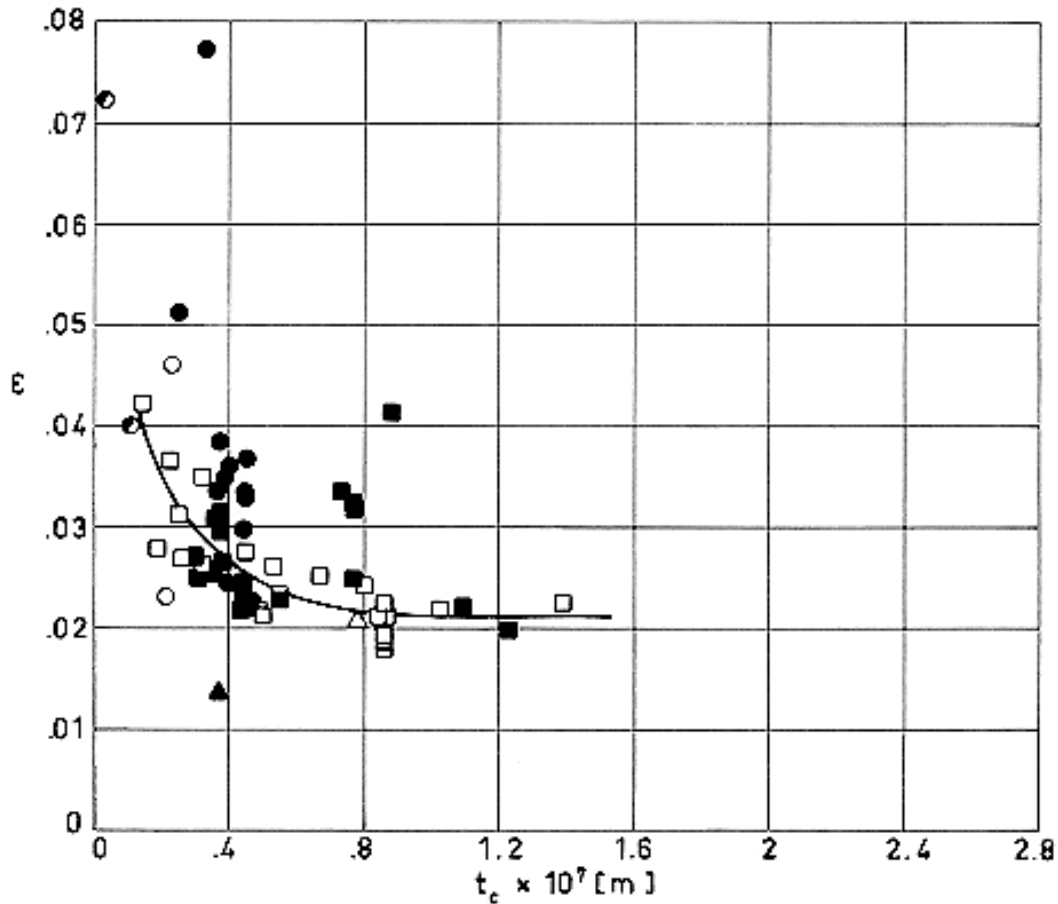
Figure 6-16: Hemispherical total emittance, ε, of Aluminized Mylar as a function of coating thickness, t_c.

The emitting surface is coated. Solid data points represent two sided coating, while open data points are for one sided coating. ◑ indicates that no details are given in the source to decide whether the specimen was single or double coated.

Explanation

Film Thickness, $t \times 10^6$ [m]	Test Method	References
6,35	t_c: Electrical Resistance. Parallel bar electrode. ε: receiver Disc exchanging heat with a closely spaced parallel sample. Sample Temperature: 307 K. Chamber Pressure: $1,33 \times 10^{-4}$ Pa.	◐: ADL (1964) [1] ☐■: ADL (1966) [2]. △: Ruccia & Hinckley (1967) [59]. ▬: Coston (1967) [13].

NOTE   Emittance of Copper Coated Mylar.
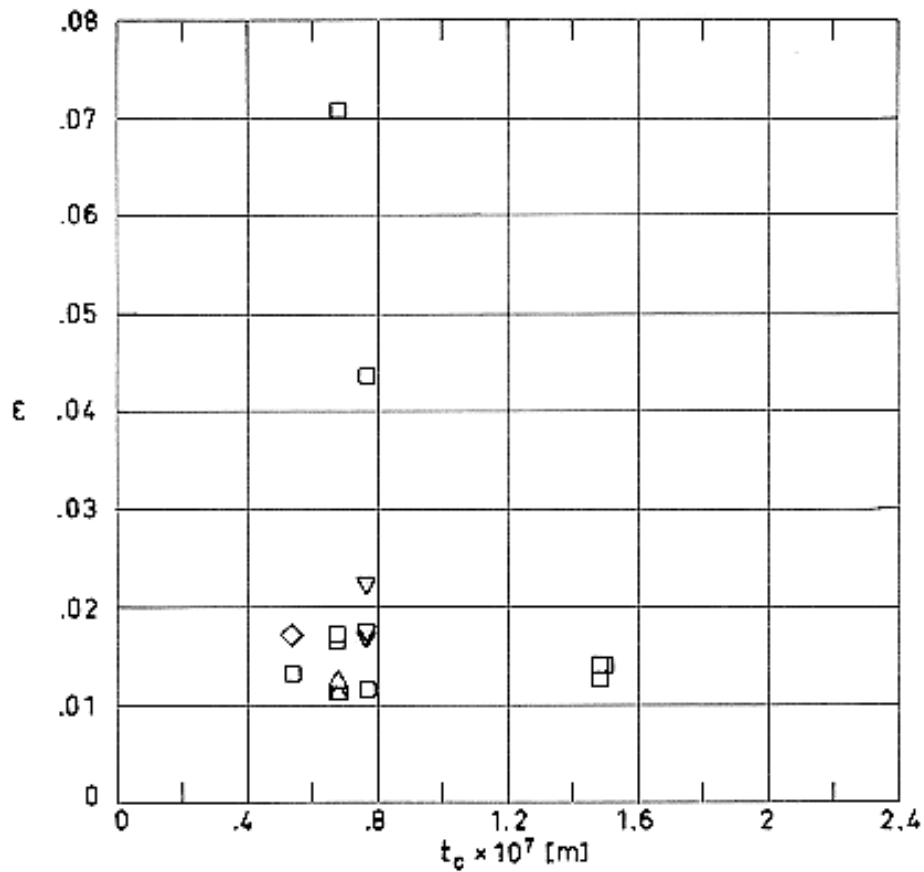
Note: non-si units are used in this figure

Figure 6-17: Hemispherical total emittance, ε, of Copper on Mylar as a function of coating thickness, t_c.

The emitting surface is coated. One sided coating in all cases. $\diamondsuit$ and ∇ are overcoated with SiO.

Explanation

Film Thickness, tx10^6 [m]	Test Method	References
6,35	t_c: Electrical Resistance. Parallel bar electrode. ε: receiver Disc exchanging heat with a closely spaced parallel sample. Sample Temperature: 307 K. Chamber Pressure: 1,33x10^{-4} Pa.	$\square$ and $\diamondsuit$: ADL (1966) [2] $\triangle$ and ∇ : Ruccia & Hinckley (1967) [59].

NOTE   Emittance of Gold Coated Mylar.
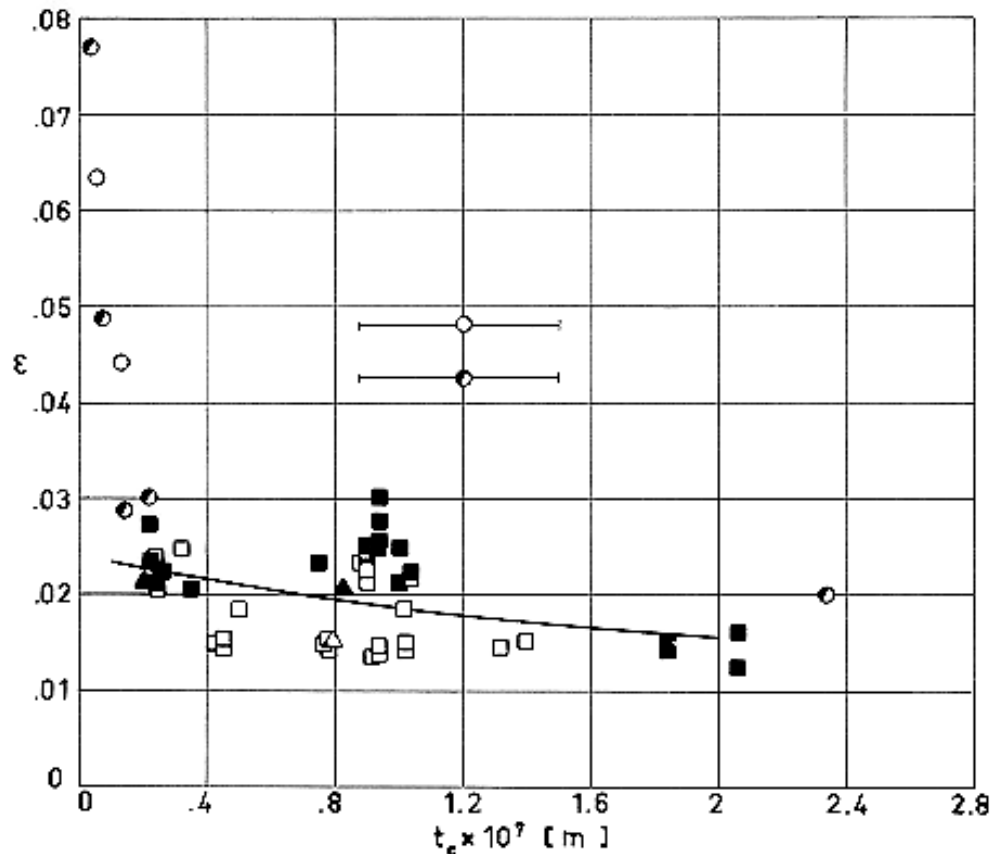
Note: non-si units are used in this figure

Figure 6-18: Hemispherical total emittance, ε, of Goldized Mylar as a function of coating thickness, t_c.

The emitting surface is coated. Solid data points represent two sided coating, while open data points are for one sided coating. ◐ indicates that no details are given in the source to decide whether the specimen was single or double coated.

Explanation

Film Thickness, tx10^6 [m]	Test Method	References
6,35	t_c: Electrical Resistance. Parallel bar electrode. ε: receiver Disc exchanging heat with a closely spaced parallel sample. Sample Temperature: 307 K. Chamber Pressure: 1,33x10^{-4} Pa.	○◐: ADL (1964) [1] □■: ADL (1966) [2]. △: Ruccia & Hinckley (1967) [59]. ▬: Coston (1967) [13].

NOTE   Emittance of Gold on Aluminized Mylar.
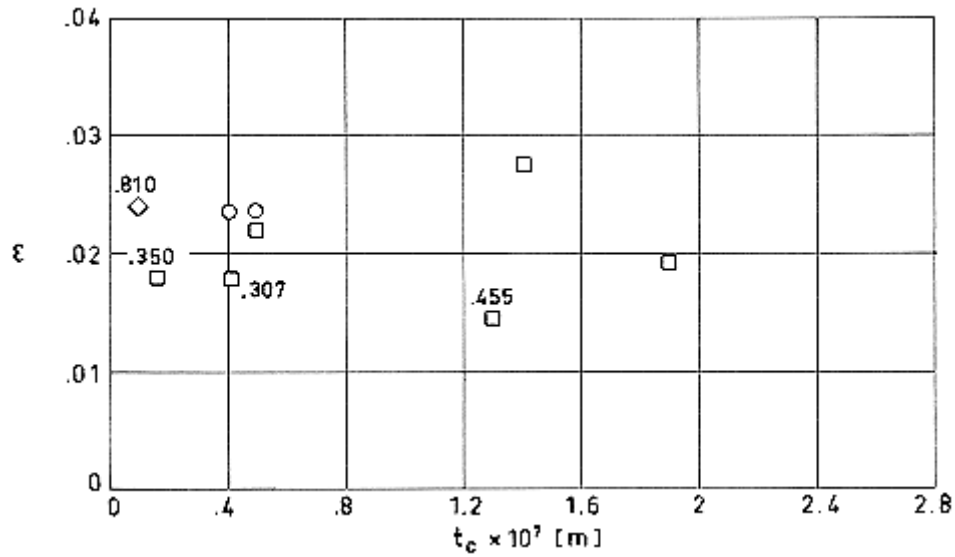
Note: non-si units are used in this figure

Figure 6-19: Hemispherical total emittance, ε, of Gold on Double Aluminized Mylar as a function of Gold thickness, t_c.

The emitting surface is the goldized one. Numbers give the Aluminium layer thickness measured in the same units as t_c . $\diamond$: Silver instead of Aluminium.

Explanation

Film Thickness, tx10^6 [m]	Test Method	References
6,35	t_c: Electrical Resistance. Parallel bar electrode. ε: receiver Disc exchanging heat with a closely spaced parallel sample. Sample Temperature: 307 K. Chamber Pressure: 1,33x10^{-4} Pa.	$\bigcirc$: ADL (1964) [1] $\square$ and $\diamond$: ADL (1966) [2].

NOTE   Emittance of Silver Coated Mylar.
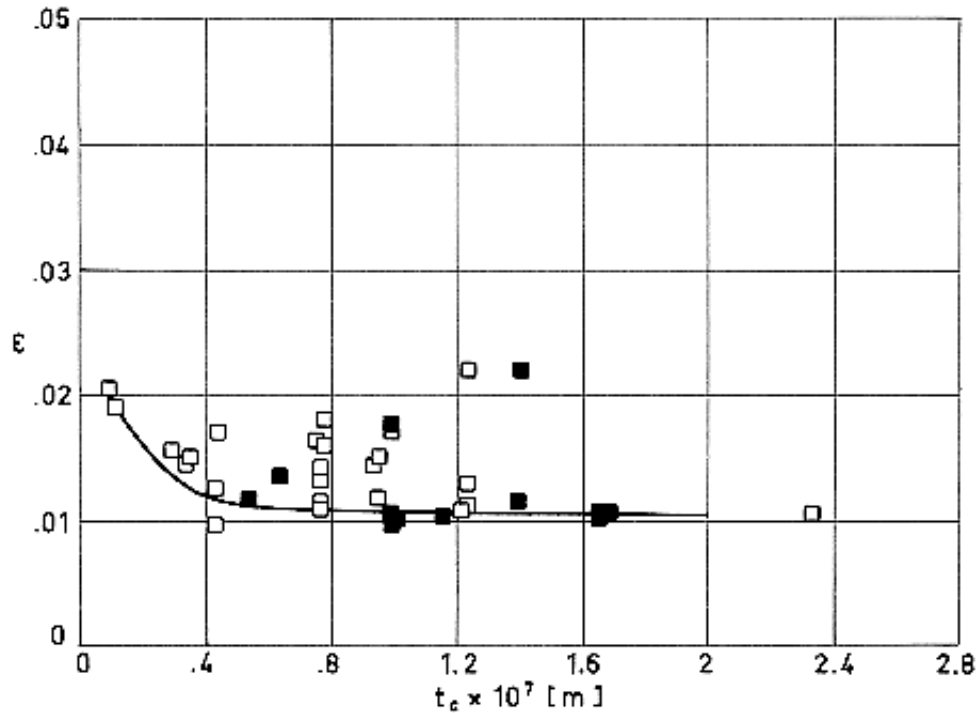
Note: non-si units are used in this figure

Figure 6-20: Hemispherical total emittance, ε, of Silvered Mylar as a function of coating thickness, t_c.

The emitting surface is coated. Solid data points represent two sided coating, while open data points are for one sided coating.

Explanation

Film Thickness, tx10^6 [m]	Test Method	References
6,35	t_c: Electrical Resistance. Parallel bar electrode. ε: receiver Disc exchanging heat with a closely spaced parallel sample. Sample Temperature: 307 K. Chamber Pressure: 1,33x10^{-4} Pa.	▢■: ADL (1966) [2]. ▬: Coston (1967) [13].

NOTE   Emittance of Silver Coated Mylar with SiO Overcoating.
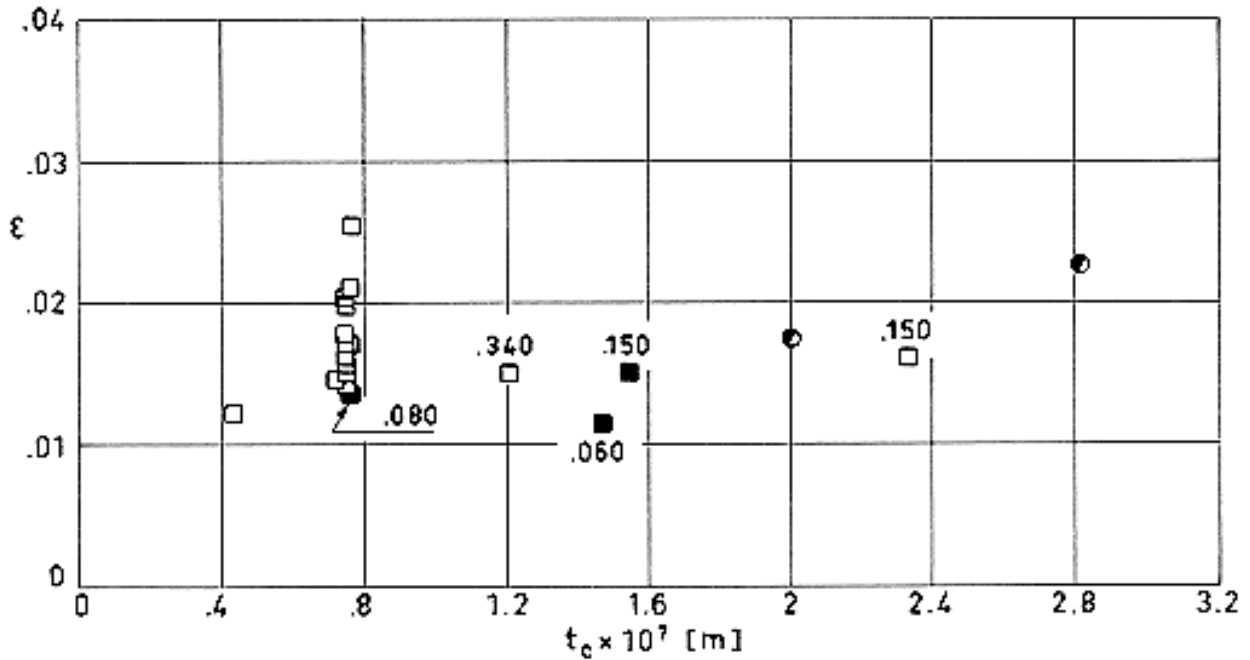
Note: non-si units are used in this figure

Figure 6-21: Hemispherical total emittance, ε, of Silvered Mylar overcoated with Silicon Monoxide as a function of Silver thickness, t_c.

The emitting surface is overcoated. Solid data points represent two sided coating plus overcoating, while open data points are for one sided coating plus overcoating. ◑ indicates that no details are given in the source to decide whether the specimen was single or double coated. Numbers give the overcoating thickness measured in the same units as t_c. Overcoating thickness of white squares is $0,75 \times 10^{-7}$ m unless otherwise indicated in the figure.

Explanation

Film Thickness, $t \times 10^6$ [m]	Test Method	References
6,35	t_c: Electrical Resistance. Parallel bar electrode. ε: receiver Disc exchanging heat with a closely spaced parallel sample. Sample Temperature: 307 K. Chamber Pressure: $1,33 \times 10^{-4}$ Pa.	◑: ADL (1964) [1] ☐■: ADL (1966) [2].

NOTE   Emittance of Aluminium Coated Kapton.

The hemispherical total emittance as a function of temperature, for several values of the coating thickness, is given in Figure 6-22. The influence of thickness, for representative temperatures, is shown in Figure 6-23 and Figure 6-24.

The table below concerns these three figures.

Explanation

Key	Film Thickness x10⁶ [m]	Coating Thickness x10⁷ [m]	Test Method	References
○		0,3		Coston (1967) [13].
□	12,7	~0,4	Calorimetrically. Specimens attached to a 2,54x10⁻² m diameter cylinder internally heated. Optical flat monitor-Interferometry	Cunnington, Zierman, Funai & Lindahn (1967) [17].
△	12,7	~0,6		
▲	12,7	~0,6		
◭	25,4	0,65		
◭		0,7		Coston (1967) [13].
▽		0,8		
▼	25,4	0,8	Same as □ .	Cunnington et al. (1967) [17]
▽		0,85		Coston (1967) [13].
▼	25,4	0,85	Same as □ .	Cunnington et al. (1967) [17]
▷	25,4	1,0		
▶		1,05	Same as □ .	Coston (1967) [13].
◁		2,2		
◀	25,4	2,2	Same as □ .	Cunnington et al. (1967) [17]

NOTE   All the data from Cunnington et al (1967) [17] are for single-aluminized specimens radiating from the coated side. No details are given by Coston (1967) [13] to decide whether the samples were single or double-coated.
Emittance of Aluminium Coated Kapton.

Note: non-si units are used in this figure
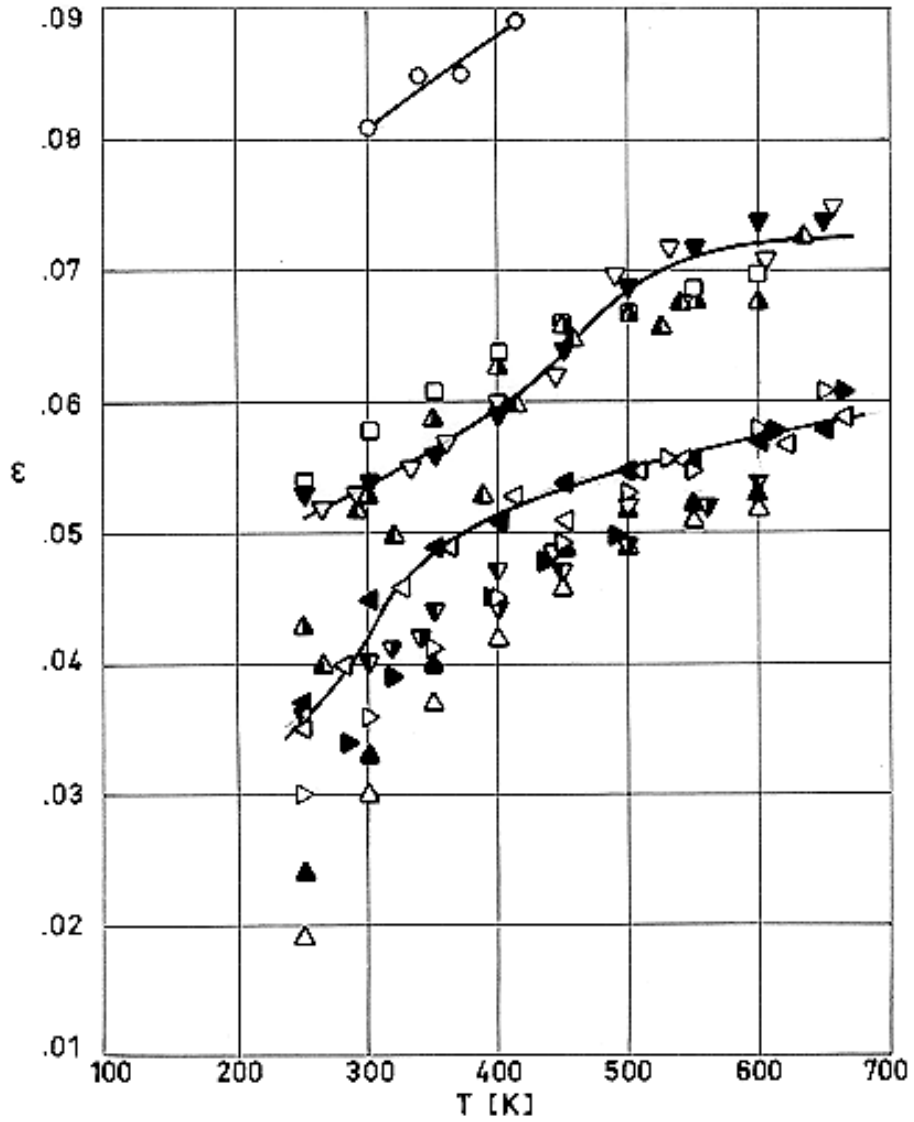
Figure 6-22: Hemispherical total emittance, ε, of Aluminized Kapton as a function of temperature, *T*.
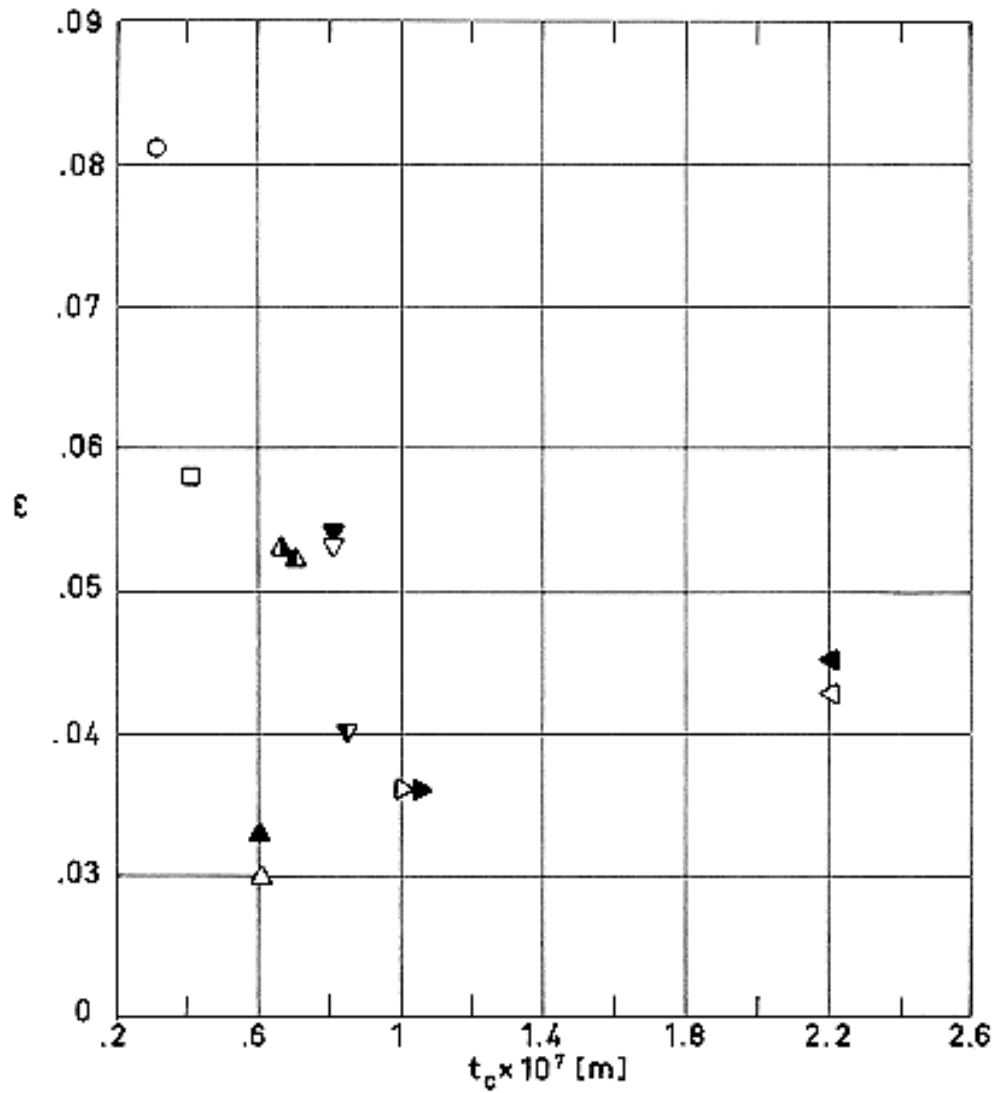
Note: non-si units are used in this figure

Figure 6-23: Hemispherical total emittance, ε, of Aluminized Kapton as a function of coating thickness, t_c, for $T = 300$ K.
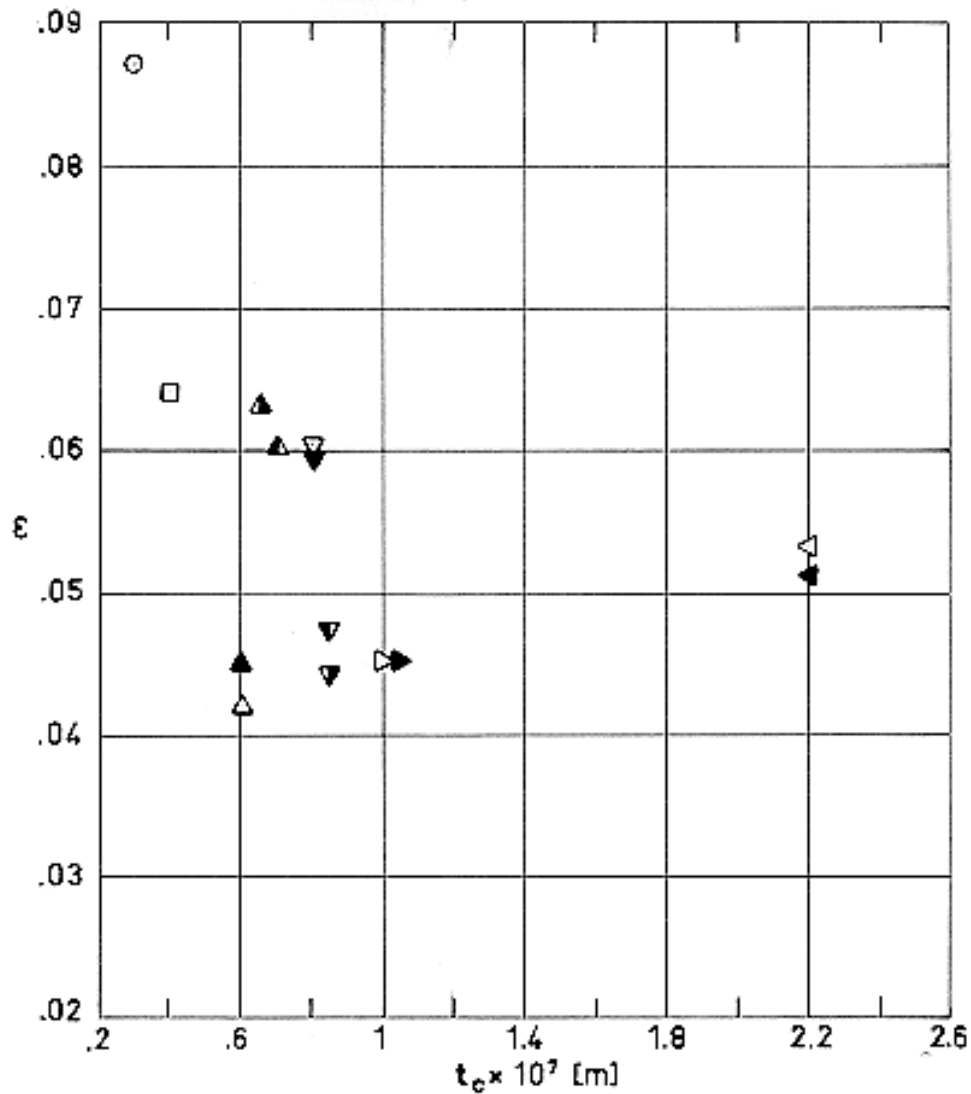
Note: non-si units are used in this figure

Figure 6-24: Hemispherical total emittance, ε, of Aluminized Kapton as a function of coating thickness, t_c, for $T = 400$ K.

Emittance of Gold Coated Kapton.
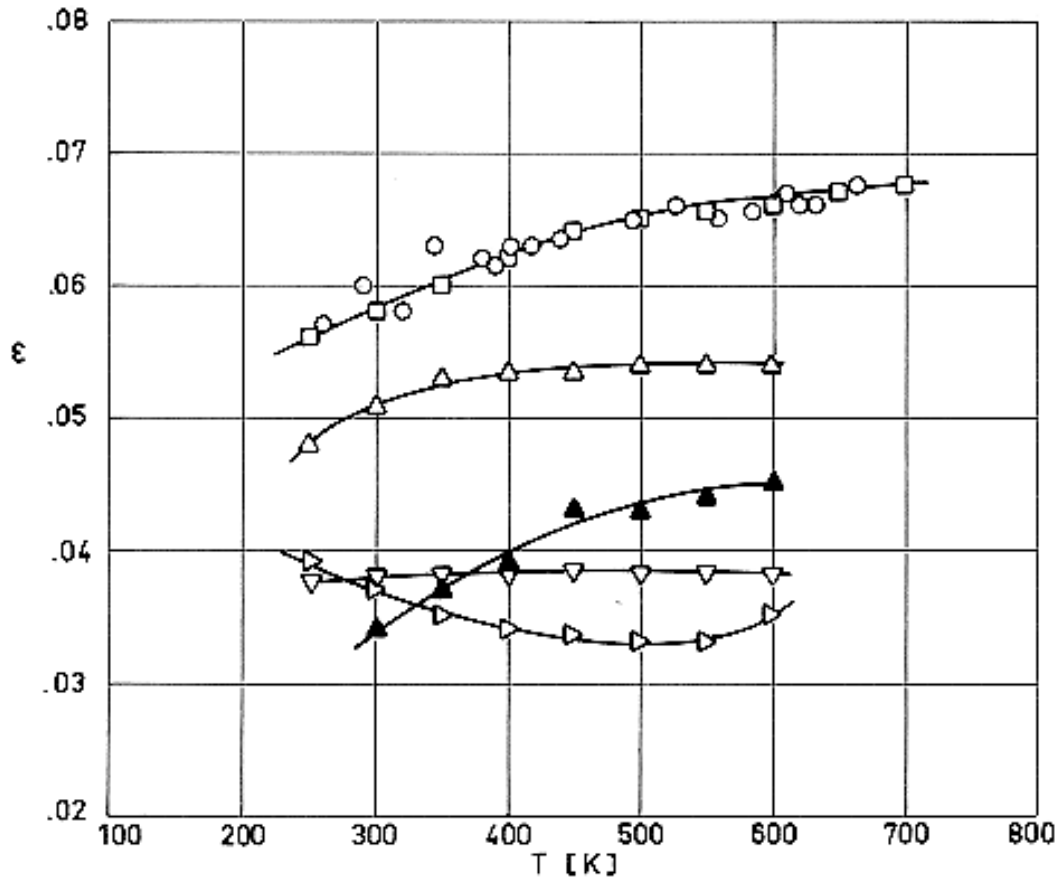
Note: non-si units are used in this figure

Figure 6-25: Hemispherical total emittance, ε, of Silgle-Goldized Kapton as a function of temperature, T.

Explanation

Key	Film Thickness x10^6 [m]	Coating Thickness x10^7 [m]	Test Method	References
○				Coston (1967) [13]
□			ε: Calorimetrically. Specimens were attached to a 2,54x10^{-2} m diameter cylinder heated internally.	Cunnington, Zierman, Funai & Lindahn (1967) [17].
△	12,7			
▲	12,7			
▽	25,4	0,6	t_c: Optical flat monitor-interferometer.	
▷	25,4	1,0	ε: Calorimetrically as above.	

NOTE   Emittance of Silver Coated Kapton.
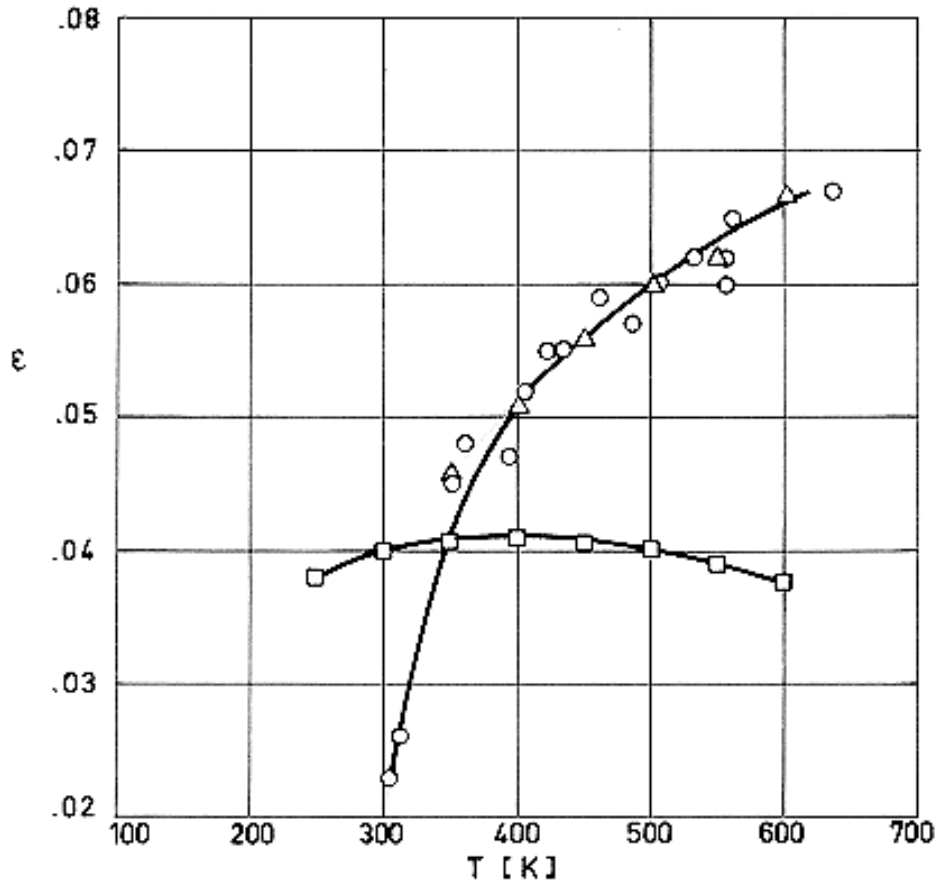
Note: non-si units are used in this figure

Figure 6-26: Hemispherical total emittance, *ε*, of Silgle-Silvered Kapton as a function of temperature, *T*.

Explanation

Key	Film Thickness x10⁶ [m]	Coating Thickness x10⁷ [m]	Test Method	References
○				Coston (1967) [13].
□	25,4	0,7	t_c: Optical flat monitor-interferometer. $ε$: Calorimetrically.	Cunnington, Zierman, Funai & Lindahn (1967) [17].
△	12,7		$ε$: Calorimetrically. Specimens were attached to a 2,54x10⁻² m diameter cylinder heated internally.	

6.5 Absorptance of metallic foils

Data regarding spectral absorptance, α'_λ, and solar absorptance, α_s, of metallic foils are given in the following pages. These data have been arranged as is indicated below.

Metal	$\alpha'_\lambda(\lambda)$ Figure	$\alpha_s (T)$ Figure
Aluminium	Figure 6-27	Figure 6-28
Copper	Figure 6-29	Figure 6-30
Gold	Figure 6-31	Figure 6-32
Molybdenum	Figure 6-33	Figure 6-34
Nickel	Figure 6-35	Figure 6-36
Incoel	Figure 6-37	Figure 6-38
Platinum	Figure 6-39	Figure 6-40
Silver	Figure 6-41	Figure 6-42

In these figures, β is the angle between the surface normal and the direction of the incident flux, λ is the wavelength of incoming radiation, and T the temperature of the sample.

Absorptance of Aluminium.
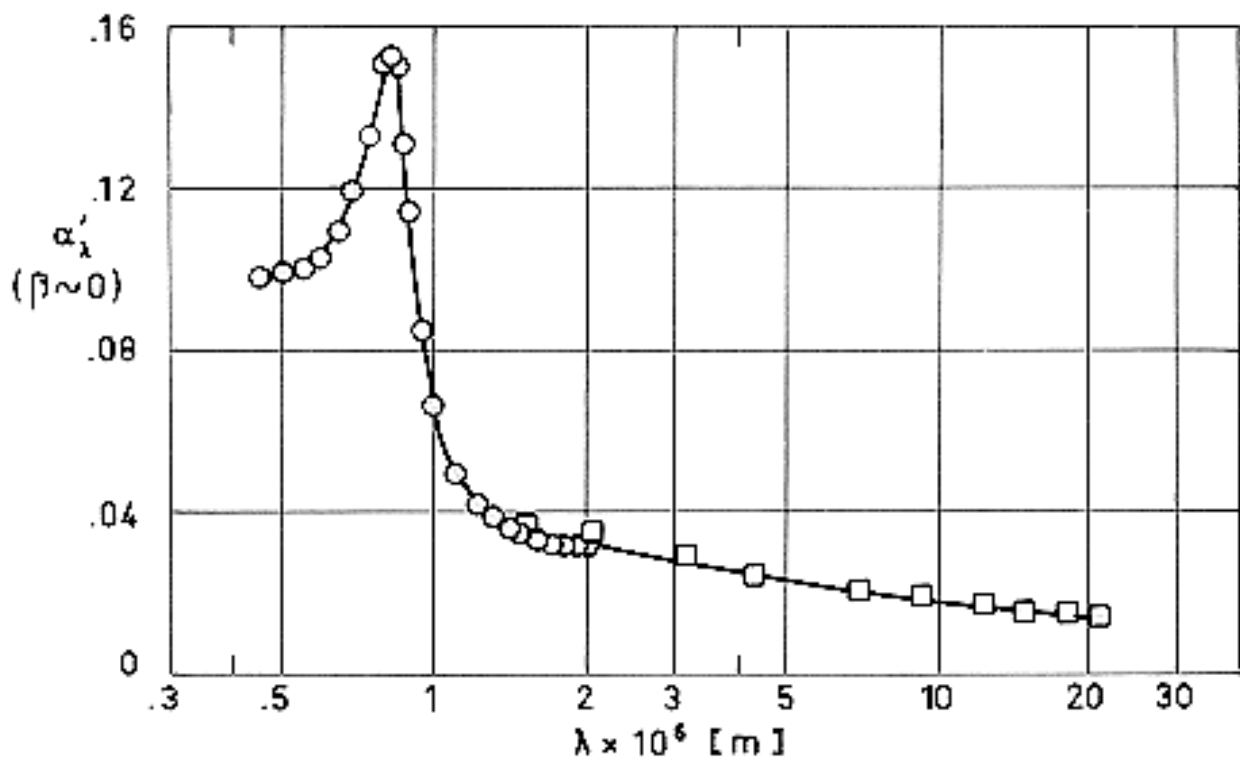
Note: non-si units are used in this figure

Figure 6-27: Normal spectral absorptance, α'_λ, of Aluminium as a function of wavelength, λ.

From Touloukian & DeWitt (1970) [74].

Explanation

Key	Description	Test Method	Comments
○	Evaporated film; evaporation rate 3x10⁻⁸ m.s⁻¹ at 2,67x10⁻³ Pa. Aged 8 days before measurement.		β ~10°. Measured in vacuum. Reported error ± 1,4%. T = 298 K.
□	Aluminium foil.	Heated cavity at approx. 1056 K with platinum reference. Authors assumed $\alpha = 1-R$ $(2\pi,25°)$.	β ~25°. Measured in dry nitrogen. T = 306 K.
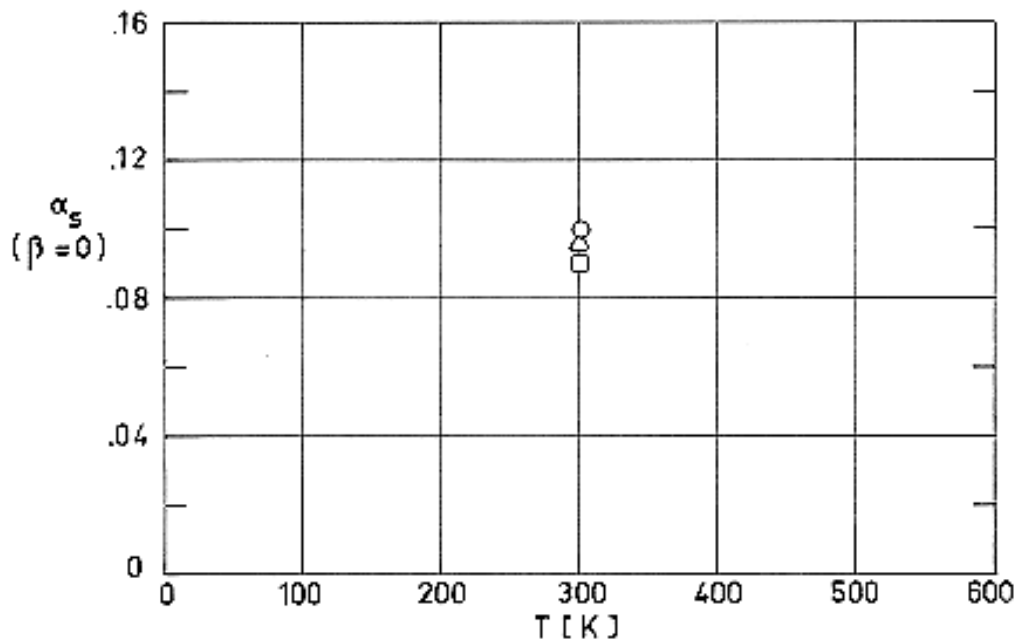
Note: non-si units are used in this figure

Figure 6-28: Normal solar absorptance, α_s, of Aluminium as a function of temperature, T.

From Touloukian & DeWitt (1970) [74].

Explanation

Key	Description	Test Method	Comments
○	Pure. 3x10⁻⁷ m thick opaque layer on glass. Freshly prepared.	Calculated from 1−ρ.	
□	Different sample. Same specimen and conditions as ○.		
△	99,99 pure. Electropolished.	Calculated from spectral reflectance.	

NOTE   Absorptance of Copper.
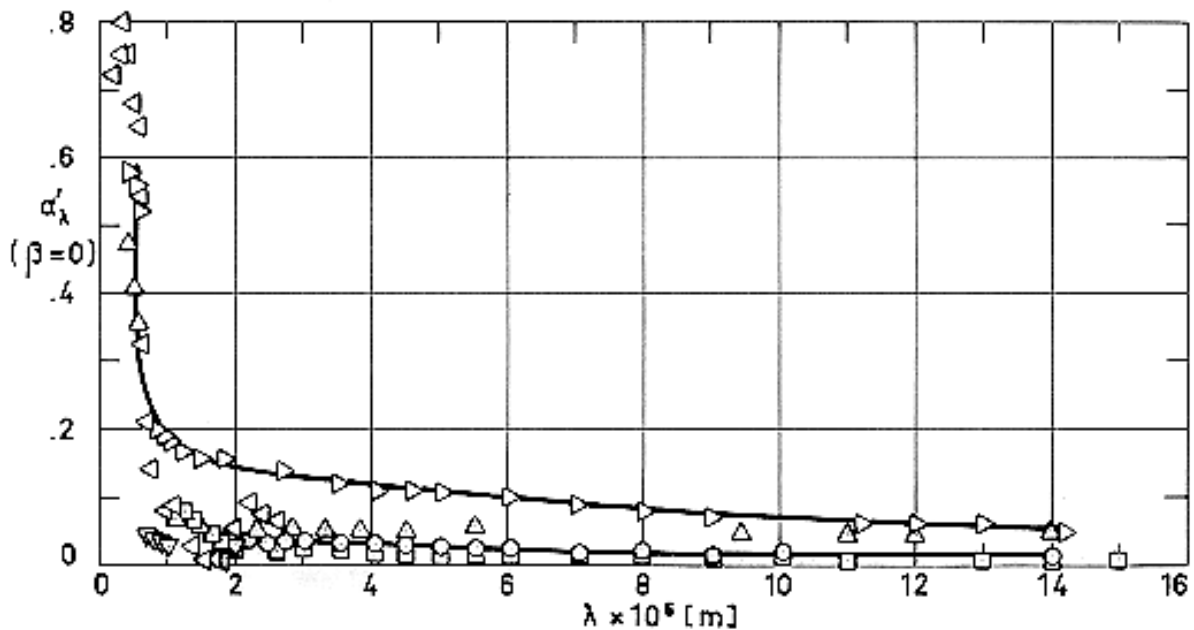
Note: non-si units are used in this figure

Figure 6-29: Normal spectral absorptance, α'_λ, of Copper as a function of wavelength λ.

From Touloukian & DeWitt (1970) [74].

Explanation

Key	Description	Test Method	Comments
◯	Mechanically polished (surface roughness $2x10^{-8}$ m peak to peak, $5x10^{-6}$ m lateral).		Measured in air. Data from smooth curve. T = 294 K.
▢	Same as ◯ except heated at 922 K for 3 h.		
△	Same as ◯ except heated at 1222 K for 102 h.		
▽	Electropolished.	Calculated from $1-\rho$.	T = 294 K.
▷	Roughened with sand paper, surface roughness $1,25x10^{-6}$ m.		
◁			Data from smooth curve. T ~298 K.
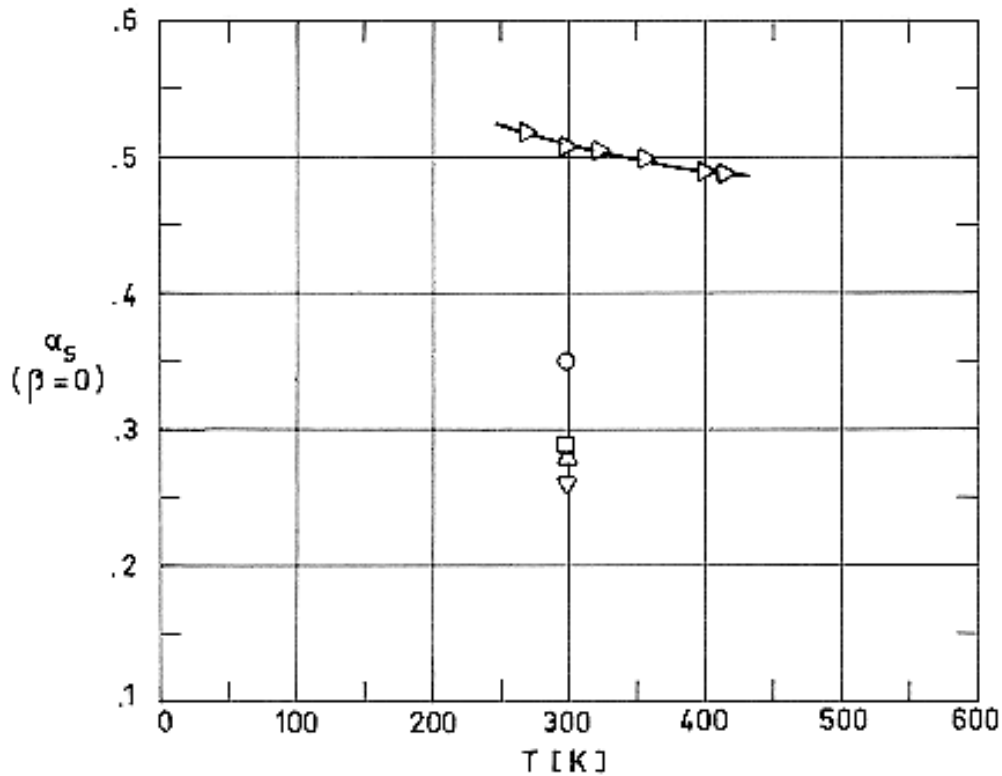
Note: non-si units are used in this figure

Figure 6-30: Normal solar absorptance, α_s, of Copper as a function of temperature T.

From Touloukian & DeWitt (1970) [74].

Explanation

Key	Description	Test Method	Comments
○	99,9 min. Cu. Turned; freshly prepared.	Calculated from $1-\rho$.	
□	Same as ○ except machine polished. Freshly prepared.		
△	Different sample. Same specimen and conditions as □ .		
▽	Different sample. Same specimen and conditions as □ .		
▷	Commercially pure. Cleaned, buffed, cleaned with carbon tetrachloride and acetone.		Measured in vacuum (1,33x10⁻⁴ Pa). Data from smooth curve.

NOTE   Absorptance of Gold.
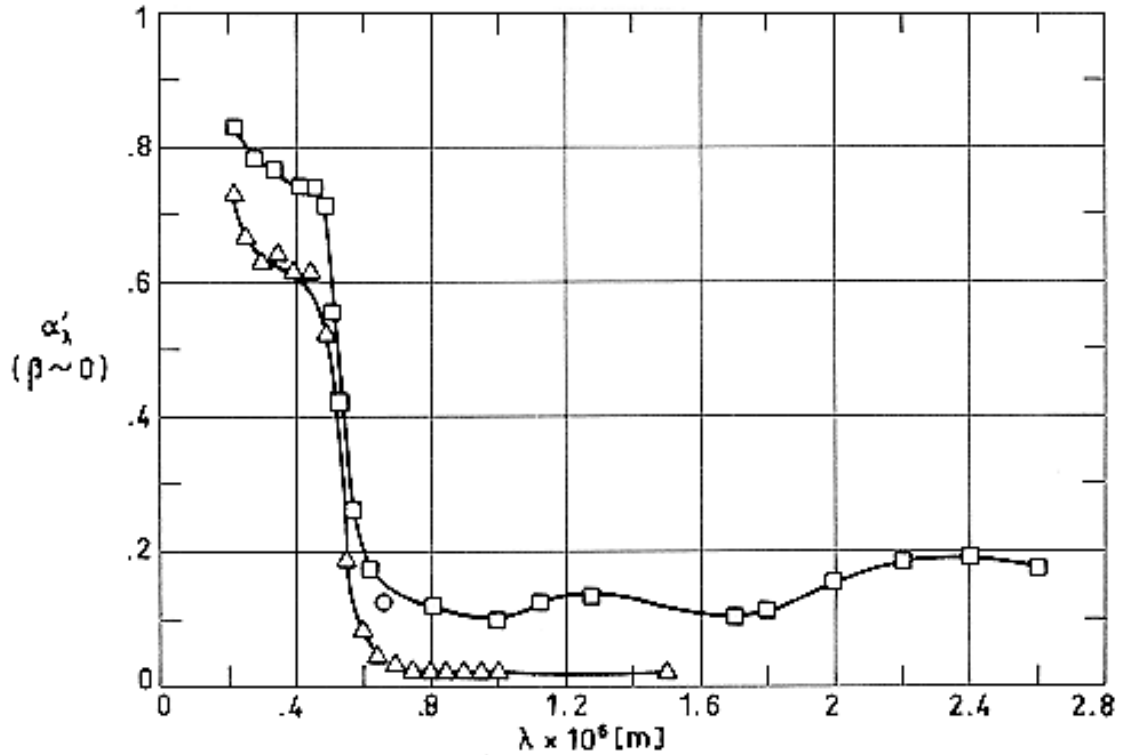
Note: non-si units are used in this figure

Figure 6-31: Normal spectral absorptance, α'_λ, of Gold as a function of wavelengthλ.

$\bigcirc$ and $\square$ from Touloukian & DeWitt (1970) [74]. $\triangle$ from Fussell, Triolo & Jerozal (1963) [22].

Explanation

Key	Description	Test Method	Comments
$\bigcirc$			Measured in burning hydrogen. Temperature range 873 K - 2073 K.
$\square$			Data from curve. T ~ 298 K.
$\triangle$			
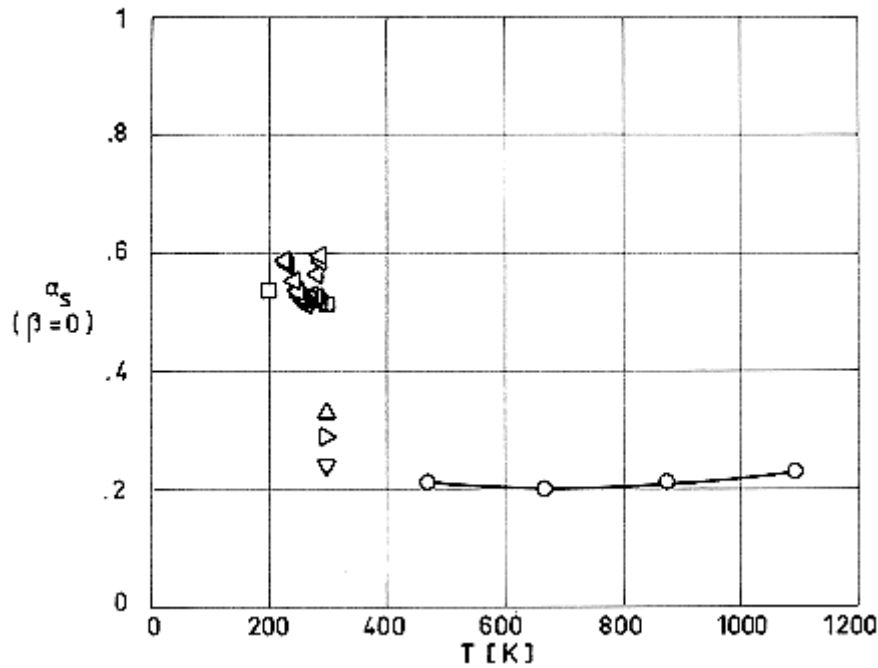
Note: non-si units are used in this figure

Figure 6-32: Normal solar absorptance, α_s, of Gold as a function of temperature T.

From Touloukian & DeWitt (1970) [74].

Explanation

Key	Description	Test Method	Comments
○	99,95 Gold. Ground with 600 grit carborundum and polished on a wet cloth lap.		Measured in vacuum (1,33x10⁻³ Pa). Reported error ≤ 10%.
□	Cleaned in sodium dichromate and dilute nitric acid solutions, buffed, cleaned with carbon tetrachloride and acetone.		Measured in vacuum (1,33x10⁻⁴ Pa). Data from smooth curve. Reported error 4%.
△	Vacuum deposited on buffed titanium.		Reported error 10%.
▽	Vacuum deposited on aluminium.		
▷	Bright foil.		
◁	Commercially pure. Cleaned, buffed, cleaned with carbon tetrachloride and acetone.		Measured in vacuum (1,33x10⁻⁴ Pa). Data from smooth curve.

NOTE   Absorptance of Molybdenum.
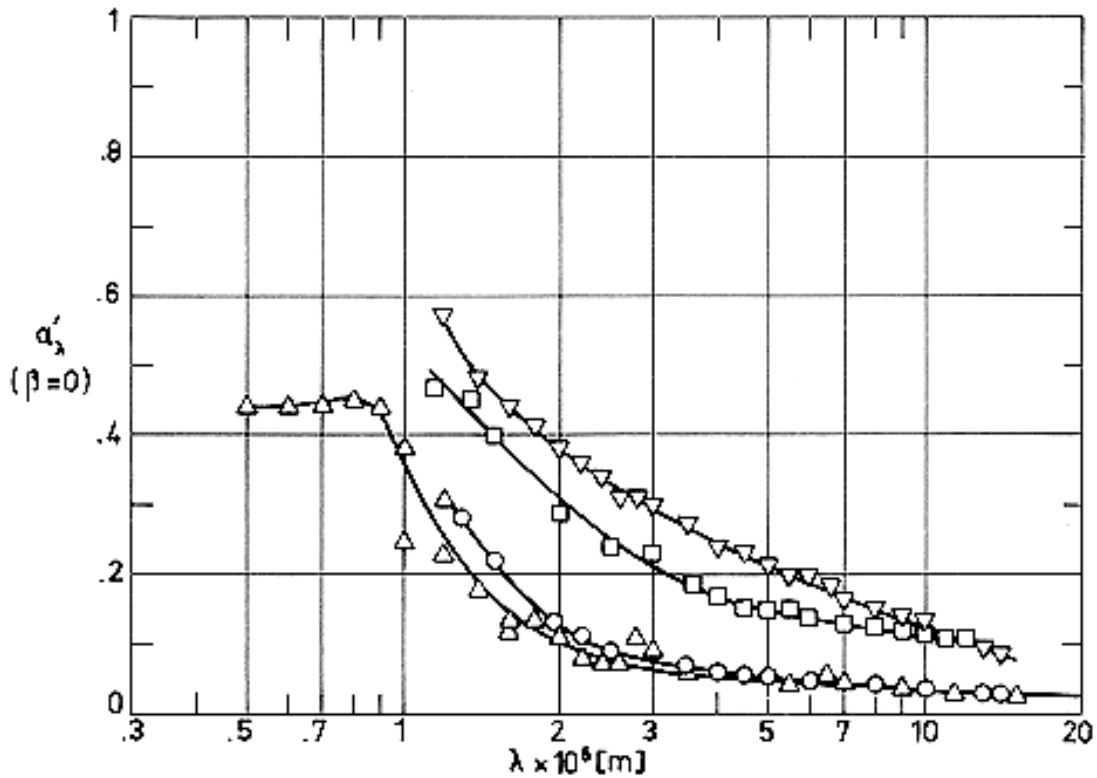
Note: non-si units are used in this figure

Figure 6-33: Normal spectral absorptance, α'_λ of Molybdenum as a function of wavelength λ.

From Touloukian & DeWitt (1970) [74].

Explanation

Key	Description	Test Method	Comments
○	Foil, 1,27x10⁻⁴ m thick. cleaned with acetone.		Measured in air. Data from smooth curve. T = 294 K.
□	Foil, 1,27x10⁻⁴ m thick. cleaned with acetone, heated in vacuum (1,33x10⁻³ Pa) 1 h at 1273 K.		
△	Polished.	Reflectance technique.	
▽	Machined smooth.	Reflectance technique.	
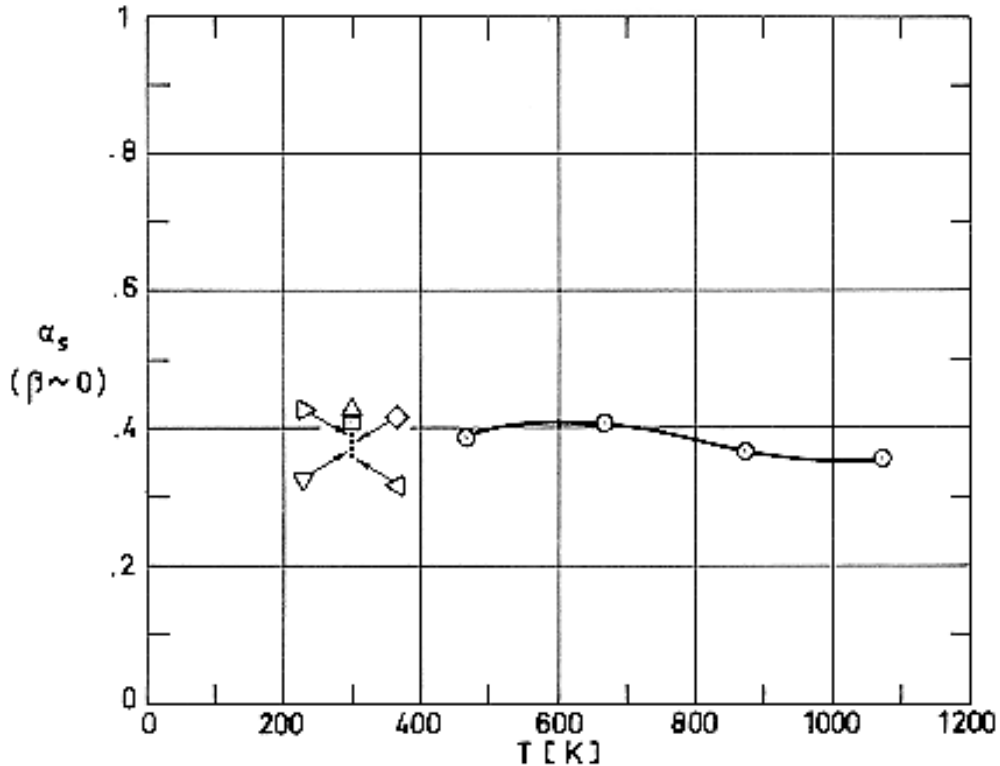
Figure 6-34: Normal solar absorptance, α_s, of Molybdenum as a function of temperature T

. From Touloukian & DeWitt (1970) [74].

Explanation

Key	Description	Test Method	Comments
○	Vacuum arc cast, machined, extruded, recrystallized, rolled. Disk 10^{-3} m thick, ground and polished.		$\beta = 0°$ Measured in vacuum ($1,33 \times 10^{-3}$ Pa).
□	Arc melted, unalloyed, as received.	From spectral reflectance.	$\beta = 9°$ Calculated for above atmosphere conditions.
△	Same as □ .		$\beta = 0°$ Calculated for sea level conditions.
▽	Same as □ except cleaned with liquid detergent.		Same as □ .
▷	Same as ▽ .		Same as △ .

Key	Description	Test Method	Comments
◁	Same as □ except polished.		Same as □.
◇	Same as ◁.		Same as △.

NOTE   Absorptance of Nickel.
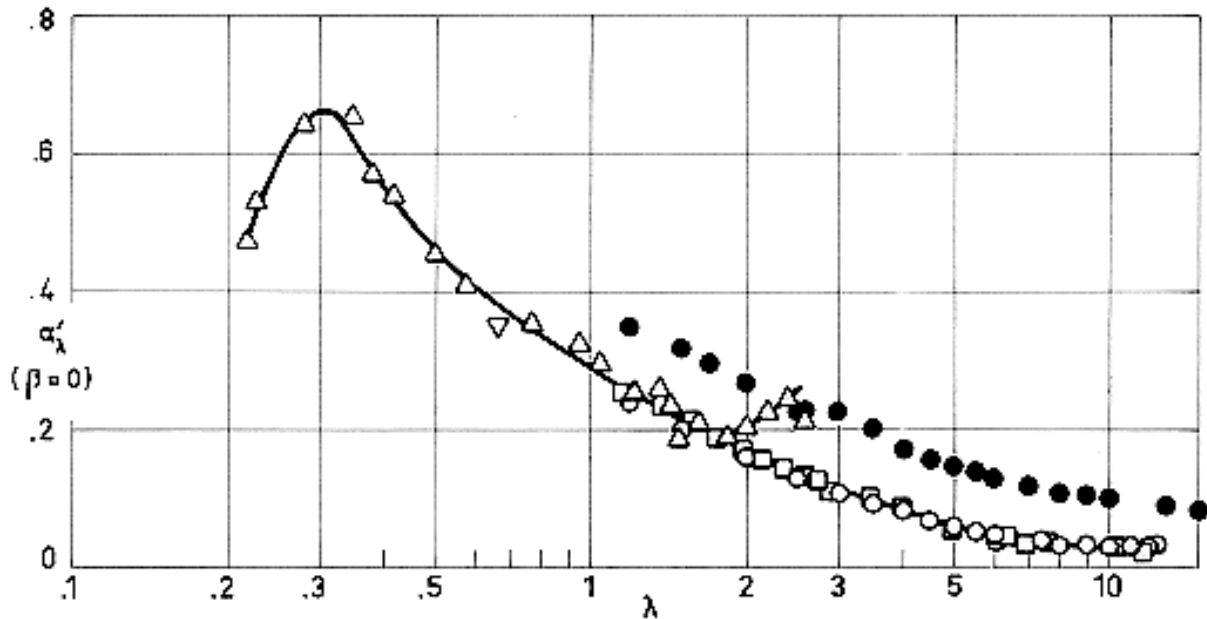
Note: non-si units are used in this figure

Figure 6-35: Normal spectral absorptance, α'_λ of Nickel as a function of wavelength λ

. From Touloukian & DeWitt (1970) [74].

Explanation

Key	Description	Test Method	Comments
○	Mechanically polished with aluminium oxide and cleaned with water (surface roughness $2,5\times10^{-8}$ m peak to peak and $2,5\times10^{-5}$ m lateral).		Measured in air. Data from smooth curve. $T = 298$ K.
●	Polished and cleaned as above. Heated in vacuum: 3 h, 588 K; 3 h, 1089 K; 4 h, 1267 K; and 48 h above 1256 K. Surface roughness (measured after 120 d) $7,5\times10^{-6}$ m peak to peak and $2,5\times10^{-5}$ m lateral.		Data from smooth curve. $T = 298$ K.

Key	Description	Test Method	Comments
□		Holraum.	T = 294 K. Reported error <5%.
△	Foil 7,62x10^{-5} m thick.		Data from smooth curve. $T \sim$ 298 K.
▽			Measured in burning hydrogen. Authors assumed $\alpha = \varepsilon$. T = 873 K.
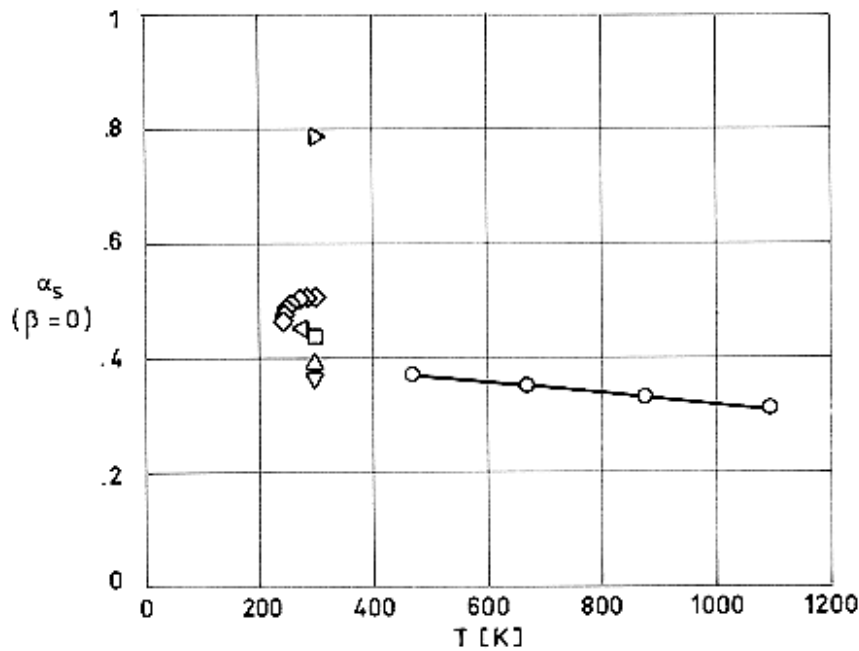
Figure 6-36: Normal solar absorptance, α_s, of Nickel as a function of temperature, T.

From Touloukian & DeWitt (1970) [74].

Explanation

Key	Description	Test Method	Comments
○	Commercially pure. Ground with 600 grit carborundum and polished.		Measured in vacuum (1,33x10⁻³ Pa).
□	Commercial grade. As received.	Spectral reflectance	Computed for sea level conditions.
△	Same as □ except cleaned with liquid detergent.		
▽	Same as □ except polished.		
▷	Same as □ except oxidized in air at red heat for 30 min.		
◁	Electroless nickel. Extraterrestrial.		Reported error 10%.
◇	Commercially pure. Cleaned with carbon tetrachloride and acetone.		Measured in vacuum (1,33x10⁻⁴ Pa). Data from smooth curve.

NOTE   Absorptance of Nickel Alloys (INCOEL).
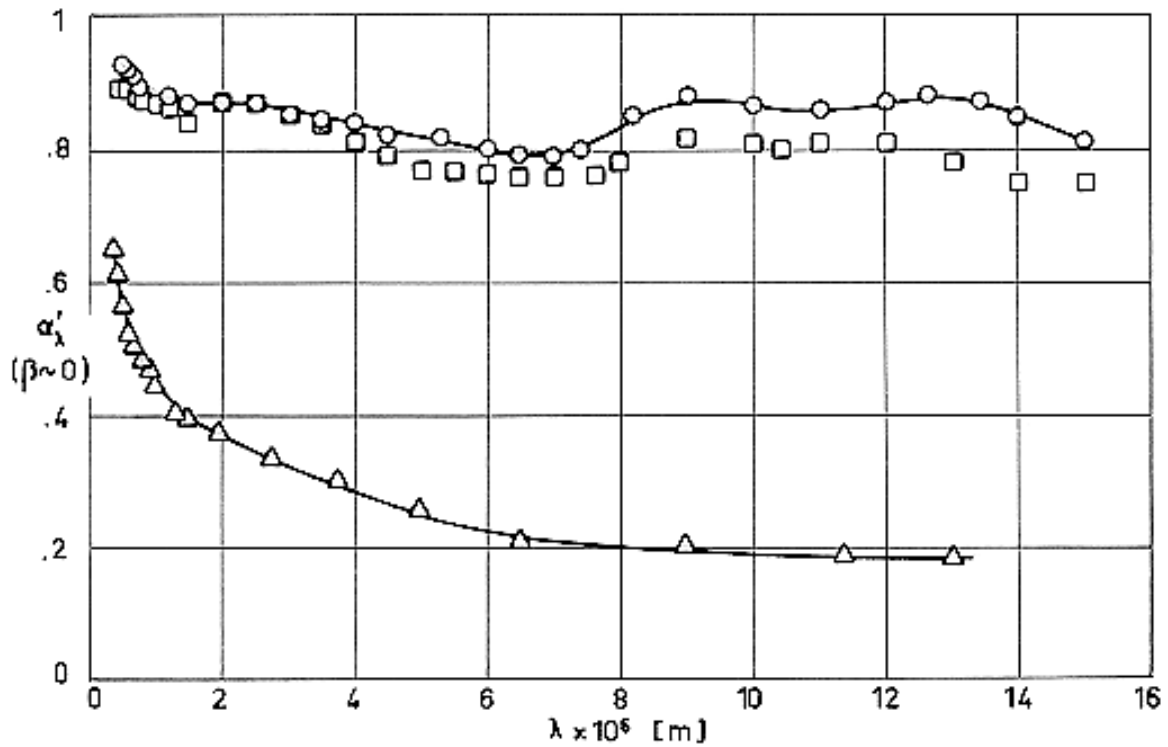
Note: non-si units are used in this figure

Figure 6-37: Normal spectral absorptance, α'_λ of Incoel as a function of wavelength λ.

From Touloukian & DeWitt (1970) [74].

Explanation

Key	Description	Test Method	Comments
○	Incoel. Nominal composition.		Measured in air. Data from smooth curve. $T = 294$ K.
□	Same as ○ .> Heated at 1250 K for 2 h and at 1467 K for 2 h.		
△	Incoel X. Nominal composition. Rolled plate.	Heated cavity at approx. 1056 K with platinum reference. Authors assumed $\alpha = 1-R\ (2\pi, 25°)$.	$\beta = 25°$. Measured in dry nitrogen. $T = 306$ K.

NOTE   Solar Absorptance of Nickel Alloys (INCOEL).
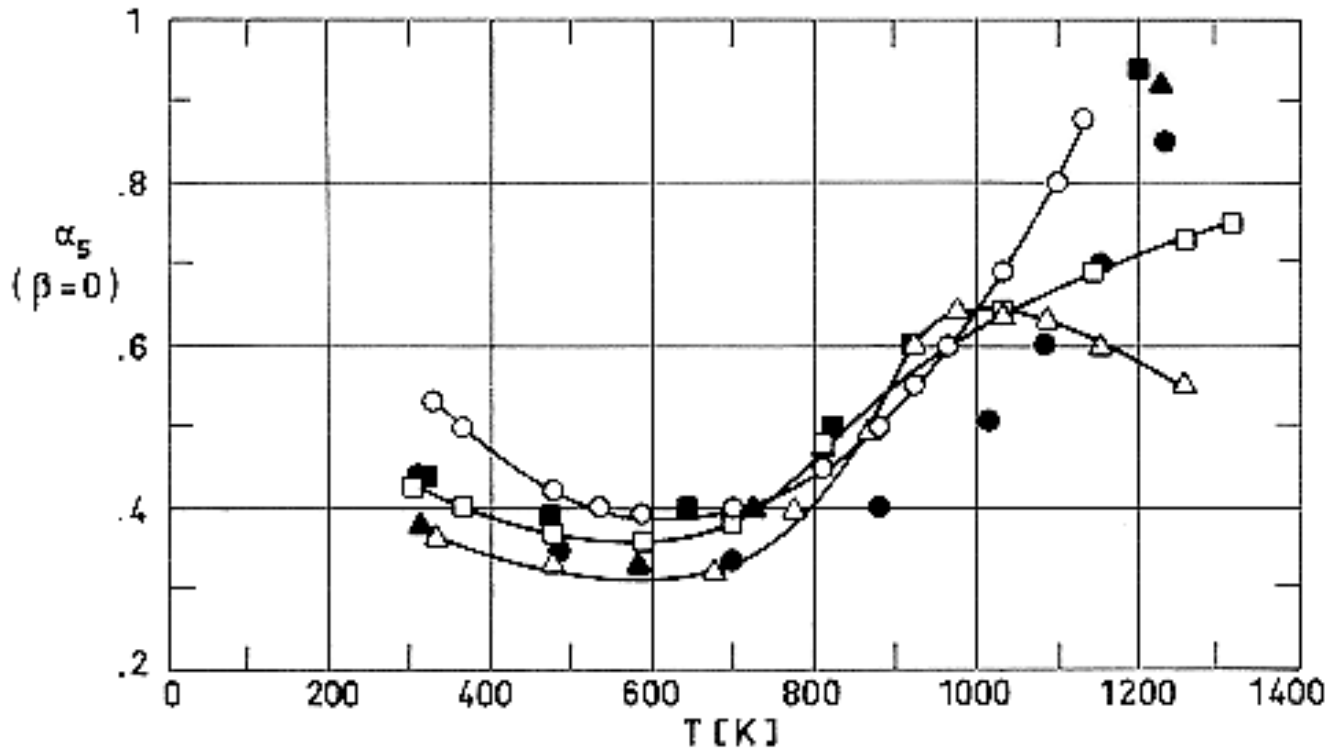
Note: non-si units are used in this figure

Figure 6-38: Normal solar absorptance, α_s, of Incoel as a function of the temperature, T, to which samples had been previously heated.

From Wood, Deem & Lucks (1961) [76].

Explanation

Key	Description	Test Method	Comments
○	Incoel B. As received.	Comparison standards. Comparison pyroheliometer. Temperature measured with thermocouples.	Measured in air at 311 K.
□	Incoel B. Clean and smooth.		
△	Incoel B. Polished.		
●	Incoel X. As received.		
■	Incoel X. Clean and smooth.		
▲	Incoel X. Polished.		

NOTE   Absorptance of Platinum.
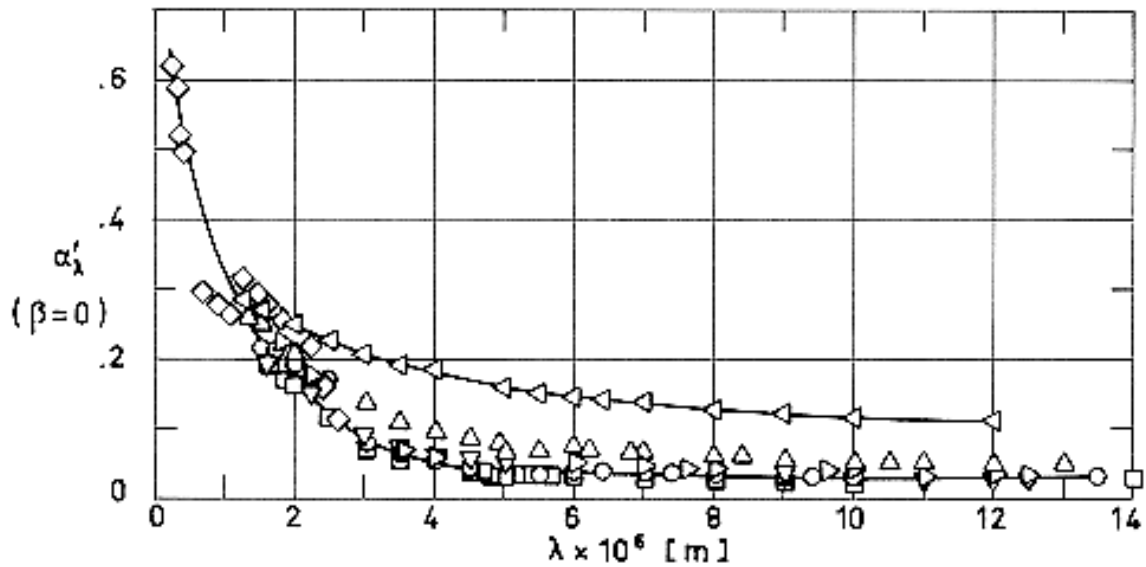
Note: non-si units are used in this figure

Figure 6-39: Normal spectral absorptance, α'_λ of Platinum as a function of wavelength λ.

From Touloukian & DeWitt (1970) [74].

Explanation

Key	Description	Test Method	Comments
○	NBS platinum. Heated in air at 1523 K for 1 h, cooled for 12 h.		Measured in air. Data from smooth curve. $T = 294$ K.
□	NBS platinum. Heated in air at 1523 K for 1 h, cooled for 12 h, heated at T1088 K for 24 h and at 1523 K for 1 h.		
△	Same as □ except after 180 d heated at T1083 K for 11 h and at T1277 K for 1 h.		Measured after a total of 240 d. $T = 294$ K.
▽	Mechanically polished with aluminium oxide and cleaned with water. Heated at 1088 K for 3 h.		Measured in vacuum (6,65 x10⁻⁴Pa). Data from smooth curve. $T = 294$ K.
▷	Polished with aluminium oxide, cleaned with water. Heated at 672 K for 3 h, 1088 K for 6 h, T1111 K for 53 h, and 1460 K for 30 h.		Measured in air. Data from smooth curve. $T = 294$ K.
◁	Heated as ▷ except heated for 58 additional hours at 1477 K.		

Key	Description	Test Method	Comments
◇			Data from smooth curve. $T \sim 294$ K.
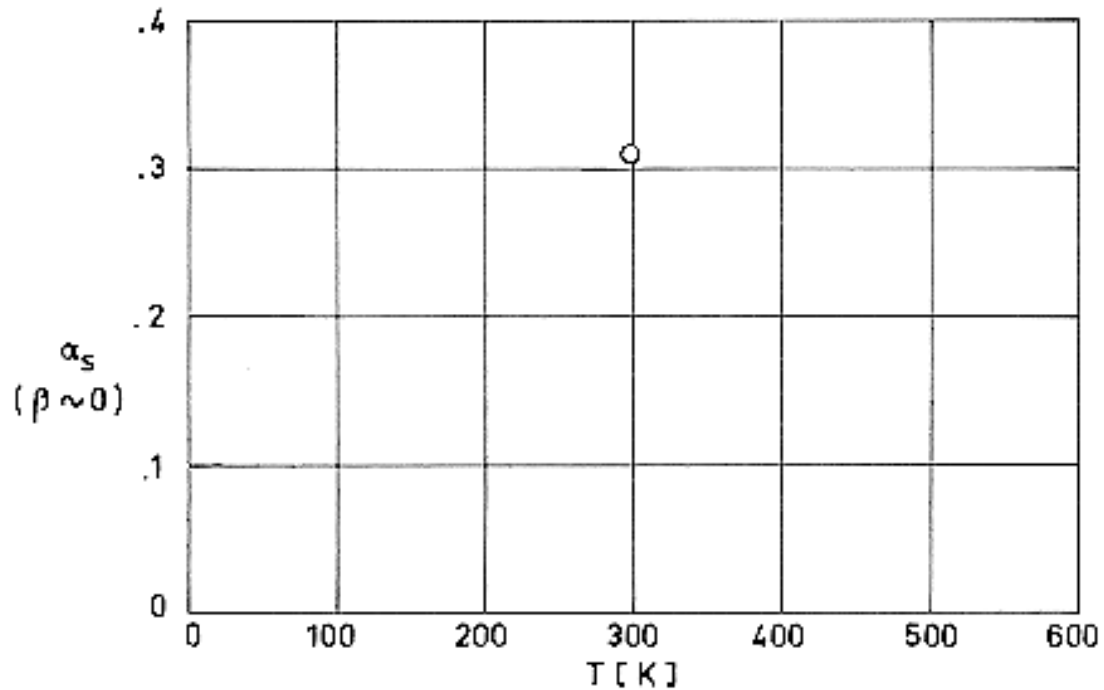
Note: non-si units are used in this figure

Figure 6-40: Normal solar absorptance, α_s, of Platinum as a function of temperature, T.

From Touloukian & DeWitt (1970) [74].
Explanation

Key	Description	Test Method	Comments
○	Pure metal. As received, bright.	Calculated from spectral reflectance data either for sea level or for above atmosphere conditions.	$\beta = 9°$.

NOTE   Absorptance of Silver.
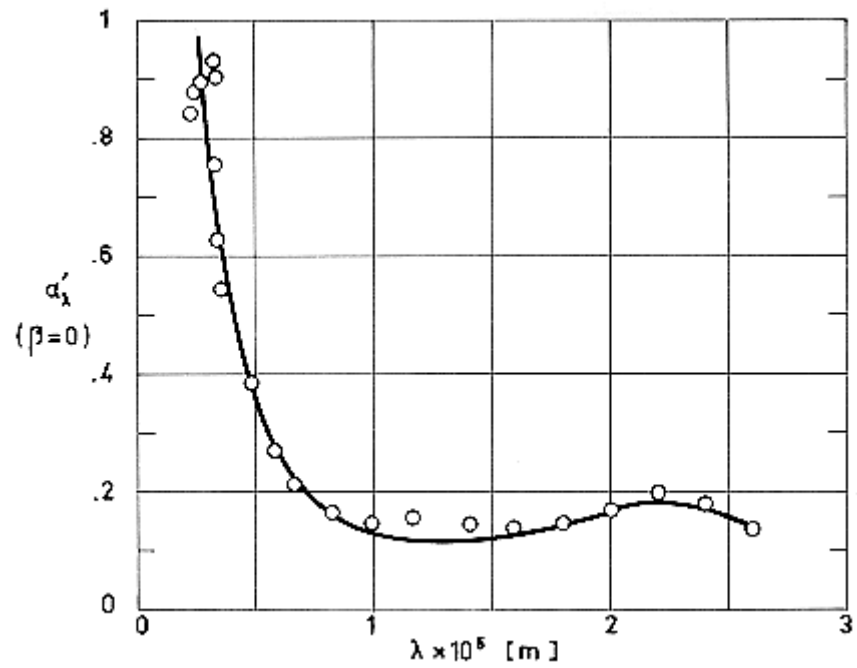
Note: non-si units are used in this figure

Figure 6-41: Normal spectral absorptance, α'_λ of Silver as a function of wavelength, λ.

From Touloukian & DeWitt (1970) [74].

Explanation

Key	Description	Test Method	Comments
○	1,27x10⁻⁴ m thick.		Data from smooth curve. $T \sim 298$ K.
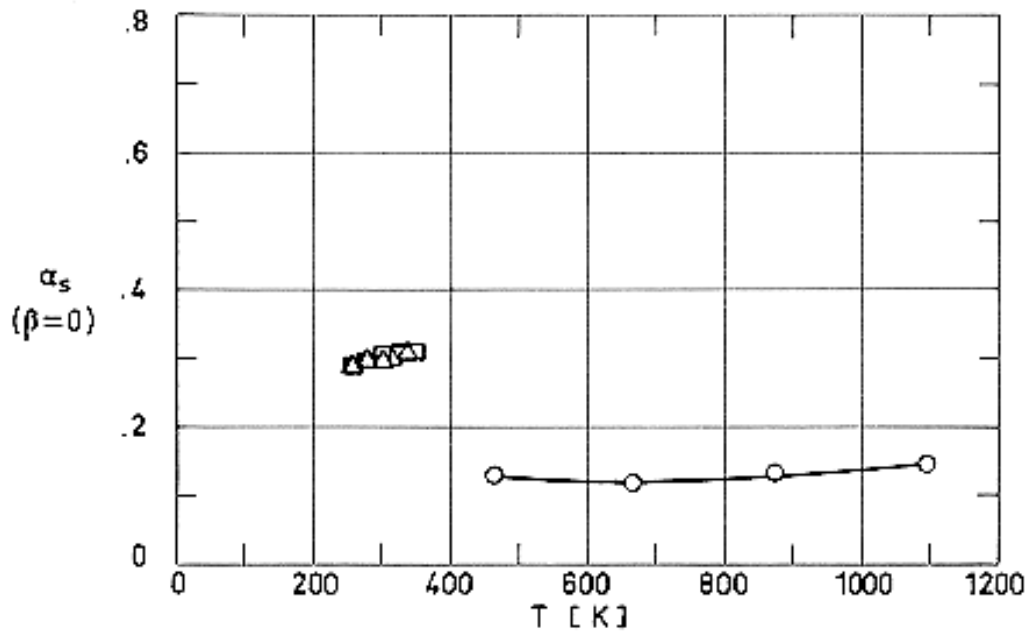
Note: non-si units are used in this figure

Figure 6-42: Normal solar absorptance, α_s, of Silver as a function of temperature, *T*.

From Touloukian & DeWitt (1970) [74].

Explanation

Key	Description	Test Method	Comments
◯	Commercial rolled plate, 99,9 pure. Ground with 600 grit Carborundum, and polished on a wet cloth lap with unlevigated jewellers rouge.		Measured in vacuum. Reported error <10%.
☐	Commercial sheet. Cleaned with both sodium dichromate and dilute nitric acid. Buffed on a felt buffing wheel and cleaned with carbon tetrachloride and acetone.		Measured in vacuum ($1{,}33 \times 10^{-4}$Pa). Data from smooth curve. Reported error 5%.
△	Commercially pure. Cleaned; buffed; cleaned with carbon tetrachloride and acetone.		Measured in vacuum ($1{,}33 \times 10^{-4}$Pa). Data from smooth curve.

6.6 Radiation shields. miscellaneous properties

Relevant properties of radiation shields are given in the next pages. The enclosed data have been arranged as follows:

Content	Table	Figure
Properties of Metallic Foils	Table 6-1	
Properties of Polymeric Films	Table 6-2	
Properties of Several Marketed Polycarbonate Resins	Table 6-3	
Tensile Strength of Mylar and Kapton H for Different Values of the Temperature	Table 6-4	
Properties of Coated Plastic Films	Table 6-5	
Linear Thermal Expansion of Goldized Mylar as a Function of Temperature		Figure 6-43
Linear Thermal Expansion of Goldized Kapton as a Function of Temperature		Figure 6-44
Flammability of Several Radiation Shields in Oxygen and in Air	Table 6-6	
Outgassing Characteristics of Non-Metallized and Metallized Plastic Films	Table 6-7	
Procurement Data	Table 6-8	

Table 6-1: Properties of Metallic Foils

Property	Aluminium	Copper	Gold	Molybdenum	Nickel	Incoel	Incoel X	Platinum	Silver
Melting Point [K]	933,2	1356	1336	2883	1726	1668-1695		2042	1233,8
Maximum Recommended Service Temperature [K]	723 [a] 772 [b]	723-1273 [a] 811 [b]	613 [c]	811 [b] 1200 [d]	811 [b] 1473 [a]	1477 [b]	1089 [b]		755 [b]
Density, ρx10^{-3} [kg.m^{-3}]	2,702	8,92	19,32	10,2	8,90	8,51	8,30 [e]	21,45	10,49
Tensile Strength σx10^{-7} [Pa]	4,7	19,3 [e] (σ_{ult})	12,4-22,1	79,3 [e]	28,3 [e] (σ_{ult})	55,2-103,4		13,8-16,6	12,6
Modulus of Elasticity, Ex10^{-10} [Pa]	6,8	12,4	7,86	29,0	20,7	21,4			
Specific Heat, cx10^{-2} [J.kg^{-1}.K^{-1}]	9,00 [e]	3,86	1,30	2,76	4,71	4,56	4,60 [e]	0,131	2,34
Thermal Conductivity, kx10^{-2} [W.m^{-1}.K^{-1}]	2,39	3,94	2,97	1,42	0,92	0,151	0,159 [e]	0,690	4,18
Linear Thermal Expansion Coefficient, βx10^6 [K^{-1}]	26,4	16,5	14,2	5,1 [e]	13,3	11,5		8,9	20,61

Property	Aluminium	Copper	Gold	Molybdenum	Nickel	Incoel	Incoel X	Platinum	Silver
Minimum Thickness Available, tx10^6 [m]	5	6	1 [f]	5 [f]	25	25	25	1 [f]	1 [f]

NOTE   All data in this table, unless otherwise stated, are from ASM (1961) [5].

[a]   From Kaganer (1969) [33].

[b]   From Rittenhouse & Singletary (1969) [55].

[c]   From Chapman & Porter (1910) [12]. Leaf becomes granular upon contraction.

[d]   From Dixon & Musgrove (1973) [18].

[e]   From Smithells (1962) [67].

[f]   Foils of the quoted thicknesses have normally small surface areas. See Table 6-8 for additional details.

Table 6-2: Properties of Polymeric Films

PROPERTY	Mylar "A" Polyester (Dupont)	Kimfol [a] Polycarbonate (Kimberley Clark)	Lexan [a] Polycarbonate (General Electric)	Kapton "H" Polyimide (Dupont)
Maximum Recommended Service Temperature [K]	422	408	405	672
Density, $\rho \times 10^{-3}$ [kg.m^{-3}]	1,395	1,21	1,20	1,42
Moisture Regain [percent]	0,37 at 297 K in a 50% relative humidity atmosphere	0,4 after 24 h immersion	0,15 at 296 K in a 50% relative humidity atmosphere	1,3 at 296 K in a 50% relative humidity atmosphere
Tensile Strength, $\sigma \times 10^{-8}$ [Pa]	1,72 [b]	2,14 0,76	0,55	1,72 [b]
Thermal Conductivity, k at 298 K, [W.m^{-1}.K^{-1}]	0,152	0,19	0,19	0,156
Flammability [e]	Slow rate of burning	Moderate. Can be made flame resistant	Slow rate of burning	Self-extinguishing
Minimum Thickness Available, $t \times 10^6$ [m]	3,81	2,03	12,70	6,35

NOTE   From Leonhard & Hyde (1971) [42]

[a]   Comparative data concerning several commercially available polycarbonates are given in Table 6-3.

[b]   For the influence of temperature see Table 6-4.

[c]   Machine direction.

[d]   Cross direction.

[e]   Additional data on the flammability of several shields are given in Table 6-6.

Table 6-3: Properties of Several Marketed Polycarbonate Resins

PROPERTY	Lexan (General Electric)	Merlon (Mobay Chemical)	Makrolon (Bayer AG)
Color	Light amber	Light straw	Light yellow
Density, ρx10^{-3} [kg.m^{-3}]	1,20	1,20	1,20
Tensile yield strength, σ_vx10^{-8} [Pa]	0,55-0,62	0,62	0,61-0,66
Tensile ultimate strength, σ_{ult}x10^{-8} [Pa]	0,62-0,72		0,78-0,88
Tensile Modulus Ex10^{-9} [Pa]	2,21	2,07	
Shear yield strength, τ_vx10^{-8}[Pa]	0,37		
Shear ultimate strength, τ_{ult}x10^{-8} [Pa]	0,63		
Specific heat, cx10^{-3} [J.kg^{-1}.K^{-1}]		1,17	1,17
Thermal conductivity, k [W.m^{-1}.K^{-1}]	0,19		0,20
Thermal linear expansion coefficient, βx10^5 [K^{-1}]	7	7	6
Heat distortion temperature [K]	411-416 (1,82x10^6 Pa)	413,5 (1,82x10^6 Pa)	408-419
	412-418 (0,46x10^6 Pa)	416,5 (0,46x10^6 Pa)	
Brittle temperature [K]	138		138
Melting point [K]	541 Crystalline		533-538 Crystalline 495-503 Amorphous
Flammability	Self-extinguishing	Self-extinguishing	Self-extinguishing
Water absorption [percent]	0,3 after 24 h immersion		0,36 after 16 d

NOTE   From Kazanjian (1974) [34].

Table 6-4: Tensile Strength of Mylar and Kapton H for Different. Values of the Temperature.

T [K]	Tensile Strength, $\sigma \times 10^{-8}$, [Pa]	
	Mylar	**Kapton H**
77,5	2,70	1,72
298	1,60	1,47
472	0,34	0,83

NOTE   From Rosato (1968) [56].

Table 6-5: Properties of Coated Plastic Films

Sample Description/ Useful Temperature Range [K]	Tensile Strength, $\sigma \times 10^{-8}$ [Pa]	Propagating Tear Strength, $F \times 10^2$ [N]	Flexure Endurance Cycles/ Load [N]	Abrasion Resistance	
				Cycles/ Load, $P \times 10^{-3}$, [Pa]	Hemispherical total emittance Before After
Mylar 6,35x10⁻⁶ m thick with vapor deposited Aluminium on both sides/ 213,5 to 422	4,1	1,3	27000 / 5	500 / 1,4	0,023 / destroyed
Kapton 12,7x10⁻⁶ m thick with vapor deposited Aluminium on both sides/ 5 to 672	4,8	2,7	11000 / 15	1000 / 1,4	0,025 / 0,20
Kapton 12,7x10⁻⁶ m thick with vapor deposited Aluminium and Germanium on both sides/ 5 to 672	4,8	2,7	26000 / 15	5000 / 1,4 to 12	0,026 / 0,028
Kapton 25,4x10⁻⁶ m thick with liquid bright Gold on both sides/ 5 to 672	5,2	7,8	16000 / 15	5000 / 1,4 to 12	0,018 / 0,025

Sample Description/ Useful Temperature Range [K]	Tensile Strength, σx10^{-8} [Pa]	Propagating Tear Strength, Fx10^2 [N]	Flexure Endurance Cycles/ Load [N]	Abrasion Resistance	
				Cycles/ Load, Px10^{-3}, [Pa]	Hemispherical total emittance Before After
Kapton 25,4x10^{-6} m thick with liquid bright Gold and vapor deposited Germanium on both sides/ 5 to 672	5,2	≥ 7,8 (estimated)	≥ 16000	1500	0,020 0,020
			15 (both estimated)	1,4 to 12	

NOTE   From Richardson, Ruccia & French (1970) [54].
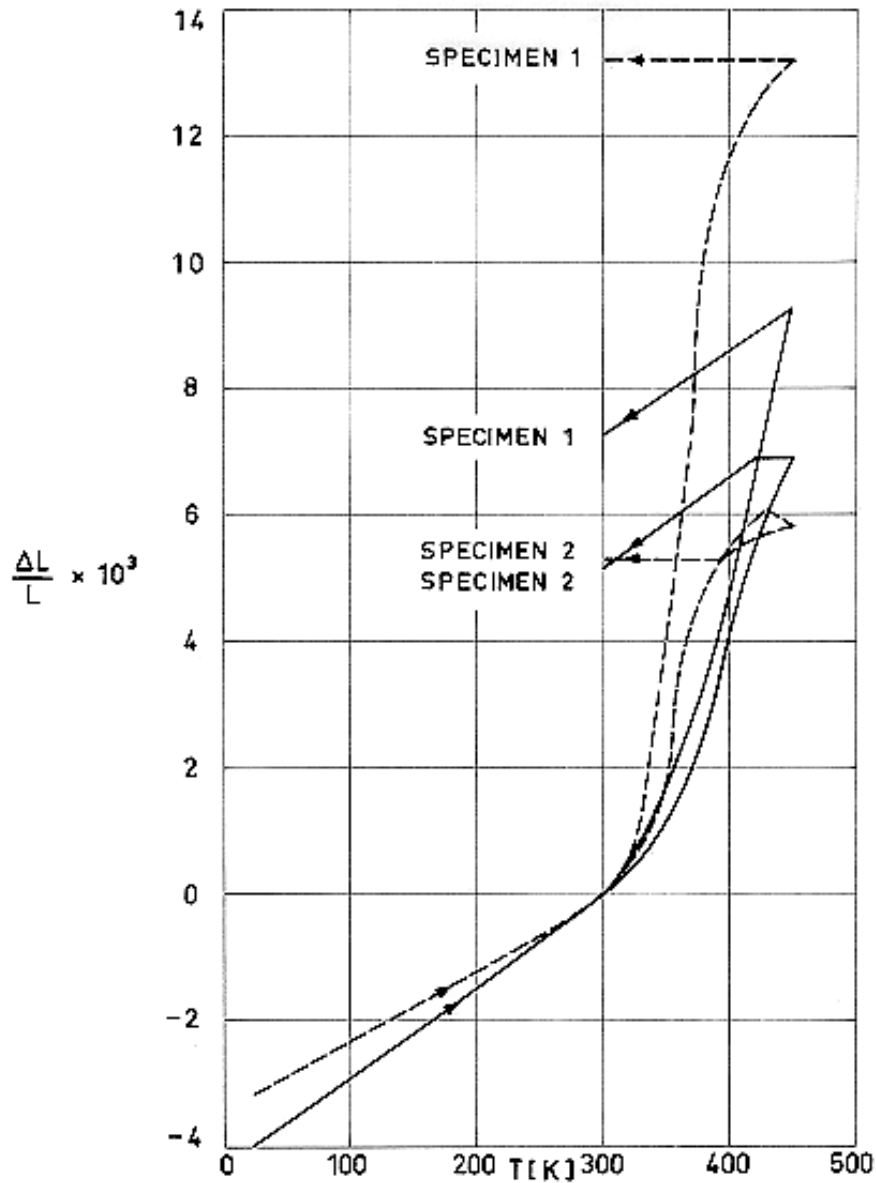
Figure 6-43: Linear thermal expansion, *ΔL/L*, of two nominally identical specimens of 6,35x10⁻⁶ m thick Mylar Double-Goldized as a function of temperature, *T*.

━━━━ : Longitudinal direction,

━━ ━━ : Transverse direction.

From Leonhard & Hyde (1971) [42].
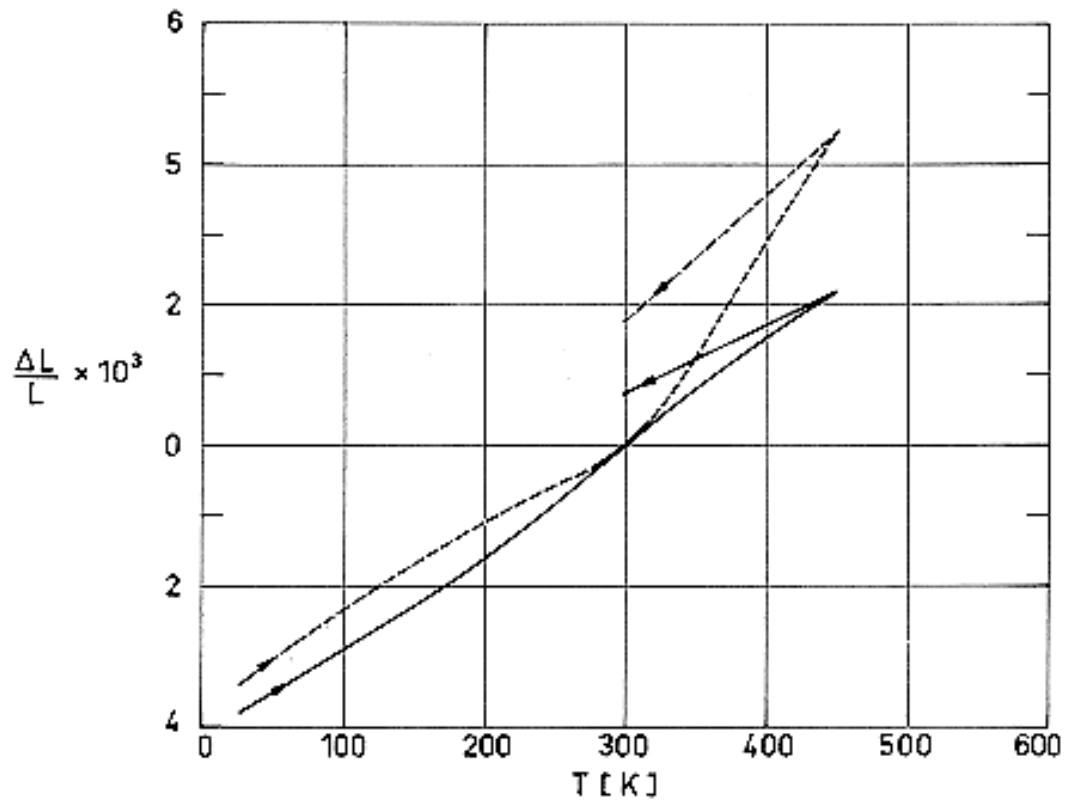
Figure 6-44: Linear thermal expansion, *ΔL*/*L* of 6,35x10⁻⁶ - 7,62x10⁻⁶ m thick Kapton Double-Goldized, with Dacron Flocking, as a function of temperature, *T*

▬▬▬ : Longitudinal direction,

▬ ▬ : Transverse direction.

From Leonhard & Hyde (1971) [42].

Table 6-6: Flammability of Several Radiation Shields in Oxygen and in Air

Shield Description	Oxygen		Air
	1,14x10^5 Pa	0,43x10^5 Pa	10^5 Pa
Mylar 6,35x10^{-6} m thick with vapor deposited Aluminium on both sides	F	F	F
Kapton 12,7x10^{-6} m thick with vapor deposited Aluminium on both sides	F	F	SE
Kapton 12,7x10^{-6} m thick with vapor deposited Aluminium and vapor deposited Germanium on both sides	F	F	SE
Kapton 25,4x10^{-6} m thick with liquid bright Gold on both sides	F	F	F
Kapton 25,4x10^{-6} m thick with liquid bright Gold and vapor deposited Germanium on both sides	F	F	SE

NOTE   From Richardson, Ruccia & French (1970) [54].
            F: Flammable
            SE: Self-extinguishing

Table 6-7: Outgassing Characteristics of Non-Metallized and Metallized Plastic Films

Material (Manufacturer)	%TWL [a]	%VCM [b]	Cure Time [h]	Cure Temp. [K]	Vacuum Conditions	Reference
Mylar 100S (DuPont)	0,220	0,120				Campbell, Marriot & Park (1973) [10]
Mylar 100T (DuPont)	0,200	0,120				
Mylar 100S (DuPont)	0,240	0,060				
Mylar LA616-1,77x10⁻⁶ m thick film (DuPont)	0,156	0,004				
Kapton 200XH667 (DuPont)	0,140	0,090				
Kapton 200XHF929A Fluorocarbon Coated (DuPont)	0,540	0,050				
Kapton FEP film 400F022 (DuPont)	0,310	0,180				
Kapton FEP film 400F022 (DuPont)	0,250	0,010	1,5	575	Air	
Kapton H film 1,27x10⁻⁶ m thick film (DuPont)	0,771	0,027				
Teflon FEP 100A (DuPont)	0,060	0,060				
Teflon FEP 500A (DuPont)	0,050	0,050				
Teflon FEP 500C (DuPont)	0,020	0,010				
Hostaflon PTFE (Hoechst)	0	0			$1,33 \times 10^{-4}$ Pa	Zwaal, Dauphin & Alonso (1971) [77]
Makrofol E (Bayer)	0,04	0,01			$1,33 \times 10^{-4}$ Pa	
Mylar Aluminized (Int. Research G.B.)	0,16	0			$1,33 \times 10^{-4}$ Pa	

Material (Manufacturer)	%TWL [a]	%VCM [b]	Cure Time [h]	Cure Temp. [K]	Vacuum Conditions	Reference
Kapton Double-Aluminized (ADL)	1,1					Richardson, Ruccia & French (1970) [54]
Kapton Double-Aluminized with Germanium Overcoating (ADL)	0,9					
Kapton Double-Goldized (ADL)	0,5					
Kapton Double-Goldized with Germanium Overcoating	0,8					

[a]   TWL: Total Weight Loss.

[b]   VCM: Volatile Condensable Materials (by weight).

NOTE   Outgassing rates of several shield materials are given in clause 6.17.2.1. in connection with evacuation under outgas controlled conditions.

Table 6-8: Procurement Data

Material	Minimum Thickness, tx10^6 [m]	Width, w [m]	Length, L [m]	Purity (percent)	Approximate Cost [US $]	Suppliers	Alternative Applications
Aluminium	5 8	0,5 1	roll roll	99 99	2,7 per kg 2,7 per kg	a a b, c, d, e, f	Thin film circuitry, electrical capacitors, fornitures, packing.
Copper	6	0,27	roll	99,9	8,83 per kg	g c	Car radiators, electrical components, heaters.
Gold	1	0,2	0,45	99,9	2520 per piece	c h	Accelerators targets, alpha counter windows, electrical components, jewellery.
Molybdenum	5 15	0,2 0,3	0,45 roll	99,9 99,93	3160 per piece 560 per kg	c i h, j, k	Accelerator targets, furnaces.
Nickel	25 80	0,1 0,2	roll roll	99,5 99,5	7,95 per kg 7,95 per kg	l, m l, m c, h	Electronic equipment transducers.
Inconel	25 80	0,1 0,2	roll roll		10,3 per kg 10,3 per kg	l, m l, m	Afterburner components, jet insulation blankets, combustion cans.
Inconel X	25 80	0,1 0,2	roll roll		8,23 per kg 8,23 per kg	l, m l, m	Thrust chamber walls, turbine housings, engine seals, support bands.

Material	Minimum Thickness, $t \times 10^6$ [m]	Width, w [m]	Length, L [m]	Purity (percent)	Approximate Cost [US $]	Suppliers	Alternative Applications
Platinum	1	0,2	0,45	99,9	4220 per piece	c h	Heat flux sensors, electrical components, jewellery.
Silver	1		0,45	99,99	4500 per piece	c h	Electrical components, jewellery.
Polyester	6 9 12 12	1,2	roll	Single or Double-Aluminized Single or Double-Aluminized Single-Aluminized	0,25 to 0,61 per m² 0,41 to 0,82 per m² 0,15 per m²	n o p q	Electrical capacitors, furnitures.
Polyimide	25	0,4	roll			r	

Key to Suppliers:

[a]   Empresa Nacional de Aluminio, S.A., General Sanjurjo, 4, Madrid-3, Spain.

[b]   Alcan Wire Ltd., Windsor Ave., Merton Abbey, London SW 19, England.

[c]   Goodfellow Metals Ltd., Ruxley Towers, Claygate-Esher, Surrey KT 10 OTS, England.

[d]   Pechiney, 23 Rue Balzac, 65360 Paris, France.

[e]   Star Aluminium Co., Ltd., 97 Penn Road, Wolverhampton, Staffs WV 3 ODM, England.

[f]   Vereingte Aluminium-Werke Aktiengesellschaft, 5300 Bonn, Germany.

[g]   Gränges Metallverken, S-721 88 Västeras, Sweden.

[h]   Reactor Experiments, Inc., 963 Terminal Way, San Carlos, California 94070, USA.

[I]   Metallwerk Plansee AG & Co. KG., A-6600 Reutte, Tirol, Austria.

[j]   Climax Molybdenum Company (American Metal Climax), 1 Greenwich Plaza, Greenwich, Connecticut 06830, USA.

[k]   Metals Research Ltd., Melbourn Royston, Hestfordshire, England.

[l]   Henry Wiggin & Company, Ltd., Holmer Road, Hereford-HR4 9SL, England.

[m]   Huntington Alloy Products Division, The International Nickel Company, Inc., Huntington, West Virginia 25720, USA.

[n]   Verolme Vacuumtechnik AG, 6228 Eltville, Sudetenstr. 3, Germany.

[o]   Imperial Chemical Industries Ltd., Millbank, London SWIP 3 JF, England.

[p]   Westfälische Metallindustrie KG, Hueck & Co., 4780 Lippstadt, Germany.

[q]   Sarrió, Compañía Papelera de Leiza, S.A., Leiza, Navarra, Spain.

[r]   Carl Huth & Söhne, 712 Bietigheim, Postfach 114, Germany.

6.7 Radiation shields. measurement of the coating thickness

The thermal performance of an evacuated multilayer insulation system depends upon the emittance of its radiation shields. When shields are formed by metal coating on substrate films, the coating thickness affects the emittance and control the portion of incident radiation which is transmitted through the shield material.

Among the different existing methods to measure the coating thickness, the Resistance Method is the most widely used by commercial metal depositors. According to Ohm's law, the electrical resistance, R, between the ends of a right prism of length, L, and cross-sectional area, wt_c, is given by

$R = \rho(L/wt_c)$,

ρ being the electrical resistivity of the metal. When $L = w$, the resistance (measured in ohms per square) is proportional to $1/t_c$.

In the practical application of the above idea two different types of electrodes may be used: the parallel bar and the two-point electrode. The reader is referred to ADL (1966) [2] for details concerning the operating methods.

When the coating thickness is comparable to the mean free path of the electrons through the metal lattice, which loosely speaking is of the order of 2×10^{-8} m, Ohm's law is modified as we see below.

Figure 6-45 compares the coating thickness, t_c, measured by several methods with that measured by use of the Resistance Method, $t_{c\Omega}$. It may be seen that the last one gives reasonably accurate values of the coating thickness for the copper, gold, and silver coating examined. For several of the aluminium coatings, large discrepancies arise between the resistance and the other methods.

The values of t_c which are plotted in Figure 6-45 have been measured by means of some of the following methods.
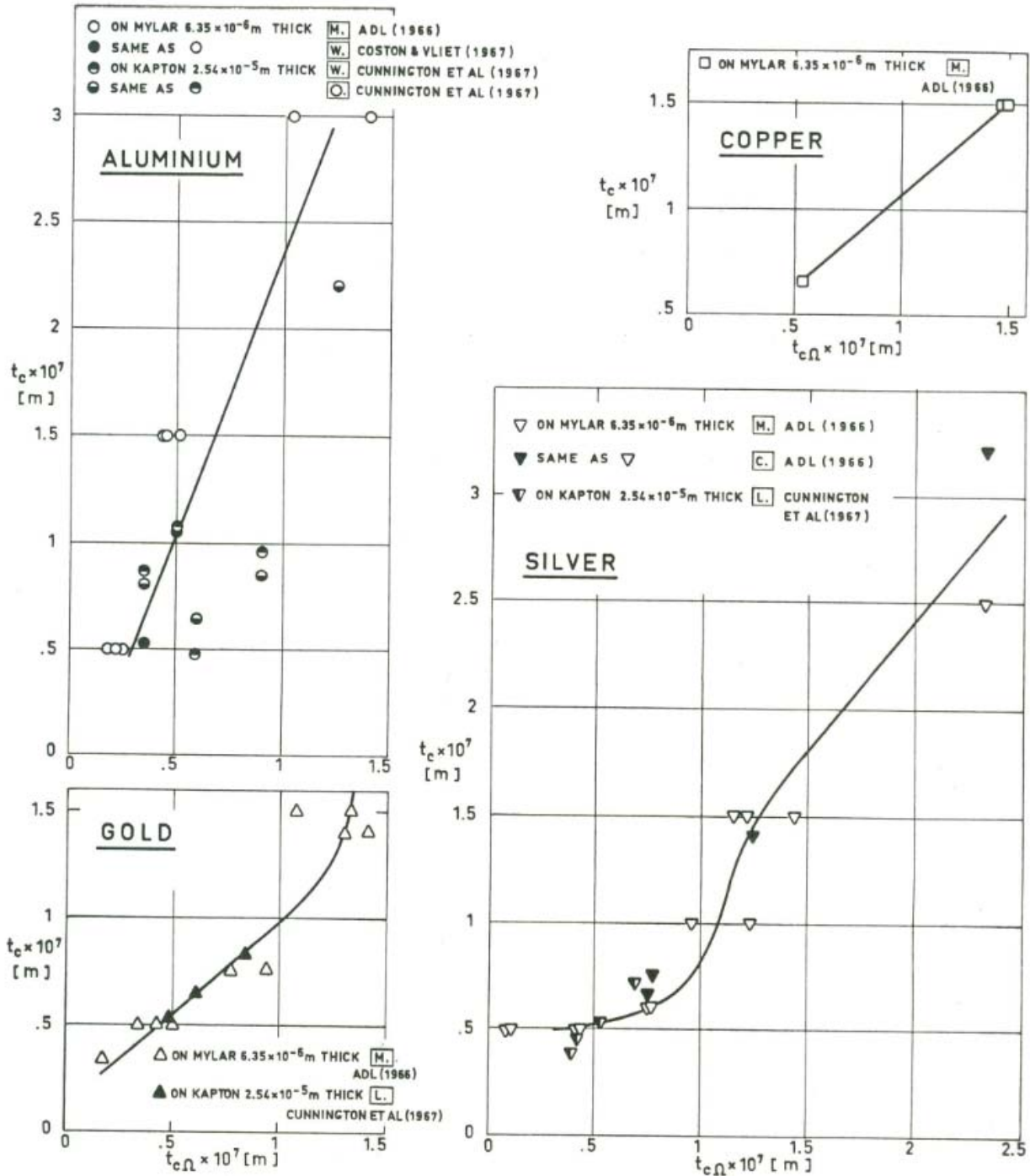
Note: non-si units are used in this figure

Figure 6-45: Coating thickness, t_c, given by several methods, compared with that gives by the electrical resistance method, $t_{c\Omega}$.

All coatings are vacuum deposited. Capital letters refer to the measuring method according to the following key: *C*, Crystal; *L*, Light transmission; *M*, Melt; *O*, Optical; *W*, Weight difference.

C. Vibrating Crystal Method. The coating is being deposited on a vibrating crystal. The shift of the natural frequency of the crystal relates to the coating thickness.

L. Light Transmission. When the sample is transparent the characteristics of the light transmitted through it, which can be analyzed with a spectrophotometer, are related to the coating thickness.

M. Melt Method. The coating is produced as in the bell-jar vacuum deposition method, from weighted amounts of metal.

O. Optical Method. Optical flats are placed adjacent to the film during the deposition process. The film coating thickness on the flats is determined by interferometry.

W. Weight-by-Difference Method. A coated film is weighted before and after removal of the coating thickness. It is important to realize that the removing solvent does not change the substrate.

To deduce the coating thickness from the electrical resistance, the following expression can be used (Maissel (1970) [45]).

$$R = \frac{\rho}{t_{c\Omega}} + \frac{3}{8} \frac{\lambda(1-p)}{t_{c\Omega}^2} \rho$$

[6-14]

Note: non-si units are used in this figure

where:

R, Resistance. [Ω per square].

p, Fraction of the electrons suffering specular reflection at the surfaces of the metallic film. In the following it is assumed that $p = 0$, although such an assumption may not be appropriate for Gold.

$t_{c\Omega}$, Coating Thickness. [m].

λ, Mean Free Path of the electrons in the metal lattice. [m].

ρ, Bulk Resistivity of the metal. [W.m].

Table 6-9 gives ρ and $3\lambda\rho/8$ for the four metals considered.

Table 6-9: ρ and $3\lambda\rho/8$ for Aluminium, Copper, Gold and Silver

Metal	ρx108 [Ω.m]	$3/8\lambda\rho$x10^{16} [Ω.m^2]
Aluminium	2,65 [a]	3,14 [a]
Copper	1,55 [b]	2,44 [c]
Gold	2,35 [b]	3,61 [d]
Silver	1,59 [a]	3,38 [a]

[a] From Cunnington et al. (1967) [17].

[b] From Bardeen (1958) [7].

[c] Calculated by the compiler ($\lambda = 4,2$x10^{-8} m at $T = 273$ K. From Kittel (1966) [36]).

[d] Calculated by the compiler ($\lambda = 4,1$x10^{-8} m at $T = 273$ K. From Kittel (1966) [36]). The value quoted by Cunnington et al. (1967) [17] seems to be a misprint.

The variation of R with $t_{c\Omega}$ is shown in Figure 6-46.
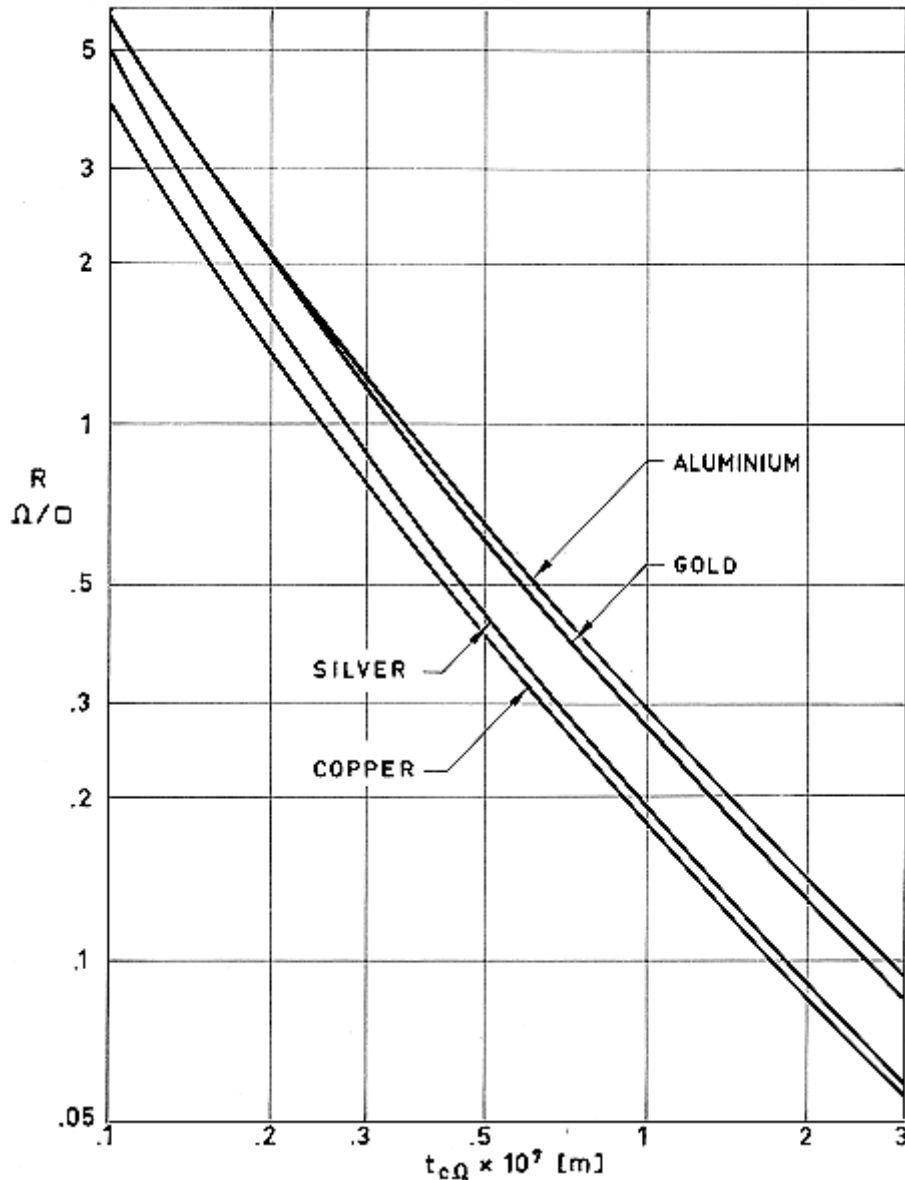
Note: non-si units are used in this figure

Figure 6-46: Thickness, $t_{c\Omega}$, of metallic coatings as a function of film electrical resistance, R. Calculated by the compiler.

6.8   Spacers

Spacers are low thermal conductivity materials whose aim is to decrease the solid conductivity between parallel neighboring radiation shields. Spacers can be classified in four groups (Glaser et al. (1967) [23]): multiple resistance, point contact, single component, and composite. "Superfloc" ("Superfloc" is a trade name of Convair Division Of General Dynamics) has several characteristics in common with the first two groups and is be classified separately.

6.8.1   Multiple-resistance spacers

Contacting particles exchange heat through their points of contact. Therefore, a mat of fibers arranged in a parallel array, in which the heat passes from each fiber to another nearly-parallel fiber to reach the next radiation shield, can be used as an effective spacer.

The contact thermal conductance grows with the force pressing the particles against each other, so that solid heat conduction through fibrous systems depends not only on the temperature gradient, fiber thermal conductivity, volume fraction of fibers, and packing geometry, but also depends upon the contacting load and mechanical properties of the fibers. For a given bulk material, the finer the fibers, the greater the resistance per unit thickness the mat presents to the heat flow.

The prediction of the thermal conductivity of a fibrous system is fairly complicated because of the random orientation of the fibers, and local variations in loading and thermal resistance at each contact area. Semi empirical correlations have been often attempted in terms of the solid fraction, thermal conductivity of the bulk material, and fiber diameter. The reader is referred to the monography by Kaganer (1969) [33] for further details concerning theoretical models of heat transfer through fibrous materials.

Glass fibers, quartz fibers, and plastic fibers are used as spacers in MLI systems. Fibrous mats are produced in thicknesses ranging from $7,5 \times 10^{-5}$ to $7,5 \times 10^{-4}$ m. Fiber diameters as small as 5×10^{-7} m are commercially available.

Problems in connection with the use of these spacers arise from their very poor dimensional stability. Bonding together the fibers could be detrimental to the performance of the MLI because of the heat flow across the bonded contact areas. In addition, bonding materials contribute to the outgassing of the spacer.

Stitching is often used to increase the stability of the MLI system without greatly decreasing its thermal performance.

6.8.2   Point-contact spacers

The dimensional stability of the MLI system can be improved by using silk, nylon or fiber-glass screens, whose knots, which can be assimilated to isolated spheres, do space neighboring radiation shields.

The mesh size of the screen, or distance between spheres, should be as large as possible, but an upper limit exists determined by the requirements that direct contact between radiation shields, produced by their sagging, should be avoided.

The thickness of the screens used as spacers in MLI systems ranges from $7,5 \times 10^{-5}$ to 6×10^{-4} m; the mesh size ranging from $1,53 \times 10^{-3}$ to $6,35 \times 10^{-3}$ m.

In addition to their dimensional stability, screen spacers allow an easy evacuation of the gas contained in the MLI.

6.8.3   Superfloc

Superfloc spacers consists of small tufts of a synthetic fiber bonded with a suitable adhesive to one side of each radiation shield.

The current configuration consists on tufts, made of 10^{-3} m long Dacron needles, arranged in a triangular pattern of approximately 10^{-2} m side, and bonded to one face of the shield with Crest 7343 polyurethane adhesive.

The method of manufacturing Superfloc, described by Leonhard & Hyde (1971) [42], is as follows:

1. A silk screen printing device is placed on the radiation shield material to which dots of adhesive are transferred by using a squeegee.

2. The shield is vibrated by being pulled across hexagonal bars that are rotating at 150 rpm.

3. The fiber tufts, arranged in the triangular pattern, "stand" about 10^{-2} m above the radiation shield base.

4. The vibration forces the needles into the adhesive while being held in an orderly vertical position.

5. Curing, whose peculiarities depend on the adhesive used, is performed.

The thickness of a typical Mylar-Superfloc MLI system having 22 shielding layers is of the order of $2,5 \times 10^{-2}$ m (Scollon & Carpitella (1970) [62]).

The main advantages of this system are that it provides low thermal conduction paths between shields; reasonable structural strength; ease purging, venting, and repressurization; density control, and simple insulation application.

6.8.4   Single-component MLI

Embossed or crinkled neighboring shields exhibit randomly distributed small contact areas having heat transfer rates which are of the same order of magnitude as those corresponding to radiative transfer.

This system can only be used with single-metallized plastic films of low thermal conductivity, such as Mylar.

Embossment pattern should be deep enough to allow for material memory, otherwise its geometrical characteristics would change with time. The problem is particularly acute when Kapton films are used.

A typical geometric component of the embossment pattern is approximately $1,5 \times 10^{-3}$ m deep, 3×10^{-3} m long and $1,5 \times 10^{-3}$ m wide, and is located on 10^{-2} m centers (Cunnington et al. (1967) [17]).

Surface emittance increases because embossment. The available information on this point is not precise enough and sometimes both the effect of embossment and of perforations are reported together. For simple geometric patterns the effect of embossment on emittance could be estimated by using the information concerning groove cavities. Unfortunately, since the aim of such cavities is to increase further the absorptance of absorptive surfaces, most of the available data concern medium and high values of the surface absorptance. Figure 6-47 gives the apparent emittance of a V-groove cavity for a range of surface absorptance which is well below that taken to calculate the data shown in D.

6.8.5   Composite spacers

As mentioned above in connection with bonded against nonbonded fibrous mat spacers, several materials which are very attractive from the insulating point of view show very poor dimensional stability. The consideration of this and similar situations leads to the concept of a spacer consisting of two or more materials: a very light, dimensionally stable one whose thermal properties are of no concern, plus a second material whose selection is guided exclusively by its thermal properties.

This concept permits a designer to select the materials best suited to the specific function and the desired performance of the complete assembly.
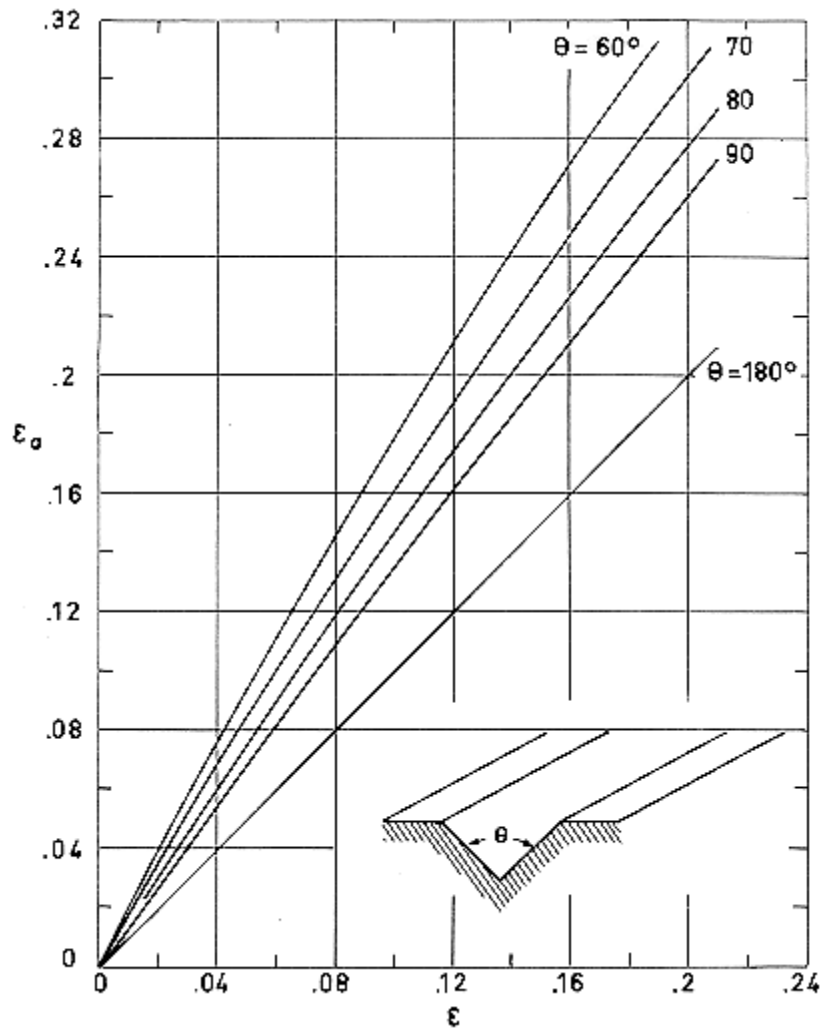
Note: non-si units are used in this figure

Figure 6-47: Apparent emittance, ε_a, of a gray V-Groove as a function of surface emittance, ε, illustrating the effect of embossing or crinkling on the optical properties of the shield. Calculated by the compiler.

6.8.6 One-dimensional heat flow through an mli with absorbing and scattering spacers

The heat transfer rate through and MLI formed by N shields, having the same emittance on both faces, and by N–1 thin spacers, is given, according to Cunnington et al. (1969) [17] by the following expression:

$$Q = \frac{n^2 \sigma A (T_N^4 - T_1^4)}{(N-1)\left(\dfrac{2}{s} - 1\right) + (a + 2s)\dfrac{t'}{2}}$$ [6-15]

Note: non-si units are used in this figure

where:

A, area normal to the temperature gradient. [m^2].

N, number of radiation shields.

Q, heat flown through the insulation. [W].

T_i, temperature of the shield i. [K]. $i = 1, N$

a, absorption coefficient of the spacer. [m^{-1}].

s, scattering coefficient of the spacer. [m^{-1}].

t', total spacer thickness. [m].

n, index of refraction of the spacer.

ε, emittance of shields, assumed to be the same for all of them.

σ, Stefan-Boltzmann Constant. [W.m^{-2}.K^{-4}].

It should be mentioned that a, n, and s depend on the spacer material, volume fraction of spacer, packing geometry and optical characteristics of the gas filling the space between shields, if any. Normally n can be assumed to be equal to unity. A limited amount of data concerning absorption and scattering coefficients is given in Table 6-10. The values presented in that table were deduced from total transmission data. The measurements were performed with the specimens at room temperature. Uncertainties of thickness measurement and spatial distribution of transmitted energy, and the errors associated with measurement of very low values of transmission, result in an estimated maximum uncertainty of 50% for the reported coefficients.

The effect of absorption and scattering by the spacers can be neglected in most cases, especially when the emittance of the shields is small.

Table 6-10: Absorption and Scattering Coefficients for Spacer Materials

Material	Nominal Density, ρ [kg.m⁻³]	Thickness, tx10⁵ [m]	Fiber Diameter, dx10⁶ [m]	Source Temp., [K]	Absorption Coefficient, ax10⁻⁴ [m]	Scattering Coefficient, sx10⁻⁴ [m⁻¹]
Dexiglas	200	7,62	<1	500 650 800 1000 1700	0,13 0,11 0,11 0,07 0,06	2,6 2,7 2,8 3,1 2,5
Tissuglas	220	1,52	<1	500 650 800	0,03 0,11 0,11	2,65 2,8 3,0
Refrasil A-100	50	4,83	1,3	500 650 800 1000	<0,02	0,38 0,57 0,73 0,76
Refrasil B-100	50	4,83	10	500 650 800 1000	<0,02	0,33 0,50 0,71 0,74
Carbon Fiber Paper			10	775 923 1123 1273	0,04 0,02 0,02 0,04	3,85 2,60 1,85 2,00

NOTE   From Cunnington, Zierman, Funai & Lindahn (1967) [17].

6.9 Spacers. miscellaneous properties

Relevant properties of spacers materials are given in the following pages. Because of the countless variety of both candidate materials and testing procedures it seems to be advisable to present the data using the same layout as in the different sources, without trying to unify them.

The table below guides in the search for these data.

Property	Table	Figure
Effect of Heat	Table 6-11, Table 6-14	
Moisture Regain	Table 6-11, Table 6-15	
Density	Table 6-11, Table 6-19	
Breaking Strength	Table 6-11	
Effect of Temperature on Breaking Strength	Table 6-16, Table 6-17, Table 6-18	
Elastic Recovery	Table 6-11	
Average Stiffness	Table 6-11	
Thermal Conductivity	Table 6-11, Table 6-19	Figure 6-48 to Figure 6-53
Specific Heat	Table 6-11, Table 6-19	Figure 6-54
Thermal Diffusivity	Table 6-19	
Flammability	Table 6-11, Table 6-20, Table 6-21	
Outgassing	Table 6-22	

Table 6-11: Properties of Staple Fibers
Data is available for the following Staple Fibers

Dacron Polyester (DuPont)	Table 6-12
Kodel Polyester (Eastman)	
Nomex Polyamide (DuPont)	
Nylon 6 Polyamide (Dupont)	
PBI a (Celanese)	Table 6-13
Silk	
Teflon Fluorocarbon (DuPont)	
"E" Glass	

NOTE   From Leonhard & Hyde (1971) [42].

a   PBI: polybenzimidazole (Polyimide).

b   Additional data are given in Table 6-14.

c   Additional data are given in Table 6-15.

d   gpd: grams per denier. The fineness of a fiber is expressed in units per denier, which is the weight in grams of a 9000 m length. Physically the tenacity is that length of fiber or yarn which causes rupture due to its own weight.
Additional data concerning the influence of thermal exposure on tenacity are given in Table 6-16, Table 6-17 and Table 6-18.

e   Thermal properties of fabrics woven of several fibersare given in Table 6-19. Effective thermal conductivities of fibrous spacers are given in Figure 6-48 to Figure 6-53.

f   Additional data are given in Figure 6-20.

g   Additional data are given in Table 6-20 and Table 6-21.

Table 6-12: Properties of Staple Fibers

Property	Dacron Polyester (DuPont)	Kodel Polyester (Eastman)	Nomex Polyamide (DuPont)	Nylon 6 Polyamide (Dupont)
Effect of Heat [b]	Melts at 522 K	Melts at 561 K	Does not melt. Degrades above 640 K. At 520 K has 60% of at room temperature strength.	Melts at 488,5 K. Yellows after 5 h at 422 K.
Moisture Regain [Percent] [c]	0,4	0,4	5	4
Density, $\rho \times 10^{-3}$ [kg.m^{-3}]	1,38	1,22	1,38	1,14
Breaking Strength [gpd] [d]	3,8-4,3	2,5-3	5,3	3,8-5,5
Elastic Recovery [percent]	80 at 8%	90-97 at 2%	100 at 4%	100 at 2%
Average Stiffness [gpd] [d]	12	11	24 (Calculated)	17-20
Thermal Conductivity, k [W.m^{-1}.K^{-1}] [e]	0,171	0,17	0,13	0,247
Specific Heat, $c \times 10^{-3}$ [J.kg^{-1}.K^{-1}] [f]	2,1-2,5	2,1-2,5	1,21	2,5
Flammability [g]	Slow burning rate	Slow burning rate	Self-extinguishing	Self-extinguishing

NOTE From Leonhard & Hyde (1971) [42].

[b] Additional data are given in Table 6-14.

[c] Additional data are given in Table 6-15.

[d] gpd: grams per denier. The fineness of a fiber is expressed in units per denier, which is the weight in grams of a 9000 m length. Physically the tenacity is that length of fiber or yarn which will just cause rupture due to its own weight.
Additional data concerning the influence of thermal exposure on tenacity are given in Table 6-16, Table 6-17 and Table 6-18.

[e] Thermal properties of fabrics woven of several fibers are given in Table 7-17. Effective thermal conductivities of fibrous spacers are given in Figure 6-48 to Figure 6-53.

[f] Additional data are given in Figure 6-20.

[g] Additional data are given in Table 6-20 and Table 6-21.

Table 6-13: Properties of Staple Fibers

Property	PBI [a] (Celanese)	Silk	Teflon Fluorocarbon (DuPont)	"E" Glass
Effect of Heat [b]	**Shrinks at 1088 K.**	**Desintegrates at 444 K.**	**Melts at 600 K. Non-degraded at 477 K. Sublimes 0,0002% per h at 560 K.**	**Softens at 1110 K. At 640 K has 50% of at room temperature strength.**
Moisture Regain [Percent] [c]	13	11	0	0
Density, ρx10^{-3} [kg.m^{-3}]	-	1,25-1,35	2,3	2,54
Breaking Strength [gpd] [d]	4,9	2,8-5,2	1,6	6,0-7,3
Elastic Recovery [percent]	-	-	-	100 at 2%
Average Stiffness [gpd] [d]	105	18	12	322
Thermal Conductivity, k [W.m^{-1}.K^{-1}] [e]	-	-	0,24	1
Specific Heat, cx10^{-3} [J.kg^{-1}.K^{-1}] [f]	-	-	1,05	0,80
Flammability [g]	Non-flammable	Moderate burning rate	Non-flammable	Non-flammable

NOTE   From Leonhard & Hyde (1971) [42].

[a] PBI: polybenzimidazole (Polyimide).

[b] Additional data are given in Table 6-14.

[c] Additional data are given in Table 6-15.

[d] gpd: grams per denier. The fineness of a fiber is expressed in units per denier, which is the weight in grams of a 9000 m length. Physically the tenacity is that length of fiber or yarn which will just cause rupture due to its own weight.
Additional data concerning the influence of thermal exposure on tenacity are given in Table 6-16, Table 6-17 and Table 6-18.

[e] Thermal properties of fabrics woven of several fibers are given in Table 7-17. Effective thermal conductivities of fibrous spacers are given in Figure 6-48 to Figure 6-53.

[f] Additional data are given in Figure 6-20.

[g] Additional data are given in Table 6-20 and Table 6-21.

Table 6-14: Effect of Heat on Several Fibers

Fiber	Sticks or Softens T [K]	Melts T [K]	Decomposes T [K]	Chars T [K]
Acrilan	508			
Nomex				722
Orlon	508			
PBI				811
Rayon			450-477	
Teflon		600 (Gel temp.)		

NOTE   From Ross for both tables (1968) [57].

Table 6-15: Moisture Regain of Several Fibers

Fiber	Moisture Regain [percent]
Nomex	7
Nylon 6	4
Nylon 6-6	4
PBI	13
Polyester	1
Rayon	13
Silk	11

Table 6-16: Effect of Exposure Temperature, Pressure and Time on the Strength of Fabrics, *T* = 450 K

Material	Breaking Strength, Fx10^{-5} [N.m^{-1}]					
	0 h	**2 h**		**6 h**		**24 h**
		1,7x10⁶ Pa	**0 Pa**	**0,34x10⁶ Pa**	**1,7x10⁶ Pa**	**1,7x10⁶ Pa**
Nylon 6-6 0,12 kg.m⁻²	0,277	0,247	0,156	0,140	0,152	-
Nylon 6-6 0,24 kg.m⁻²	0,587	0,515	0,177	0,229	0,240	-
Nylon 6-6 0,48 kg.m⁻²	1,26	0,963	0,672	0,692	0,660	-
Dacron 0,12 kg.m⁻²	0,256	-	0,250	0,247	0,247	-
Nomex 0,13 kg.m⁻²	0,242	0,236	0,236	0,235	0,233	0,243
Glass 0,31 kg.m⁻²	0,678	-	0,753	0,683	0,753	-
Glass 0,64 kg.m⁻²	1,16	-	1,10	1,19	1,11	-

NOTE   From Ross (1968) [57].

Table 6-17: Fiber Strength after 10 min Exposure to Temperature

T [K]	Breaking Strength [gpd]				
	Nomex	Nylon 6-6	PBI	"E" Glass	Fusel Silica
Room	6,6	6,5	4	13,8	15
399,5	6,5	4,6	-	-	15,6
422	-	-	4,4	-	-
455	4,8	3,8	-	-	-
505	-	No strength	3,2	-	-
511	3,8	-	-	13,7	16,3
566,5	2,8	-	-	-	-
588,5	-	-	2,6	-	-
622	1,1	-	-	9,9	9,3
672	-	-	1	-	-
677,5	-	No strength	-	-	-
699,5	-	-	0,4	-	-
733	-	-	-	8,6	8,9
811	-	-	-	7,6	8,8
866,5	-	-	-	6,5	8,2
922	-	-	-	4,2	6,3
1033	-	-	-	No strength	5,2

NOTE   From Ross (1968) [57].

Table 6-18: Effect of Cycling vs. Continuous Exposure to Temperature of Two Fibers in Woven Forms

Material	Strength Change [percent]			
	394 K		422 K	
	Cycling, 2 h soaks, 3 soaks	Continuous 6 h	Cycling, 2 h soaks, 3 soaks	Continuous 6 h
Dacron Sewing thread size E, natural	0,3	0	− 1,3	− 0,9
Sewing thread size E, sage green	1,3	1,0	3,5	− 2,1
Nylon 6-6 Fabric 5,42x10^{-2} kg.m^{-2} 3/1 twill, warp	− 6,7	1,4	− 21	− 20,7
Fabric 7,63x10^{-2} kg.m^{-2} dobby weave, warp	− 0,5	0,6	− 21,9	− 14,7
Fabric 16,1x10^{-2} kg.m^{-2} 2/2 twill, warp	5,6	4,4	− 24,3	− 14,5
Webbing, untreated 38700 N min, strength	− 1,5	− 2,7	− 33,4	− 36,8
Webbing, treated 38700 N min, strength	− 23,5	− 2,5	− 52,2	− 52,4

NOTE   From Ross (1968) [57].

Table 6-19: Thermal Properties of Fabrics Woven of Several Fibers

Fiber and Fabric	Pressure $px10^{-4}$ [Pa]	Temperature T [K]	Density $\rho x10^{-2}$ [kg.m^{-3}]	Thickness under Load $tx10^4$ [m]	Mass/Area $\rho tx10^2$ [kg.m^{-2}]	Avg. Thermal Conductivity $kx10^2$ [W.m^{-1}.K^{-1}]	Specific Heat $cx10^{-3}$ [J.kg^{-1}.K^{-1}]	Thermal Diffusivity $\alpha x10^7$ [m².s^{-1}]
Nomex 6x61x10^{-2} kg.m^{-2} Dobby weave	11,7	477,5	4,53	1,45	6,59	3,63	1,47	0,981
	0,204	477,5	4,53	1,45	6,59	1,38	1,47	0,361
	11,7	588,5	4,53	1,45	6,59	4,33	1,47	1,16
	0,204	588,5	4,53	1,45	6,59	1,73	1,47	0,465
Nylon 7,68x10^2 kg.m^{-2} 2/1 Twill	11,7	477,5	6,12	1,17	7,13	3,81	2,39	0,310
	0,204	477,5	6,12	1,17	7,13	2,60	2,39	0,178
Glass fiber 30,2x10^2 kg.m^{-2} Satin weave	11,7	588,5	9,02	3,34	30,17	6,58	1,09	0,671
	0,204	588,5	9,27	3,34	30,17	3,81	1,09	0,387
Fused Silica 30,2x10^2 kg.m^{-2}	11,7	588,5	8,25	3,93	32,42	7,27	1,05	0,852
	0,056	588,5	8,25	3,93	32,42	4,33	1,05	0,516
	12,1	922	8,25	3,93	32,42	10,38	1,09	1,16

Fiber and Fabric	Pressure $p\text{x}10^{-4}$ [Pa]	Tempe-rature T [K]	Density $\rho\text{x}10^{-2}$ [kg.m^{-3}]	Thickness under Load $t\text{x}10^4$ [m]	Mass/Area $\rho t\text{x}10^2$ [kg.m^{-2}]	Avg. Thermal Conductivity $k\text{x}10^2$ [W.m^{-1}.K^{-1}]	Specific Heat $c\text{x}10^{-3}$ [J.kg^{-1}.K^{-1}]	Thermal Diffusivity $\alpha\text{x}10^7$ [m^2.s^{-1}]
Satin weave	0,056	922	8,25	3,93	32,42	5,71	1,09	0,645
Graphic	12	922	4,95	5,23	25,88	28,73	1,67	0,877
	0,216	922	5,06	5,11	25,88	20,77	1,67	2,45

NOTE   From Ross (1968) [57].
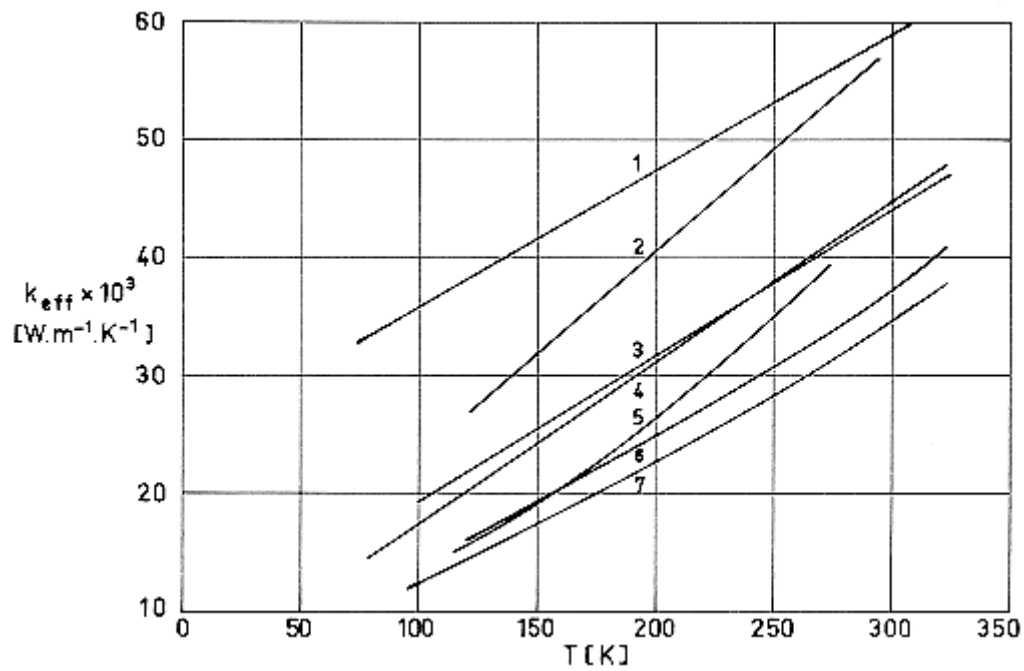
Figure 6-48: Effective thermal conductivity, k_{eff}, of several fibrous spacers as a function of mean temperature, T.

From Kaganer (1969) [33].

Explanation

Key	Description	Test Method	Comments
1	Cotton wool $\rho = 81$ kg.m^{-3}		Measured in air at normal temperature.
2	Rock wool 400		
3	Rock wool 260		
4	Glass wool 50		
5	Cotton wool 42		
6	Floss silk 58		
7	Rock wool 95		
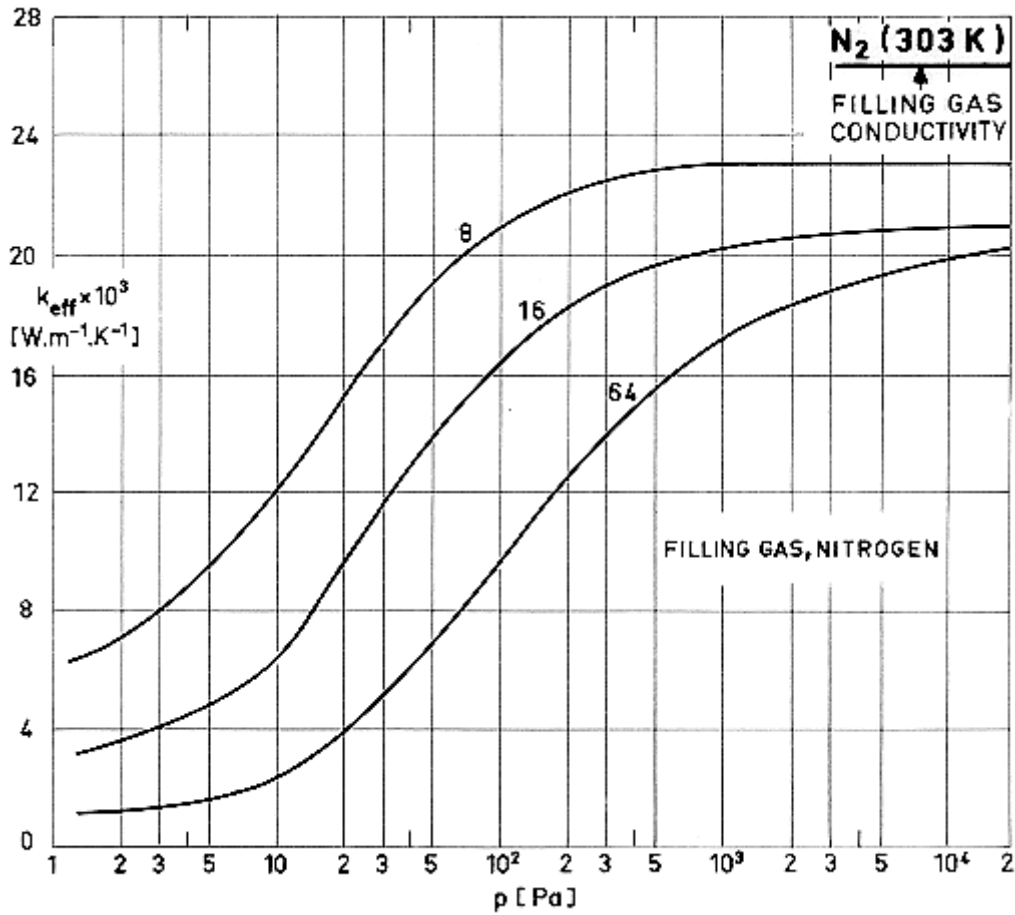
Figure 6-49: Effective thermal conductivity, k_{eff}, of Fiber-glass batting as a function of Nitrogen gas pressure, p.

Numbers on curves indicate batting densities in $kg.m^{-3}$. T_H = 303 K, T_C = 80,5 K. Thermal conductivity of Nitrogen at 303 K is indicated for comparison.

From Coston (1967) [13].
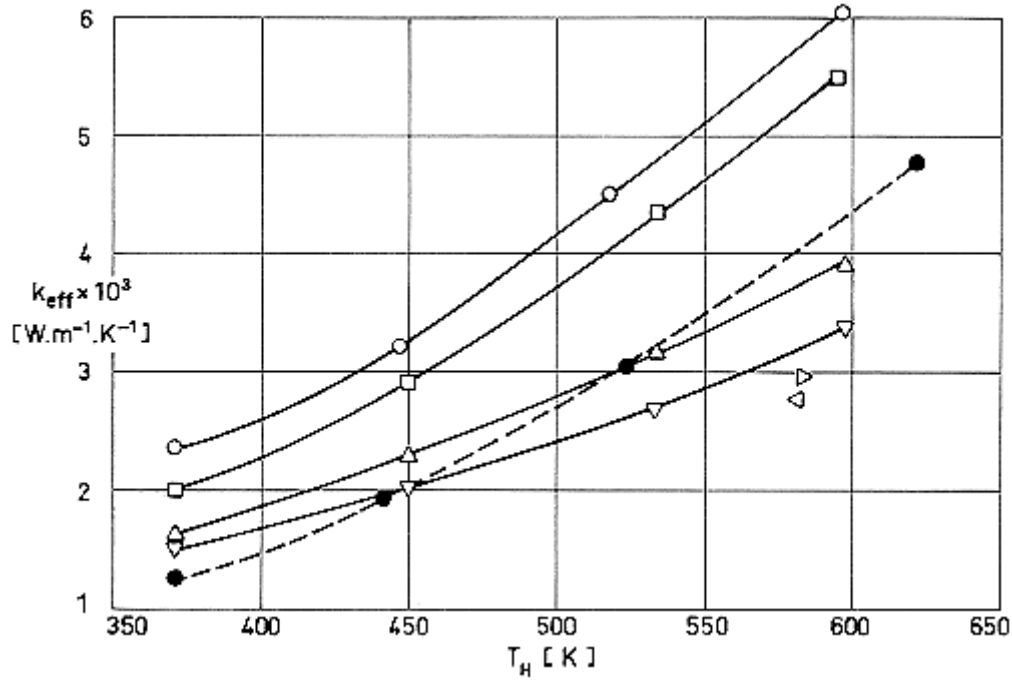
Figure 6-50: Effective thermal conductivity, k_{eff}, of Dexiglas as a function of warm-boundary temperature, T_H.

From Cunnington, Zierman, Funai & Lindahn (1967) [17].

Explanation

Key	ρ_{bulk} [kg.m^{-3}]	Layers.m^{-1}	Test Method	Comments
○	69,5	4650	Flat-Plate Calorimeter. Heat flux related to boil-off rate of liquid butane.	T_C= 273,5 K. Measured in vacuum (<1,33x10^{-2} Pa)
□	74	4920		
△	118	7870		
▽	147	9840		
▷	197	13110		
◁	236	15750		
●	69,5	4650	Flat-Plate Calorimeter. Heat flux related to boil-off rate of liquid nitrogen.	T_C = 77,5 K. Measured in vacuum (<1,33x10^{-2} Pa)
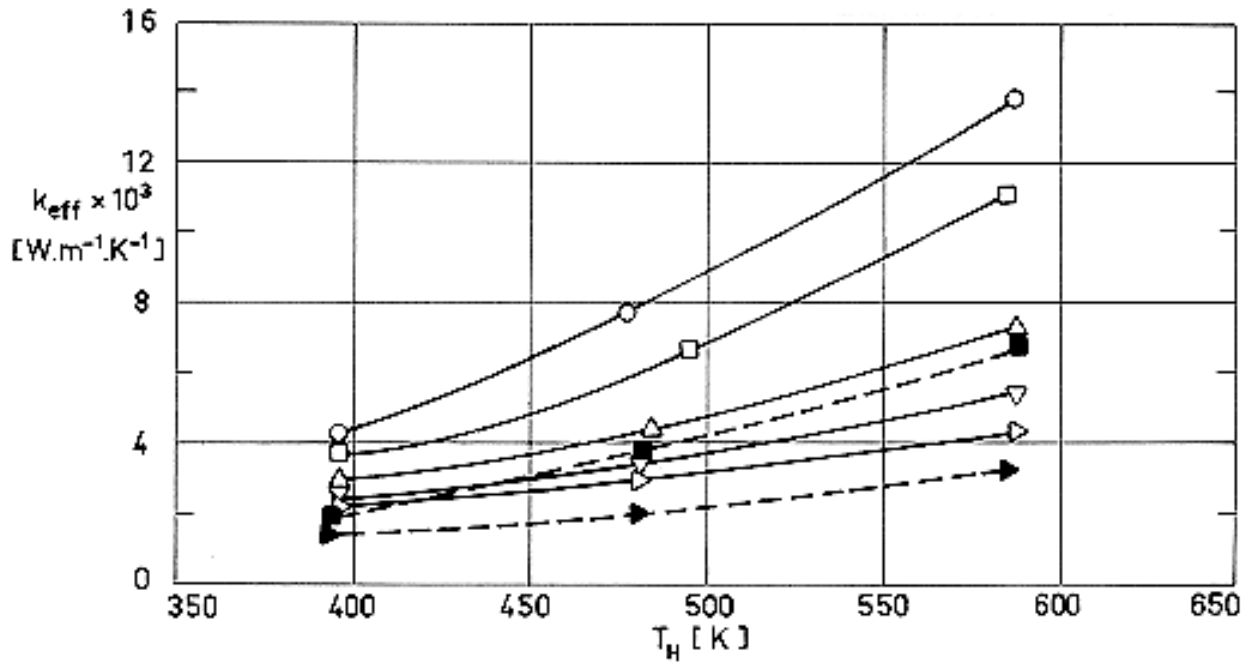
Figure 6-51: Effective thermal conductivity, k_{eff}, of Tissuglas as a function of warm-boundary temperature, T_H.

From Cunnington, Zierman, Funai & Lindahn (1967) [17].

Explanation

Key	ρ_{bulk} [kg.m^{-3}]	Layers.m^{-1}	Test Method	Comments
○	26,6	6570	Flat-Plate Calorimeter. Heat flux related to boil-off rate of liquid butane.	T_C= 273,5 K. Measured in vacuum (<1,33x10^{-2} Pa)
□	40	9840		
△	53,2	13110		
▽	80,2	19720		
▷	107	26380		
■	40	9840	Flat-Plate Calorimeter. Heat flux related to boil-off rate of liquid nitrogen.	T_C= 77,5 K. Measured in vacuum (<1,33x10^{-2} Pa)
▶	107	26380		
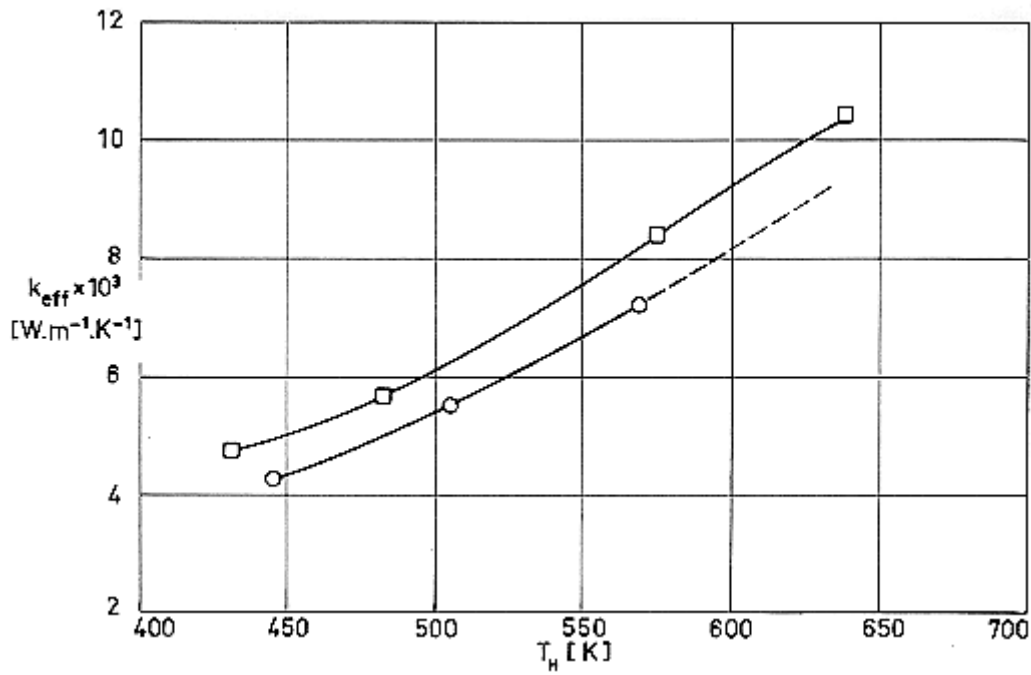
Figure 6-52: Effective thermal conductivity, k_{eff}, of Refrasil as a function of warm-boundary temperature, T_H.

From Cunnington, Zierman, Funai & Lindahn (1967) [17].

Explanation

Key	Description	Test Method	Comments
○	Refrasil A-100 Fiber Batt. Nominal fiber diameter, 10^{-6} - 2×10^{-6} m. ρ_{bulk} = 128,5 kg.m^{-3}	Flat-Plate Calorimeter. Heat flux related to boil-off rate of liquid butane.	T_C = 273,5 K. Measured in vacuum (<1,33x10^{-2} Pa)
□	Refrasil B-100 Fiber Batt. Nominal fiber diameter, $10,2 \times 10^{-6}$ m. ρ_{bulk} = 125 kg.m^{-3}		
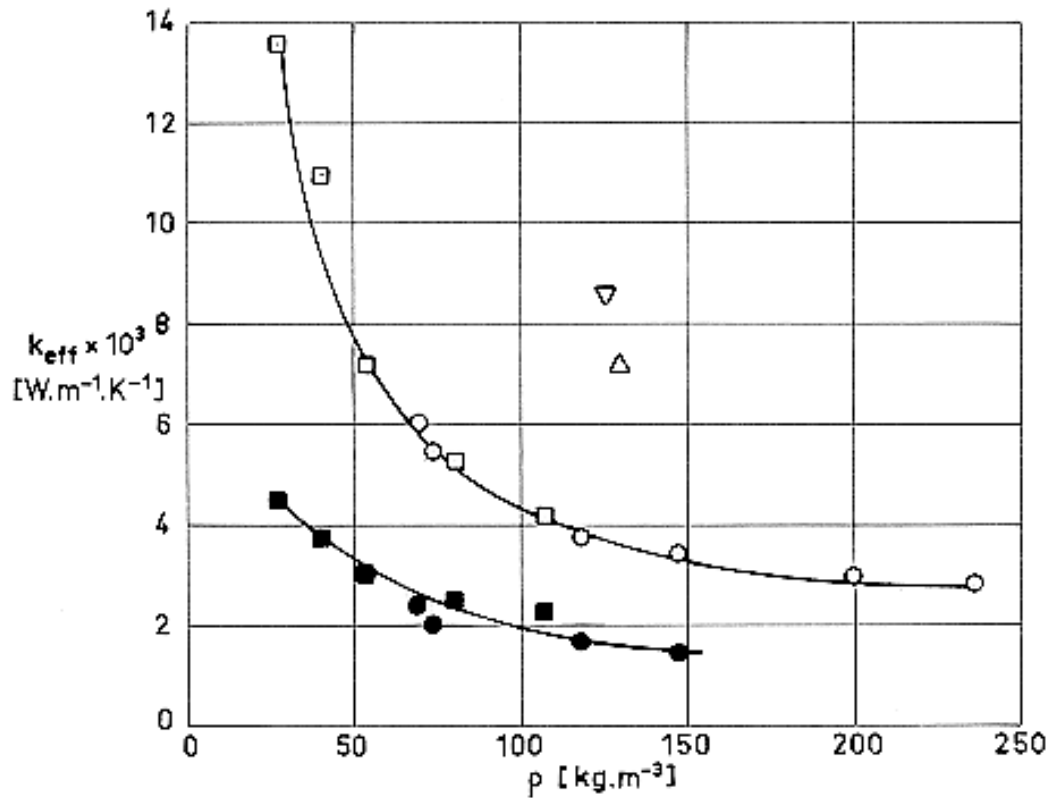
Figure 6-53: Effective thermal conductivity, k_{eff}, of several spacer materials as a function of bulk density, ρ.

From Cunnington, Zierman, Funai & Lindahn (1967) [17].

Explanation

Key	Description	Test Method	Comments
○	Dexiglas.	Flat-Plate Calorimeter. Heat flux related to boil-off rate of liquid butane.	T_H= 580 K. T_C = 273,5 K. Measured in vacuum (<1,33x10^{-2} Pa$^)$
□	Tissuglas.		
△	Refrasil A-100.		
▽	Refrasil B-100.		
●	Dexiglas.	Same as ○ .	T_H= 400 K. T_C = 273,5 K. Measured in vacuum (<1,33x10^{-2} Pa$^)$
■	Tissuglas.		
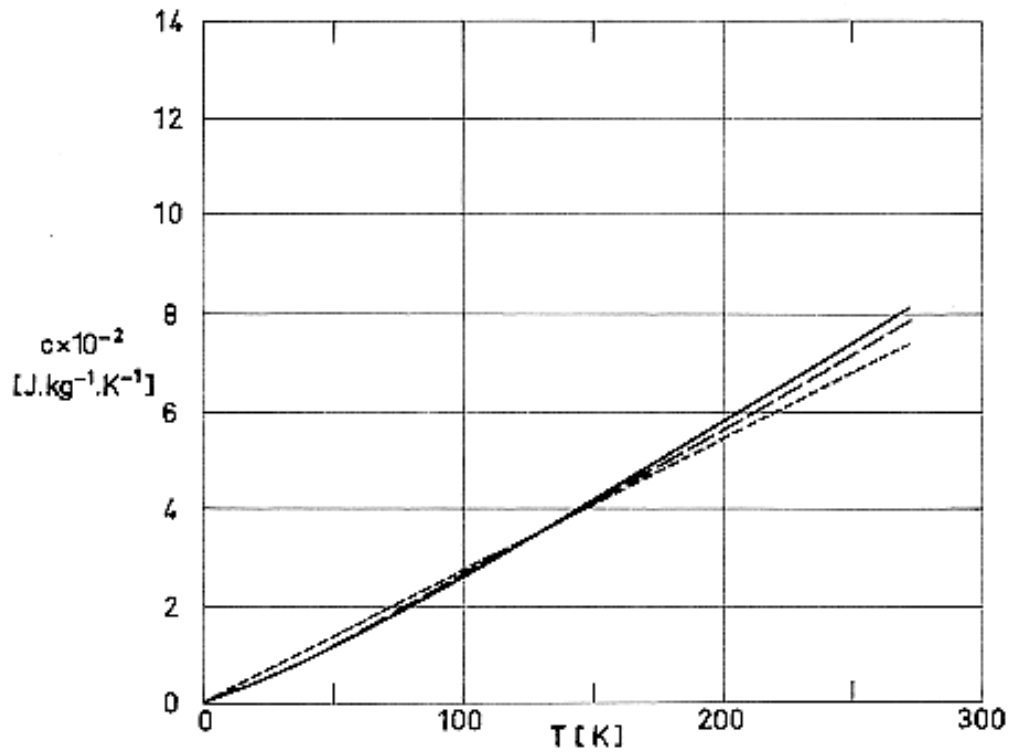
Figure 6-54: Specific Heat, *c*, of several spacer materials as a function of temperature, *T*.

From Coston (1967) [13].

Explanation

Key	Description	Comments
———	Dexiglass.	Deduced from the specific heat of Aluminium foil with Dexiglass paper spacers.
— —	Glass Fibers.	
•••••••	Quartz.	

Table 6-20: Flammability per Vertical Flame Tests

Material	Flame Time [s]	Glow Time [s]	Char Length [m]
Nomex OG. 0,11 kg.m^{-2}	0	12,8	0,081
Nomex OG. 0,17 kg.m^{-2}	0	15,2	0,086
PBI, Gold 0,10 kg.m^{-2}	0	0	0,058
PBI, Gold 0,17 kg.m^{-2}	0	0	0,015
Kynol [a] 0,20 kg.m^{-2}	0	2,8	0,003

NOTE   From Ross & Stanton (1973) [58].

[a]   Kynol is a phenol formaldehyde from The Carborundum Company.

Table 6-21: Flammability of Several Spacers in Oxygen and in Air

Material	Oxygen		Air
	1,14x10^5 Pa	0,43x10^5 Pa	10^5 Pa
Dacron batt-nonwoven, 18x10^{-3} kg.m^{-2}, 3,81x10^{-5} m thick	F	F	F
Fiber-glass Beta Marquisette, Style 2530	NF	NF	NF
Fiber-glass Plainweave Style 104 (unstabilized)	NF	NF	NF
Fiber-glass Plainweave Style 104, stabilized with 5 to 8 percent (by weight) of L-3306 Fluorel	SE	SE	NE
Polyurethane foam 4x10^3 pores per m, 7,62x10^{-4} m thick	F	F	F

NOTE   From Richardson, Ruccia & French (1970) [54].
          F : Flammable.
          NF: Non-flammable.
          SE: Self-extinguishing.

Table 6-22: Outgassing Characteristics of Several Spacers

Material (Manufacturer)	% TWL [a]	% VCM [b]	Cure Time [h]	Cure Temp. [K]	Vacuum Conditions	References
Dacron Cloth 302 Caprollon	0,050	0,040				Campbell, Marriot & Park (1973) [10]
Dacron Netting 70886-10 (Berkshire Hathaway)	0,190	0,060				
Dacron Polyester Mesh Style 15320 (Stern & Stern Textiles)	0,127	0,016				
Silk Netting Style 5517 (Jordan Marsh)	2,533	0,077				
Silk Netting Style 5517 (Jordan Marsh)	2,452	0,115	24 [c] 5 4	298 [c] 363 298	$1,33 \times 10^{-4}$ Pa $1,33 \times 10^{-4}$ Pa $1,33 \times 10^{-4}$ Pa	
Silk Netting Style 5517 (Jordan Marsh)	2,342	0,125	24 [c] 5 4	298 [c] 398 298	$1,33 \times 10^{-4}$ Pa $1,33 \times 10^{-4}$ Pa $1,33 \times 10^{-4}$ Pa	
Fiberil-Oberflächenvlies Typ T 1751 (Viledon-Werk Carl Freudenberg)	1,44	0,03			$1,33 \times 10^{-4}$ Pa	Klippel & Langer (1974) [37]
Fibrex-Polyestervlies Typ H 3002 (Viledon-Werk Carl Freudenberg)	0,36	0,03			$1,33 \times 10^{-4}$ Pa	
Perlon-Wirktüll Net F 134 (Textilwerk Schauenstein)	1,23	0,031			$1,33 \times 10^{-4}$ Pa	
Perlon-Wirktüll Net F 152 (Textilwerk Schauenstein)	1,70	0,04			$1,33 \times 10^{-4}$ Pa	
Polyester-Bobinet-Tüll Net 1946 (Textilwerk Schauenstein)	0,12	0,038			$1,33 \times 10^{-4}$ Pa	
Fiberglass Beta Marquisette Stevens Style 2530	0,9					Richardson & Ruccia & French (1971) [54]

6.10 Complete systems

As it has emphasized repeatedly, the calculation of the insulation characteristics of an MLI is a difficult task. Hence it seems useful to collect as many experimental data as possible on the performance of existing systems. This collection is the objective of clauses 6.11 to 6.17.

Ideally an MLI system is supposed to be placed normally to the temperature gradient, so that most of the data presented regard the performance of ideal systems as measured on normal calorimeters (Clause 6.11). However, thermal conductivities obtained on spacecraft can be considerably higher than those obtained in an idealized system, because of the discontinuities which are necessarily introduced in real configurations. Information on non-normal heat transfer is given in Clause 6.12. The effect of singularities such as overlaps, stitches and patches appears in Clause 6.13. In addition to these discontinuities, which are introduced during the assembling process, holes may be made in the shields to ease evacuation. These holes increase the shield transmittance, and consequently the thermal conductivity of the system. Data on the degrading effect of these holes are presented in Clause 6.14.

A limited amount of information on the effect of other type of holes, those introduced because of mechanical damage, is given in clause 6.15.

An important point concerns the effect of the inner gas on the blanket thermal conductivity. This gas may be either air, a purge gas, or species absorbed or adsorbed in the system. Since MLI systems exhibit low thermal conductivity when evacuated, two questions arise:

1.   How the inner gas degrades the thermal performance of the system (clause 6.16), and

2.   how such gases will be evacuated (clause 6.17).

The interaction of the evacuation system with the heat transfer processes is also worth being considered since holes made in the shields degrade the performance of the system. This point has been already discussed in connection with

6.11 Normal heat transfer

Effective thermal conductances of MLI systems under temperatures gradients normal to the insulation surface are given in this clause. In particular, the effects of layer density and boundary temperatures on the thermal conductance are considered.

For each MLI system at least three among the following four plots have been drawn.

1.   The effective thermal conductance, k_{eff}, as a function of the layer density measured by the number of radiation shields per unit thickness, N/t.

2.   The product of apparent density and affective thermal conductivity, ρk_{eff}, as a function of N/t. This product provides a measure of the MLI usefulness in space applications and a basic for comparing it with other systems.

3.   The compressive mechanical load, P, versus the resulting layer density, N/t. Since compression increases solid conduction, degrading the insulating characteristics of the system, some feeling on how sensitive the system is to mechanical loads is required.

4.   The variation of the effective thermal conductance with temperature for a given layer density.

It has been common practice the plotting of apparent thermal conductivity of a given system versus the warm-boundary temperature, T_H. It can be shown that for large temperature differentials the effective thermal conductivity is approximately proportional to T_H^3. When the cold-boundary temperature, T_C, is not constant, T_H is not the most appropriate parameter. The experimental evidence indicates that, when T_H is held constant, a higher thermal conductivity results from increasing T_C. The following options are now open to the compiler:

1.   For results corresponding to the same MLI with the same value of T_C, the Plotting of k_{eff} vs. T_H seems to be the best choice.

2.   When neither the maximum nor the minimum temperatures are constant a combination of both values -the characteristic temperature T- is used.

$$T = \sqrt[3]{\frac{T_H^4 - T_C^4}{4(T_H - T_C)}}$$

[6-16]

Note: non-si units are used in this figure

The data presented are arranged as follows. The MLI systems are grouped according to their shields, and for each shield, according to their spacers. The first page dealing with a given system shows k_{eff} and $\rho\ k_{eff}$ as a function of N/t. The second page gives P vs. N/t and k_{eff} vs. T. A fairly detailed description of the samples involved is given in the third page. This description includes the conditions under which the tests have been performed, such as chamber pressure, boundary temperatures and type of calorimeter used. Appropriate references are precisely identified.

In those cases where the available information has allowed the drawing of only three figures among the four abovementioned, the explanatory table is enclosed in the second of the pages corresponding to the system involved.

An index of the compiled data is given in the next page.

System			Data		
Shield	**Spacer**	**Fig.**	k_{eff} *(N/t),* ρ_{keff} *(N/t)*	*P (N/t)*	k_{eff} *(T)*
Aluminium	Fiber-glass	Figure 6-55, Figure 6-56	X	X	
Single-Aluminized Mylar Crinkled		Figure 6-57	X		X
Aluminized Mylar Dimpled		Figure 6-62	X		X
Double-Aluminized Mylar	Glass Fabric	Figure 6-64	X	X	
	Foam	Figure 6-66	X	X	X
	Silk Net	Figure 6-69	X	X	X
	Silk+Foam	Figure 6-72	X	X	
	Silk+Paper	Figure 6-74	X	X	
Single-Aluminized Kapton	Dexiglass	Figure 6-78	X		X
	Tissuglas	Figure 6-80	X		X
Double-Goldized Kapton	Dacron	Figure 6-82	X	X	
	Nomex	Figure 6-84	X	X	
Superfloc		Figure 6-86	X	X	X
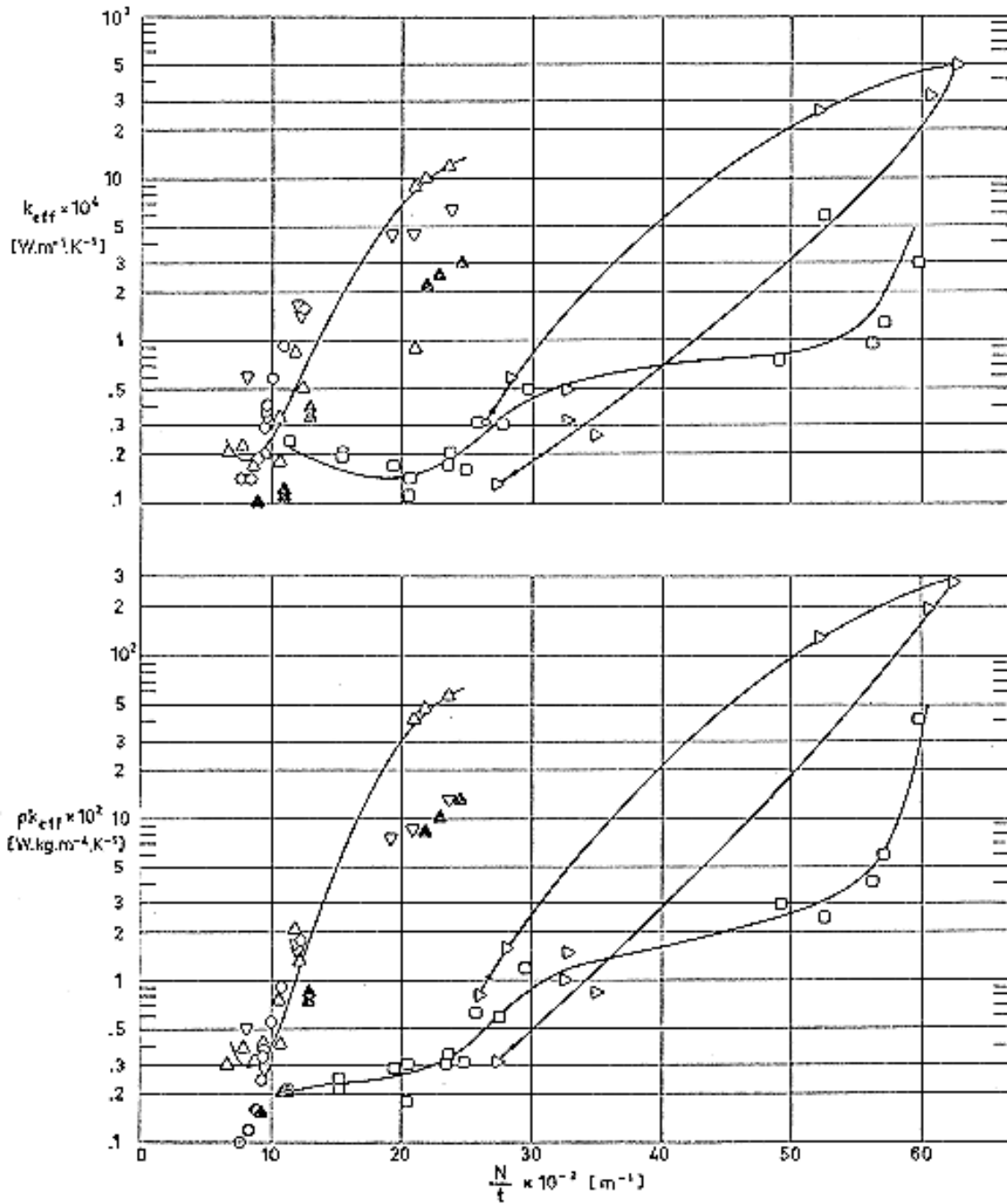
Note: non-si units are used in this figure

Figure 6-55: Effective thermal conductivity, *k*eff, and product of apparent density and effective thermal conductivity, ρ*k*eff, vs. the number of radiation shields per unit thickness, *N/t*.

Arrows in curves indicate whether the system is being loaded or unloaded.
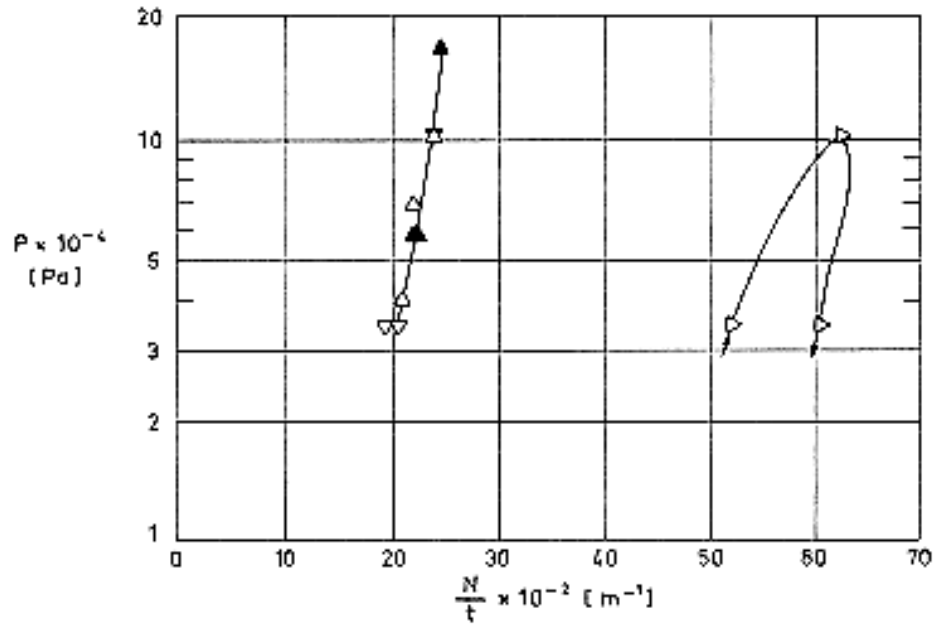
Figure 6-56: Compressive mechanical load, *P*, on the multilayer insulation vs. the number of radiation shields per unit thickness, *N/t*.

Explanation

Key	Sample Description	$t \times 10^2$ [m] Uncompressed	$\rho \times 10^3$ [Pa]	T_H [K]	T_C [K]	Calorimeter Type	References
○	N = 10 Shields. 12,7x10⁻⁶ m thick smooth Aluminium. 11 Spacers. 3,56x10⁻⁴ m thick Fiber-glass mat.	1,28	<1,33	293,5± 5	77,5	ADL Model 12. Flat-Plate (double-guarded cold-plate).	ADL (1964) [1] p. II-17.
□ ◫ ■	N = 10 Shields. 12,7x10⁻⁶ m thick smooth Aluminium. 11 Spacers. Each consisting of 3 layers of 25,4x10⁻⁶ m thick glass fiber cloth (genin). Spacers thickness 10⁻⁴ m.	0,88	<1,33	□: 288± 2,5 ◫: 284± 1,5 ■: 293± 0,5	77,5 20,5 20,5	Same as ○.	ADL (1964) [1] p. II-18.
△	N = 10 Shields. 5,08x10⁻⁵ m thick Al alloy 1145-H19 bright both sides. 11 Spacers. 5,08x10⁻⁴ m thick and 144 kg.m⁻³ CTL-449 Fiber-glass mat. CTL Div of Sudebaker Corp.	1,49 [a]		282± 2	20,5	Same as ○.	ADL (1964) [1] p. II-33.
▲	Same as △. Slots cut in the spacer to produce 11% support area.	1,11 [a]	<0,67	291,5± 1	20,5	Same as ○.	ADL (1964) [1] p. II-36.

Key	Sample Description	tx10^2 [m] Uncompressed	ρx10^3 [Pa]	T_H [K]	T_C [K]	Calorimeter Type	References
▽	N = 10 Shields. 12,7x10^{-6} m thick Aluminium Embossed. 11 Spacers. 3,56x10^{-4} m thick Fiber-glass mat.	1,22	<1,33	281± 1,5	20,5	Same as ○.	ADL (1964) [1] p. II-19.
▷	Same as squares except Aluminium Embossed, wave-like pattern.	0,38	<0,13	280,5± 1,5	20,5	Same as ○.	ADL (1964) [1] p. II-20.
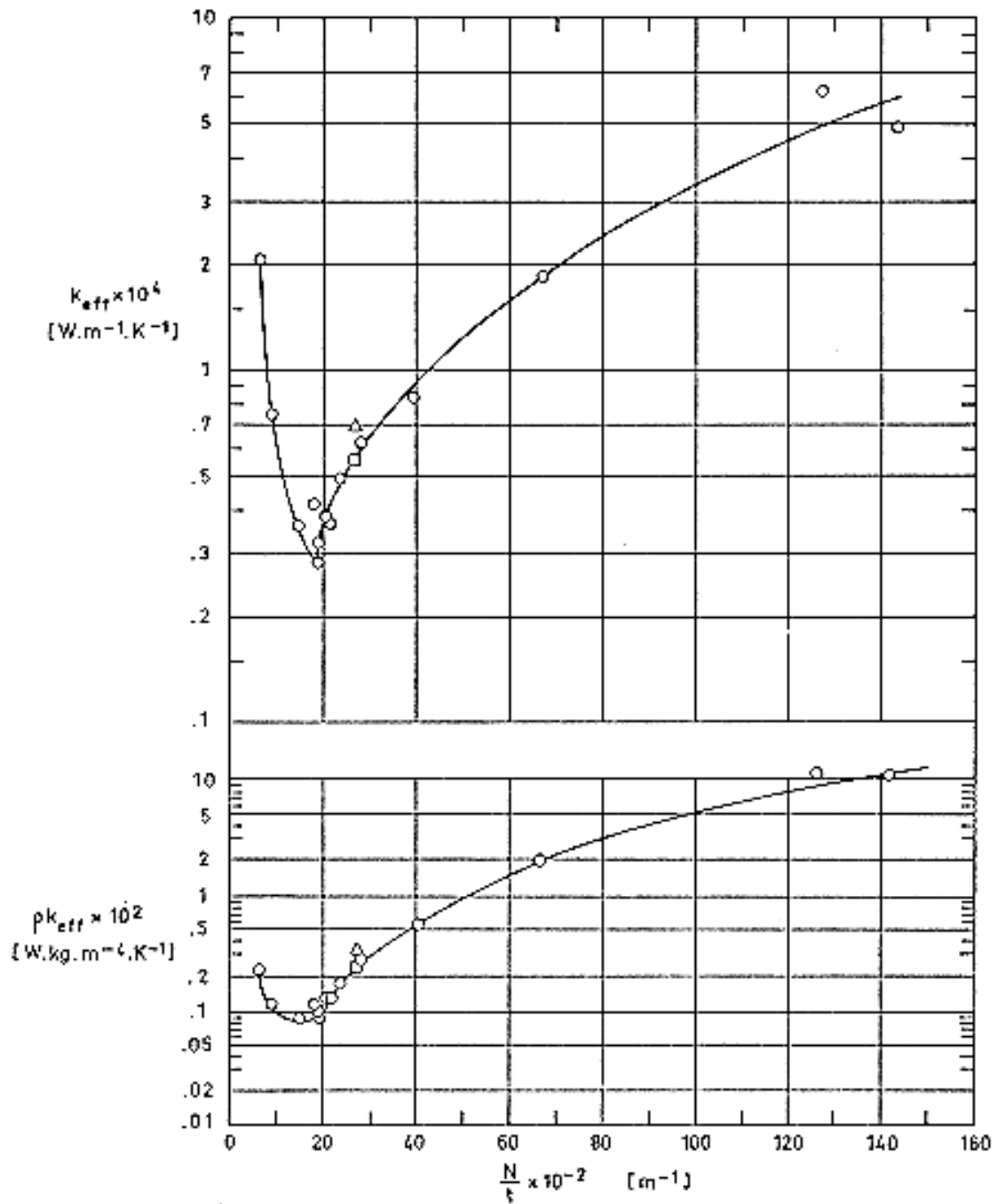
ᵃ   Largest quoted value

Figure 6-57: Effective thermal conductivity, k_{eff}, and product of apparent density and effective thermal conductivity, ρk_{eff}, vs. the number of radiation shields per unit thickness, N/t.
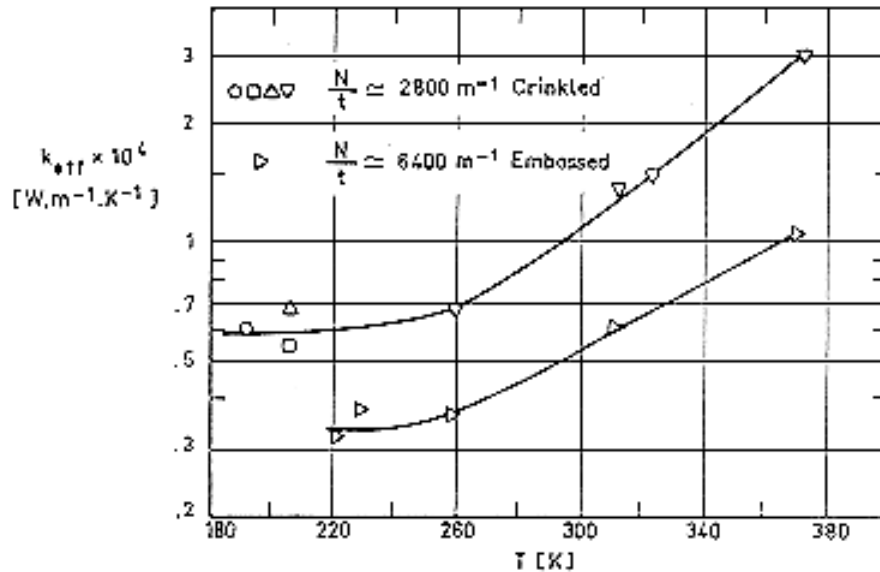
Note: non-si units are used in this figure

Figure 6-58: Effective thermal conductivity, k_{eff}, as a function of the characteristic temperature, T.

Explanation

Key	Sample description	tx10² [m] Uncom-pressed	px10³ [Pa]	T_H [K]	T_C [K]	Calorimeter Type	References
○	N=20 shields 6,35x10⁻⁶ m thick Mylar Single-Aluminized Crinkled	3,29 [a]	< 1,33	294,5	20,5	ADL Model 12 Flat-Plate (double-guarded cold-plate)	ADL (1964) [1] p. II-24
□	N=35 shields 6,35x10⁻⁶ m thick Mylar Single-Aluminized Crinkled	1,27		296	76,5		Scollon & Carpitella (1970) [62] p. B-6
△	N=35 shields 33 layers of 6,35x10⁻⁶ m thick Mylar Single-Aluminized Crinkled 2 layers of 12,7x10⁻⁶ m thick Kapton Single-Aluminized Crinkled and installed next to cold plates	1,27		295,5	76		Same as □

Key	Sample description	tx10² [m] Uncompressed	px10³ [Pa]	T$_H$ [K]	T$_C$ [K]	Calorimeter Type	References
▽	N=70 shields 6,35x10^{-6} m thick Mylar Single-Aluminized Crinkled	2,54		313,5 335,5 262 375	308 308 255 366	Lockheed/ Huntsville Cylindrical	Scollon & Carpitella (1970) [62] p. B-11 after Hale et al. (1967) [27]
▷	N=81 shields 6,35x10^{-6} m thick Mylar Single-Aluminized Embossed	1,27	0,373 0,613 0,453 0,373 0,307	238 273 321,5 384 295,5	204,5 244 300 355,5 147,5	Lockheed/ huntsville Cylindrical	Hale (1969) [27] p. 41

a   Largest quoted value.
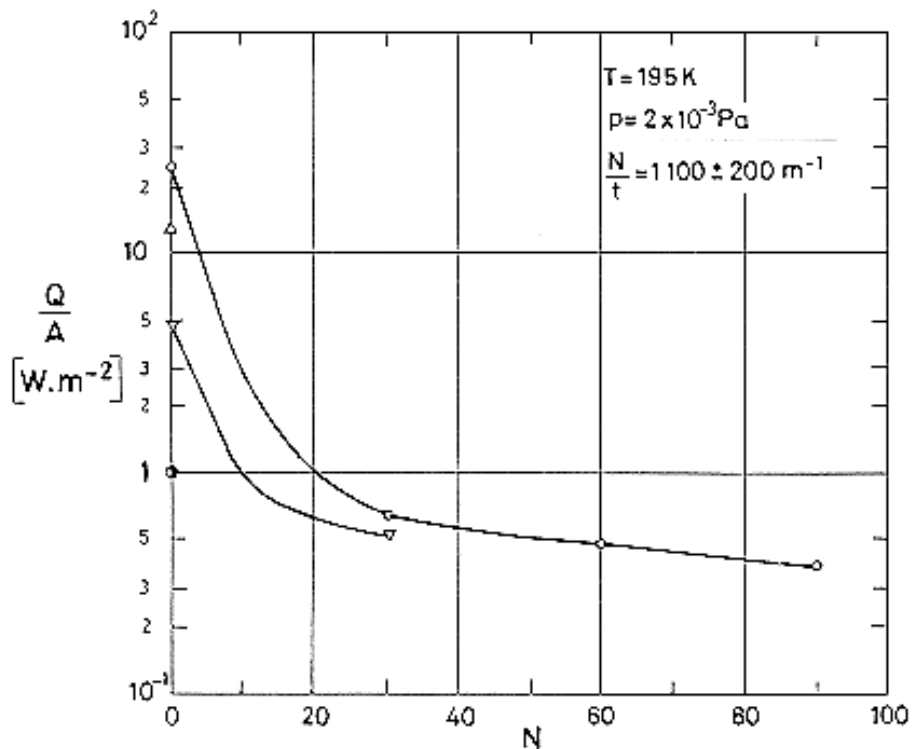
Figure 6-59: Heat flux, *Q/A*, across a single-aluminized Mylar, crinkled, MLI on different substrate plates, as a function of the number of radiation shields, *N*. *T* = 195 K, *p* = 2 x 10^{-3} Pa. *N/t* = 1100 ± 200 m^{-1}.

From Shu, Fast & Hart (1986) [65].

Explanation

Key	Substrate Plate	T_H [K]	T_C [K]	Calorimeter Type
○	Black Painted Copper	277	77	Vertical inner copper plate 2,26 m² refrigerated by a thermosiphon LN2 tube and within a copper box at room temperature. Box enclosed in an insulating vacuum cylinder. Pressure measured in the box. Nitrogen boil-off rate measured with a wet test meter.

Copper-Constantan thermocouples in the inner plate and between selected layers of the MLI. |
◐	Black Painted Copper (MLI with cracks)			
△	Polished Copper			
▽	Al Taped Copper			

Figure 6-60: Effective thermal conductivity, k_{eff}, of a single-aluminized Mylar, crinkled, MLI on two different substrate plates, as a function of the number of radiation shields, N.

MLI description and calorimeter type as in Figure 6-59 above. ○ : black painted copper substrate plate. ▽ : Al taped copper substrate plate. From Shu, Fast & Hart (1986) [65].
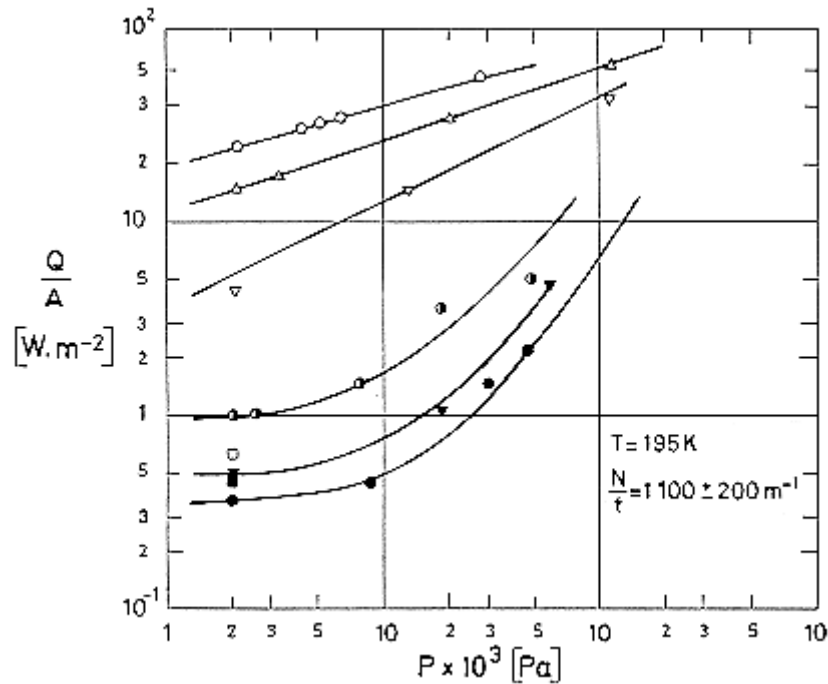
Figure 6-61: Heat flux, *Q/A*, across a single-aluminized Mylar, crinkled, MLI on different substrate plates, as a function of the pressure, *p*. T = 195 K. Layer density, *N/t* = 1100 ± 200 m⁻¹ in any case.

From Shu, Fast & Hart (1986) [65].

Explanation

Key	N	Substrate Plate	T_H [K]	T_C [K]	Calorimeter Type
○	0	Black Painted Copper	277	77	Vertical inner copper plate 2,26 m² refrigerated by a thermosiphon LN2 tube and within a copper box at room temperature. Box enclosed in an insulating vacuum cylinder. Pressure measured in the box. Nitrogen boil-off rate measured with a wet test meter.
◑	90 (cracks)				
●	90				
□	30				
■	60				Copper-Constantan thermocouples in the inner plate and between selected layers of the MLI.
△	0	Polished Copper (by hand)			
▽	0	Taped Copper (3M 425 Al tape)			
▼	30				

Note: non-si units are used in this figure

Figure 6-62: Effective thermal conductivity, k_{eff}, and product of apparent density and effective thermal conductivity, ρk_{eff}, vs. the number of radiation shields per unit thickness, N/t.

Values of N are given in parenthesis.
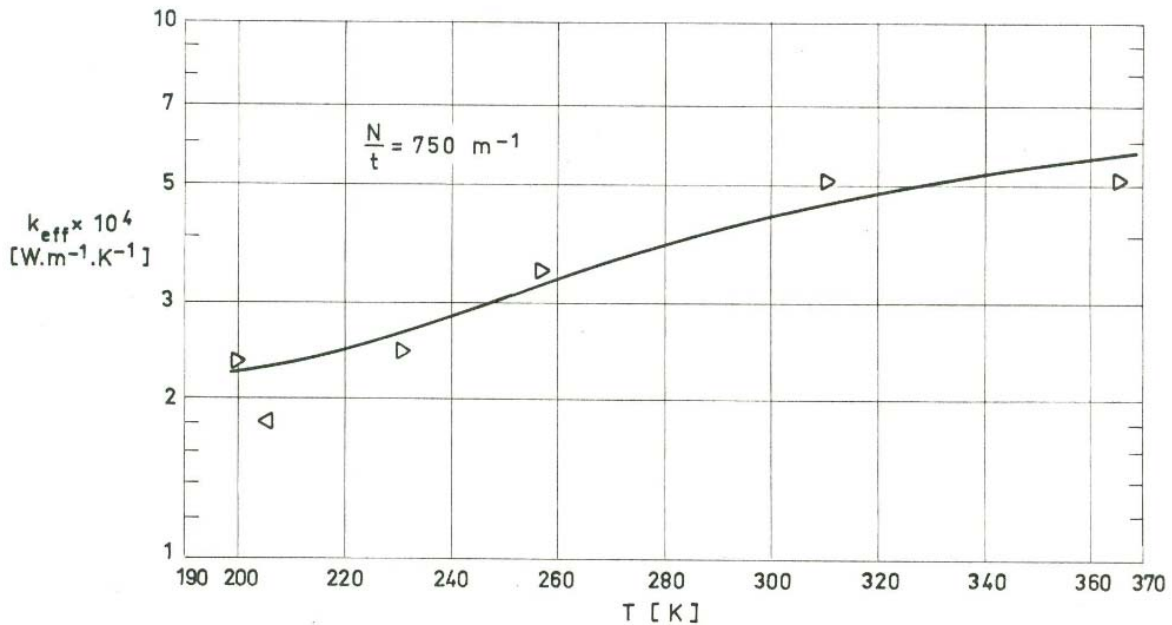
Figure 6-63: Effective thermal conductivity, k_{eff}, as a function of the characteristic temperature, T.

Explanation

Key	Sample description	t×10² [m] Uncompressed	p×10³ Pa]	T_H [K]	T_C [K]	Calorimeter Type	References
○	N=10 10 layers 12,7x10⁻⁶ m thick Mylar Double-Aluminized 10 layers 12,7x10⁻⁶ m thick Mylar Double-Aluminized Dimplar	2,54		294,5	78	NBS - Cryostat Cylindrical	Coston (1967) [13] pp. 4,3-5, 4,3-11
□	Variable number of layers. Same components as ○ .			393	78	Same as ○	
△	Same as □ .			296	20,5	Flat-Plate	
▽	Same as △ .					Same as △	
▷	N=22 22 layers of 6,35x10⁻⁶ m thick Mylar Single-Aluminized Dimplar 22 layers of 6,35x10⁻⁶ m thick Mylar Single-Aluminized	2,92	0,333 0,133 0,506 0,506 0,440	210 267 290 319,5 376,5	189 245,5 159 301,5 356	Lockheed/ huntsville Cylindrical	Hale (1969) [27] p. 42

Key	Sample description	tx10² [m] Uncompressed	px10³ Pa]	T$_H$ [K]	T$_C$ [K]	Calorimeter Type	References
	Embossed						
◁	N=8 8 layers of 12,7x10^{-6} m thick Mylar Single-Aluminized Deeply Corrugated 8 layers of 12,7x10^{-6} m thick Mylar Smooth Reflector	1,90 2,16		295 295,5	77 76		Scollon & Carpitella (1970) [62] p. B-7
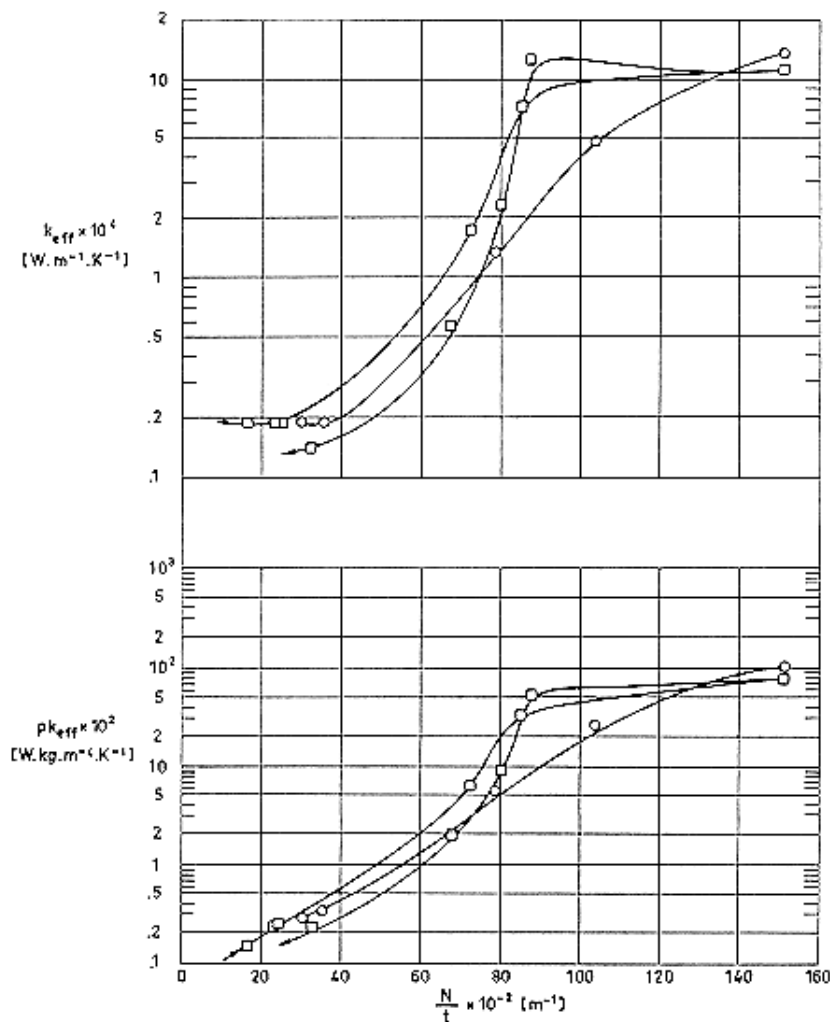
Note: non-si units are used in this figure

Figure 6-64: Effective thermal conductivity, k_{eff}, and product of apparent density and effective thermal conductivity, ρk_{eff}, vs. the number of radiation shields per unit thickness, N/t.

Arrows in curves indicate whether the system is being loaded or unloaded.
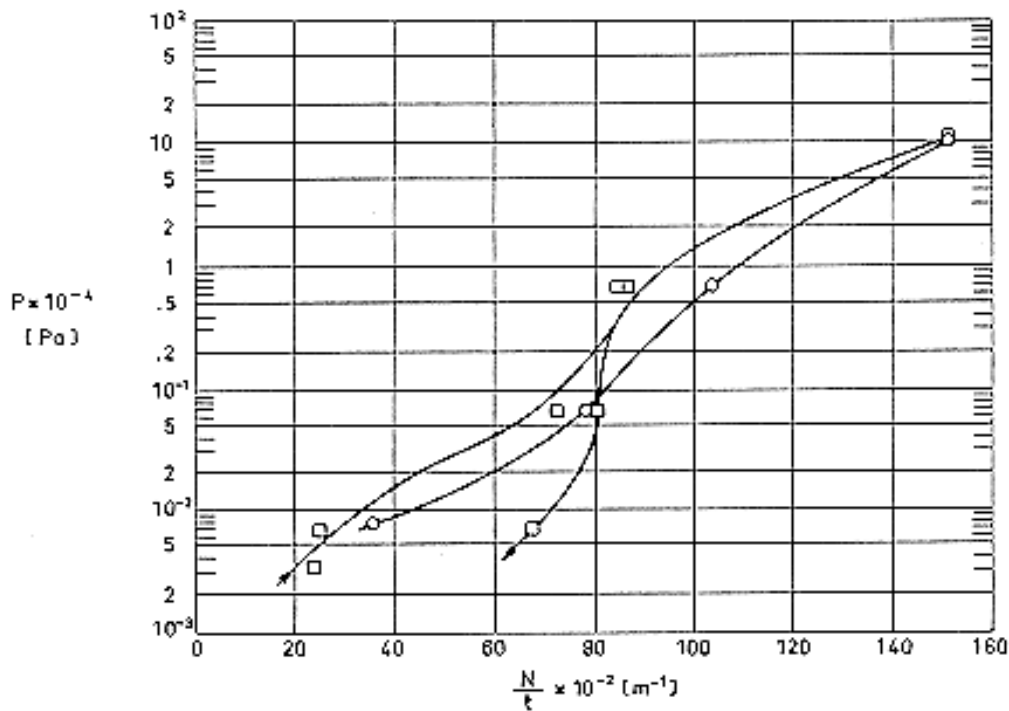
Note: non-si units are used in this figure

Figure 6-65: Compressive mechanical load, *P*, on the multilayer insulation vs. the number of radiation shields per unit thickness, *N*/*t*.

Explanation

Key	Sample Description	$tx10^2$ [m] Uncompressed	$px10^3$ [Pa]	T_H [K]	T_C [K]	Calorimeter Type	References
○	*N* = 10 Shields. 6,35x10⁻⁶ m thick x 0,279 m diameter Mylar. Double-Aluminized. 21 Spacers. 25,4x10⁻⁶ m thick x 0,305 m diameter Glass fabric.	0,330	<6,67	277,5± 1	77,5	ADL Model 12. Flat-Plate (double-guarded cold-plate).	ADL (1966) [2] p. II-33.
□	*N* = 10 Shields. 6,35x10⁻⁶ m thick x 0,279 m diameter Mylar. Double-Aluminized. 22 Spacers. 25,4x10⁻⁶ m thick x 0,305 m diameter Glass fabric.	0,599	<0,67	294± 3	77,5	Same as ○.	ADL (1966) [2] p. II-87.
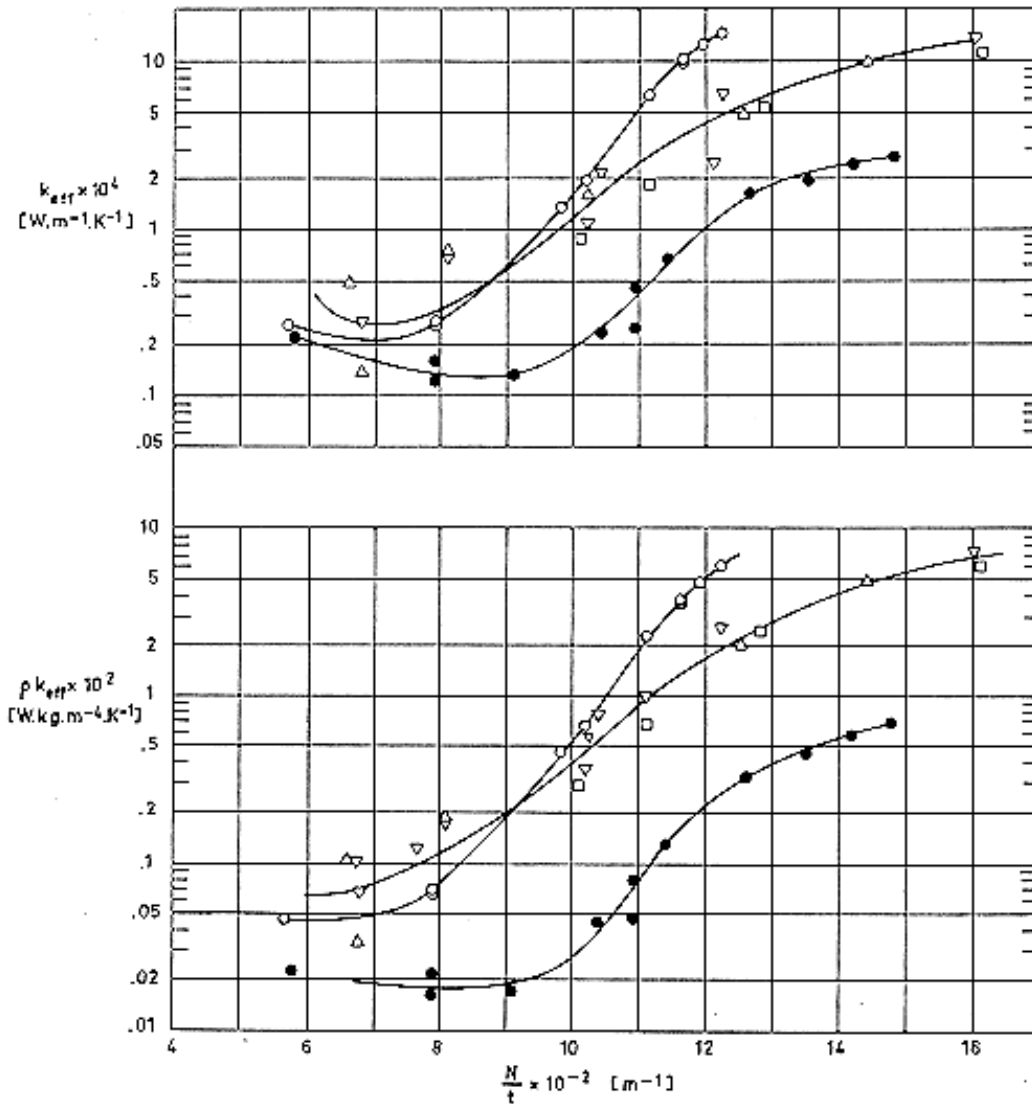
Note: non-si units are used in this figure

Figure 6-66: Effective thermal conductivity, k_{eff}, and product of apparent density and effective thermal conductivity, ρk_{eff}, vs. number of radiation shields per unit thickness, N/t.
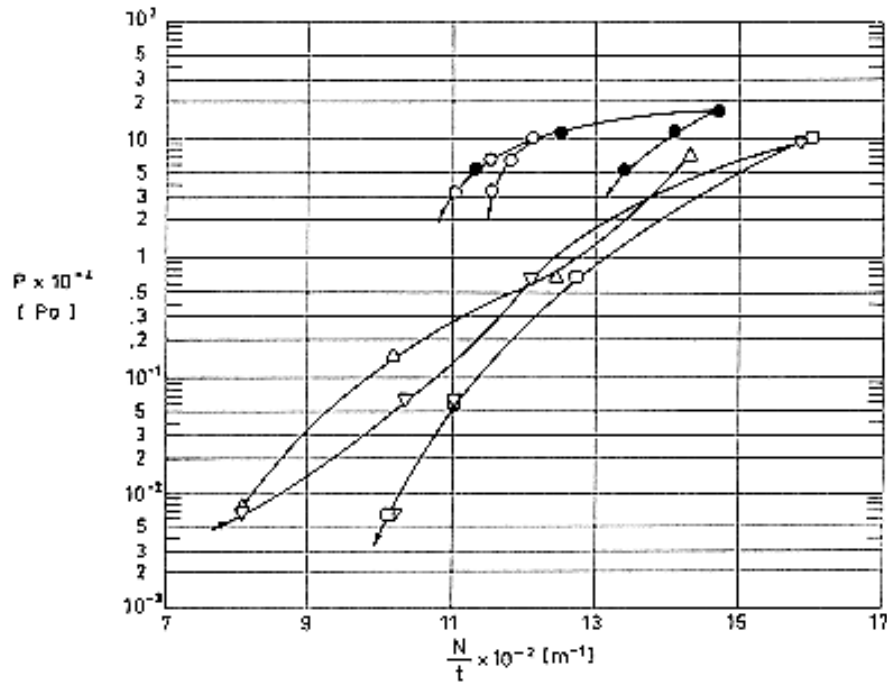
Note: non-si units are used in this figure

Figure 6-67: Compressive mechanical load, *P*, on the multilayer insulation vs. the number of radiation shields per unit thickness, *N*/*t*.

Arrows in curves indicate whether the system is being loaded or unloaded.
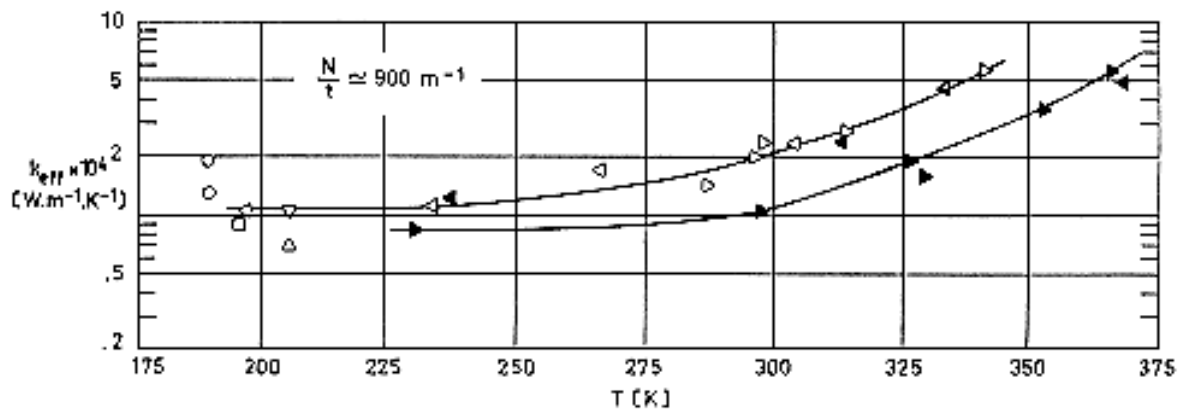
Note: non-si units are used in this figure

Figure 6-68: Effective thermal conductivity, k_{eff}, as a function of the characteristic temperature, *T*.

Explanation

Key	Sample Description	tx10^2 [m]	px10^3 [Pa]	T_H [K]	T_C [K]	Calorimeter Type	References
○	N = 10 Shields 11 Spacers 32 Kg.m^{-3} Freon blown polyurethane foam. 5x10^{-4} m thick. The spacers were formed by placing two semicircles together and cementing them only near the outer edge.	1,74 [a]	< 6,7	293± 0,5	20,5	ADL Model 12 Flat-Plate (double-guarded cold-plate).	ADL (1964) [1] p. II-34
●	Same as ○ Slots were cut in the spacers to produce 11% support area.	1,71 [a]	< 6,7	293,5± 1	20,5	Same as ○	ADL (1964) [1] p. II-35
□	N = 10 Shields 11 Spacers 32 Kg.m^{-3} Freon blown polyurethane foam. 5x10^{-4} m thick x 0,305 m diameter	0,99 [a]	< 4,0	277,5	77,5	Same as ○	ADL (1966) [2] p. II-72
△	Same as □	1,51 [a]	< 6,7	279± 1	77,5	Same as ○	ADL (1966) [2] p. II-32
▽	Same as □	1,52 [a]	< 4,0	295± 1	77,5	Same as ○	Same as □

Key	Sample Description	tx10^2 [m]	px10^3 [Pa]	T_H [K]	T_C [K]	Calorimeter Type	References
▷	N = 22 Shields 21 Spacers 7,62x10^{-4} m thick Goodyear foam (before outgassing of foam at 366,5 K)	2,54	< 1,1	300,5 316,5 344 289,5 299	295 311 338 283,5 292,5	Lockheed/ Huntsville/ Cylindrical	Scollon & Carpitelle (1970) [62]. pp. B-11, B-12
▶	Same as ▷. (after outgassing of foam at 366,5 K)	2,54	< 1,1	369 298 356 332,5 300 232	362,5 148 349 325,5 294 227	Same as ▷	Same as ▷
◁	N = 24 Shields 23 Spacers 7,11x10^{-4} m thick Goodyear foam (before outgassing of foam at 366,5 K)	2,54	0,400 0,533 0,533 0,987	210 246,5 278 311,5	184 219 254,5 297,5	Same as ▷	Hale (1969) [27] p. 39
◀	Same as ◁. (during outgassing of foam at 366,5 K)	2,54	2,67	344	322,5	Same as ▷	Same as ◁
◀	Same as ◁. (after outgassing of foam at 366,5 K)	2,54	1,87 0,480 0,200	379 325,5 299	357 301,5 166	Same as ▷	Same as ◁

a   Largest quoted value.
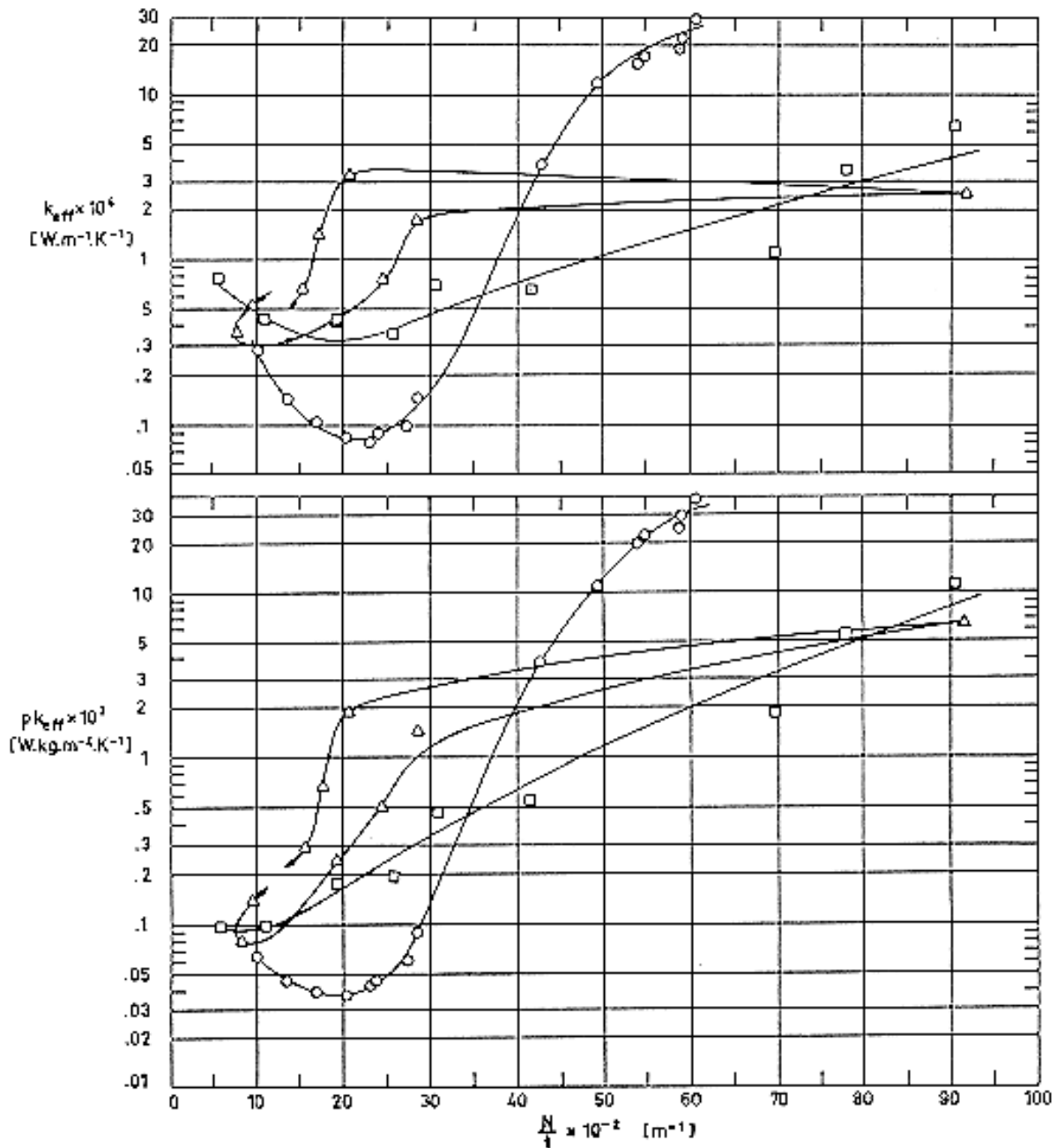
Note: non-si units are used in this figure

Figure 6-69: Effective thermal conductivity, k_{eff}, and product of apparent density and effective thermal conductivity, ρk_{eff}, vs. the number of radiation shields per unit thickness, N/t. Arrows in curves indicate whether the system is being loaded or unloaded.
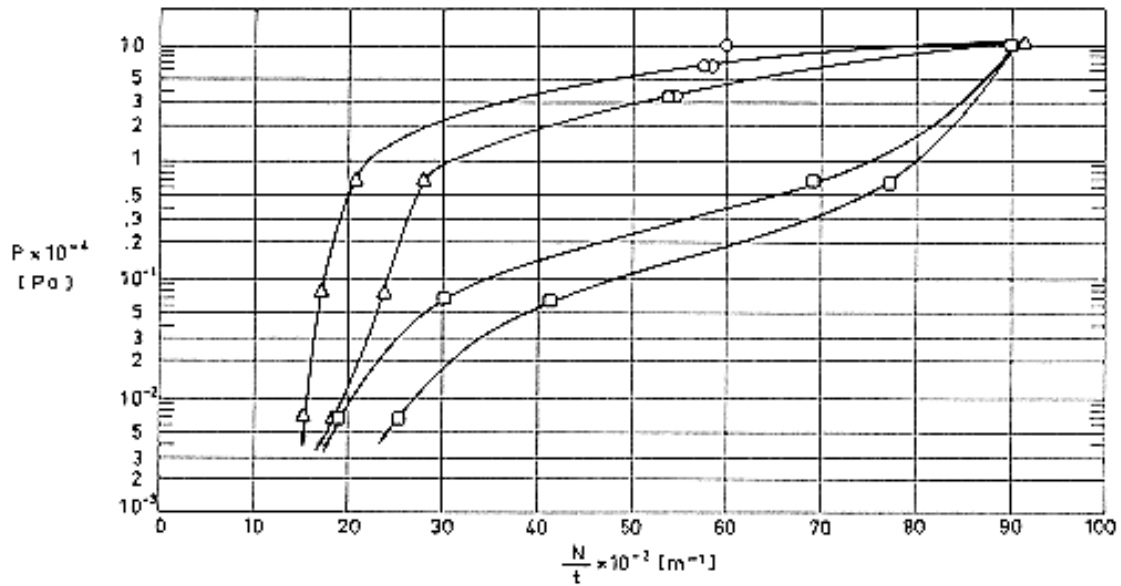
Note: non-si units are used in this figure

Figure 6-70: Compressive mechanical load, *P*, on the multilayer insulation vs. the number of radiation shields per unit thickness, *N*/*t*.
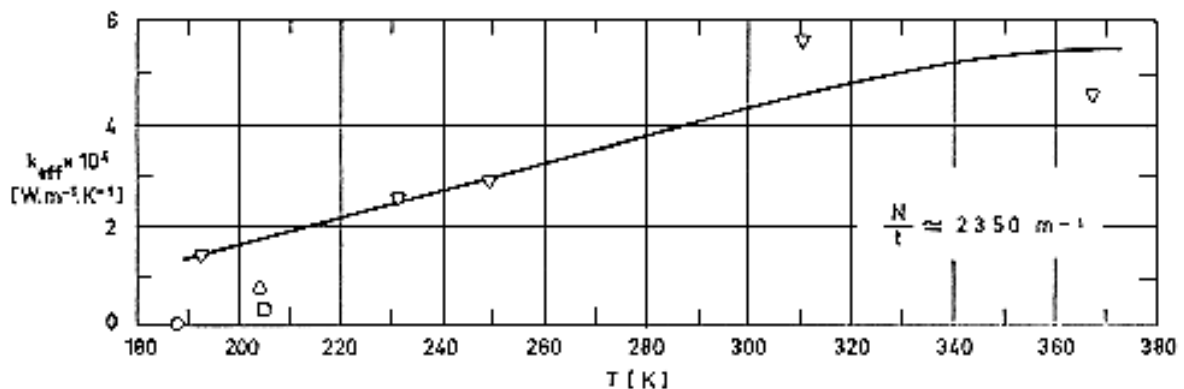
Figure 6-71: Effective thermal conductivity, *k*$_{eff}$, as a function of the characteristic temperature, *T*.

Explanation for above Figures

Key	Sample Description	*t*x10² [m] Uncompressed	*p*x10³ [Pa]	T$_H$ [K]	T$_C$ [K]	Calorimeter Type	References
○	*N* = 10 Shields 6,35x10⁻⁶ m thick Mylar Double-Aluminized 11 Spacers 1,78x10⁻⁴ m thick Nylon Netting	1 [a]	< 0,53	292± 1	20,5	ADL Model 12 Flat-Plate (double-guarded cold-plate)	ADL (1964) [1] p. II-37

Key	Sample Description	$t\text{x}10^2$ [m] Uncompressed	$p\text{x}10^3$ [Pa]	T_H [K]	T_C [K]	Calorimeter Type	References
□	N = 10 Shields $6,35\text{x}10^{-6}$ m thick x $2,79\text{x}10^{-1}$ m diameter Mylar Double-Aluminized 22 Spacers $7,62\text{x}10^{-5}$ m thick x $3,05\text{x}10^{-1}$ m diameter Silk Netting	1,73 [a]	< 6,67	295± 1,5	77,5	Same as ○	ADL (1966) [2] p. II-35
△	N = 10 Shields $6,35\text{x}10^{-6}$ m thick x $2,79\text{x}10^{-1}$ m diameter Mylar Double-Aluminized 33 Spacers $7,62\text{x}10^{-5}$ m thick x $2,79\text{x}10^{-1}$ m diameter Silk Netting	1,24	< 6,67	294± 3	77,5	Same as ○	ADL (1966) [2] p. II-34
▽	N = 60 Shields $6,35\text{x}10^{-6}$ m thick Mylar Single-Aluminized Embossed 60 Spacers White Nylon Netting	2,54	< 0,96	209 261,5 296 320 378	176 236,5 152,5 301,5 357	Lockheed/ Huntsville Cylindrical	Hale (1969) [27] p. 43

[a]   Largest quoted value.

Figure 6-72: Effective thermal conductivity, k_{eff}, and product of apparent density and effective thermal conductivity, ρk_{eff}, vs. the number of radiation shields per unit thickness, N/t.

Arrows in curves indicated whether the system is being loaded or unloaded.
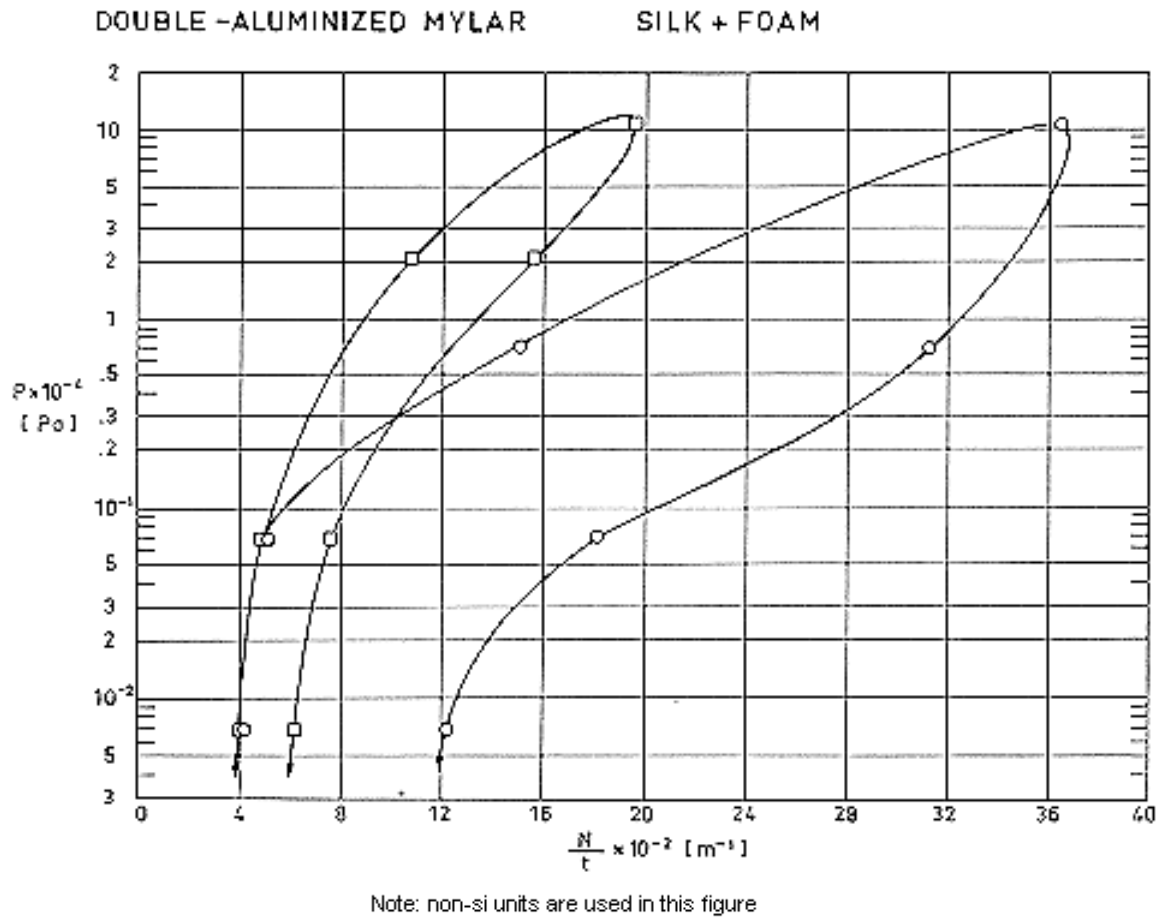
Figure 6-73: Compressive mechanical load, *P*, on the multilayer insulation vs. the number of radiation shields per unit thickness, *N*/*t*.

Explanation for above Figures

Key	Sample Description	tx10² [m] Uncompressed	px10³ [Pa]	T_H [K]	T_C [K]	Calorimeter Type	References
○	N = 10 Shields 6,35x10⁻⁶ m thick x 0,279 m diameter Mylar Double-Aluminized. 11 Spacers. 7,62x10⁻⁵ m thick x 3,05x10⁻¹ m diameter Silk Netting Having 2,54x10⁻³ m thick x6,35x10⁻³ m wide x5,72x10⁻² m long flexible polyurethane foam (Scott Paper Co) strips heat sealed by a polyester film strip.	3,20 [a]	< 6,67	294± 3	77,5	ADL Model 12. Flat-Plate (double-guarded cold-plate)	ADL (1964) [1] p. II-61.
□	Same as ○ except polyurethane foam rigid. A soft cushion consisting of 3 layers of 1,78x10⁻³ m thick flexible polyurethane foam was placed between the test sample and the warm plate. The temperature of the face toward the sample of the cushion was monitored at 294 K.	3,60 [a]	< 6,67	294± 3	77,5	ADL Model 12. Flat-Plate (double-guarded cold-plate)	ADL (1966) [2] p. II-62.

[a]   Largest quoted value.
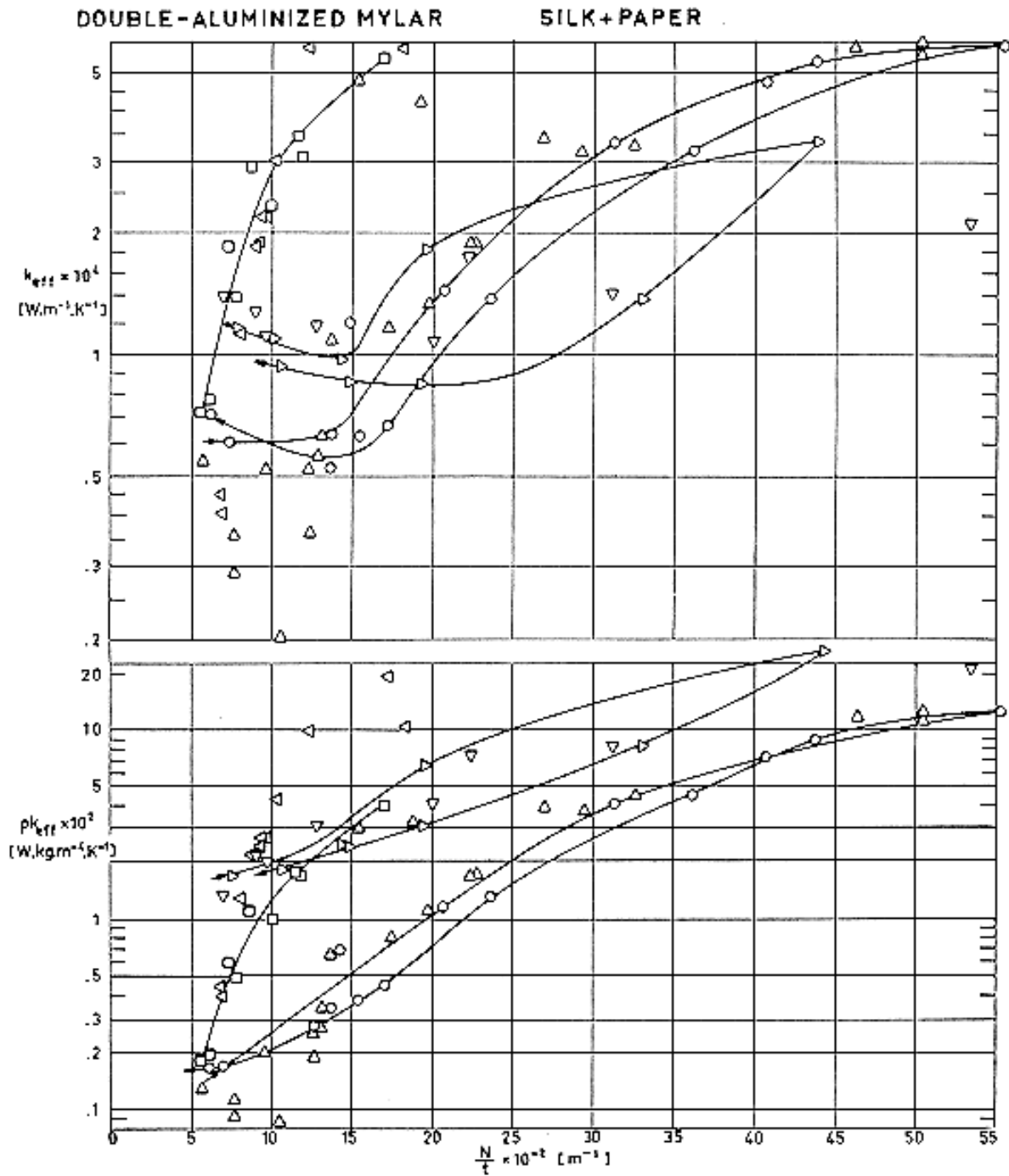
Note: non-si units are used in this figure

Figure 6-74: Effective thermal conductivity, k_{eff}, and product of apparent density and effective thermal conductivity, ρk_{eff}, vs. the number of radiation shields per unit thickness, N/t.

Arrows in curves indicated whether the system is being loaded or unloaded.

Figure 6-75: Effective thermal conductivity, *k*eff, and product of apparent density and effective thermal conductivity, ρ*k*eff, vs. the number of radiation shields per unit thickness, *N*/*t*. Complete loading-unloading history of system (△).

DOUBLE-ALUMINIZED MYLAR   SILK + PAPER

Note: non-si units are used in this figure

Figure 6-76: Compressive mechanical load, *P*, on the multilayer insulation vs. the number of radiation shields per unit thickness, *N/t*.
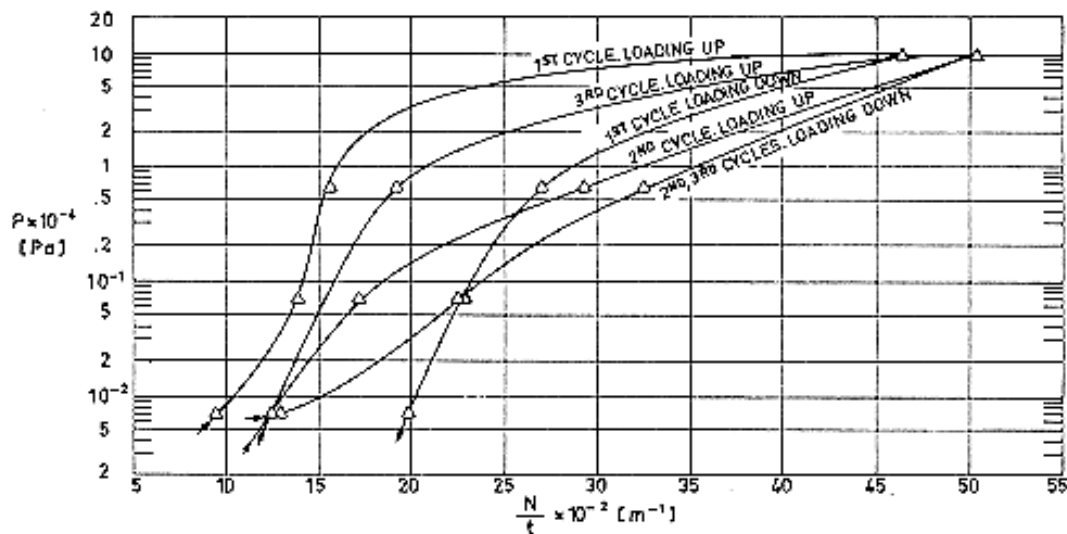

Note: non-si units are used in this figure

Figure 6-77: Compressive mechanical load, *P*, on the multilayer insulation vs. the number of radiation shields per unit thickness, *N/t*. Complete loading-unloading history of system (△).

Explanation for above Figures

Key	Sample Description	tx10^2 [m] Uncompressed	px10^3 [Pa]	T_H [K]	T_C [K]	Calorimeter Type	References
◯	N = 10 Shields 6,35x10^{-6} m thick x 2,79x10^{-1} m diameter Mylar Double-Aluminized. 11 Spacers. 7,62x10^{-5} m thick x 3,05x10^{-1} m diameter Silk Netting plus 1,02x10^{-4} m thick Glass Paper strips 1,27x10^{-2} m wide sewed on both sides of silk netting 2,54x10^{-2} m apart	1,36 [a]	< 2,67	94± 1,5	77,5	ADL Model 12. Flat-Plate (double-guarded cold-plate)	ADL (1966) [2] p. II-45.
▢	N = 10 Shields 6,35x10^{-6} m thick x 2,79x10^{-1} m diameter Mylar Double-Aluminized. 11 Spacers. 7,62x10^{-5} m thick x 3,05x10^{-1} m diameter Silk Netting plus 2,54x10^{-4} m thick Glass Paper sewed on both sides of silk netting	1,72 [a]	< 2,67	295± 2	77,5	Same as ◯	ADL (1966) [2] p. II-46.
△	N = 10 Shields 6,35x10^{-6} m thick x 2,79x10^{-1} m diameter Mylar Double-Aluminized. 11 Spacers. 7,62x10^{-5} m thick x 3,05x10^{-1} m diameter Silk Netting plus 2,03x10^{-4} m thick Glass Paper strips 6,35x10^{-3} m wide sewed on both sides of silk netting 3,18x10^{-2} m apart	1,71 [a]	< 1,33	294± 1	77,5	Same as ◯	ADL (1966) [2] p. II-48, II-49.

Key	Sample Description	tx10^2 [m] Uncompressed	px10^3 [Pa]	T_H [K]	T_C [K]	Calorimeter Type	References
▽	N = 10 Shields 6,35x10^{-6} m thick x 2,79x10^{-1} m diameter Mylar Double-Aluminized. 11 Spacers. 7,62x10^{-5} m thick x 3,05x10^{-1} m diameter Silk Netting plus 2,03x10^{-4} m thick Glass Paper disks 6,35x10^{-3} m diameter sewed on both sides of silk netting on 3,81x10^{-2} m centers with 1,52x10^{-4} m diameter thread	1,40 [a]	< 1,33	294± 2	77,5	Same as ○	ADL (1966) [2] p. II-52.
▷	Same as ▽ although threads were removed	1,31 [a]	< 5,33	296± 3	77,5	Same as ○	ADL (1966) [2] p. II-55.
◁	N = 10 Shields 6,35x10^{-6} m thick x 2,79x10^{-1} m diameter Mylar Double-Aluminized. 11 Spacers. 7,62x10^{-5} m thick x 3,05x10^{-1} m diameter Silk Netting plus 22 disks 2,03x10^{-4} m thick Glass Paper 0,305 m diameter placed on both sides of silk netting	1,43 [a]	< 9,33	296± 3	77,5	Same as ○	ADL (1966) [2] p. II-56.

[a]   Initial Value.

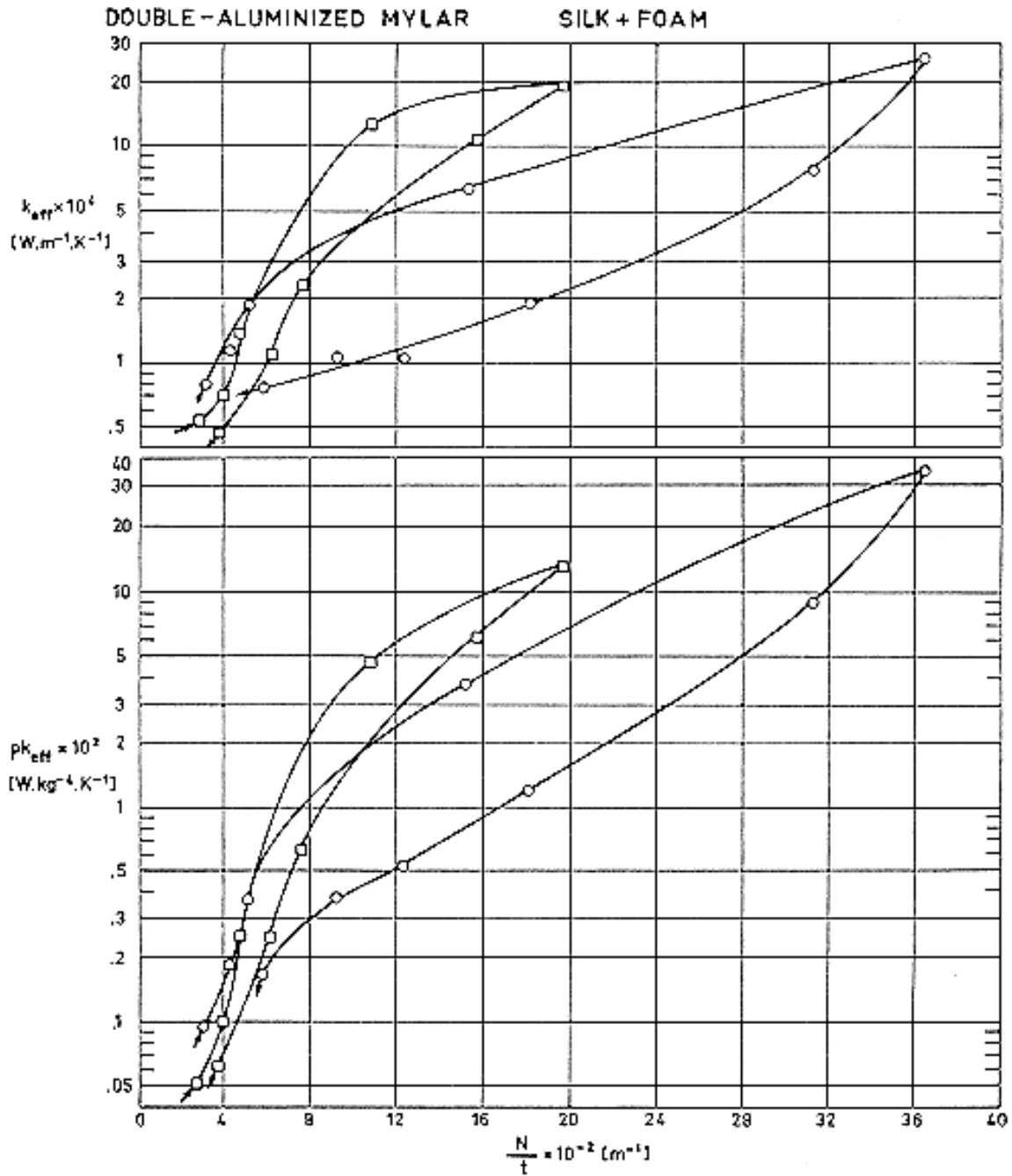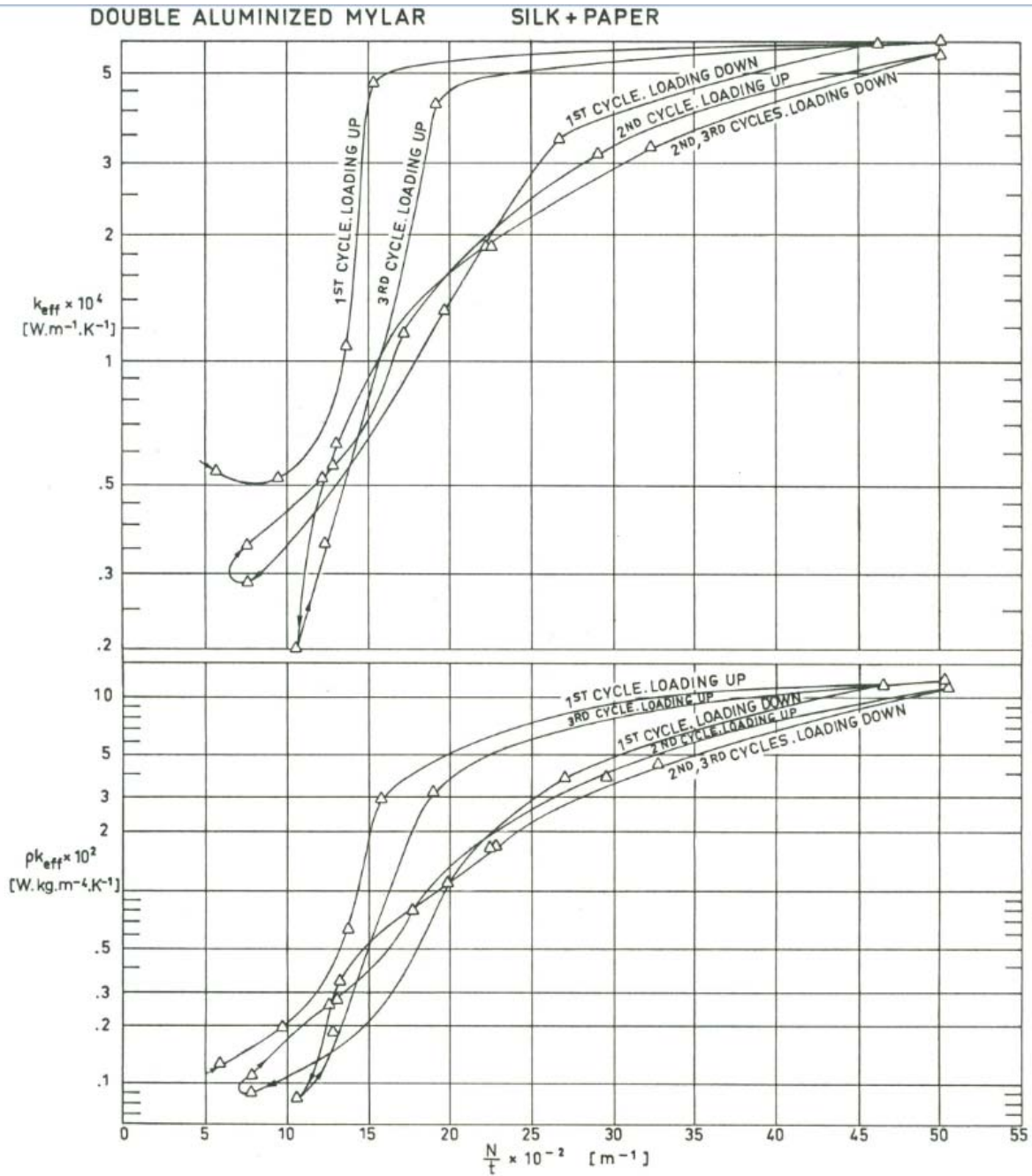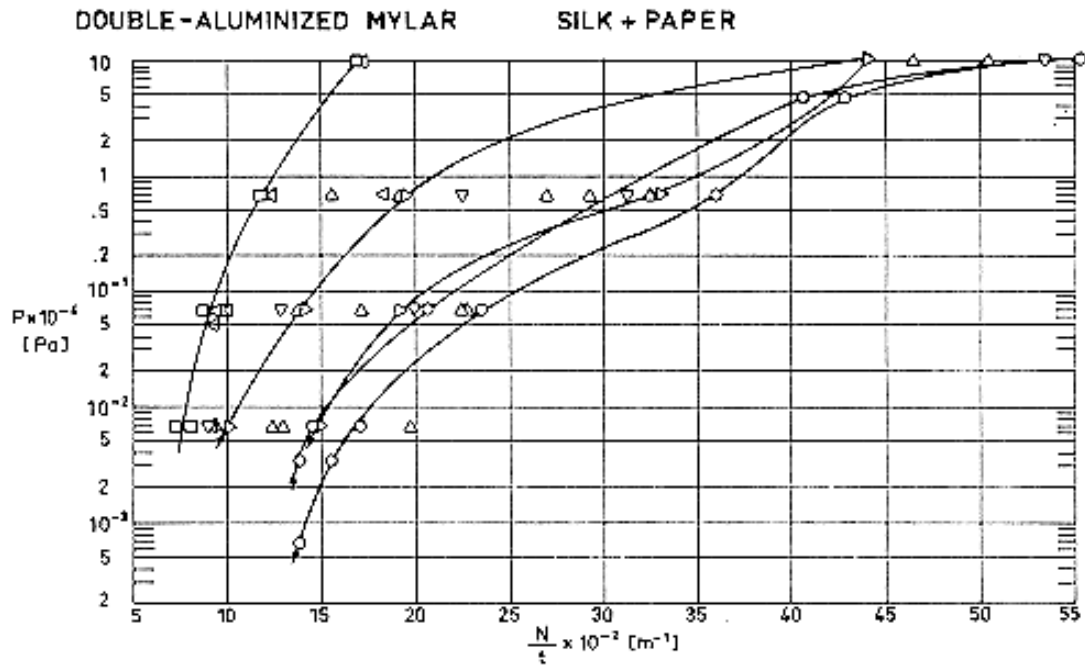Note: non-si units are used in this figure

Figure 6-78: Effective thermal conductivity, k_{eff}, and product of apparent density and effective thermal conductivity, ρk_{eff}, vs. the number of radiation shields per unit thickness, N/t.
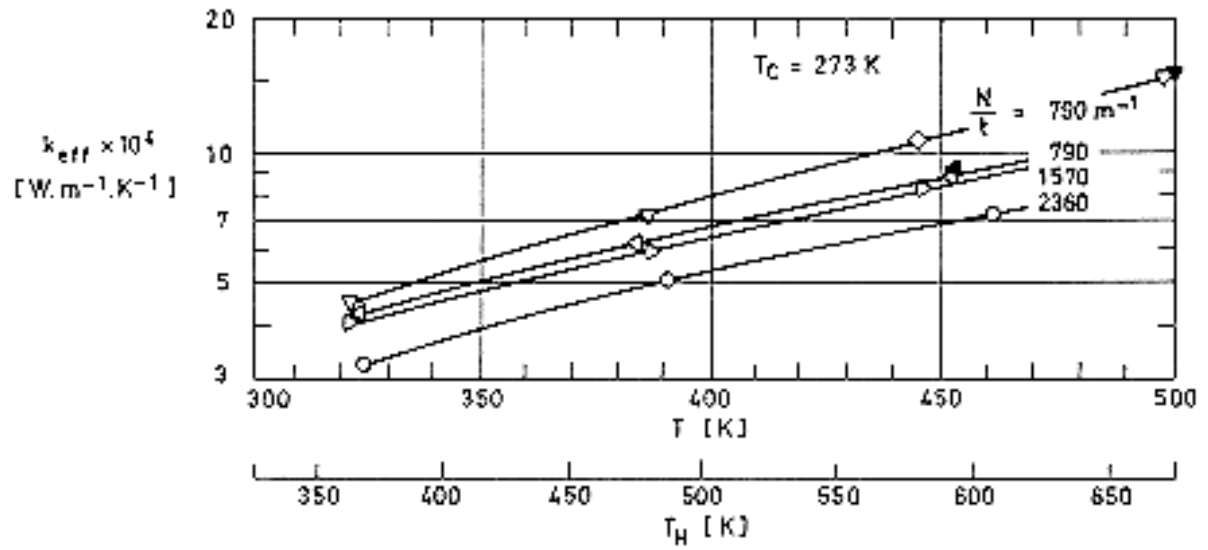
Figure 6-79: Effective thermal conductivity, k_{eff}, as a function of the characteristic temperature, T.

Explanation for above figures

Key	Sample Description	tx10^2 [m] Uncompressed	px10^3 [Pa]	T_H [K]	T_C [K]	T_E [a] [K]	Calorimeter Type	References
○	N = 30 Shields 25,4x10^{-6} m thick Kapton Single-Aluminized 31 Spacers 76,2x10^{-6} m thick Dexiglas paper	1,27	< 6,7	371 489 609	273 273 273		LMSC/ Sunnyvale Flat-Plate	Cunnington et al. (1967) [17] p. 66
□		1,07	< 6,7	602	273			
△		0,92	< 6,7	582	273			
▲		0,92	< 6,7	602	273			
▽	N = 10 Shields 25,4x10^{-6} m thick Kapton Single-Aluminized 11 Spacers 230x10^{-6} m thick Dexiglas paper	1,27	< 6,7	365 482 670	273 273 273	300 300 300		Cunnington et al. (1967) [17] p. 68
▼		1,27	< 6,7	675	273	420		
▷		0,635	< 6,7	365 482 584	273 273 273			
◁	N = 10 Shields 25,4x10^{-6} m thick Kapton Single-Aluminized 11 Spacers	1,27	< 6,7	368 478 595	273 273 273	300 300 300		Cunnington et al. (1967) [17] p. 69
◀		1,27	< 6,7	596	273	420		

Key	Sample Description	tx10^2 [m] Uncompressed	px10^3 [Pa]	T_H [K]	T_C [K]	T_E [a] [K]	Calorimeter Type	References
◇	380x10^{-6} m thick Dexiglas paper	0,950	< 6,7	586	273			
◆		0,635	< 6,7	582	273			
◆		0,508	< 6,7	578	273			

[a]   Edge boundary heat exchange have been used in some experiments to evaluate the two-dimensional effects. T_E is the resulting edge temperature.

Figure 6-80: Effective thermal conductivity, k_{eff}, and product of apparent density and effective thermal conductivity, ρk_{eff}, vs. the number of radiation shields per unit thickness, N/t.
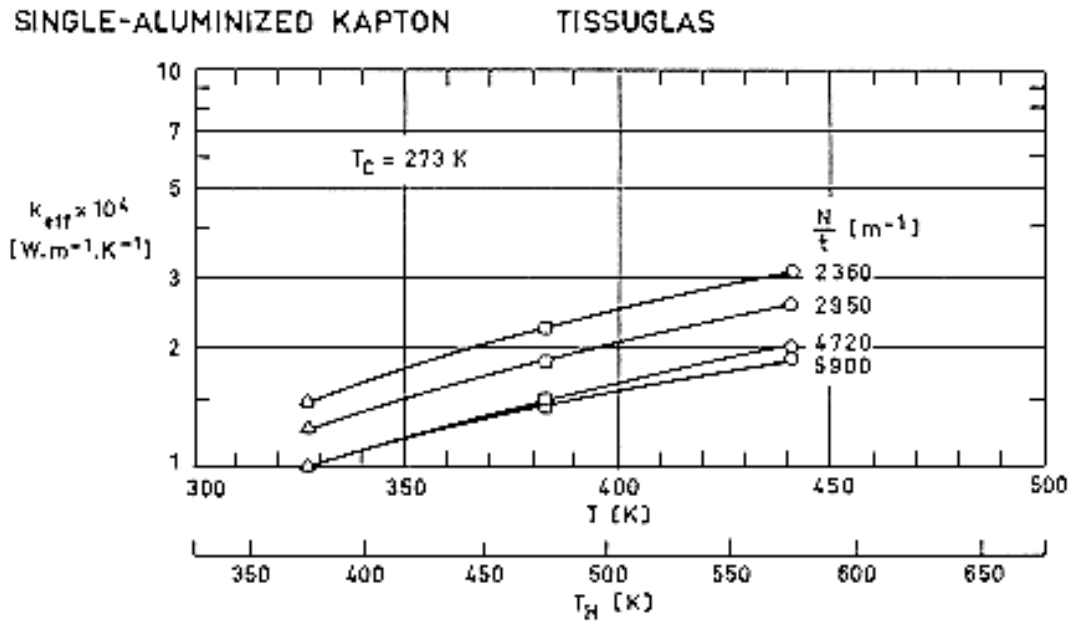
Figure 6-81: Effective thermal conductivity, k_{eff}, as a function of the characteristic temperature, T.

Explanation for above figures

Key	Sample Description	tx10² [m] Uncompressed	px10³ [Pa]	T_H [K]	T_C [K]	Calorimeter Type	References
○	N = 30 Shields 25,4x10⁻⁶ m thick Kapton Single-Aluminized 16 Spacers 15,2x10⁻⁶ m thick Tissuglas A single layer of Tissuglas for each spacer	0,64 [a]	< 6,7	575	273	LMSC/ Sunnyvale Flat-Plate	Cunnington et al. (1967) [17] p. 72
□		0,64 [a]	< 6,7	475	273		
△		0,64 [a]	< 6,7	375	273		
▽		0,64 [a]	< 6,7	475	77		
▷		0,64 [a]	< 6,7	375	77		

[a]   Deduced from layer density.
     Comments: To calculate ρ the following values have been used:
     Aluminized Kapton: 3,58x10⁻² Kg/m² (Cunnington et al. (1967) [17], p. 47)
     Tissuglas: 3,4x10⁻³ Kg/m² (Cunnington et al. (1967) [17], p. 65)
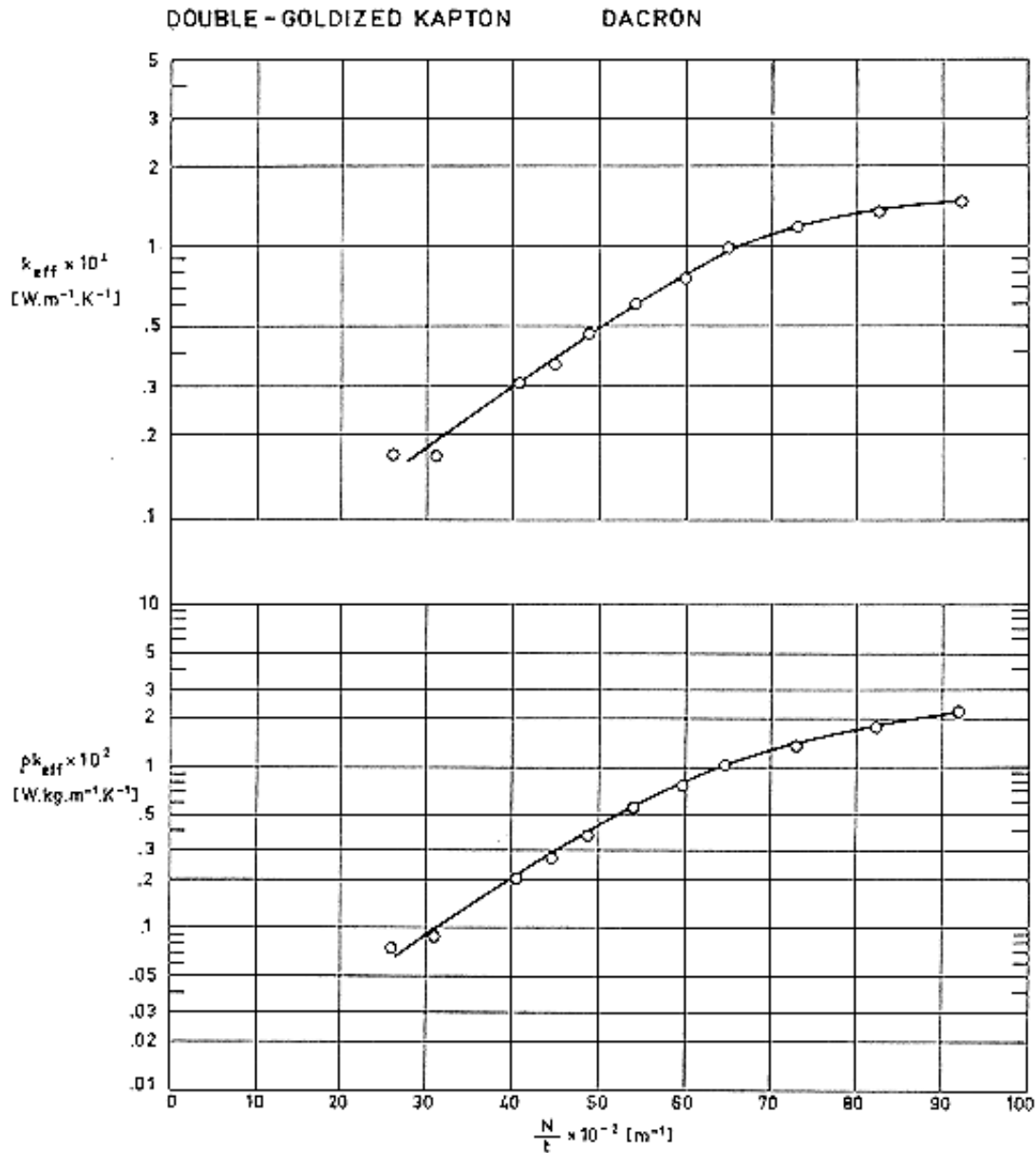
Figure 6-82: Effective thermal conductivity, k_{eff}, and product of apparent density and effective thermal conductivity, ρk_{eff}, vs. the number of radiation shields per unit thickness, N/t.
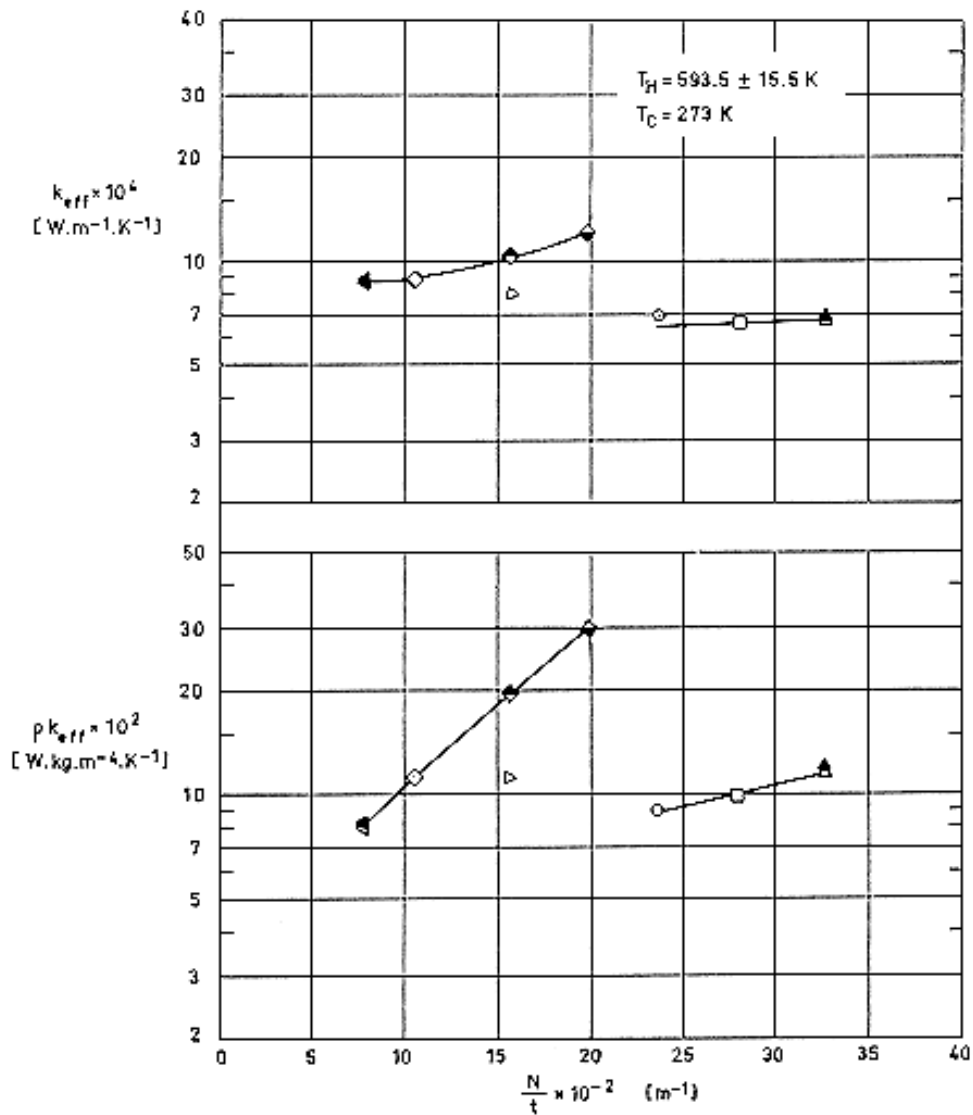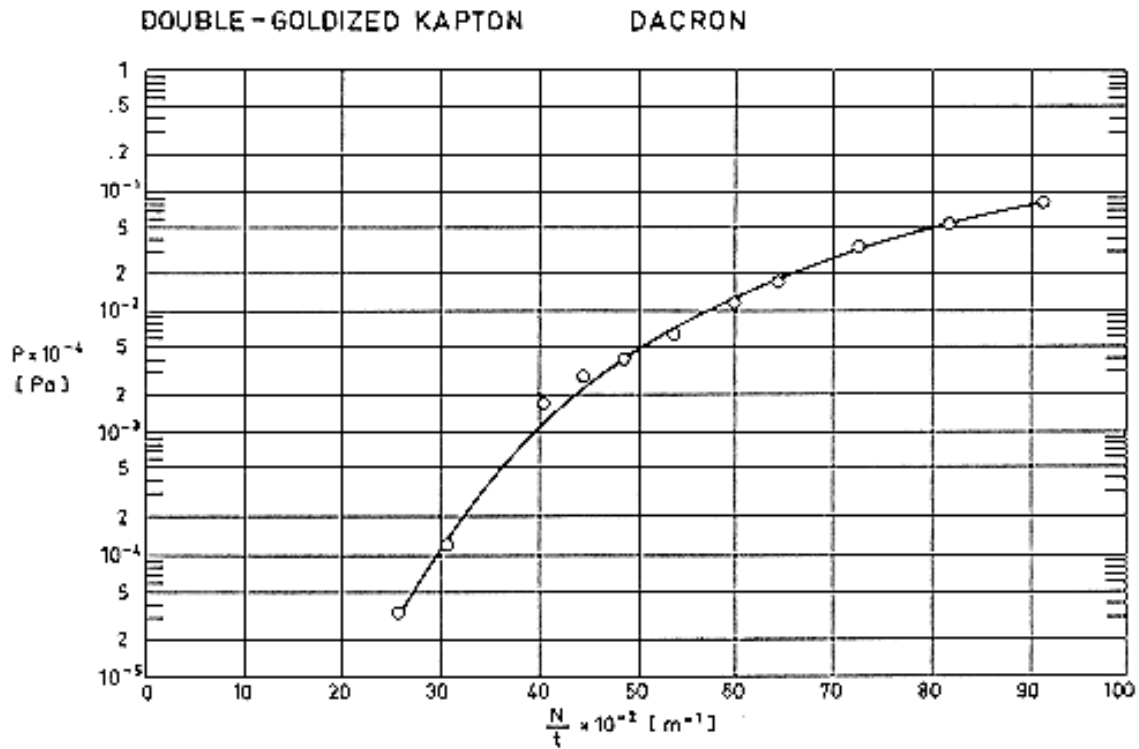
Note: non-si units are used in this figure

Figure 6-83: Compressive mechanical load, *P*, on the multilayer insulation vs. the number of radiation shields per unit thickness, *N/t*.

Explanation for above figures

Key	Sample Description	tx10^2 [m] Uncompressed	px10^3 [Pa]	T_H [K]	T_C [K]	Calorimeter Type	References
○	$N = 10$ Shields. 6,35x10^{-6} – 8,13x10^{-6} m thick Kapton. Double-Goldized. 10 Spacers 16,7x10^{-5} m thick Dracon B4A.	0,386 [a]	< 0,13	~288	77,5	Double-guarded cold-plate.	Holmes, McCrary & Krause (1972) [30] p. 794. Krause (1974) [40].

[a]   Largest quoted value.
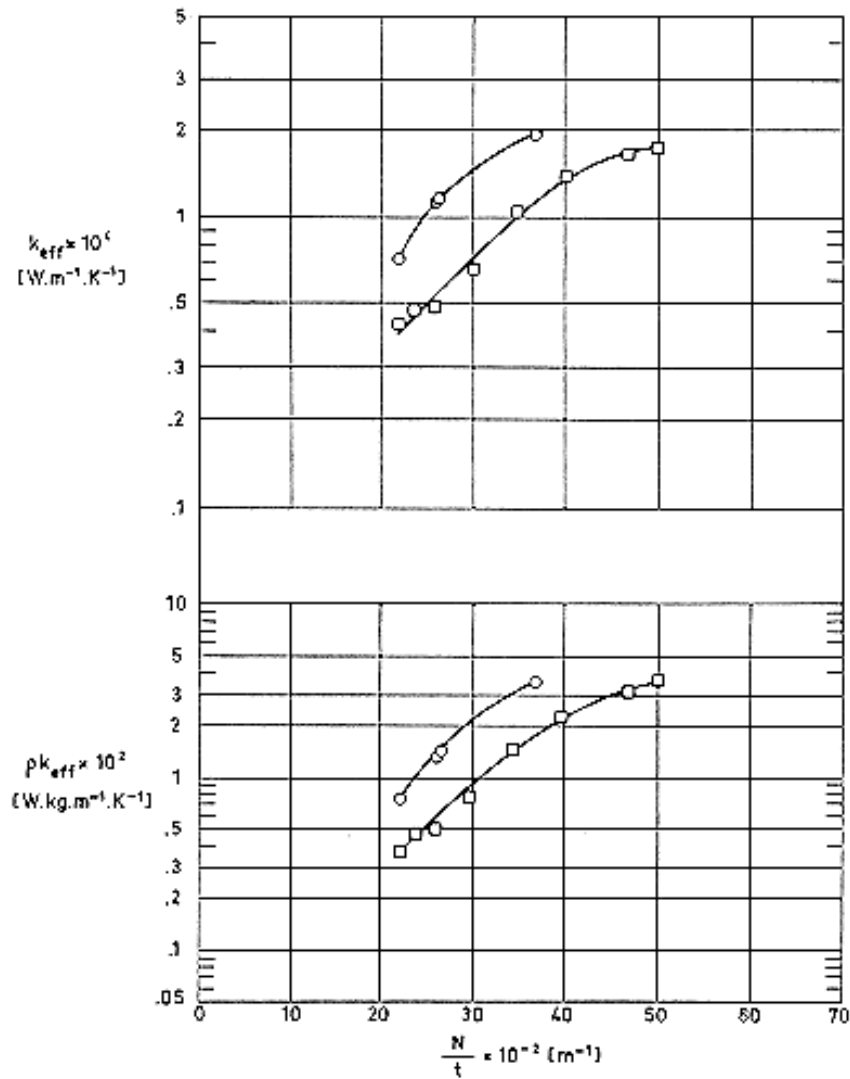
Note: non-si units are used in this figure

Figure 6-84: Effective thermal conductivity, k_{eff}, and product of apparent density and effective thermal conductivity, ρk_{eff}, vs. the number of radiation shields per unit thickness, N/t.

Note: non-si units are used in this figure
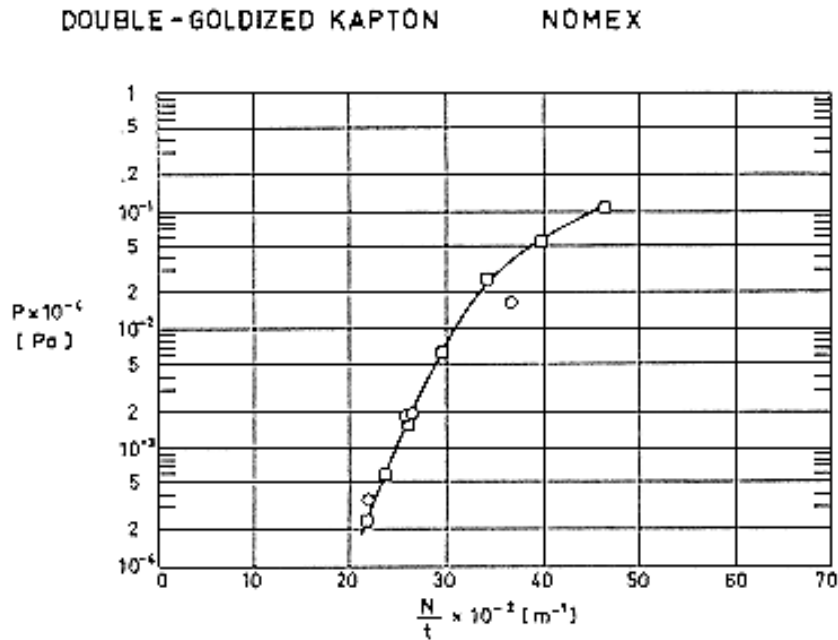
Figure 6-85: Compressive mechanical load, *P*, on the multilayer insulation vs. the number of radiation shields per unit thickness, *N*/*t*.

Explanation for above figures

Key	Sample Description	tx10^2 [m] Uncompressed	px10^3 [Pa]	T_H [K]	T_C [K]	Calorimeter Type	References
○	N = 10 Shields. 6,35x10^{-6} – 8,13x10^{-6} m thick Kapton. Double-Goldized. 10 Spacers 17,8x10^{-5} m thick Nomex HT-287.	0,459 [a]	< 0,13	~288	77,5	Double-guarded cold-plate.	Holmes, McCrary & Krause (1972) [30] p. 794. Krause (1974) [40].
□	N = 10 Shields. 6,35x10^{-6} – 8,13x10^{-6} m thick Kapton. Double-Goldized. 10 Spacers 31,8x10^{-5} m thick Nomex HT-96.	0,462 [a]	< 0,13	~288	77,5		

[a]   Largest quoted value.
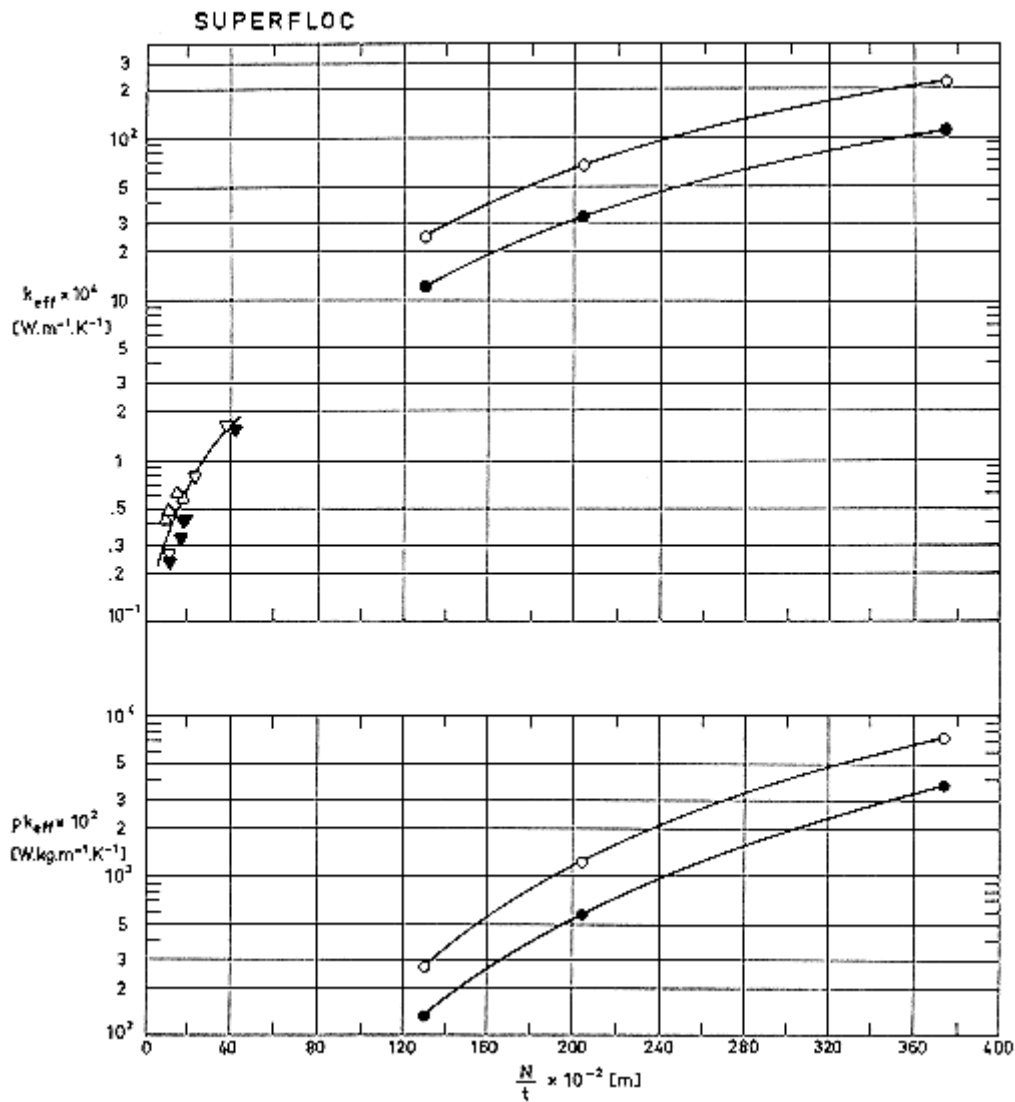
Note: non-si units are used in this figure

Figure 6-86: Effective thermal conductivity, k_{eff}, and product of apparent density and effective thermal conductivity, ρk_{eff}, vs. the number of radiation shields per unit thickness, N/t.
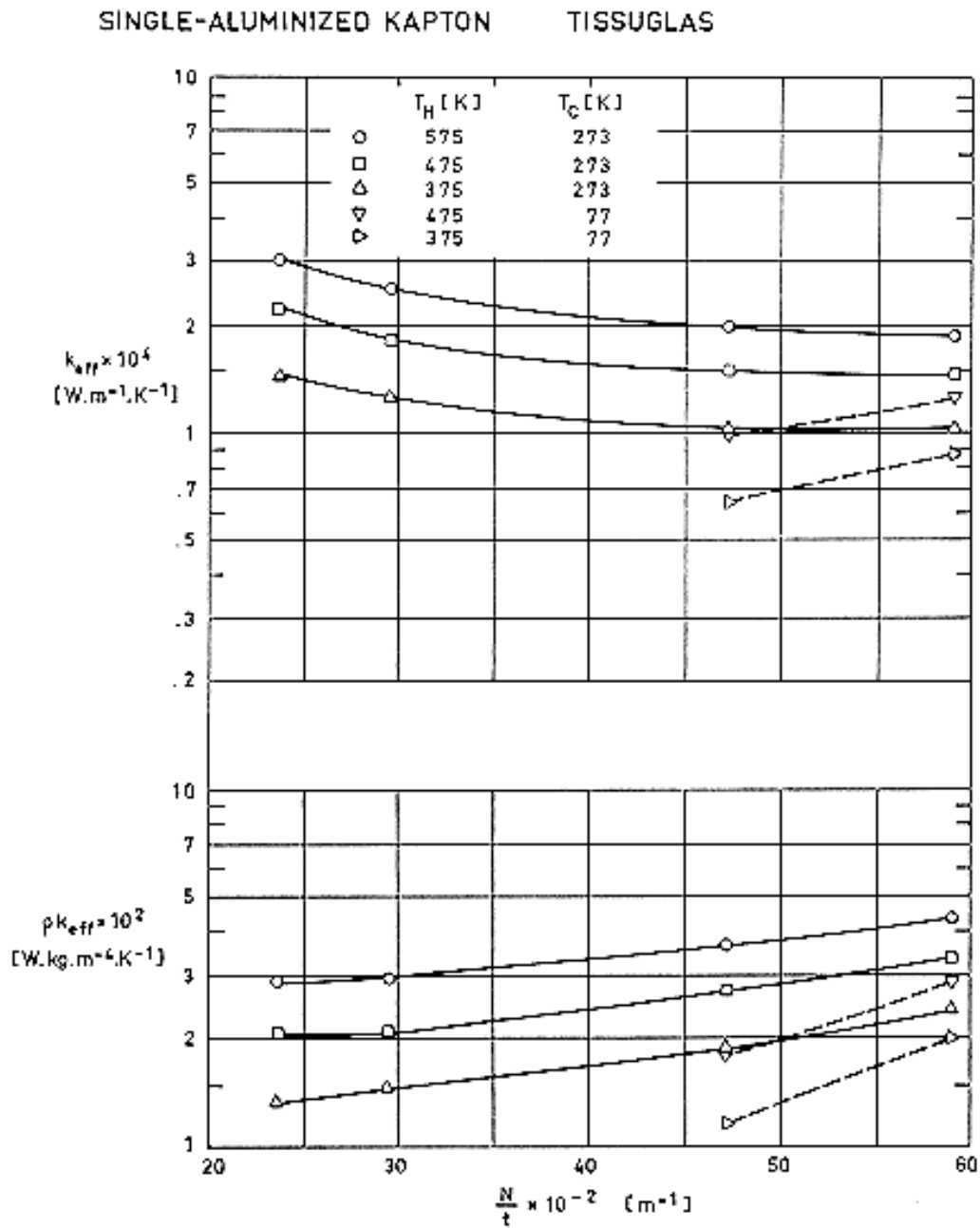
SUPERFLOC
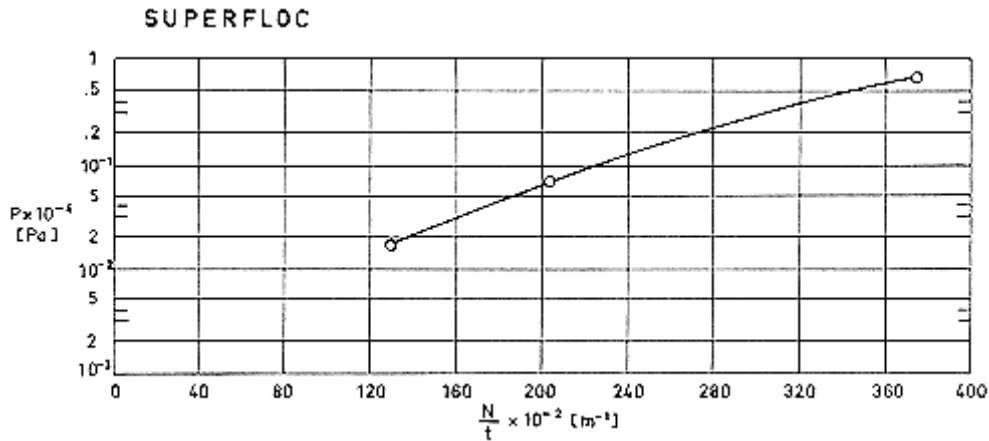
Figure 6-87: Compressive mechanical load, P, on the multilayer insulation vs. the number of radiation shields per unit thickness, N/t.
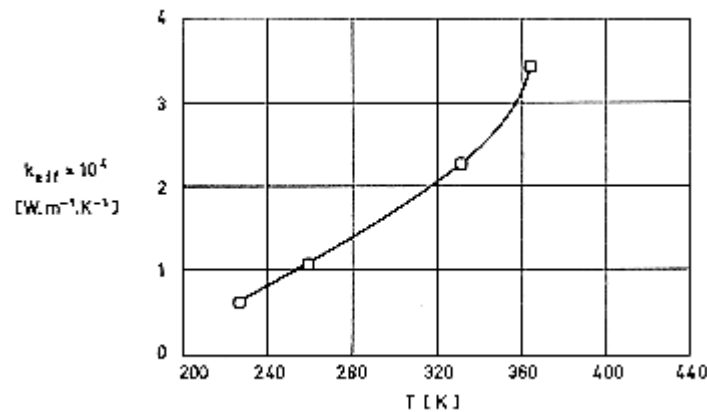
Figure 6-88: Effective thermal conductivity, k_{eff}, as a function of the characteristic temperature, T.

Explanation

Key	Sample Description	$t\text{x}10^2$ [m] Uncompressed	$p\text{x}10^3$ [Pa]	T_H [K]	T_C [K]	Calorimeter Type	References
○	Superfloc.			255	255		Hale (1969) [27] p. 46.
●				222	22,2		
□	N = 22 Shields 6,35x10⁻⁶ m thick Mylar Double-Aluminized Separated by flocking of glass fibers 1,27x10⁻⁴ m long on 1,27x10⁻² m centers.	2,54		230 262,5 335,5 368	225 257 330 361	Lockheed/ Huntsville Cylindrical	Scollon & Carpitella (1970) [62] p. B-13. After Hale et al (1967) [27].

Key	Sample Description	$t \times 10^2$ [m] Uncompressed	$p \times 10^3$ [Pa]	T_H [K]	T_C [K]	Calorimeter Type	References
△	Mylar Double-Aluminized Superfloc 0,95x10⁻² m spacing.			300	77,5		Leonhard & Hyde (1971) [42].
▽	N = 15 Shields 6,35x10⁻⁶ m thick Kapton. Double-Goldized Separated by flocking of Dracon tufts 1,57x10⁻³ m diameter, 1,02x10⁻³ m length on 1,27x10⁻² m centers. Adhesive Crest 7343 Silane modified.	1,27 [a]	< 1,33	300	77,5	ADL Model 12 Flat-Plate (double-guarded cold-plate).	p. 655.
▼	Same as ▽ except tufts placed on 0,95x10⁻² m centers.	1,27 [a]	< 1,33	300	77,5		

[a] Largest quoted value.

6.12 Lateral heat transfer

Multilayer insulations are usually designed to reduce the heat transfer normal to the surface of the insulation. However, these systems have thermal conductivities parallel to the layers which are 10^3 to 10^6 times greater than those perpendicular to them. As a consequence, the efficiency of the system may be impaired by three-dimensional effects, as occurs in the cases of edges, joints and penetrations.

Data concerning the effective lateral thermal conductivity, $k_{eff(lat)}$, of typical multilayer systems are plotted against the characteristic temperature, T, in the following sheets.

The effective thermal conductivity is given by

$k_{eff(lat)} = (Q/A)[L/(T_H - T_C)]$

where:

A is the cross-sectional area. [m²],

Q is the heat transfer rate along the insulation. [W],

T_C is the cold boundary temperature. [K],

T_H is the hot boundary temperature. [K].

The cross-sectional area, A, may be defined either as the bulk cross-sectional area, A_b, or the metallic cross-sectional area, A_m. The relationship between $k_{eff(lat),b}$ (based on A_b), and $k_{eff(lat),m}$ is:

$k_{eff(lat),b} = k_{eff(lat),m} j t_c (N/t)$

where:

N is the number of radiation shields,

j is the numerical factor. $j = 1$ for single-coated layers, and $j = 2$ for double-coated layers,

t is the total thickness of the insulation. [m],

t_c is the metallic-coating thickness. [m].

Throughout this compilation only the form $k_{eff(lat),m}$ of $k_{eff(lat)}$ is be used, although the subscript *(lat),m* will be deleted to simplify the notation. This choice is advantageous when trying to correlate the experimental data with the results of existing theoretical models (Tien, Jagannathan & Chan (1972) [71]).

Based on similar considerations, the characteristic temperature used to plot the data is defined as

$$T = \sqrt[3]{\frac{T_H^4 - T_C^4}{4(T_H - T_C)}}$$
[6-17]

Note: non-si units are used in this figure

The theory predicts that in the optically thick case (*aL > h*) k_{eff} is a linear function of T^3. In the parenthetic inequality, *a* is the transmission constant depending on the shield surface reflectance and the spacer scattering coefficient, and *h* is the spacing between neighboring shields. This optically thick condition is fulfilled in many actual situations of interest to MLI systems.
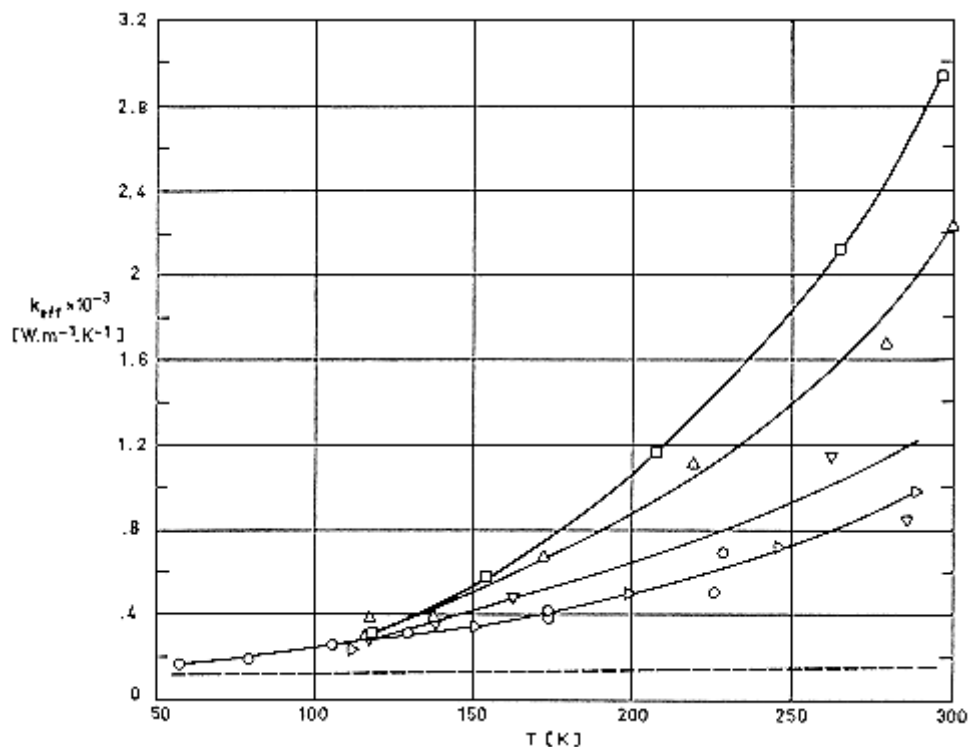
Note: non-si units are used in this figure

Figure 6-89: Lateral effective thermal conductivity, k_{eff}, as a function of characteristic temperature, T.

Explanation

All shields, unless otherwise stated, are 6,35x10⁻⁶ m thick Mylar Single-Aluminized, Crinkled.

Key	n_s	N/t [m⁻¹]	L [m]	t_cx10¹⁰ [m]	Method used to measure t_c	px10³ [Pa]	Apparatus	References
◯		2050	0,101 and 0,280	300	Electrical Resistance	<1,33	Cylindrical	Vliet & Coston (1968) [75] p. 674
▢		1380	0,0762 and 0,152	256	Electrical Resistance	1,33x10⁻³	Cylindrical	Androulakis (1970) [3] p. 4
△		1850	0,0762 and 0,152	256	Electrical Resistance	1,33x10⁻³	Cylindrical	Androulakis (1970) [3] p. 4
▽		3230	0,0762 and 0,152	256	Electrical Resistance	1,33x10⁻³	Cylindrical	Androulakis (1970) [3] p. 4
▷		4530	0,0762 and 0,152	256	Electrical Resistance	1,33x10⁻³	Cylindrical	Androulakis (1970) [3] p. 4

▬ ▬ : Thermal conductivity of the metallic coating estimated by Tien et al. (1972) [71], p. 120.
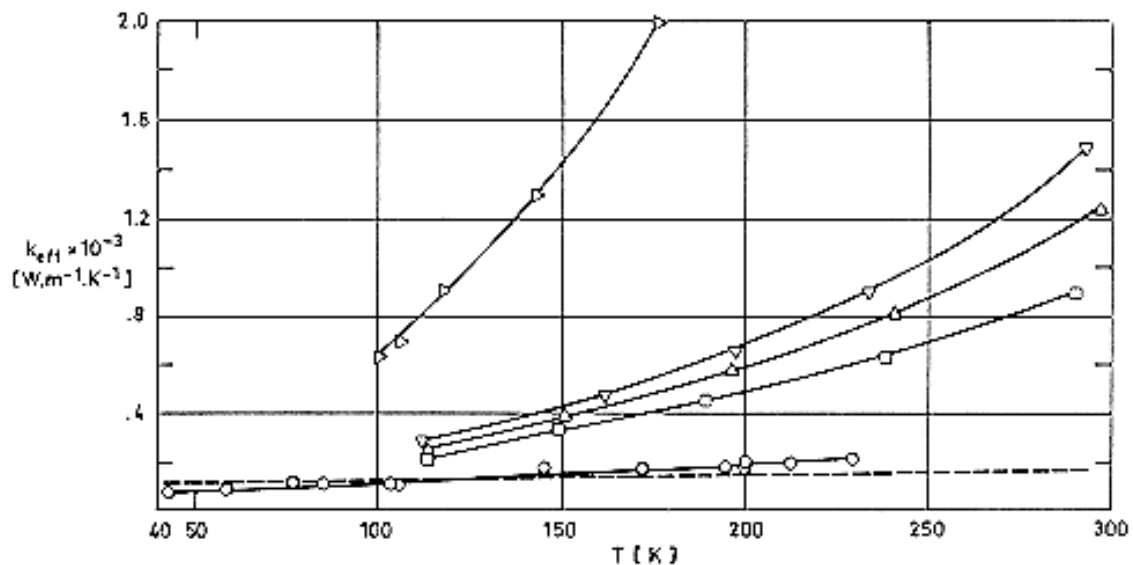
Note: non-si units are used in this figure

Figure 6-90: Lateral effective thermal conductivity, k_{eff}, as a function of characteristic temperature, T.

Explanation

All shields, unless otherwise stated, are 6,35x10⁻⁶ m thick Mylar Double-Aluminized. The spacers are Dexiglas 71x10⁻⁶ m thick, unless otherwise stated. The number, n_s, of spacer layers per shield is given below.

Key	n_s	N/t [m⁻¹]	L [m]	t_cx10¹⁰ [m]	Method used to measure t_c	px10³ [Pa]	Apparatus	References
○	1	3230	0,0864 to 0,28	378 525 [a]	Electrical Resistance	<1,33	Cylindrical	Coston & Vliet (1967) [14] p. 914
□	1	3350	0,0762 and 0,152	194	Electrical Resistance	1,33x10⁻³	Cylindrical	Androulakis (1970) [3] p. 4
△	2	2080	0,0762 and 0,152	194	Electrical Resistance	1,33x10⁻³	Cylindrical	Androulakis (1970) [3] p. 4
▽	3	1380	0,0762 and 0,152	194	Electrical Resistance	1,33x10⁻³	Cylindrical	Androulakis (1970) [3] p. 4
▷	1	1000	0,371	400± 3	Electrical Resistance	<1,33x10⁻³	Plane (transient conduction)[c]	Tien et al. (1972) [71] p. 120
▬ ▬: Thermal conductivity of the metallic coating, measured by Tien et al. (1972) [71], p. 120.								

[a]   A value of t_c = 400x10⁻¹⁰ m has been assumed by Tien et al. (1972) [71].

[b]   Mylar thickness: 76,2x10⁻⁶ m. Dexiglass thickness 600x10⁻⁶ m.

[c]   See Jagannathan & Tien (1971) [31].
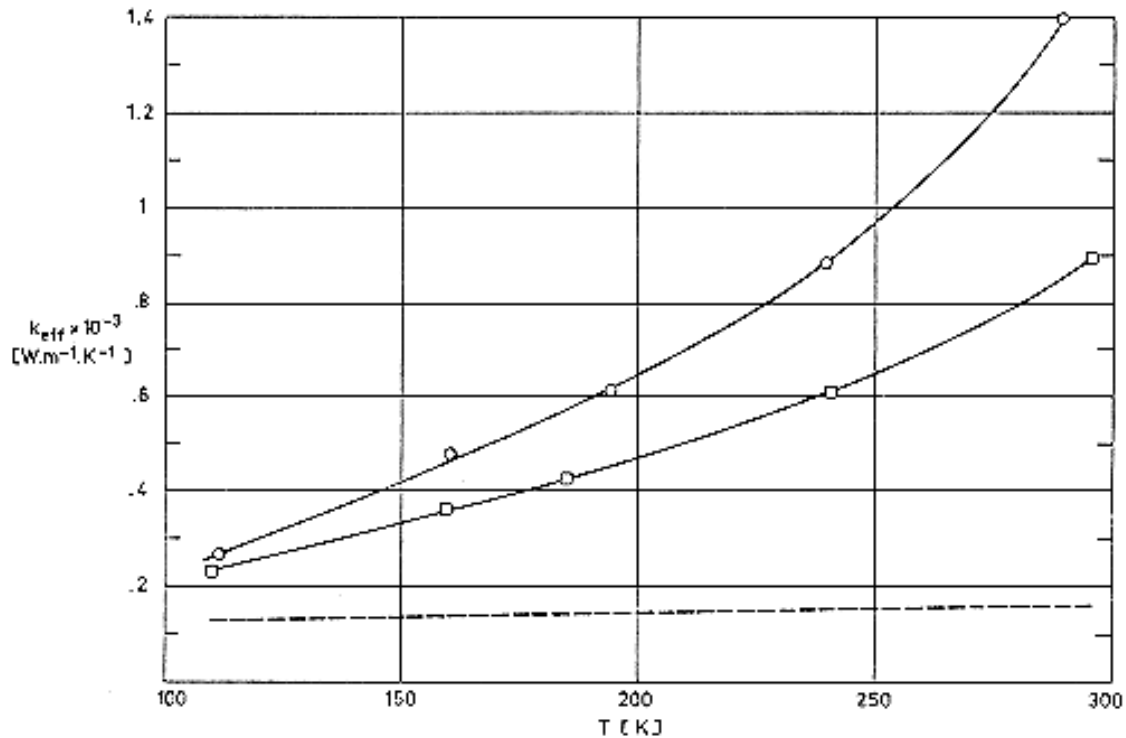
Note: non-si units are used in this figure

Figure 6-91: Lateral effective thermal conductivity, k_{eff}, as a function of characteristic temperature, *T*.

Explanation

All shields, unless otherwise stated, are $6,35\times10^{-6}$ m thick Mylar Double-Aluminized, with perforations having an open area of 0,5% and a hole size of $1,17\times10^{-3}$ m diameter. The spacers are 127×10^{-6} m thick Nylon net, unless otherwise stated. The number, n_s, of spacer layers per shield is given below.

Key	n_s	N/t $[m^{-1}]$	*L* [m]	$t_c x10^{10}$ [m]	Method used to measure t_c	$p x10^3$ [Pa]	Apparatus	References
○	2	2080	0,0762 and 0,152	194	Electrical Resistance	$1,33\times10^{-3}$	Cylindrical	Androulakis (1970) [3] p. 4
□	2	3310	0,0762 and 0,152	194	Electrical Resistance	$1,33\times10^{-3}$	Cylindrical	Androulakis (1970) [3] p. 4
▬ ▬ : Thermal conductivity of the metallic coating, estimated by Tien et al. (1972) [71], p. 121.								
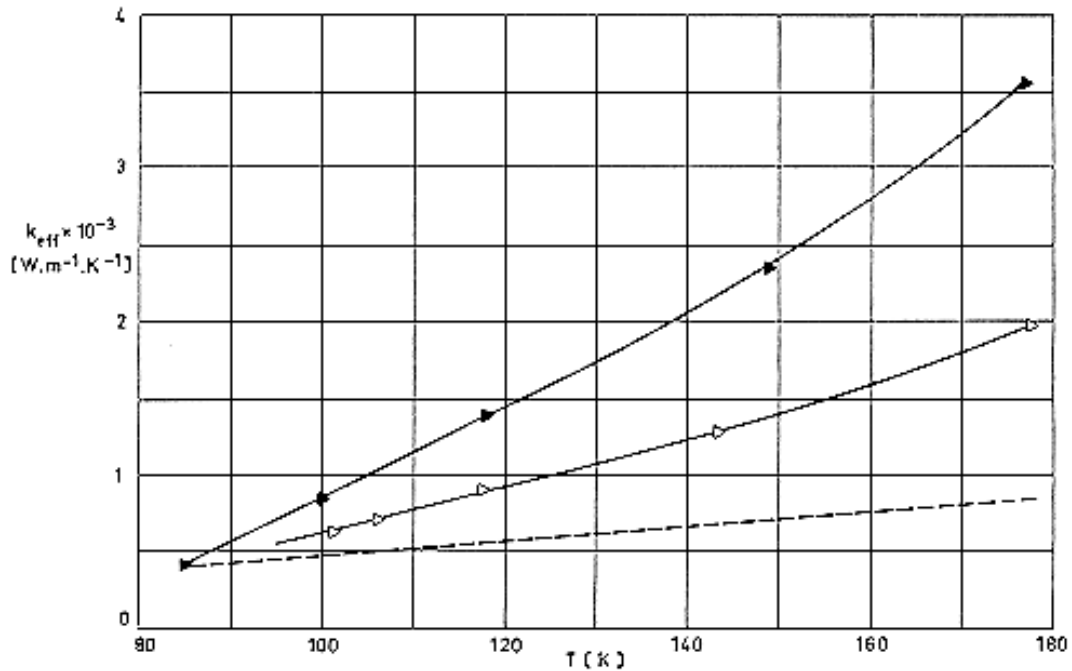
Figure 6-92: Lateral effective thermal conductivity, k_{eff}, as a function of characteristic temperature, T.

Explanation

The performance of a system of 32 parallel films, $76,2 \times 10^{-6}$ m thick Mylar Double-Aluminized, Uncrinkled, is compared with that of a similar system of shields separated by layers of 600×10^{-6} m thick Dexiglas blotting paper. The number, n_s, of spacer layers per shield is given below.

Key	n_s	N/t [m^{-1}]	L [m]	t_cx10^{10} [m]	Method used to measure t_c	px10^3 [Pa]	Apparatus	References
▷	1	1000	0,371	400± 3	Electrical Resistance	1,33x10^{-3}	Plane (transient conduction)[a]	Tien et al. (1972) [71] p. 120
▶	0	1000	0,371	400± 3	Electrical Resistance	1,33x10^{-3}	Plane (transient conduction)[a]	Tien et al. (1972) [71] p. 120
▬ ▬: Thermal conductivity of the metallic coating, measured by Tien et al. (1972) [71], p. 120.								

[a] See Jagannathan & Tien (1971) [31].

6.13 Effect of singularities

The performance of an idealized MLI is normally degraded because of the discontinuities introduced in the insulation by securing devices, penetrations, overlaps, stitches, and by many other artifices used to contour flat layers onto complicated surfaces.

The aim of this item is to present data which can be used to evaluate the effect of these singularities on the heat transfer characteristics of an MLI system.

6.13.1 Joints

Although attempts have been made to numerically analyze the thermal degradation of high-performance MLI systems in the vicinity of a joint, the results obtained are too limited in scope. Hence, it is more straightforward to collect as many experimental data as possible in order to quantify the heat losses through MLI discontinuities and thus enable the designer to predict the blanket performance.

Experimental studies have been undertaken by several investigators with the aim of relating the heat transfer through an MLI blanket in which well defined discontinuities have been introduced, to the heat transfer characteristics of the same blanket without these discontinuities.

The total heat flow rate through the blanket can be expressed as:

$$Q_{total} = Q_{ideal} + \Delta Q \qquad [6\text{-}18]$$

where Q_{ideal} is the heat flow rate of an ideal blanket having the same surface area as the real one, while ΔQ accounts for the effect of the discontinuities. This effect is normally related to the boundary temperatures, T_H and T_C, and to the surface area of the blanket, A, by means of an effective emittance, $\Delta\varepsilon_{eff}$, such that

$$\left(\Delta Q / A\right) = \sigma \Delta\varepsilon_{eff}\left(T_H^4 - T_C^4\right) \qquad [6\text{-}19]$$

According to Knopf & Murray (1970) [39], the influence of additional joints can be taken into account by means of the following linear relationship

$$\Delta s_{eff} = \frac{1}{A}\sum_i C_i\left(T_H\right)L_i \qquad [6\text{-}20]$$

Note: non-si units are used in this figure

where:

C_i is the joint coefficient for joint i. [m],

L_i is the length of joint i. [m],

A limited amount of the data presented is based on an effective thermal conductivity, Δk_{eff},

$$\left(\Delta Q / A\right) = \Delta k_{eff}\left[\left(T_H - T_C\right)/t\right] \qquad [6\text{-}21]$$

t being the blanket thickness. These data have been obtained numerically. The geometrical model used for the computation is an infinitely long slab of width *L*. The singularity, an overlap, underlap or whatever could be, spans along the whole length of the slab. The presence of the singularity changes the heat flow through the blanket. If the width of an ideal slab transferring one-dimensionally the same heat flow rate as the blanket considered is *L+L**, the effective thermal conductivity increment, Δk_{eff}, will be:
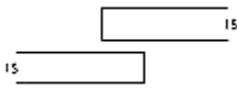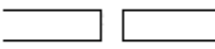
$$\Delta k_{eff} = (L^*/L)k_{eff(nor)} \qquad [6\text{-}22]$$
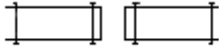
where $k_{eff(nor)}$ is the normal effective thermal conductivity of the ideal blanket.
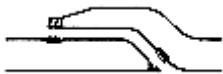
The length *L** is negative in the case of an edge rejecting heat to the space, because the slab transfers less heat, normally to its surface, than an equal slab having an adiabatic edge.
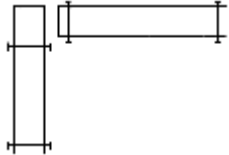
Experimental data regarding several types of joints are given in the following pages. Source data are based either on C_i, an $\Delta\varepsilon_{effi}$, or on $\Delta Q_i/A$; nevertheless, provided that sufficient details are available, it is not difficult to relate the different functions involved. Heavily bounded boxes in Table 6-23 indicate that the enclosed data have been taken from the quoted reference, while data in the lightly bounded boxes have been calculated by the compiler.
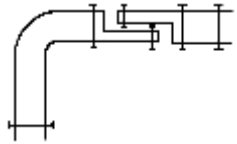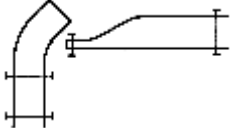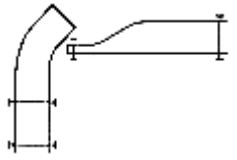
Table 6-23: Thermal Effects of Joints

Description	Sketch	$C_i \times 10^3$ [m]	$\Delta\varepsilon_{effi} \times 10^3$	$\Delta Q_i/A$ [W/m²]	Comments
1 N = 15 Shields 3,17x10⁻⁶ m thick Mylar Double-Aluminized 1,58x10⁻³ m diam holes on 1,4x10⁻² m centers 14 Spacers. Nylon Net 7,62x10⁻² m Simple Overlap		3,34 (T_H = 300 K)	3,80	1,70	From Crosby (1970) [16]. See Comments concerning configuration 21-26. The variation of effective emittance vs. overlap is given in Figure 6-93.
2 N = 15 Shields 6,35x10⁻⁶ m thick Mylar Double-Aluminized 6,35x10⁻³ m diam holes on 0,15 m centers 14 Spacers, 2,30x10⁻⁴ honeycomb Nylon Net 2 Outer Layers 2,54x10⁻⁵ thick Teflon 7,62x10⁻² m Simple Overlap		2,20 (300 K)	2,51	1,12	From Crosby (1970) [16], Stimpson & Jaworski (1972) [69]. See Comments concerning configuration 21-26. The variation of effective emittance vs. overlap is given in Figure 6-93.
3 Two semi-infinite blankets having the following effective conductivities: $k_{eff(nor)}$ = 8,6x10⁻⁴ W.m⁻¹.K⁻¹ (normal) $k_{eff(lat)}$= 1,7x10⁻² W.m⁻¹.K⁻¹ (lateral) 2,5x10⁻² m Overlapping of alternate layers		0,0938 (700 K)	0,0469	0,618	From Cunnington, Zierman, Funai & Lindahn (1967) [17]. Authors give their results in terms of the length, $L+L^*$, of an ideal blanket transferring one-dimensionally the same amount of heat that the real blanket of length L. Calculated values of L^* are given in the following figures: Overlapping effect: Figure 6-94. Underlapping effect: Figure 6-95. Edge
4 Two semi-infinite blankets having the following effective conductivities: $k_{eff(nor)}$ = 8,6x10⁻⁴ W.m⁻¹.K⁻¹ (normal) $k_{eff(lat)}$= 1,7x10⁻² W.m⁻¹.K⁻¹ (lateral) 2,5x10⁻² m Underlapping		0,660 (700 K)	0,330	4,35	
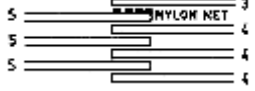
Description	Sketch	$C_i \times 10^3$ [m]	$\Delta\varepsilon_{effi} \times 10^3$	$\Delta Q_i/A$ [W/m²]	Comments
5 A semi-infinite blanket having the following effective conductivities: $k_{eff(nor)}$ = 8,6x10⁻⁴ W.m⁻¹.K⁻¹ (normal) $k_{eff(lat)}$= 1,7x10⁻²W.m⁻¹.K⁻¹ (lateral) Edge rejecting heat.		− 0,264 (700 K)	− 0,132	− 1,74	effects: Figure 6-96. Values of $\Delta Q/A$ have been deduced from Eq. [6-21] and [6-22] with: $k_{eff(nor)}$ = 8,6x10⁻⁴ W.m⁻¹.K⁻¹.L = 1 m. T_H = 700 K. T_C = 295 K. t = 2x10⁻² m $\Delta\varepsilon_{eff}$ deduced from Eq. [6-19] with: σ = 5,6697x10⁻⁸ W.m⁻².K⁻¹. $C_i(T_H)$ from Eq. [6-20] with L_i/A = 0,5 m⁻¹.
6 N = 30 Shields 6,35x10⁻⁶ m thick Mylar Single-Aluminized Crinkled Butt, laced buttons on 5,08x10⁻² m spacing.		3,20 (366 K) 3,81 (389 K)	3,11 3,70	1,68 3,04	From Knopf & Murray (1970) [39]. See Comments in the following.
7 N = 30 Shields 6,35x10⁻⁶ m thick Mylar Single-Aluminized Crinkled. 7,62x10⁻² m Shiplap, laced buttons on 5,08x10⁻² m spacing.		0,610 (T_H = 366 K) 0,732 (389 K)	0,593 0,711	0,320 0,583	From Knopf & Murray (1970) [39]. The effective emittance of a blanket with joints was measured by using an internally heated cylinder over which the insulation was wrapped. The dimensions of the cylinder were 0,61 m in diameter, 1,52 m to 1,83 m in length. The area of the test frame varied between 3,16 and 3,62 m². Length of a typical axial joint: 1,22 to 1,52 m. Length of a circumferential joint: 1,92 m. Temperatures were measured by eight
8 N = 30 Shields 6,35x10⁻⁶ m thick Mylar Double-Aluminized Embossed (Tile Geometric Square) 7,62x10⁻² m Shiplap, laced buttons on 5,08x10⁻² m spacing.		0,610 (366 K) 0,732 (389 K)	0,593 0,711	0,320 0,583	
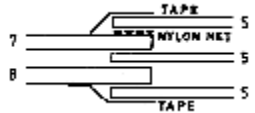
Description	Sketch	C_ix10^3 [m]	$\Delta\varepsilon_{effi}$x10^3	$\Delta Q_i/A$ [W/m^2]	Comments
9 N = 22 Shields 6,35x10^{-6} m thick Mylar Double-Aluminized 21 Spacers Tissuglas. 7,62x10^{-2} m Shiplap, laced buttons on 5,08x10^{-2} m spacing.		0,335 (366 K)	0,325	0,175	internal and eleven external thermocouples. ε_{eff} is deduced from the heating power required to stabilize the temperature. One-dimensional flat-plate data concerning effective emittances of undisturbed specimens were obtained from different sources. $\Delta\varepsilon_{eff}$ has been deduced by the compiler from the reported values of C_i, by using Eq. [6-20] with L_i = 3,4 m, A = 3,5 m^2. $\Delta Q/A$ deduced from Eq. [6-19] with σ = 5,6697x10^{-8} W.m^{-2}.K^{-4}. T_C = 303 K.
10 N = 30 Shields 6,35x10^{-6} m thick Mylar Double-Aluminized Embossed (Tile Geometric Square). 15,2x10^{-2} m Overlap, stitched Velcro·		0,640 (366 K) 0,762 (389 K)	0,622 0,740	0,336 0,607	
11 N = 30 Shields 6,35x10^{-6} m thick Mylar Single-Aluminized Crinkled. Butt, stitched Velcro.		8,99 (366 K) 9,97 (389 K)	8,73 9,69	4,71 7,95	
12 N = 30 Shields 6,35x10^{-6} m thick Mylar Single-Aluminized Crinkled. 7,62x10^{-2} m Shiplap, stitched Velcro base, laced exterior.		3,44 (366 K)	3,34	1,80	

Description	Sketch	$C_i \times 10^3$ [m]	$\Delta\varepsilon_{effi} \times 10^3$	$\Delta Q_i/A$ [W/m²]	Comments
13 N = 30 Shields $6{,}35 \times 10^{-6}$ m thick Mylar Double-Aluminized Embossed (Tile Geometric Square). Exposed edge, corner buttoned on $15{,}2 \times 10^{-2}$ m spacing.		0,945 (T_H = 366 K) 1,25 (389 K)	0,918 1,21	0,495 0,993	
14 N = 30 Shields $6{,}35 \times 10^{-6}$ m thick Mylar Double-Aluminized Embossed (Tile Geometric Square). Exposed edge, corner buttoned on $15{,}2 \times 10^{-2}$ m spacing, with Dexiglas.		0,945 (366 K) 1,097 (389 K)	0,918 1,066	0,495 0,875	
15 N = 30 Shields $6{,}35 \times 10^{-6}$ m thick Mylar Single-Aluminized Crinkled. Exposed edge, corner buttoned on $5{,}08 \times 10^{-2}$ m spacing, with reflective tape.		1,34 (366 K) 1,71 (389 K)	1,30 1,66	0,701 1,36	
16 N = 22 Shields $6{,}35 \times 10^{-6}$ m thick Mylar Double-Aluminized 21 Spacers Tissuglas Exposed edge, corner buttoned on $5{,}08 \times 10^{-2}$ m spacing, with reflective tape.		0,732 (366 K)	0,711	0,384	

Description	Sketch	C_ix10³ [m]	$\Delta\varepsilon_{effi}$x10³	$\Delta Q_i/A$ [W/m²]	Comments
17 N = 30 Shields 6,35x10⁻⁶ m thick Mylar Single-Aluminized Crinkled 7,62x10⁻² m Shiplap, laced buttons with compound corner.		1,16 (366 K) 1,46 (389 K)	1,13 1,42	0,610 1,16	
18 N = 22 Shields 6,35x10⁻⁶ m thick Mylar Double-Aluminized 21 Spacers Tissuglas 7,62x10⁻² m Shiplap, laced buttons with compound corner.		0,640 (366 K)	0,622	0,336	
19 N = 30 Shields 6,35x10⁻⁶ m thick Mylar Single-Aluminized Embossed (Tile Geometric Square). Exposed edge, corner single line stitching.		2,47 (366 K) 2,71 (389 K)	2,40 2,63	1,29 2,16	
20 N = 30 Shields 6,35x10⁻⁶ m thick Mylar Double-Aluminized Embossed (Tile Geometric Square). Exposed edge, corner single line stitching.		5,27 (T_H = 366 K) 5,49 (389 K)	5,12 5,33	2,76 4,37	

Description	Sketch	C_ix10³ [m]	$\Delta\varepsilon_{effi}$x10³	$\Delta Q_i/A$ [W/m²]	Comments
21 N = 15 Shields 6,35x10⁻⁶ m thick Mylar Double-Aluminized. Holes 6,35x10⁻³ m diam., 0,15 m centers 14 Spacers 2,30x10⁻⁴ m thick Nylon Net 2 Outer Layers 2,54x10⁻⁵ m thick Teflon 7,62x10⁻² m Overlap, stitched.		3,31 (300 K)	3,77	1,69	From Stimpson & Jaworski (1972) [69]. Effective emittance of a blanket with joints was measured by using cylindrical calorimeter. The dimensions of the cylinder were 0,254 m in diameter, 0,71 m in length. Since the actual test section length is 0,406 m, the effective area of the shield in the test section is approximately 0,325 m². Temperatures were measured with thermocouples. Heat losses were estimated by means of the electrical power required to maintain a desired equilibrium temperature inside the blanket. The heat losses through the undisturbed blanket were calculated as a function of the number of layers, shield emittance and percentage of holes. C_i has been deduced by the compiler from the reported values of $\Delta\varepsilon_{eff}$, by using Eq. [6-20] with L_i = 0,37 m and A = 0,325 m². $\Delta Q/A$ has been deduced from Eq. [6-19] with σ = 5,6697x10⁻⁸ W.m⁻².K⁻⁴. T_H = 300 K, T_C = 120 K.
22 N = 15 Shields 6,35x10⁻⁶ m thick Mylar Double-Aluminized. Holes 6,35x10⁻³ m diam., 0,15 m centers 14 Spacers 2,30x10⁻⁴ thick Nylon Net 2 Outer Layers 2,54x10⁻⁵ m thick Teflon 7,62x10⁻² m Overlap. Interleaved. Number of layers indicated in the sketch.		2,14 (300 K)	2,44	1,092	
23 N = 15 Shields 6,35x10⁻⁶ m thick Mylar Double-Aluminized. Holes 6,35x10⁻³ m diam., 0,15 m centers 14 Spacers 2,30x10⁻⁴ thick Nylon Net 2 Outer Layers 2,54x10⁻⁵ m thick Teflon 7,62x10⁻² m Overlap. Interleaved.		1,88 (300 K)	2,14	0,958	

Description	Sketch	C_ix10³ [m]	$\Delta\varepsilon_{effi}$x10³	$\Delta Q_i/A$ [W/m²]	Comments
Number of layers indicated in the sketch.					
24 N = 15 Shields 6,35x10⁻⁶ m thick Mylar Double-Aluminized. Holes 6,35x10⁻³ m diam., 0,15 m centers 14 Spacers 2,30x10⁻⁴ thick Nylon Net 2 Outer Layers 2,54x10⁻⁵ m thick Teflon 7,62x10⁻² m Overlap. Interleaved. Number of layers indicated in the sketch.		1,70 (300 K)	1,94	0,869	
25 N = 15 Shields 6,35x10⁻⁶ m thick Mylar Double-Aluminized. Holes 6,35x10⁻³ m diam., 0,15 m centers 14 Spacers 2,30x10⁻⁴ thick Nylon Net 2 Outer Layers 2,54x10⁻⁵ m thick Teflon 7,62x10⁻² m Overlap. Interleaved. Number of layers indicated in the sketch.		1,70 (300 K)	1,94	0,869	

Description	Sketch	$C_i \times 10^3$ [m]	$\Delta\varepsilon_{effi} \times 10^3$	$\Delta Q_i/A$ [W/m²]	Comments
26 N = 15 Shields 6,35x10⁻⁶ m thick Mylar Double-Aluminized. Holes 6,35x10⁻³m diam., 0,15 m centers 14 Spacers 2,30x10⁻⁴ thick Nylon Net 2 Outer Layers 2,54x10⁻⁵ m thick Teflon 7,62x10⁻² m Overlap. Interleaved. Number of layers indicated in the sketch.		1,62	1,84	0,822	

Note: non-si units are used in this figure
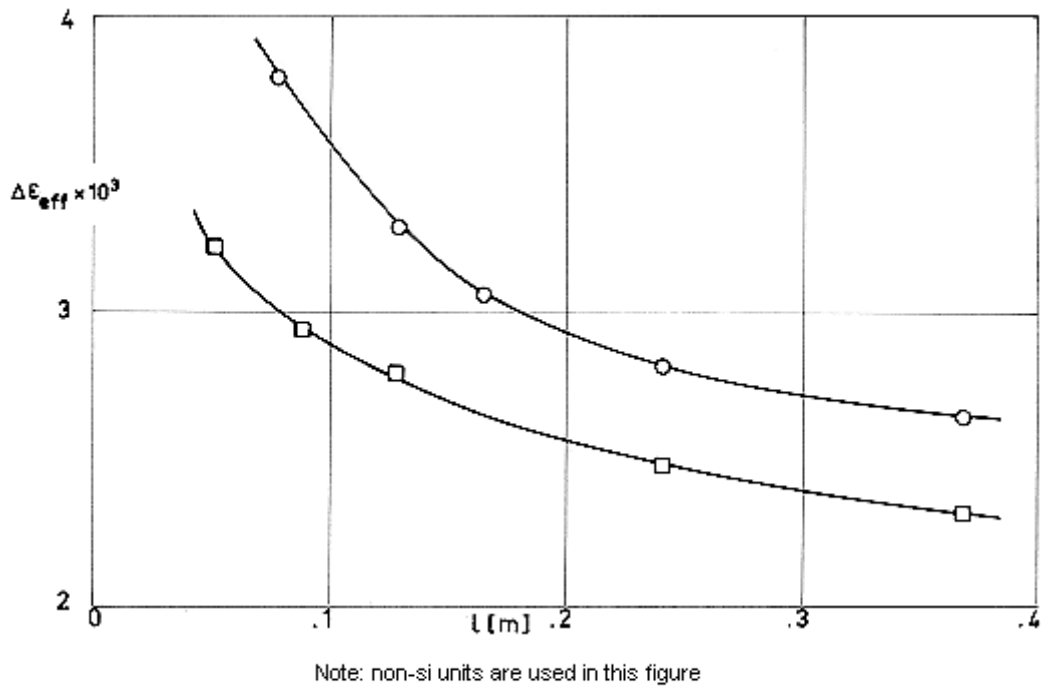
Figure 6-93: Effective emittance, $\Delta\varepsilon_{eff}$, vs. overlap, l

○ : Configuration 1 of Table 6-23.

□ : Configuration 2. From Crosby (1970) [16].

Note: non-si units are used in this figure
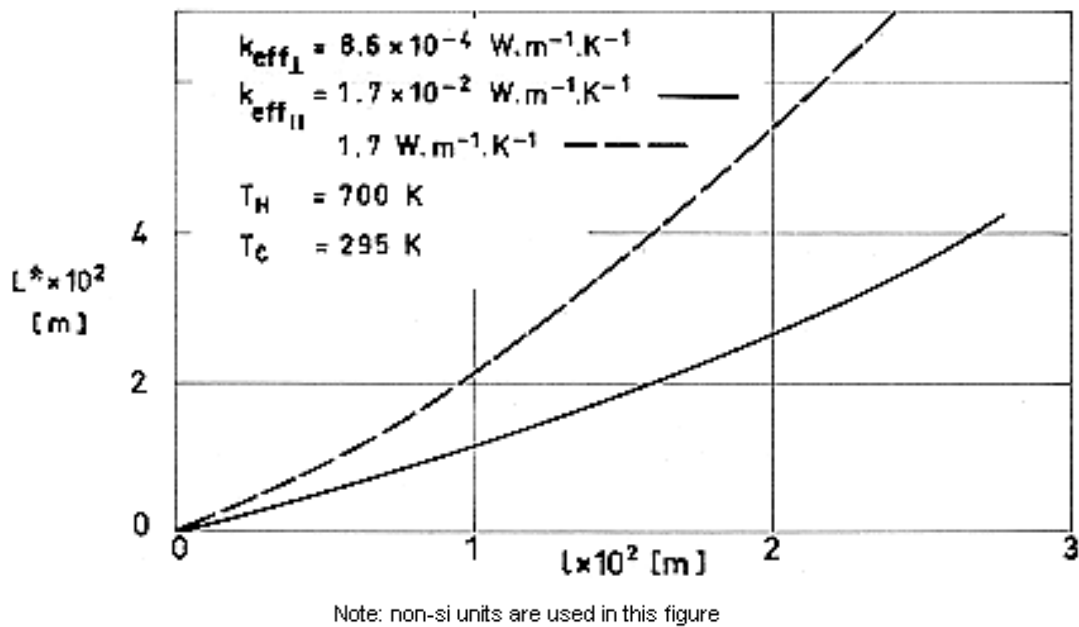
Figure 6-94: Length, L^*, vs. overlap, l, of alternate layers.

From Cunnington et al. (1967) [17].
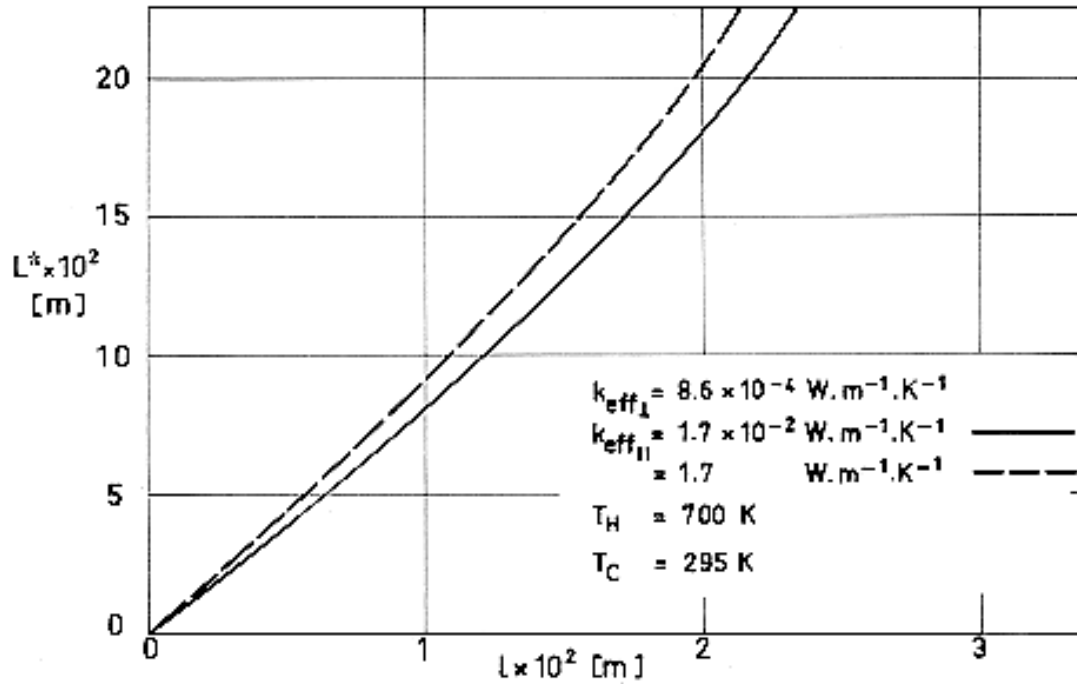
Figure 6-95: Length, *L**, vs. underlap, *l*.

From Cunnington et al. (1967) [17].
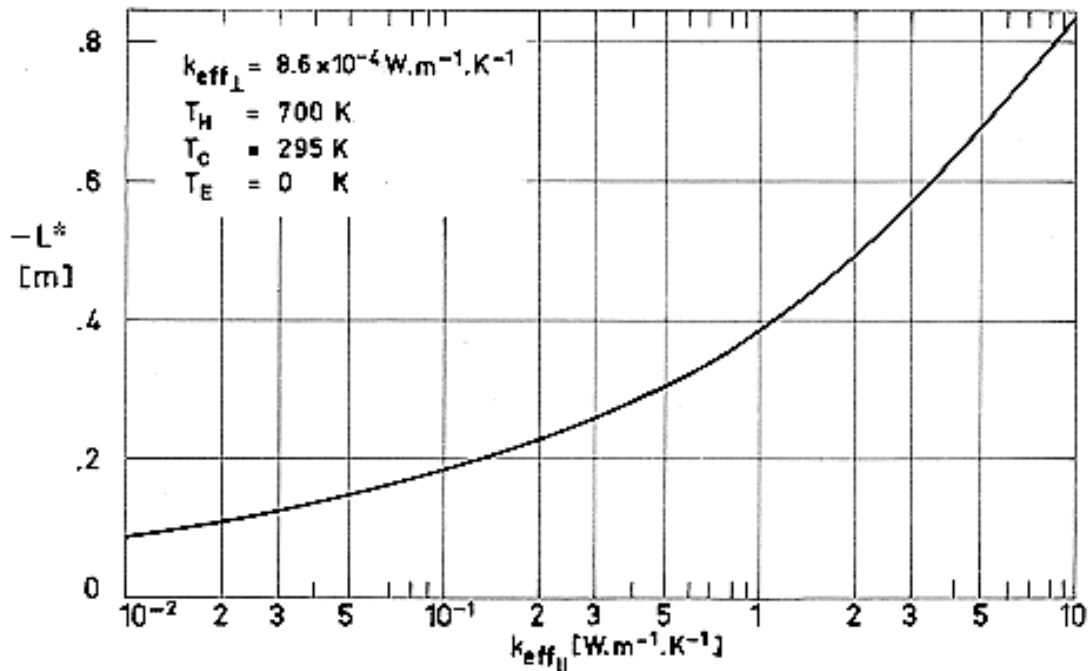
Figure 6-96: Length, *L**, vs. *k_{eff}*. Edge rejection.

From Cunnington et al. (1967) [17].

6.13.2 Stitches and patches

Stitches are extensively used in spacecraft MLI systems to contain cutting debris and to improve the dimensional stability of the blanket enabling ease of handling during extensive testing and repeated use.

Stitching increases locally the layer density and subsequently the blanket thermal conductivity.

According to Stimpson & Jaworski (1972) [69], the heat loss caused by stitching may be approximated by the following straight-line relationship based upon the length, *L*, of the stitch

$\mathit{\Delta}Q = 0{,}0335 + 0{,}88\,L$

where:

ΔQ, heat loss due to stitching. [W].

L, length of stitch. [m].

This relationship is represented in Figure 6-97, where several experimental data points have been also plotted.
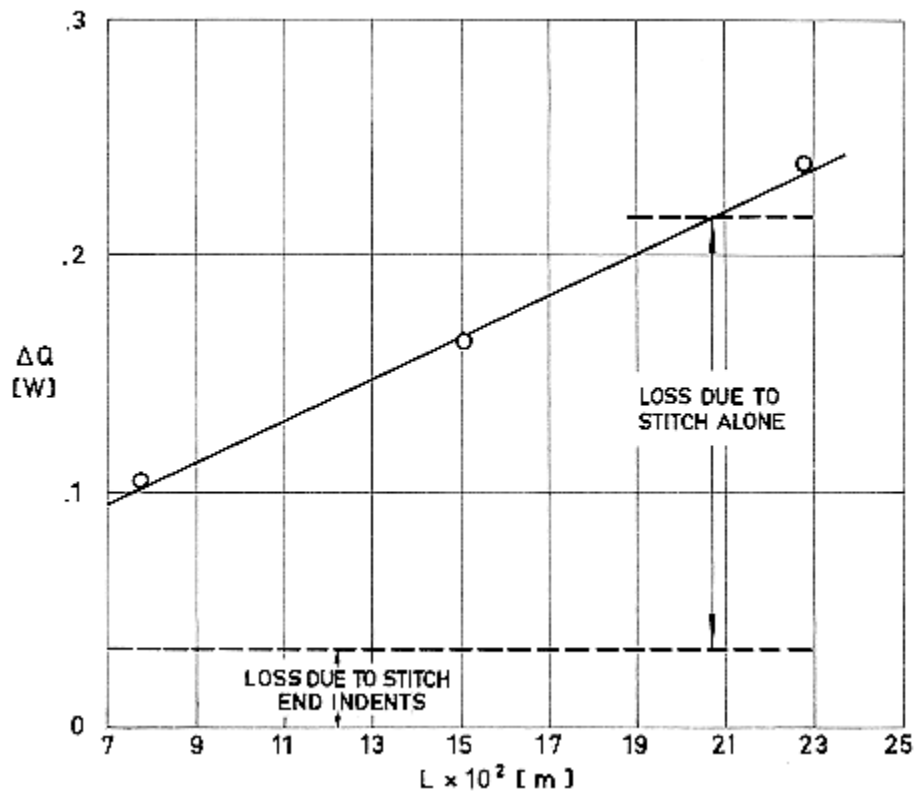
Note: non-si units are used in this figure

Figure 6-97: Heat loss, *ΔQ*, due to stitching vs. the length of Stitch, *L*.

From Stimpson & Jaworski (1972) [69].

Explanation

Undisturbed System	Stitching	Test method
15 Shields $6,35 \times 10^{-6}$ m thick Mylar Double-Aluminized; holes $6,35 \times 10^{-3}$ m diameter on 0,15 m centers. 14 Spacers $2,30 \times 10^{-4}$ thick Nylon Net. 2 Outer Layers $2,54 \times 10^{-5}$ m thick Teflon Single aluminized. Wrapped around the heater cylinder.	3 axial 0,228 m in length stitches. The stitch was shortened to 0,152 m and then to 0,076 m by removing threads. A circumferential stitch was then installed and tested for the same lengths.	Effective emittance of the system was measured by using an electrically heated cylindrical calorimeter. The dimensions of the cylinder were 0,254 m in diameter, 0,711 m in length. The heat losses through the undisturbed blanket were calculated.

For shorter stitch lengths (*L* < 0,07 m) the above relationship is no longer valid. Tests on individual button ties resulted in an average heat loss of 0,012 W, which is about a third of the sum of two stitch indent losses from a longer stitch.

Patches have been used to reduce the heat loss caused by stitches. Patching shields locally the blanket, reducing the temperature differential across it. The influence of the patches on the heat loss is given in

Figure 6-98. As a general rule it can be said that patches on the hot side are more effective that on the cold side, and on both sides only slightly better.
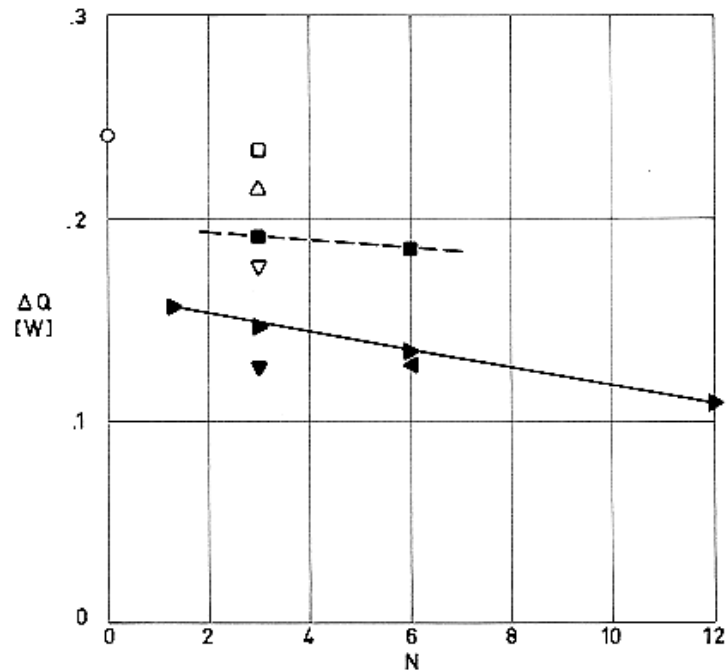
Note: non-si units are used in this figure

Figure 6-98: Heat loss, *ΔQ*, due to stitch patching vs. the number of patch layers, *N*. Undisturbed system and test method as in Figure 6-97.

From Stimpson & Jaworski (1972) [69].

Explanation

Patch Layer Description	Key	Patching
3 Layers of Mylar Double-Aluminized. 3 Nylon Net spacers. 1 Layer of Teflon Single-Aluminized.	○	Stitch 0,228 m length. Unpatched.
	□	0,1x0,33 m. Type B. Cold Side.
	■	0,1x0,33 m. Type A. Cold Side.
	△	0,2x0,4 m. Type B. Cold Side.
In Type A the Teflon layer was extended 4x10⁻³m beyond the patch borders. Type B had no Teflon extension.	▽	0,1x0,33 m. Type B. Both Sides.
	▼	0,1x0,33 m. Type A. Both Sides.
	▶	0,1x0,33 m. Type A. Hot Side.
	◀	0,15x0,38 m. Type A. Hot Side.

6.14 Effect of evacuating holes
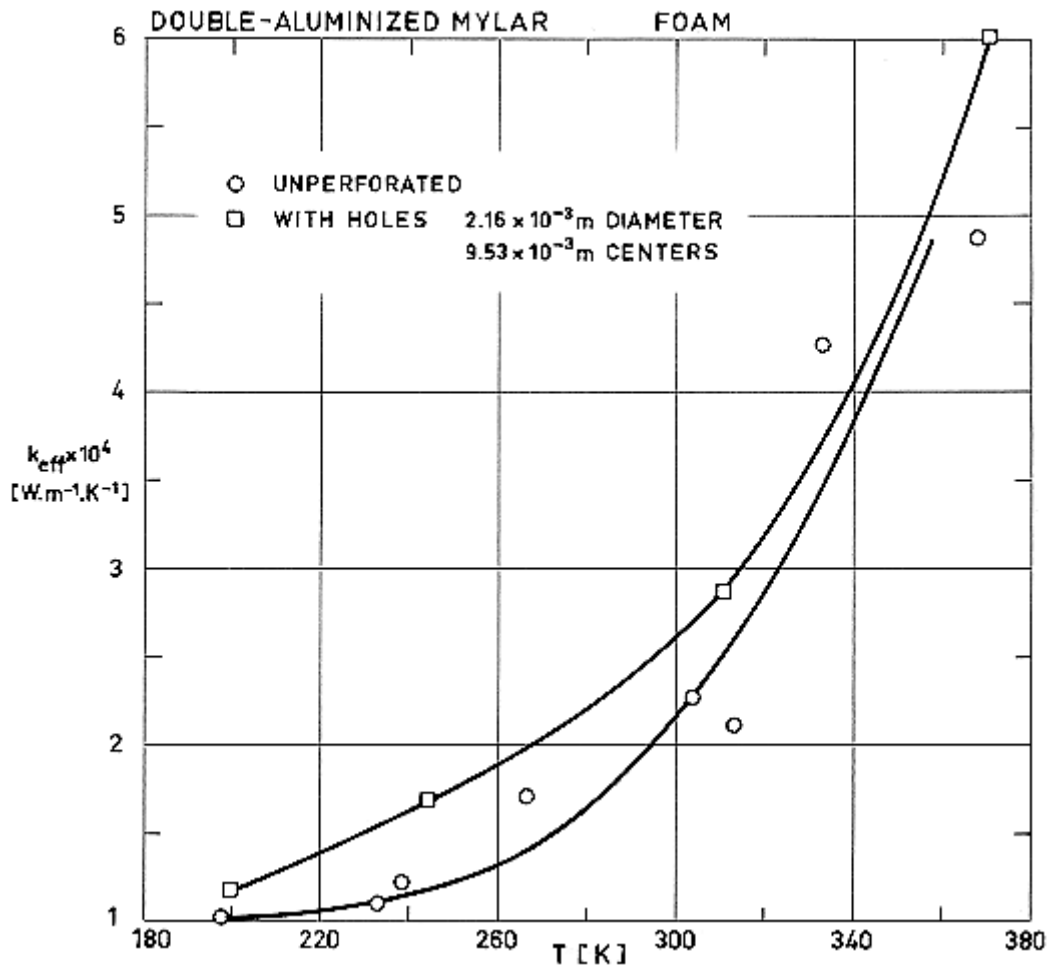
Figure 6-99: Effect of perforations on the effective thermal conductivity of a multilayer insulation formed by 24 Radiation Shields 6,35x10⁻⁶ m thick Mylar Double-Aluminized, and 23 Spacers 7,11x10⁻⁴ m thick Polyurethane Foam.

From Hale (1969) [27].
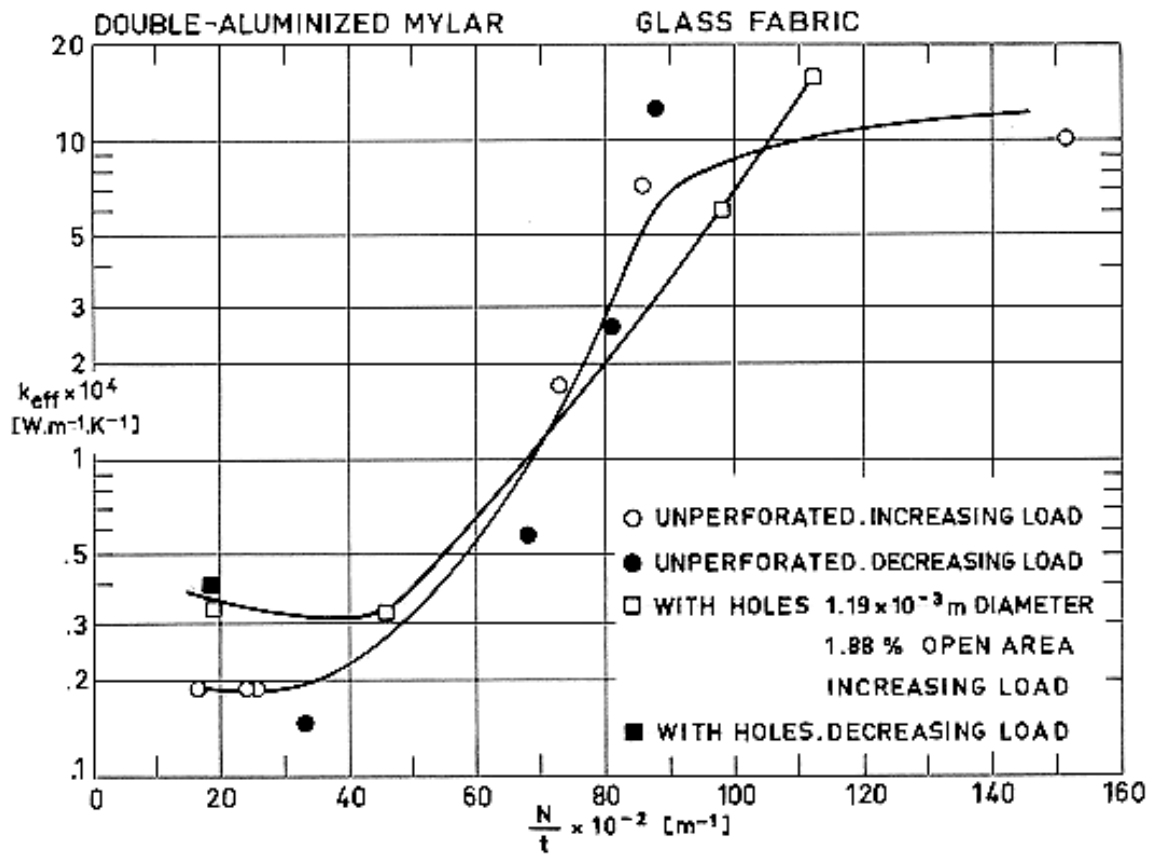
Figure 6-100: Effect of perforations on the effective thermal conductivity of a multilayer insulation formed by 10 Radiation Shields 6,35x10⁻⁶ m thick by 0,279 m diameter Mylar Double-Aluminized, and 22 Spacers 2,54x10⁻⁵ m thick by 0,305 m diameter Glass Fabric.

From ADL (1966) [2].
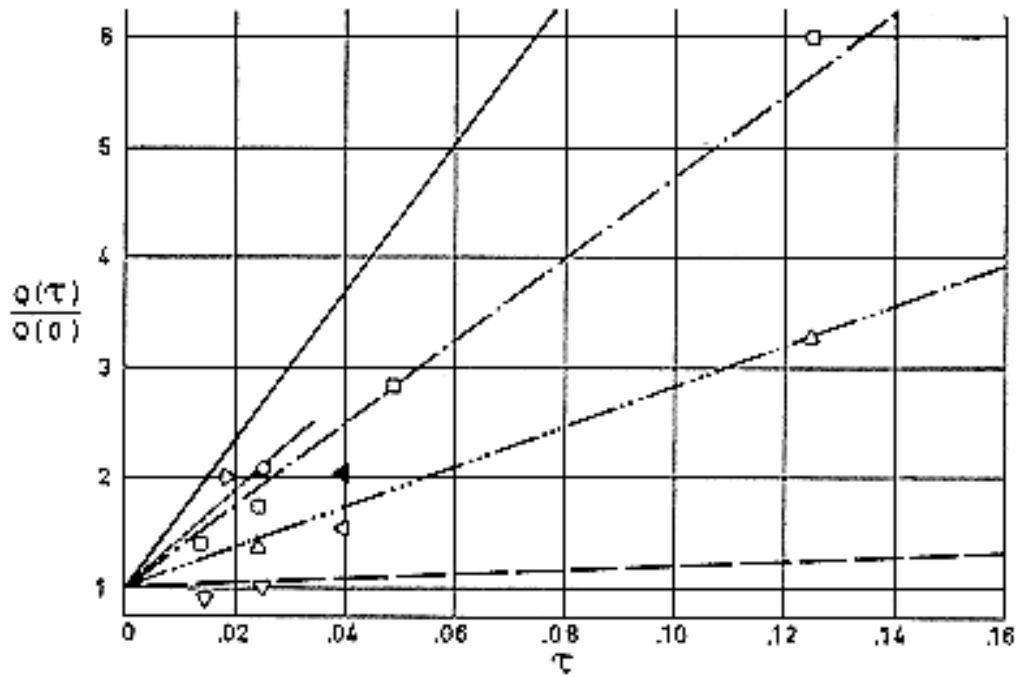
Note: non-si units are used in this figure

Figure 6-101: Effect of percentage of perforations, τ, on the heat flux through a multilayer insulation.

Explanation

Key	Description	Hole dia. x10³ [m]	T [K]	References
▬▬▬	$Q(\tau)/Q(0) = [(2-\varepsilon)\tau+\varepsilon]/[\varepsilon(1-\tau)]$. Boundary for small holes $\varepsilon = 0,033$			Tien & Cunnington (1973) [70].
▬ ▬	$Q(\tau)/Q(0) = (1+2\tau)$. Boundary for large holes			
○	10 Shields. Tempered aluminium 11 spacers. $3,18 \times 10^{-3}$ m by $3,18 \times 10^{-3}$ m thick Vinyl-Coated Fiber-Glass Screen	1,59	$T_C = 77$	Glaser et al. (1967) [23] pp. 58-59
········	Straight-line through ○ points			
□	Same as ○	3,18		
▬·▬	Straight-line through square points			
△	Same as ○	6,35		
▬··▬	Straight-line through triangle points			
▽	20 Shields. Mylar Single-Aluminized Crinkled	3,18	$T_C = 20$	

Key	Description	Hole dia. x10³ [m]	T [K]	References
▷	10 Shields. 6,35x10⁻⁶ m thick Mylar Double-Aluminized 22 Spacers. 2,54x10⁻⁵ m thick by 30,48x10⁻² m diameter Glass Fabric.	1,85	$T_H = 294$ $T_C = 77$	ADL (1966) [2] pp. II-87; II-91.
◁	24 Shields. 6,35x10⁻⁶ m thick Mylar Double-Aluminized 23 Spacers. 7,11x10⁻⁴ m thick. Polyurethane Foam	9,53	$T \sim 200$ [a]	Hale (1969) [27] p. 39
◀	Same as ◁	9,53	$T \sim 240$ [a]	

[a] T is the characteristic temperature.

6.15 Effect of mechanical damage

Note: non-si units are used in this figure
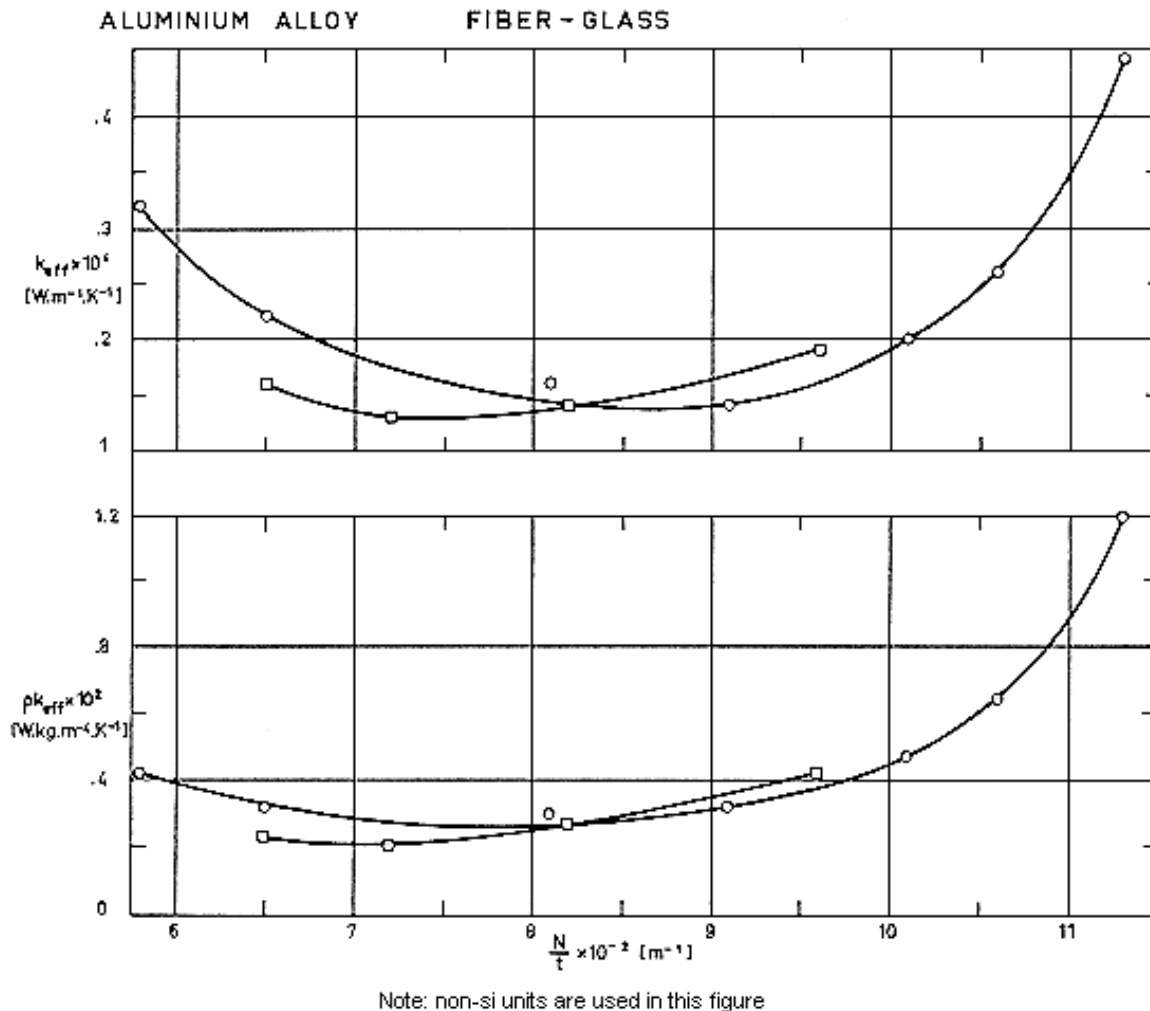
Figure 6-102: Effect of Meteoroid-Bumper debris damage on the effective thermal conductivity, k_{eff}, and product of apparent density and effective thermal conductivity, ρk_{eff}.

Both functions are plotted vs. the number of radiation shields per unit thickness, *N/t*.

Sample represented by circles was damaged by being fired upon by hypervelocity pellets. Sample represented by squares was not damaged.

Explanation

Key	Sample Description	tx10^2 [m] Uncompressed	px10^3 [Pa]	T$_H$ [K]	T$_C$ [K]	Calorimeter Type	References
○	N = 5 Shields 5,08x10^{-5} m thick Al. Alloy 1145-0 6 Spacers	0,86 [a]	<0,93	293± 1	20,5	ADL Model 12 Flat-Plate (double-guarded	ADL (1964) [1] p. II-63

Key	Sample Description	tx10^2 [m] Uncompressed	px10^3 [Pa]	T$_H$ [K]	T$_C$ [K]	Calorimeter Type	References
	5,08x10^{-4} m thick Vinyl-Coated Glass-Fiber screen 3,18x10^{-3} x 3,18x10^{-3} m mesh. Damaged.					cold-plate)	
☐	Same as ◯ . Undamaged	0,77 [a]	<0,93	293± 1	20,5		

[a] Largest quoted value.

6.16 Effect of inner gas pressure

Evacuated MLI exhibit low thermal conductivity, since the effect of gas conduction decreases when pressure decreases.

According to kinetic theory, the thermal conductivity, k_g, of a gas is a function of the product of the density, ρ, times the mean free path, λ, of the gas molecules

$$k_g \propto \rho \lambda c_p \overline{c}$$

Note: non-si units are used in this figure

[6-23]

where neither the specific heat at constant pressure, c_p, nor the mean molecular speed, $\overline{c}$,

depend upon the pressure. (Strictly speaking c_p is a slowly varying function of pressure).

In the continuous region, where the pressure goes from an atmosphere to a few hundred pascals, the molecular mean free path of the gas is much smaller than the characteristic length of the spacer voids. Under these conditions, the gas conduction is independent of pressure, as the decrease in density is compensated for by the increase in the mean free path.

On the other hand, if the pressure is low enough the characteristic length of the spacer voids may become much smaller than the gaseous mean free path. Thence, the thermal conductivity decreases in proportion to pressure because the characteristic length, d, is now that of the void rather than the mean free path of the gas (free molecular region).

It is obvious that the transition from one region to the other depends upon the dimensions of the individual components of the insulation. The larger the voids, the lower the pressure required to approach the free molecular region.

At atmospheric pressure the thermal conductivity of a complete multilayer insulation system approaches that of the inner gas, and is independent of the thermal conductivity of the evacuated system. At very low pressure the gaseous conduction is negligible compared to solid and radiative conduction, and the thermal conductivity of the system becomes again independent of pressure. Because of these reasons, the thermal conductivity of the multilayer insulation relates to gas pressure by an S-like curve.

Concerning the type of gas, it should be said that gases of high thermal conductivity (e.g., helium or hydrogen) cause more drastic degradation of the performance of the system than gases with low

conductivity (e.g., nitrogen or air). At low temperature, the condensations of the inner gases reduces the insulation effectiveness, in addition to damaging the blanket (upon pressurization due to subsequent heating), and constituting a fire and explosion hazard when the condensates come in contact with the organic components of the spacer.

Gas within the insulation may be evacuated with a vacuum system connected to a cryogenic storage tank. As an alternative, cryopumping may be achieved by using carbon dioxide, which is a gas at room temperature but freezes on a surface cooled below 190 K, thus reducing the gas pressure in a sealed space. A third technique for preventing condensation of air is to purge the insulation with helium gas, which does not condense at liquid hydrogen temperatures. Purging with warm helium is often used to improve outgassing of organic materials. The principal advantage of purging is that it greatly reduces the need for leak reliability in a protective enclosure, however, failure to provide venting may result in a rupture of the enclosure and degradation of the insulation.

Thermal conductivities of several multilayer insulation systems containing different pages are plotted versus gas pressure in the following data sheets.
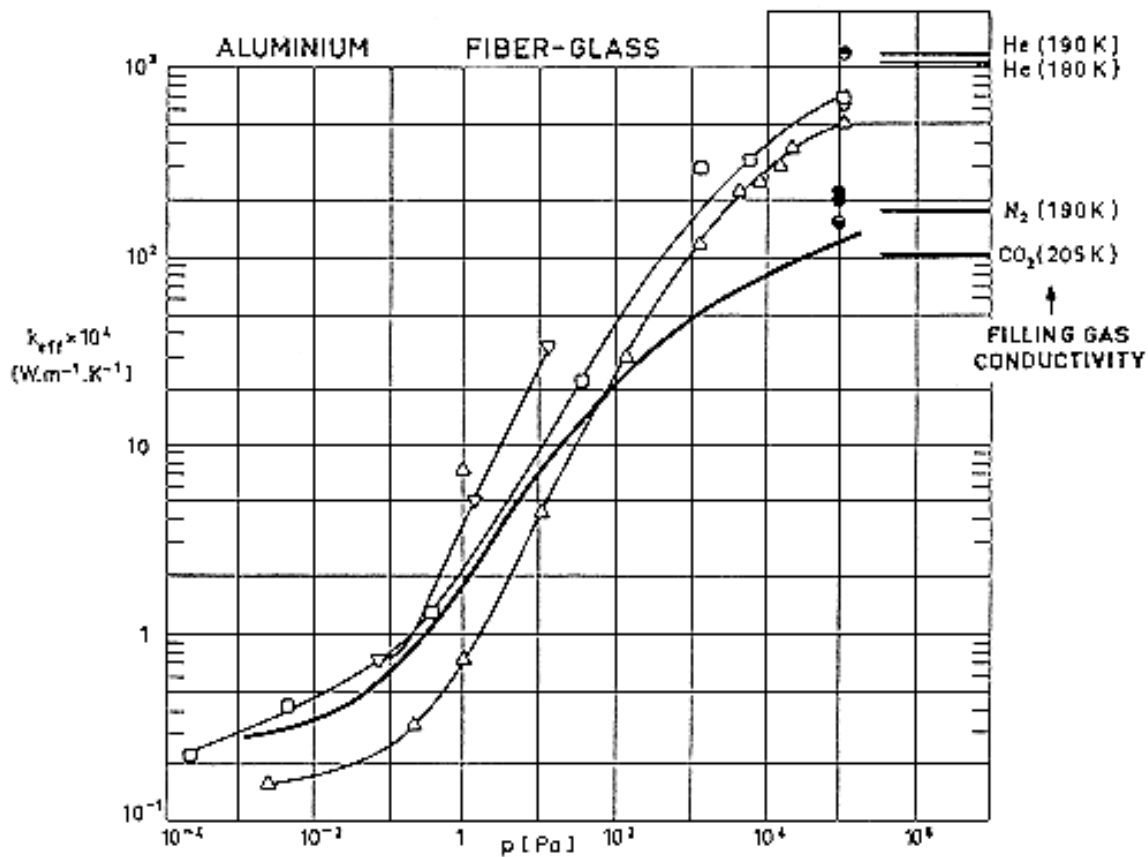
Figure 6-103: Effective thermal conductivity, k_{eff}, as a function of gas pressure, p.

The thermal conductivities of the filling gases at the characteristic temperatures are indicated for comparison.

Explanation

Key	Sample Description	$t \times 10^2$ [m] Uncompressed	Filling Gas	T_H [K]	T_C [K]	Calorimeter Type	References
○	N = 10 Shields 5,08x10⁻⁵ m thick Al. Alloy 1145-H19 bright both sides 11 Spacers 5,08x10⁻⁴ m thick Glass Fiber screen 3,175x10⁻³ by 3,175x10⁻³ m mesh [a]	0,94	He	273	20,5	ADL Model 12 Flat-Plate (double-guarded cold-plate)	ADL (1964) [1] p. II-48
●	Same as ○	0,89	N_2	264,5± 6	77,5	Same as ○	Same as ○
◑	Same as ○	0,94	N_2	265,5	20,5	Same as ○	Same as ○
◒	Same as ○	0,91	CO_2	293,5	77,5	Same as ○	Same as ○
□	Shields: Tempered Aluminium Spacers: Vinyl-Coated Fiber Glass Screen		He		77		Glaser et al. (1967) [23] p. 56
△	Shields: N not quoted. N/t = 1417 m⁻¹. Aluminium Spacers: Fiber Glass		N_2 N_2	294 294	20,7 20,7		Coston (1967) [13] p. 4,3-25
▬	Shields: Aluminium Spacers: Fiber Glass		N_2	294	20,7		
▽	Shields: Aluminium Spacers: Glass Wool		Air				Same as □

[a]   The sample was enclosed in a polyester film container for purging.
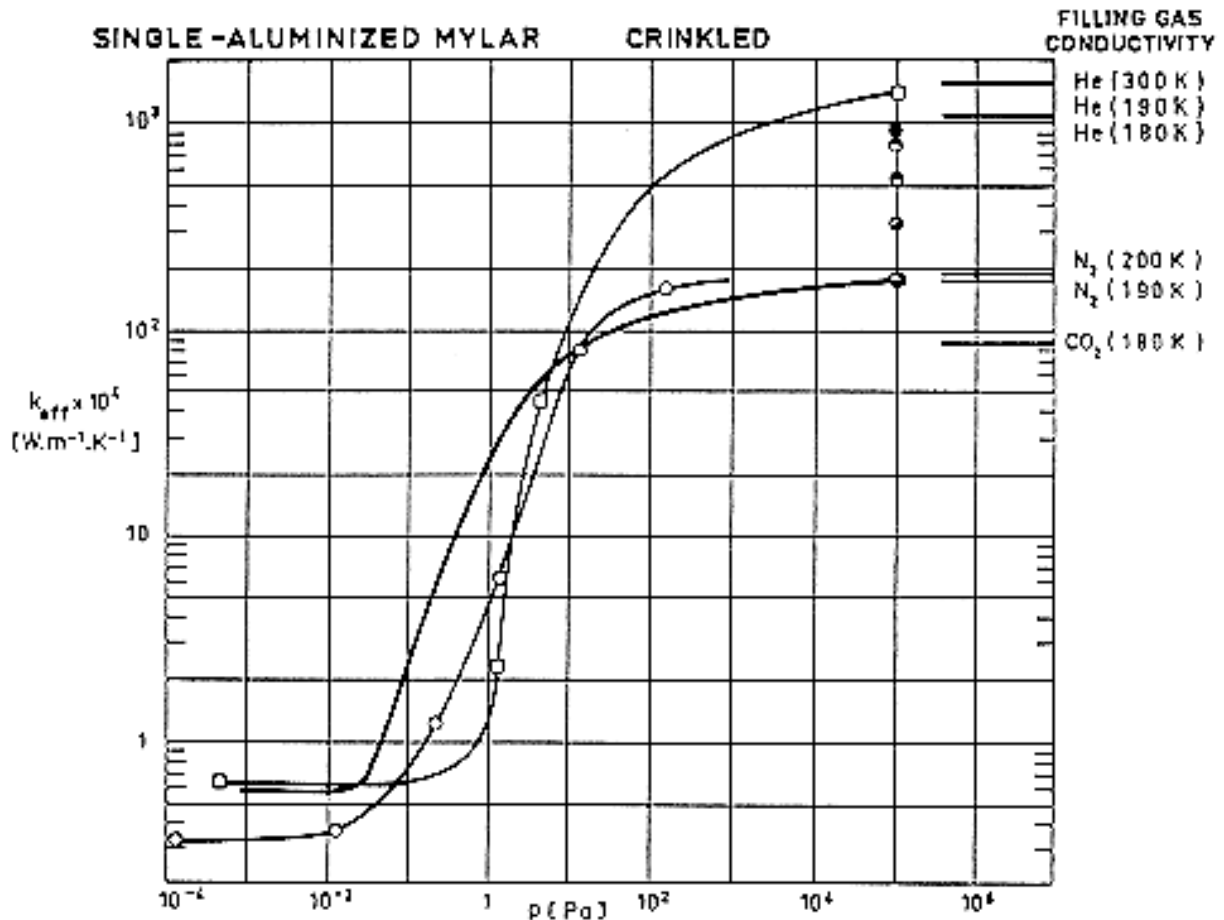
Figure 6-104: Effective thermal conductivity, k_{eff}, as a function of gas pressure, p.

The thermal conductivities of the filling gases at the characteristic temperatures are indicated for comparison.

Explanation

Key	Sample Description	tx10² [m] Uncompressed	Filling Gas	T_H [K]	T_C [K]	Calorimeter Type	References
◯	Mylar Single-Aluminized Crinkled		Air				Glaser et al. (1967) [23] p. 56
●	*N* = 20 Shields 6,35x10⁻⁶ m thick Mylar Single-Aluminized Crinkled	0,94 ᵃ	He	274	77,5	ADL Model 12 Flat-Plate (double-guarded cold-plate)	ADL (1964) [1] p. II-49
◓	Same as ●	0,94 ᵃ	He	274	20,5	Same as ●	Same as ●
◒	Same as ●	0,94 ᵃ	CO₂	261	77,5	Same as ●	Same as ●
◑	Same as ●	0,94 ᵃ	N₂	275,5	77,5	Same as ●	Same as ●

Key	Sample Description	$t \times 10^2$ [m] Uncompressed	Filling Gas	T_H [K]	T_C [K]	Calorimeter Type	References
◑	Same as ●		N_2	268,5	20,5	Same as ●	Same as ●
▬	Shields N not quoted. N/t = 1575 m⁻¹ 6,35x10⁻⁶ m thick Mylar Single-Aluminized Crinkled		N_2	294	79,4		Coston (1967) [13] p. 4,3-25
☐	N = 81 Shields 6,35x10⁻⁶ m thick Mylar Single-Aluminized Embossed	1,27	He	312± 9,5	300,5± 1	Lockheed/ Huntsville Cylindrical	Hale (1969) [27] p. 41

a   Largest quoted value.
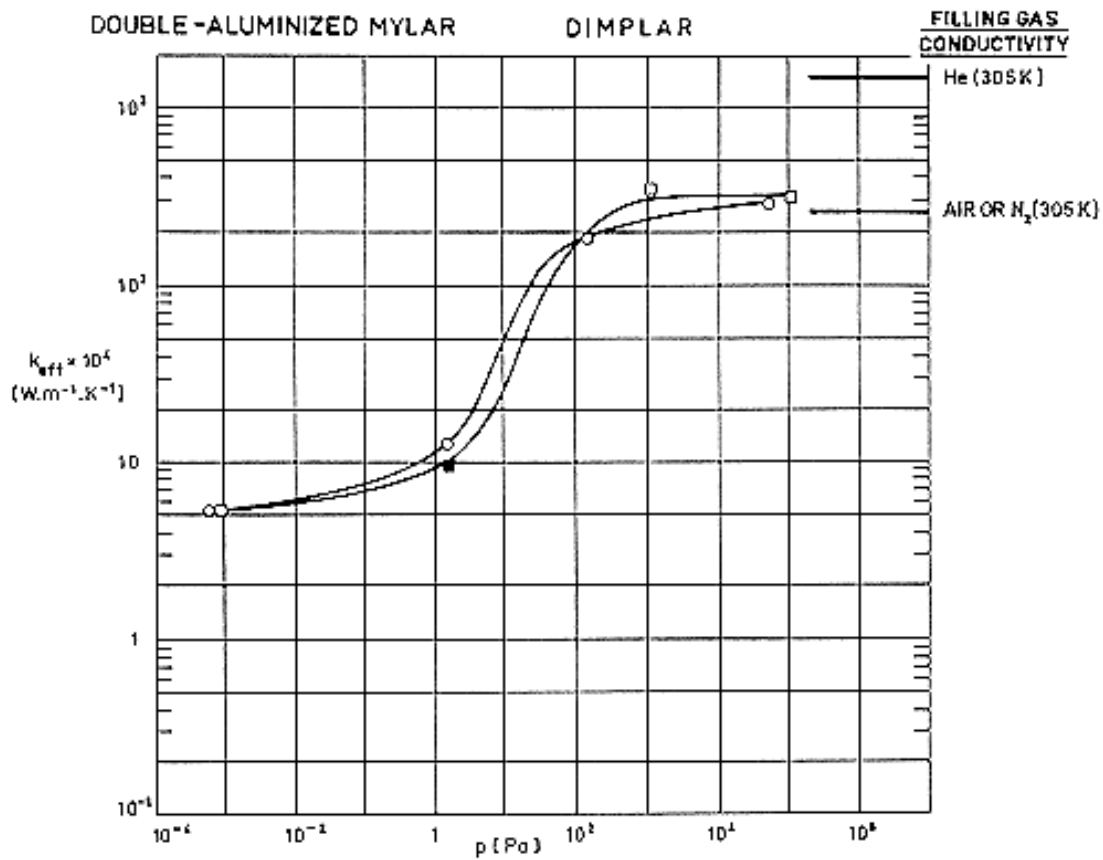
Figure 6-105: Effective thermal conductivity, k_{eff}, as a function of gas pressure, p.

The thermal conductivities of the filling gases at the characteristic temperatures are indicated for comparison.

Explanation

Key	Sample Description	$t \times 10^2$ [m] Uncompressed	Filling Gas	T_H [K]	T_C [K]	Calorimeter Type	References
○	$N = 22$ 22 Layers 6,35x10⁻⁶ m thick Mylar Single-Aluminized Dimpled 22 Layers 6,35x10⁻⁶ m thick Mylar Single-Aluminized Embossed	2,92	He ?	311,5 ± 8	301,5 ± 1,5	Lockheed/ Huntsville Cylindrical	Hale (1969) [27] p. 42
☐	$N = 60$ Shields 6,35x10⁻⁶ m thick Mylar Single-Aluminized Embossed 60 Spacers White Nylon Net	2,54	He ?	316 ± 4,5	304 ± 2,5		Hale (1969) [27] p. 43
■		2,54	He ?	266	255		

Comments: Although the author claims that the system has been purged with helium preheated to 394 K, it seems obvious that the filling gas is either nitrogen or air.
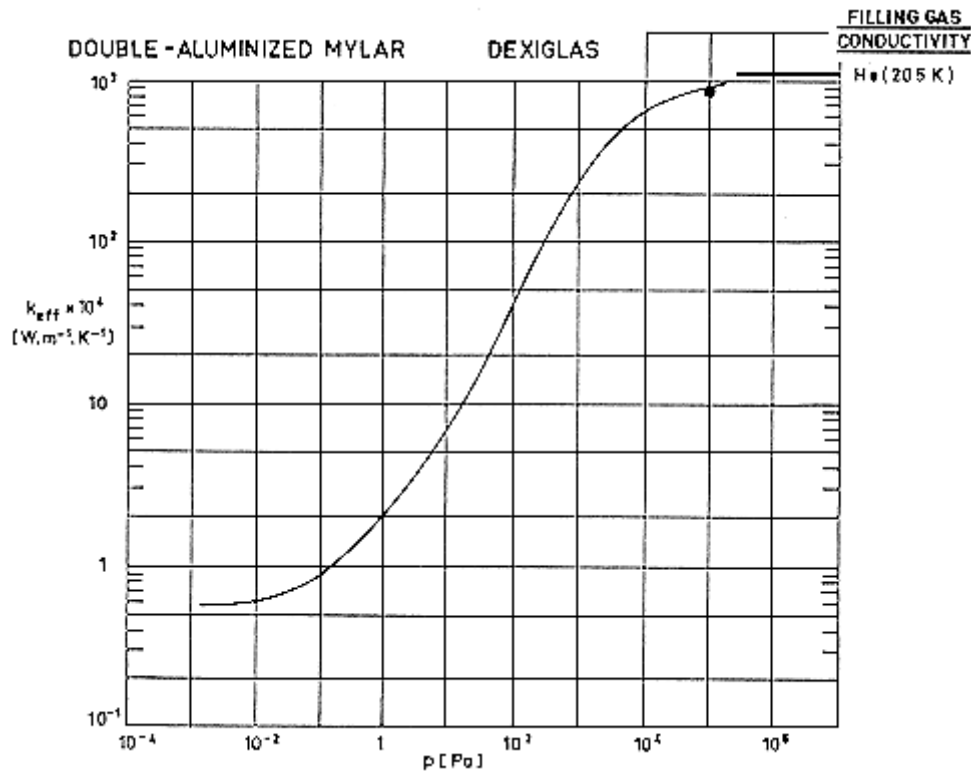
Figure 6-106: Effective thermal conductivity, k_{eff}, as a function of gas pressure, p.

The thermal conductivity of the filling gas at the characteristic temperature is indicated for comparison.

Explanation

Key	Sample Description	$t \times 10^2$ [m] Uncompressed	Filling Gas	T_H [K]	T_C [K]	Calorimeter Type	References
———	Shields N not quoted. N/t = 2677 m^{-1} 6,35x10^{-6} m thick Mylar Double-Aluminized Spacers 7,11x10^{-6} m thick Dexiglas buttons on 0,1 m centers		He	294	77,2		Coston (1967) [13] p. 4,3-25
●	N = 20 Shields 6,35x10^{-6} m thick Mylar Single-Aluminized Crinkled	0,94 [a]	He	274	77,5	ADL Model 12 Flat-Plate (double-guarded cold-plate)	ADL (1964) [1] p. II-49

[a] Largest quoted value.
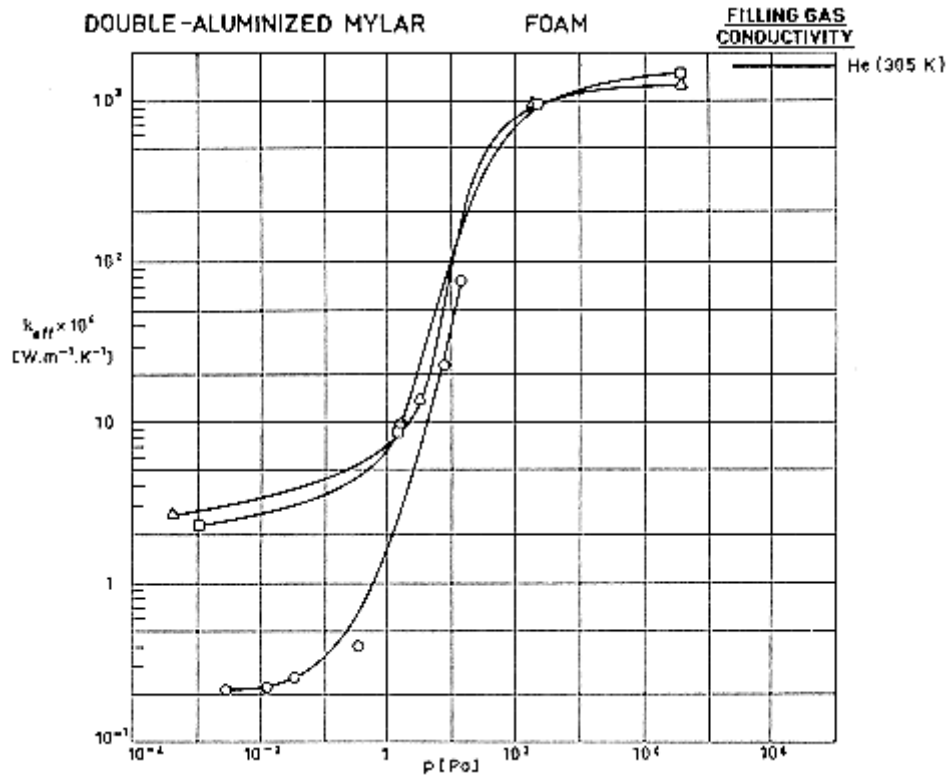
Figure 6-107: Effective thermal conductivity, k_{eff}, as a function of gas pressure, p.

The thermal conductivity of the filling gases at the characteristic temperatures are indicated for comparison.

Explanation

Key	Sample Description	tx10² [m] Uncompressed	Filling Gas	T_H [K]	T_C [K]	Calorimeter Type	References
◯	Shields: Mylar Spacers: Foam		He				Glaser et al. (1967) [23] p. 56
▢	N = 24 Shields 6,35x10⁻⁶ m thick Mylar Double Aluminized 23 Spacers 7,11x10⁻⁶ m thick Red Polyurethane Goodyear Foam	2,54	He	307± 4,5	301± 4	Lockheed/ Huntsville Cylindrical	Hale (1969) [27] p. 39
△	Same as ▢ .> Perforated-Shields having holes of 2,16x10⁻³ m diameter 9,53x10⁻³ m between centers.	2,54	He	312± 9,5	301± 1		

6.17 Evacuation

The thermal conductivity of an MLI system can be reduced to a very low level provided that the interstitial pressure is kept below roughly 10^{-3} Pa so that gaseous conduction is practically eliminated. This pressure level can be achieved, before or after launch, by certain pumping processes.

During ascent flight the inner gas pressure should be reduced rapidly enough to prevent high stresses on the shields, and to decrease the transient heating and associated propellant boil-off. As the gas pressure is reduced, outgassing from the insulation materials becomes important, seriously prolonging the evacuation period.

There have been two pumping procedures in practice, namely the edge pumping, which causes the gas to flow parallel to the shield layers, and the broadside pumping in which the gas flows, normally to the layers, through small holes made in the shields.

To study the evacuation -and repressurization- processes the MLI system is assimilated to a porous medium. The motion of a gas through a porous medium is fairly well understood, at least for engineering purposes. The characteristics of the gas flow depend on the ratio of the molecular mean free path, λ, to the pore diameter, d. λ/d is often called the Knudsen number.

At the outset of evacuation, when the pressure is of the order of one atmosphere (10^5 Pa), $\lambda/d \ll 1$, the intermolecular collisions are dominant, and the gas behaves as a continuum medium.

For very low pressures, when outgassing from the material controls the fluid motion, $\lambda/d > 1$, collisions with the walls dominate, and the so called free molecular flow prevails.

In the intermediate range of pressures the problem is extremely complicated, however, useful semi empirical correlations exist which can be used for the present purposes.

6.17.1   Interstitial pressure during rapid evacuation

Although the gas flow through an MLI can be three-dimensional, a conservative estimate of the pressure variation may be achieved by use of the results of one-dimensional theory wherein the minimum linear flow path is used as the half-length of the equivalent one-dimensional configuration.

In the case of edge pumping the minimum linear flow path, L, is the distance from center of blanket to the nearest open edge. This case has been considered by Kneisel & Bennet (1970) [38].

For broadside pumping L would be equal to the blanket thickness, t.

In order to analyze the flow of the gas through the MLI system it is assumed that the gas is perfect, and that the temperature and the gas properties are constant.

6.17.1.1   Continuum regime

Near the atmospheric pressure, the mass flow rate per unit cross-sectional area, m, is given by Darcy's law

$$m = \frac{\kappa}{\mu} \rho \frac{\partial p}{\partial x}$$

[6-24]

Note: non-si units are used in this figure

where:

p, Gas pressure, depending on coordinate, x, and time, t. [Pa].

x, Coordinate parallel to flow direction. [m].

κ, Permeability of the porous medium. [m²].

μ, Gas viscosity at the average blanket temperature. [Pa.s].

ρ, Mean density of the gas. [kg.m⁻³].

Taking into account the mass preservation condition in a differential control element

$$\frac{\partial \rho}{\partial t} = \frac{\partial m}{\partial x}$$

[6-25]

Note: non-si units are used in this figure

the following equation results:

$$\frac{\mu}{\kappa} \frac{\partial p}{\partial t} = \frac{\partial}{\partial x}\left(p \frac{\partial p}{\partial x} \right)$$

[6-26]

Note: non-si units are used in this figure

The initial boundary conditions are:

Initial condition: $p(x,0) = p_0(0)$

Boundary conditions:

Blanket Center ($x = 0$): $\partial p/\partial x = 0$ for any t

Blanket Edge ($x = L$): $p(L,t) = p_0(t)$

$p_0(t)$ being the outer pressure at instant t.

In the case of edge pumping, once this model of fluid flow has been postulated, κ can be estimated from data giving the variation of pressure with time. Conversely, from the value of κ it can be deduced the pressure time relationship in an MLI system of given evacuation length, L.

Values of κ for several MLI systems are shown in Figure 6-108.
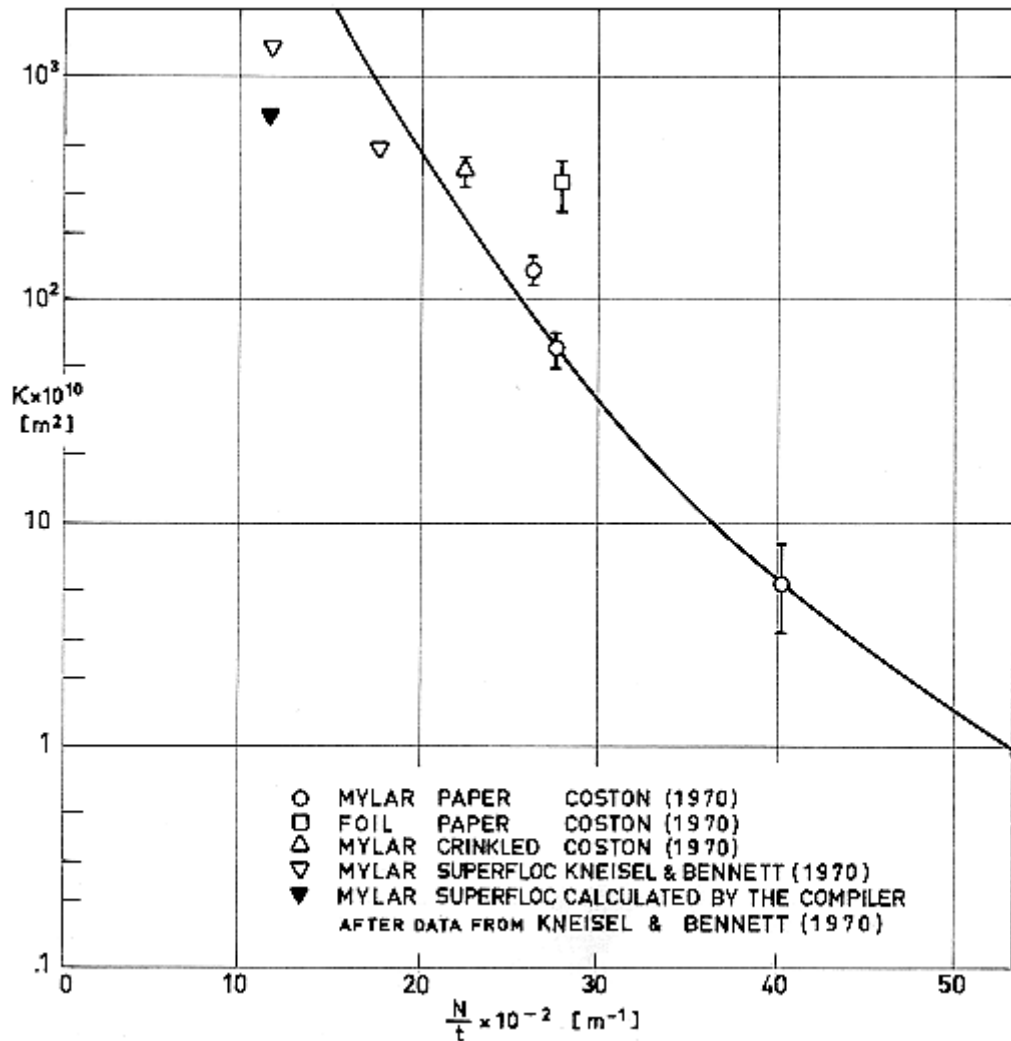
Note: non-si units are used in this figure

Figure 6-108: Permeability, κ, of several multilayer insulation configurations as a function of the layer density, N/t.

In the case of broadside pumping the fitting of the one-dimensional model is not so obvious if the hole diameter is smaller than the diameter of the pores in the spacer. This small hole limiting case has some technical interest since the shield emittance would be degraded because increased transmittance produced by large holes.

When the hole diameter is of the same order or smaller than the pore diameter, the resistance to fluid flow is localized in the holes. Hence, it can be assumed that the pressure in each one of the spaces between two neighboring shields is uniform although different from a space to the other. The pressure difference between two consecutive spaces is equal to the pressure loss experimented by the fluid when flowing through the hole.

For Reynolds numbers, defined in terms of the hole diameter and the mean fluid velocity through the hole, smaller than one, the mass flow rate per unit cross-sectional area, m_h, of an isolated, circular, hole is given (Happel & Brenner (1965) [29]) by the following expression:

$$m_h = \frac{d^2}{6\pi\mu} \rho \frac{\Delta p}{d}$$

[6-27]

Note: non-si units are used in this figure

where:

d, Hole diameter. [m].

Δp, Pressure loss through the hole. [Pa].

Since the number of shields per unit blanket thickness, N/t, is normally large, the multiple-step-like pressure distribution across the blanket can be substituted by a continuous one, so that the mass flow rate, m, per unit area of the shield becomes

$$m = \frac{\tau d}{6\pi(n/t)\mu} \rho \frac{\partial p}{\partial x}$$

[6-28]

Note: non-si units are used in this figure

τ being the fractional open area or transmittance of the perforated shields.

By comparing Eq. [6-28] to Eq. [6-24] it is deduced that the above one-dimensional approach can be applied to the hole-controlled broadside pumping provided that the following value of the permeability is used

$$\kappa_h = \frac{\tau d}{6\pi(N/t)}$$

[6-29]

6.17.1.1.1   Edge pumping vs. broadside pumping

A simple dimensional reasoning, based on Eq. [6-26], indicates that the characteristic edge-evacuation time, t_e, will obey the following order of magnitude relationship

$$t_e \approx \frac{\mu}{p} \frac{L^2}{\kappa}$$

[6-30]

Likewise, for the hole-controlled broadside pumping case

$$t_h \approx \frac{\mu}{p} \frac{6\pi t^2(N/t)}{\tau d}$$

[6-31]

Note: non-si units are used in this figure

Expression [6-30] and [6-31] supply a criterion for guiding in the selection of the evacuation procedure, which could be useful, at least for the pressure range considered. When

$$\frac{L^2}{\kappa} < 6\pi \frac{Nt}{\tau d}$$

[6-32]

the edge pumping should be preferred, otherwise broadside evacuation would allow a faster outgoing of the inner gas.

At very low pressures, when the main problem is to manage the outgassing products, broadside evacuation is normally preferred.

6.17.1.1.2   Mathematical solution of the problem

Although Eq. [6-26], with the appropriate initial and boundary conditions, has been numerically integrated by Kneisel & Bennet (1970) [38] in several particular cases, it is possible to obtain very simple results of more general usefulness.

Owing to obvious structural reasons, the maximum to minimum pressure difference should be small compared to the outer pressure, thence one can write.

$$p(x,t) = p_o(t) + \pi(x,t) \quad , \quad |\pi(x,t)| << p_o(t) \qquad [6\text{-}33]$$

The differential equation giving $\pi(x,t)$ is, to a first approximation:

$$\frac{\partial^2 p}{\partial x^2} = \frac{\mu}{\kappa p_o} \frac{dp_o}{dt} \qquad [6\text{-}34]$$

which can be easily integrated, leading to the following expression:

$$p(x,t) = p_o(t) + \frac{\mu}{2\kappa} \frac{1}{p_o} \frac{dp_o}{dt} \left(x^2 - L^2 \right) \qquad [6\text{-}35]$$

It has been assumed that, for a typical booster pressure profile

$$\left. \frac{dp_o}{dt} \right|_{t=0} = 0 \qquad [6\text{-}36]$$

otherwise slight changes should be made in this mathematical treatment in order to fulfill the initial condition.

Values of $p(0,t)$–$p_0(t)$ deduced from Eq. [6-35] have been compared to those given by Kneisel & Bennet (1970) [38], both calculated and measured, in Figure 6-109. It can be seen that the results of the present calculation agree fairly closely with those obtained by Kneisel & Bennet using similar values of κ, μ, and $p_0(t)$), and that the fitness of the present analytical prediction to experimental results is excellent when the value of the blanket permeability, κ, is appropriately chosen.
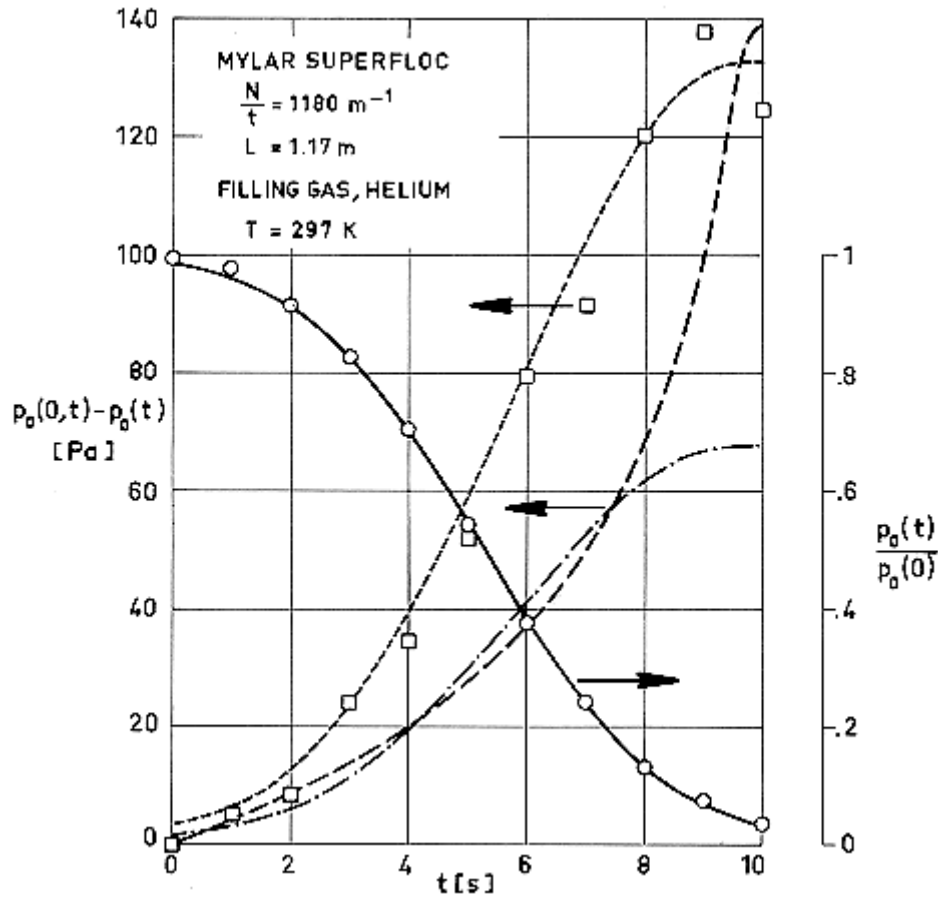
Figure 6-109: Pressure differential, *p(0,t)–p₀(t)*. Vs. time, *t*.

□: Experimental> (Kneisel & Bennett (1970)).

▬ ▬: Computed by> the same authors.

▬•▬: Eq. [6-35]. $\kappa = 1{,}37 \times 10^{-7}$ m².

•••••••: Eq. [6-35].> $\kappa = 0{,}70 \times 10^{-7}$ m².

O: Vacuum> chamber pressure as measured by Kneisel & Bennett [38].

▬▬▬: Curve given> by the expression

$$\frac{p_o(f)}{p_o(0)} = \frac{1}{2}\left\{1 - erf\left[0{,}3(t - 5{,}28) - 0{,}0012(t - 5{,}28)^3\right]\right\},$$

Which has been used to calculate dp_o/dt.

6.17.1.2 Intermediate regime

When the pressure is low, rarefaction effects are taken into account, so that the equation giving the mass flow rate, *m*, through unit cross-sectional area of a porous body, becomes

$$m = \left(\frac{\kappa p}{\mu} + D_K\right)\rho\frac{\partial}{\partial x}\ln p \qquad [6\text{-}37]$$

where:

D_K, Knudsen Diffusion Coefficient. [m.s⁻¹].

$$D^K = \frac{4}{3}\bar{c}K_o \qquad [6\text{-}38]$$

$\bar{c}$

Note: non-si units are used in this figure

, Average Molecular> Speed. [m.s⁻¹].

$$\bar{c} = \sqrt{\frac{8RT}{\pi m}} \qquad [6\text{-}39]$$

R, Boltzmann Constant,

$R = 1,38054 \times 10^{-23}$ J.K⁻¹.

T, Temperature. [K].

m, Mass of one molecule. [kg].

$m = M.N_A^{-1}$

M, Gas Molecular mass. [kg.mol⁻¹].

N_A, Avogadro Constant,

$N_A = 6,02252 \times 10^{23}$ mol⁻¹.

K_0, Constant dependent on the interaction between the gas and the porous medium. [m].

From Eq. [6-37] following the same procedure as above, it is obtained:

$$\frac{\mu}{\kappa}\frac{\partial p}{\partial t} = \frac{\partial}{\partial x}\left(p\frac{\partial p}{\partial x}\right) + \frac{D_\kappa \mu}{\kappa}\frac{\partial^2 p}{\partial x^2} \qquad [6\text{-}40]$$

Note: non-si units are used in this figure

When the pressure is so low that $\kappa p/D_\kappa \mu \ll 1$, the first term in the right hand side can be neglected, and the following equation results

$$\frac{\partial p}{\partial t} = D_K \frac{\partial^2 p}{\partial x^2} \qquad [6\text{-}41]$$

Note: non-si units are used in this figure

Values of D_K, obtained under different conditions, have been represented in Figure 6-110. The curve, which appears in that figure, has been plotted assuming that D_K depends only on M regardless of the interaction of the gas molecules with the porous medium; and this interaction is assumed to be always that corresponding to Argon flowing through a Mylar-Crinkled blanket at 295 K.
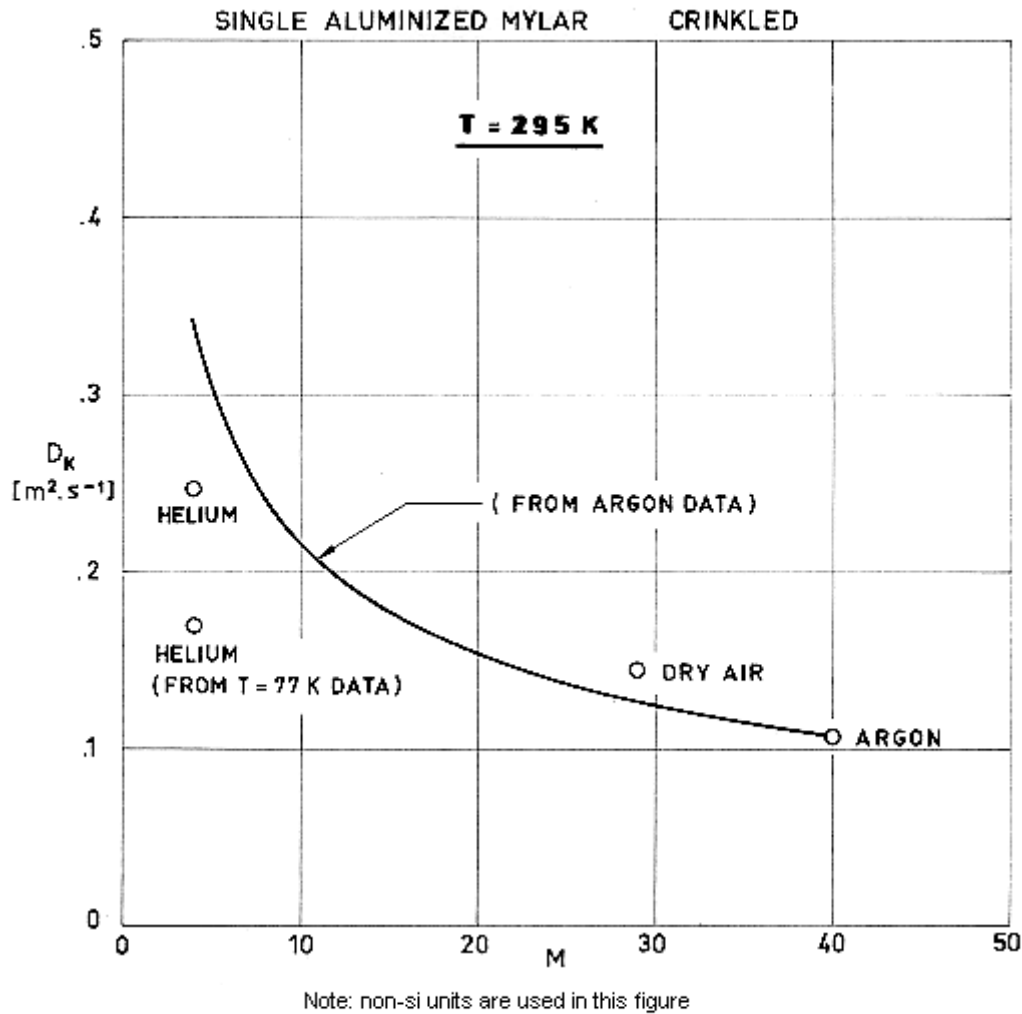
Figure 6-110: Knudsen Diffusion Coefficient, D_K, as a function of gas molecular mass, M. From Coston (1967) [13], p. 4,3-31.

The pressure evolution is given by the following equation:

$$p(x,t) = p_o(t) + \frac{1}{2D_K}\frac{dp_o(t)}{dt}(x^2 - L^2)$$

[6-42]

Note: non-si units are used in this figure

6.17.2   Interstitial pressure in outgas controlled situations

When the pressure in the MLI has been reduced, outgassing from the insulation surfaces becomes dominant.

For normal satellite temperatures there is not outgassing at atmospheric or higher pressures. The outgassing rate increases as the pressure decreases, reaching appreciable values at very low pressures. In the very low-pressure ranges, such as those considered presently, the outgassing rate is almost independent of pressure.

Outgassing data for several shields and spacers, and one complete MLI system are given in Figure 6-111 to Figure 6-116. The influence of purging, prepumping and ambient temperature on the

outgassing rate can be deduced from these figures. Outgassing rates are usually given in units of pressure times volume per unit time per unit apparent surface area as a function of time, for constant experimental temperature and negligible ambient pressure.

Broadside pumping is normally used for evacuating outgassing products, which come from sources homogeneously distributed throughout the different layers of the insulation material.
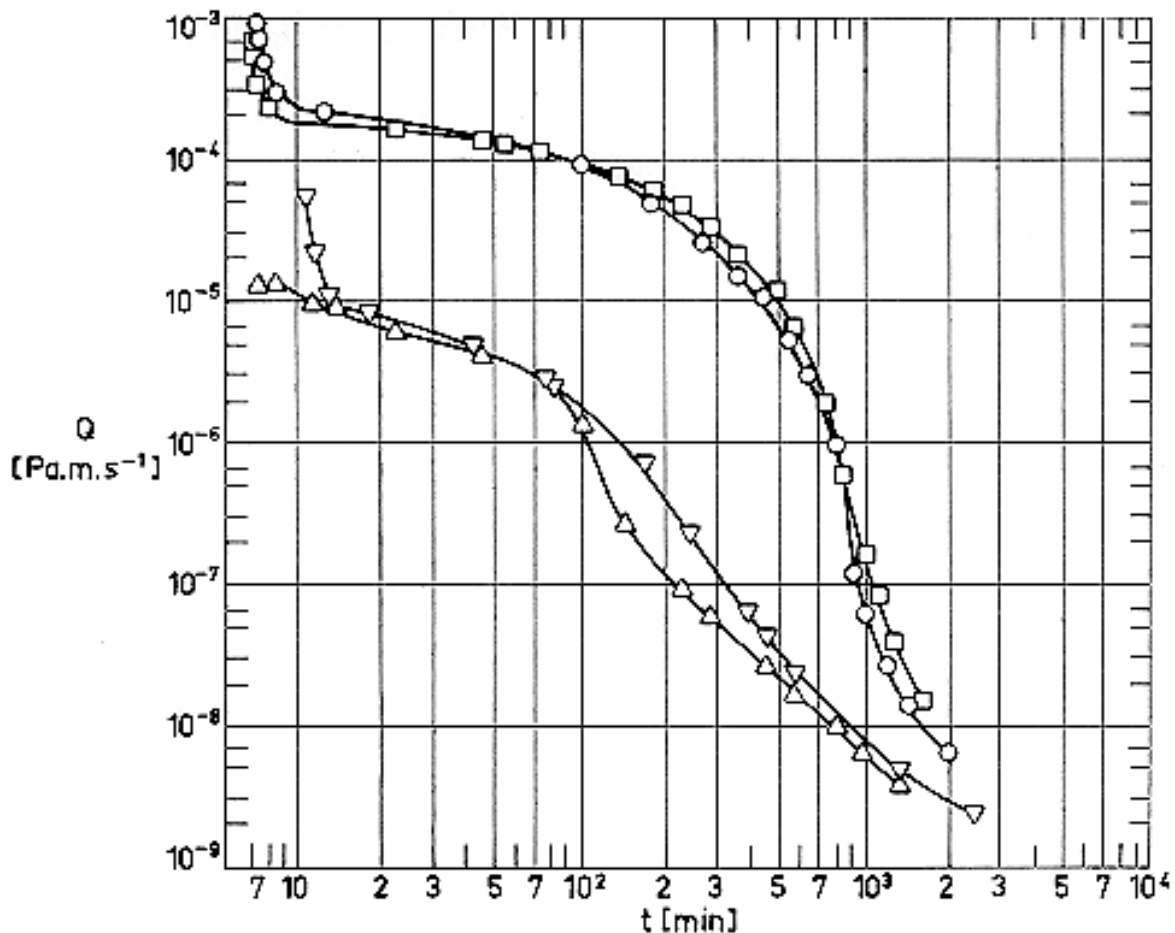
Figure 6-111: Outgassing rate, *Q*, as a function of pumping time, *t*, for Mylar Double-Aluminized. Effect of preconditioning. From Glassford (1970) [24].

Explanation

Sample Description	Test Method	Key	Preconditioning
Film thickness, $t = 6{,}35 \times 10^{-6}$ m. Coating thickness, $t_c = 0{,}5 \times 10^{-7}$ m.	Q found from the difference in slopes of the pressure histories for the chamber plus sample and the empty chamber. Slopes deduced from graphically	○	As received.
		□	Purged at ambient temperature with Helium ($4{,}2 \times 10^{-3}$ m³.min⁻¹ for 30 min).

Sample Description	Test Method	Key	Precondioning
	smoothed pressure vs. time data. Reproducibility of pressure data: 2%. Chamber temperature: 297 K. Chamber pressure below $1{,}33 \times 10^{-2}$ Pa.	$\triangle$	Purged at 373 K with Helium. (Same flow rate and purging time).
		$\triangledown$	Purged at 373 K with Nitrogen. (Same flow rate and purging time).
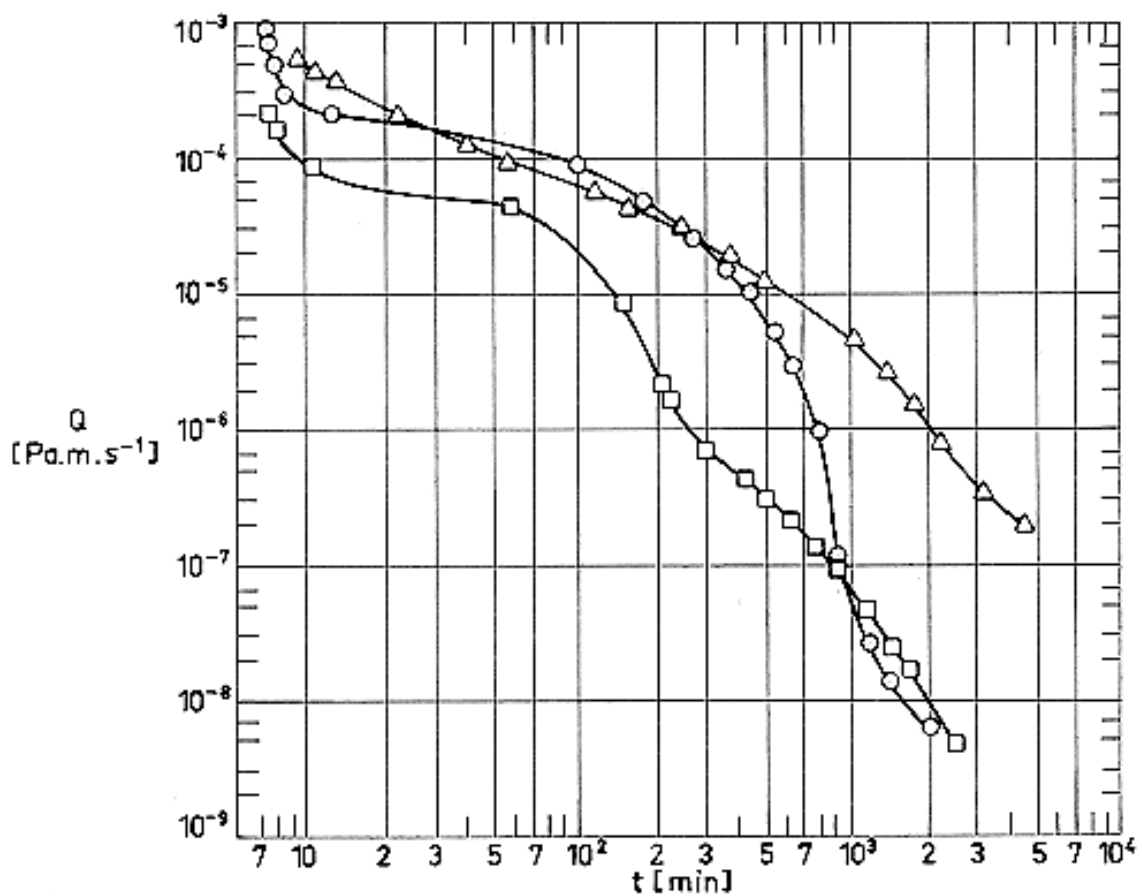
Figure 6-112: Outgassing rate, *Q*, as a function of pumping time, *t*, for Mylar Double-Aluminized. Effect of prepumping. From Glassford (1970) [24].

Explanation

Sample Description	Test Method	Key	Prepumping
Film thickness, $t = 6,35 \times 10^{-6}$ m. Coating thickness, $t_c = 0,5 \times 10^{-7}$ m.	Q found from the difference in slopes of the pressure histories for the chamber plus sample and the empty chamber. Slopes deduced from graphically smoothed pressure vs. time data. Reproducibility of pressure data: 2%. Chamber temperature: 297 K. Chamber pressure below $1,33 \times 10^{-2}$ Pa.	○	As received.
		□	Prepumped as in normal test and pressurized back to atmospheric pressure with He. Exposed to atmosphere (35% humidity) for 5 d and 31 d (identical curves). Then tested.
		△	Prepumped as in normal test and pressurized back to atmospheric pressure with Air. Exposed to atmosphere for 1 d. Then tested.
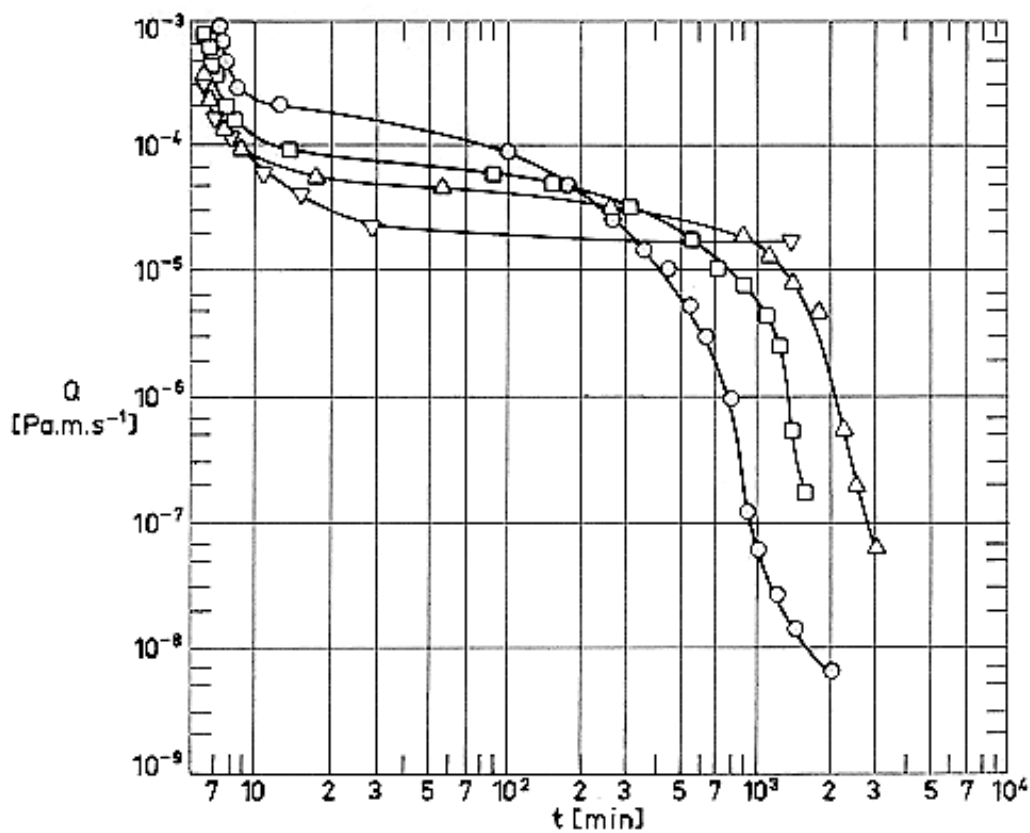
Figure 6-113: Outgassing rate, Q, as a function of pumping time, t, for Mylar Double-Aluminized, as received. Effect of test temperature.

From Glassford (1970) [24].

Explanation

Sample Description	Test Method	Key	Test Temperature
Film thickness, $t = 6,35 \times 10^{-6}$ m. Coating thickness, $t_c = 0,5 \times 10^{-7}$ m.	Q found from the difference in slopes of the pressure histories for the chamber plus sample and the empty chamber. Slopes deduced from graphically smoothed pressure vs. time data. Reproducibility of pressure data: 2%. Chamber temperature: 297 K. Chamber pressure below $1,33 \times 10^{-2}$ Pa.	○	$T = 297$ K
		□	$T = 282$ K. Coolant: Melting water-glycerine solution.
		△	$T = 273$ K. Coolant: Melting ice.
		▽	$T = 262$ K. Coolant: Melting water-ethylene glycol solution.
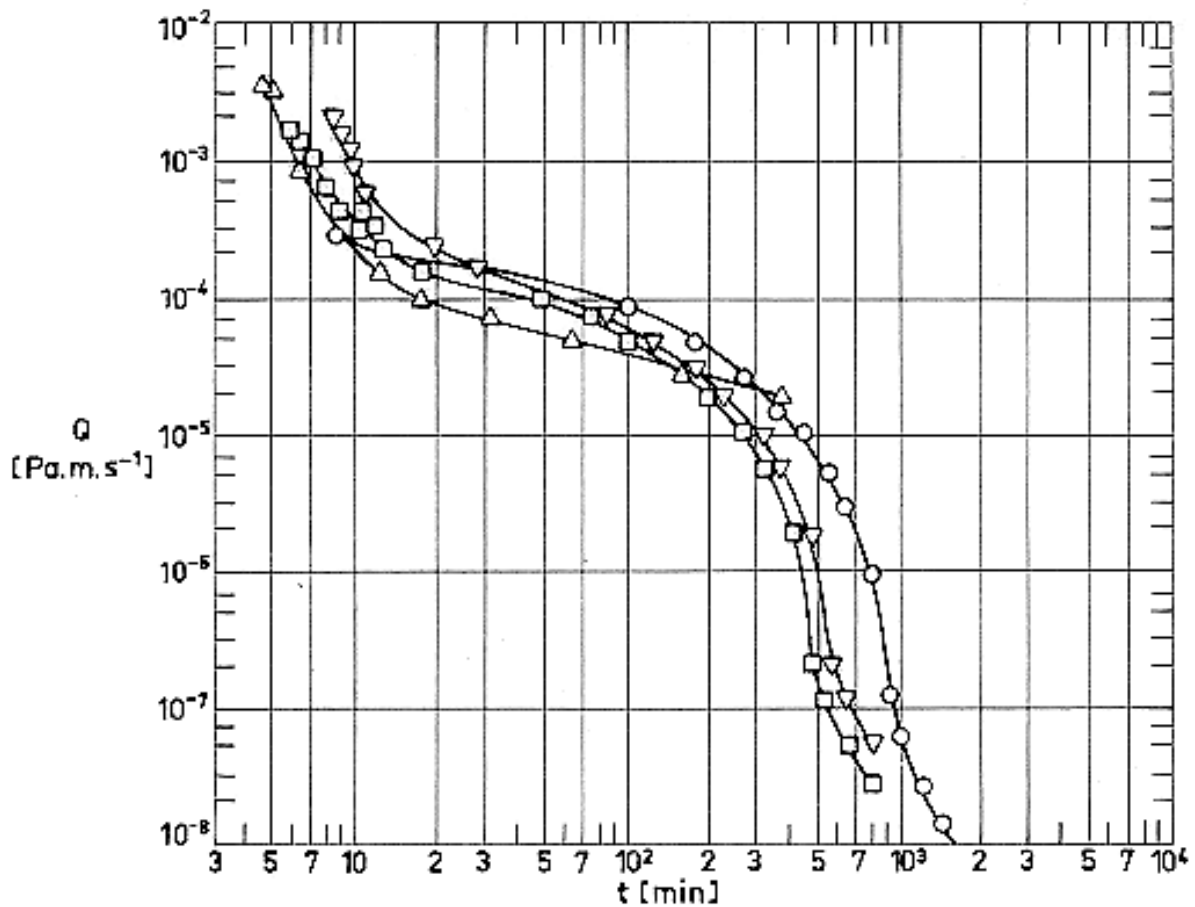
Figure 6-114: Outgassing rate, Q, as a function of pumping time, t, for several shielding materials, as received.

From Glassford (1970) [24].

Explanation

Key	Sample Description	T [K]	Test Method
○	6,35x10⁻⁶ m thick Mylar Double-Aluminized. Coating thickness, t_c = 0,5x10⁻⁷ m.	297	Q found from the difference in slopes of the pressure histories for the chamber plus sample and the empty chamber.
□	3,81x10⁻⁶ m thick Mylar Double-Aluminized Crinkled. t_c = 0,5x10⁻⁷ m.	297	
△		273	Slopes deduced from graphically smoothed pressure vs. time data.
▽	6,35x10⁻⁶ m thick Mylar Double-Aluminized flocked with Dacron tufts on 1,27x10⁻² m centers. t_c = 0,5x10⁻⁷ m.	297	Reproducibility of pressure data: 2%. Chamber pressure below 1,33x10⁻² Pa.
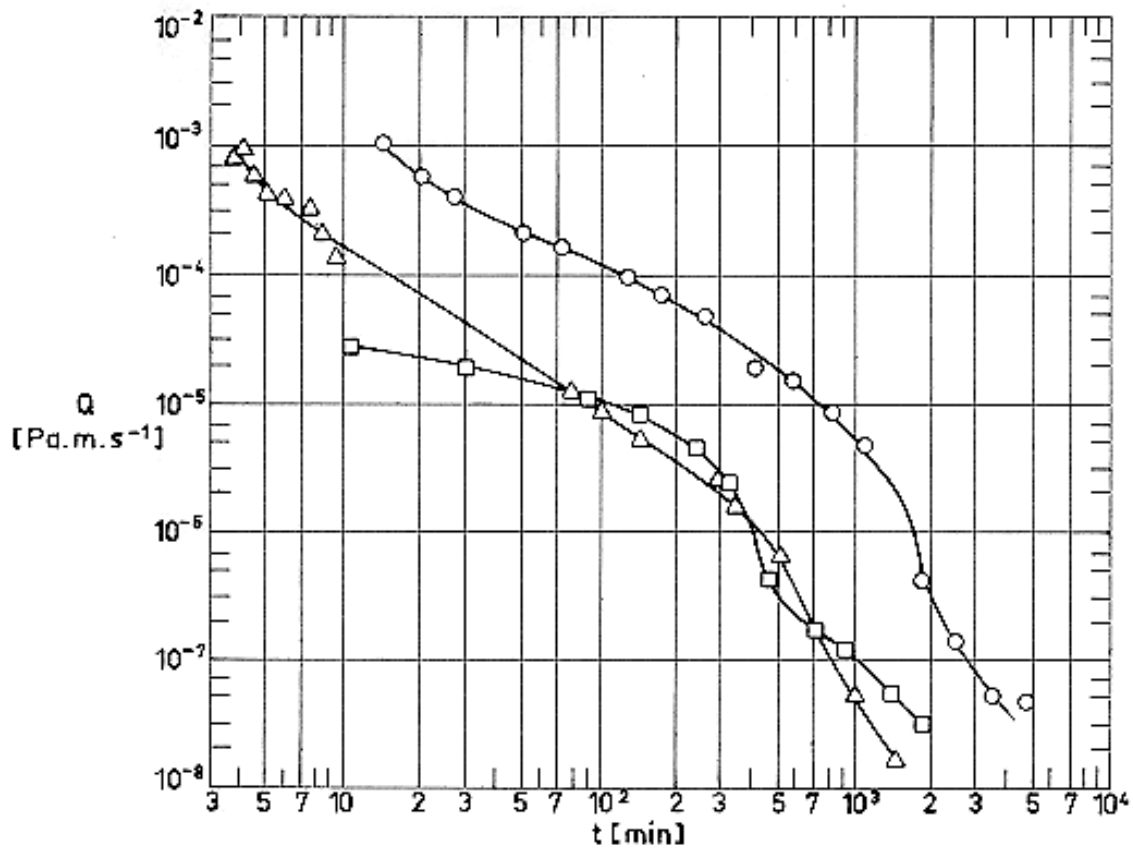
Figure 6-115: Outgassing rate, *Q*, as a function of pumping time, *t*, for several spacing materials.

From Glassford (1970) [24].

Explanation

Key	Sample Description	Test Method
◯	15,2x10⁻⁶ m thick Tissuglas. Nominal density, ρ = 224 kg.m⁻³. As received.	*Q* found from the difference in slopes of the pressure histories for the chamber plus sample and the empty chamber.
◻	Same as ◯. Purged with Helium at 373 K.	Slopes deduced from graphically smoothed pressure vs. time data. Reproducibility of pressure data: 2%. Chamber temperature: 297 K.
△	6,35x10⁻⁶ m thick Mylar. Uncoated. Density, ρ = 1,41x10³ kg.m⁻³.	Chamber pressure below 1,33x10⁻² Pa.
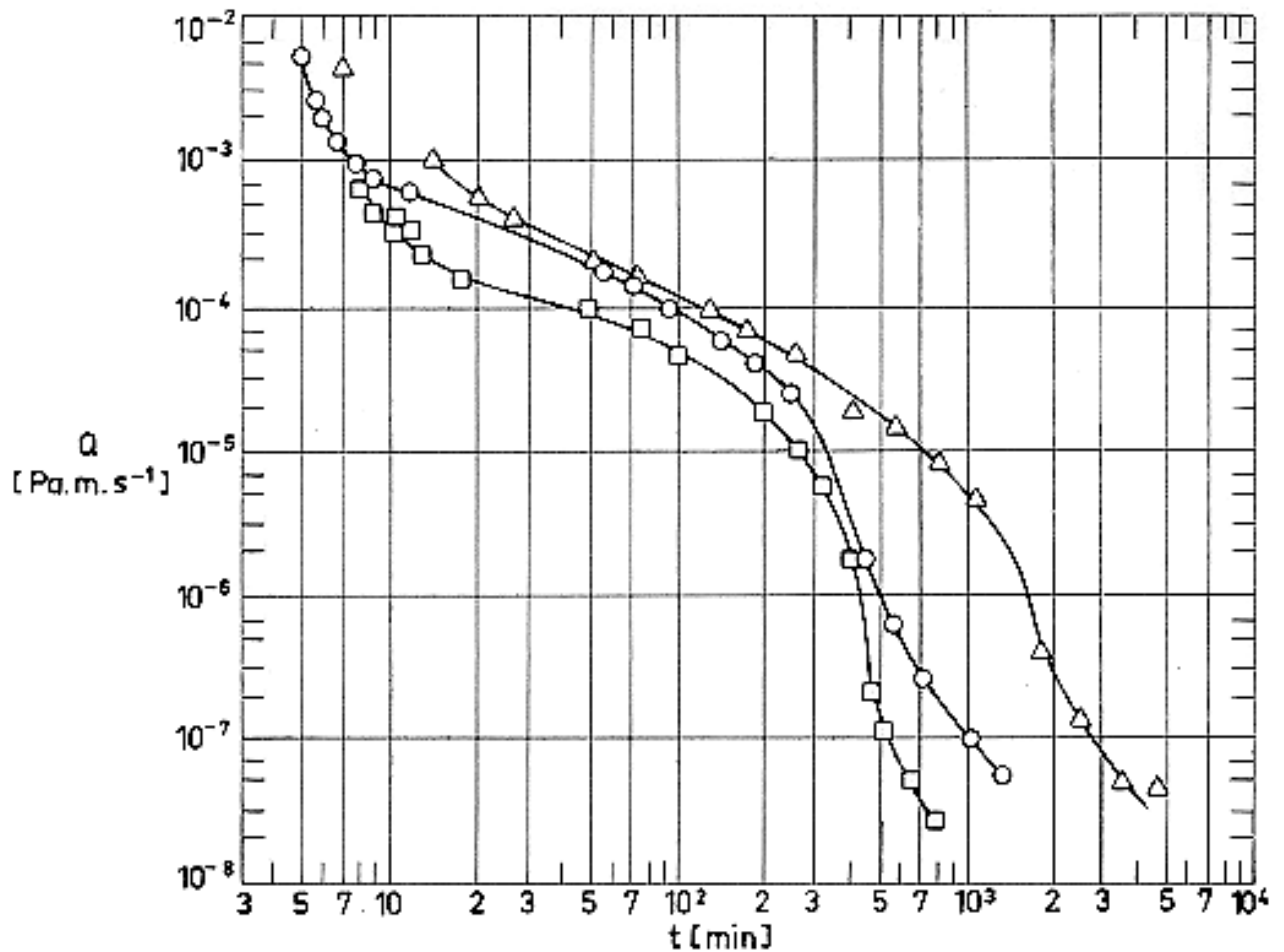
Figure 6-116: Outgassing rate, _Q_, as a function of pumping time, _t_, for an MLI system and for its components. No preconditioning. From Glassford (1970) [24].

Explanation

Key	Sample Description	Test Method
○	Two layers of $3,81 \times 10^{-6}$ m thick Mylar Double-Aluminized Crinkled. Coating thickness, $t = 0,5 \times 10^{-7}$ m. one layer of $15,2 \times 10^{-6}$ m thick Tissuglas. Nominal density, $\rho = 224$ kg.m^{-3}.	Q found from the difference in slopes of the pressure histories for the chamber plus sample and the empty chamber.
□	$3,81 \times 10^{-6}$ m thick Mylar Double-Aluminized Crinkled. Coating thickness, $t_c = 0,5 \times 10^{-7}$ m.	Slopes deduced from graphically smoothed pressure vs. time data. Reproducibility of pressure data: 2%. Chamber temperature: 297 K. Chamber pressure below $1,33 \times 10^{-2}$ Pa.
△	$15,2 \times 10^{-6}$ m thick Tissuglas. Nominal density, $\rho = 224$ kg.m^{-3}.	

6.17.2.1 Analysis of gas flow in an mli with outgassing

Broadside pumping of an MLI at very low pressures has been considered by Lin (1973,1974) [43]. His approach can be outlined as follows:

1. The gas properties are uniform in each space between adjacent shields. This assumption is satisfied when the percentage area of perforation, τ, is small, and the number of shields per unit thickness, N/t, is large.

2. The fluid motion is low, and the relevant properties, namely: temperature and partial pressures of the species, can be calculated by use of the equations of conservation of mass and energy. Notice that there are as many mass conservation equations as outgassing species. However, for most MLI systems the outgassing products are mainly constituted by water vapor originally absorbed or adsorbed in the system.

3. At very low pressures, such as those existing in an outgas dominated situation, the heat transfer is controlled by thermal radiation between insulation layers. Assuming that shield emittances are constant, and that absorption and scattering of radiation by the spacers is negligible, the energy equation is replaced by:

$$T(x) = \sqrt[4]{T_C^4 + \left(T_H^4 - T_C^4\right)\frac{x}{t}}$$

[6-43]

Note: non-si units are used in this figure

where:

T_C, cold boundary temperature. [K].

T_H, warm boundary temperature. [K].

t, insulation thickness. [m].

x, distance to the cold boundary. [m].

4. The mass conservation equation for the species j in the interstice i may be written as:

$$t_i \frac{\partial p_i^{(j)}/T_i}{\partial t} = \frac{\tau_{i-1}}{4}\left[\frac{p_{i-1}^{(j)}}{T_{i-1}}c_{i-1}^{(j)} - \frac{p_i^{(j)}}{T_i}c_i^{(j)}\right] -$$
$$-\frac{\tau_i}{4}\left[\frac{p_i^{(j)}}{T_i}c_i^{(j)} - \frac{p_{i+1}^{(j)}}{T_{i+1}}c_{i+1}^{(j)}\right] +$$
$$+\left(2 - \tau_{i-1} - \tau_i\right)\frac{Q_i^{(j)}}{T_i}$$

[6-44]

Note: non-si units are used in this figure

where:

$Q_i^{(j)}$, outgassing rate of species j in space i. [Pa.m.s^{-1}].

$c_i^{(j)}$, molecular speed of species j in space i. [m.s^{-1}].

$p_i^{(j)}$, partial pressure of species j in space i. [Pa].

t, time. [s].

t_i, thickness of interstitial space i. [n].

τ_i, percentage area of perforation for the shield placed between spaces i and i+1.

Since the gas in any interstitial space is in thermal equilibrium, the expression of the molecular speed $c_i^{(j}$ is that given in connection with Eq. (7) above, with $T = T_i$ and $m = m^{(j}$.

The outgassing rates are supposed to be known functions of temperature; the effect of pressure is negligible in the pressure range under consideration.

5.   By taking into account the initial and boundary conditions, the system of simultaneous first order differential equations [6-44] for the partial pressures $p_i^{(j}$ can be numerically solved.

6.17.3   Self-pumping multilayer insulations

The dependence of the effective thermal conductivity, k_{eff}, of an MLI on the pressure, as measured outside the insulation, is as follows (see Figure 6-103 to Figure 6-107): At 10^{-3} Pa, k_{eff} approaches a residual value. Over the range from 10^{-1} Pa to 10 Pa the thermal conductivity varies linearly with pressure due to gas thermal conduction, and at higher pressures it approaches the value corresponding to the filling gas thermal conductivity.

Extensive pumping and thermal vacuum procedures do not reduce the residual conductance any further once a pressure below 10^{-3} Pa is achieved outside the insulation.

The effective gas pressure inside the insulation, which is not known and difficult to measure anyway, is probably 10 to 50 times higher than that externally measured, due to residual outgassing which cannot be reduced further by thermal vacuum techniques, since the allowable bake-out temperature of most plastic materials is limited.

Scurlock & Saull (1976) [63] had reported spectacular test results with MLIs to which a getter material had been incorporated to absorb outgassed molecules and maintain an internal pressure below 10^{-2} Pa. The values of the effective thermal conductivity of the MLIs tested by the said authors are one order of magnitude smaller than those reported in the literature for similar systems. To the best of our knowledge (see Barth & Lehman (1988) [8]) these reductions never have been achieved with realistically large systems and, even worse, conductivity increases have been reported by other authors (Halaczek & Rafalowicz (1986a,b) [25] & [26]).

The available information on these MLIs is introduced emphasizing the different methods used to incorporate the absorbing material and to obtain the experimental results.

The main distinguishing characteristics of the different systems tested up to now are introduced in Table 6-24 and Figure 6-117. The bulk of the reported information is summarized in Table 6-25 and the most salient results are given in Table 6-26.

Table 6-24: Characteristics of Self-Pumping MLIs the performances of which are given in Table 6-25

Shield Spacer	N	$(N/t)\times10^{-2}$ [m^{-1}]	A [m^2]	Absorbent	Calorimeter	References
Al foil or Double Al. Mylar Paper	10	30	0,10	Hand or Machine made carbon loaded glass fiber paper (Whatman GFG3) + Getter (as fine powder)	NBS Cylindrical P=10^{-4} Pa to 10^{-1} Pa	Scurlock & Saull [63]
Single Component Single Al. Plastic film	10	27	0,10	Cellulose paper, 50% carbon loaded. Single aluminized.	NBS Cylindrical P=5x10^{-4} Pa to 10 Pa	Matsuda & Yoshikiyo (1980) [46]
Al foil Paper	11	25	0,08	Glass fiber paper. Carbon loaded in the wet state. BAU[a] carbon concentration 2 % to 30 %	Flat-Plate (unguarded) P=10^{-3} Pa	Halaczek & Rafalowicz (1986a,b) [25] & [26]
Single Al. Plastic film Paper	40	8	4	Carbon Paper (China scientific Instruments and Materials Co.)	LN$_2$ filled parallelepipedic tank in ≤ 10^{-4} Pa environment	Barth & Lehmann (1988) [8]

[a]   Russian designation.
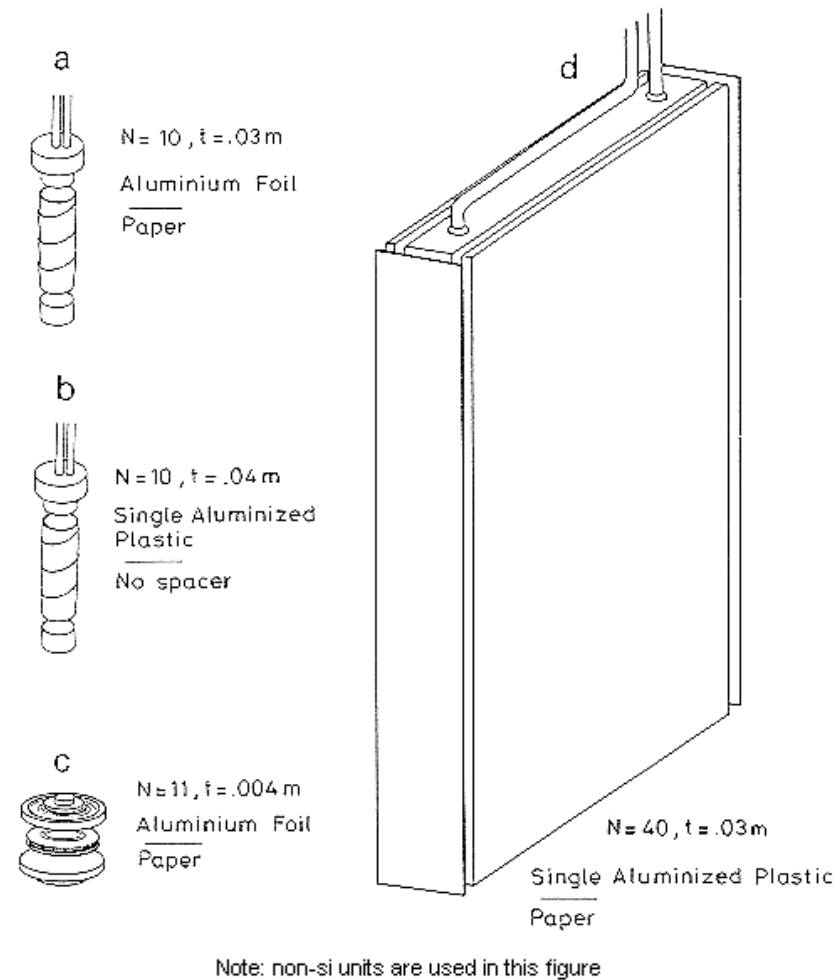
Figure 6-117: Main characteristics of the different self-evacuated MLIs and experimental methods used to obtain the results summarized in Table 6-25.

a) From Scurlock & Saull (1976) [63]. b) From Matsuda & Yoshikiyo (1980) [46]. c) From Halaczek & Rafalowicz (1986a) [25]. d) From Barth & Lehmann (1988) [8].

Table 6-25: Characteristics of Several Self-Pumping Multilayer Insulations

Spec No.	Sample Description	$t \times 10^2$ [m]	$p \times 10^{3\ a}$ [Pa]	T_H [K]	T_C [K]	Preconditioning	Calorimeter	Q/A [W.m^{-2}] $k_{eff} \times 10^6$ [W.m^{-1}.K^{-1}]	References
1	N=10 shields, 8,7x10^{-6} m thick. Aluminium foil. 10 spacers. Machine made Carbon loaded paper. The base unloaded paper is described in Specs. Nos. 25, 26. Carbon powder diameter 10^{-5} m.	0,324	1 Self Pump.	294	77		NBS-Cryostat Cylindrical. d =0,1035 m A=1,015x10^{-3} m². LN$_2$ evaporation volume flow rate measured at room temperature with a rotameter. Apparently the inner temperature distribution was not measured.	1,02 15,2	Scurlock & Saull (1976) [63]
2			0,4 Ext. Pump.					0,966 14,4	
3	N=10 shields as for Specs. Nos. 1,2. 10 spacers as for Specs. Nos. 1,2. Paper baked at 450 K with N$_2$ purge.	0,298	0,13 Self Pump.			Paper baked		0,670 9,2	
4			0,53 Ext. Pump.					0,778 10,7	
5	N=10 shields as for Specs. Nos. 1,2. 10 spacers as for Specs. Nos. 1,2 + Getter	0,305	2,4 Self Pump.					1,08 15,2	
6			0,4 Ext. Pump.					0,921 12,8	

Spec No.	Sample Description	$t \times 10^2$ [m]	$p \times 10^{3\ a}$ [Pa]	T_H [K]	T_C [K]	Preconditioning	Calorimeter	Q/A [W.m^{-2}] $k_{eff} \times 10^6$ [W.m^{-1}.K^{-1}]	References
7	N=10 shields as for Specs. Nos. 1,2. 10 spacers as for Specs. Nos. 1,2. Paper baked at 450 K with N$_2$ purge.	0,324	1,9 Self Pump.			Paper baked before getter introduction		0,527 7,9	
8			-- Ext. Pump.					0,517 7,7	
9			5,3 Self Pump.			Paper baked as for Specs. Nos. 7,8. Rotary pump down.		0,667 9,9	
10			0,4 Ext. Pump.					0,507 7,6	
11	N=10 shields as for Specs. Nos. 1,2. 10 Spacers GFG3 Paper as received.	0,285	27 Self Pump.					2,14 28,1	
12			0,13 Ext. Pump.					1,73 22,8	

Spec No.	Sample Description	$t \times 10^2$ [m]	$p \times 10^{3\ a}$ [Pa]	T_H [K]	T_C [K]	Preconditioning	Calorimeter	Q/A [W.m^{-2}] $k_{eff} \times 10^6$ [W.m^{-1}.K^{-1}]	References
13	N=10 shields as for Specs. Nos. 1,2. 10 spacers as for Specs. Nos. 11,12. Paper baked at 450 K with N$_2$ purge.	0,209	107 Self Pump.			Paper baked		2,46 23,9	
14			0,4 Ext. Pump.					1,87 17,9	
15	N=10 shields as for Specs. Nos. 1,2. 10 spacers as for Specs. Nos. 13,14 + Getter.	0,209	1,6 Self Pump.			Paper baked before getter introduction		1,06 11,0	
16			0,4 Ext. Pump.					1,01 10,8	
17	N=10 shields as for Specs. Nos. 1,2. 10 Spacers Nylon Net.	0,311	67. Self Pump.					4,58 65,5	
18			0,53 Ext. Pump.					0,916 13,1	
19	N=10 shields as for Specs. Nos. 1,2. 10 Spacers Nylon Net, tightly wound.	0,184	133. Self Pump.					7,19 61,2	
20			0,67 Ext.					2,01 17,0	

Spec No.	Sample Description	$t \times 10^2$ [m]	$p \times 10^{3\ a}$ [Pa]	T_H [K]	T_C [K]	Preconditioning	Calorimeter	Q/A [W.m^{-2}] $k_{eff} \times 10^6$ [W.m^{-1}.K^{-1}]	References
			Pump						
21	N=10 shields 12,5x10^{-6} m thick Mylar film double aluminized t_c=200x10^{10} m. 10 Spacers. Machine made	0,184	12 Self Pump.					4,22 35,7	
	Carbon loaded paper.	0,216	40 Self Pump.					2,58 25,6	
22		0,184	1,33 Ext. Pump.					3,73 31,2	
		0,216	6,67 Ext. Pump.					2,23 21,5	
23	N=10 shields as for Specs. Nos. 21,22. 10 spacers as for Specs. Nos. 21,22. Paper baked at 450 K with N$_2$ purge.	0,324	5,33 Self Pump.			Paper baked		1,76 26,3	
24			0,6 Ext. Pump.					1,78 26,5	

Spec No.	Sample Description	tx10² [m]	px10³ ª [Pa]	T$_H$ [K]	T$_C$ [K]	Preconditioning	Calorimeter	Q/A [W.m⁻²] k_{eff}x10⁶ [W.m⁻¹.K⁻¹]	References
25	N=10 shields as for Specs. Nos. 21,22. 10 Spacers GFG3 glass fiber paper 18x10⁻³ kg.m⁻² 10⁻⁴ m thick. Fiber diameter 10⁻⁶ m.	0,267	133. Self Pump.					3,40 41,7	
26			0,93 Ext. Pump.					2,48 30,5	
27	N=10 shields as for Specs. Nos. 21,22. 9 spacers. Hand made carbon paper. Sheets 0,2 m x 0,2 m but joined with tape.	0,280	1,33 Ext. Pump.					1,16 15.	
28	N=10 shields as for Specs. Nos. 21,22. 5 spacers as for Spec. No. 27.	0,180	0,27 Ext. Pump.					1,35 12.	
29	N=10 shields as for Specs. Nos. 21,22. 3 spacers as for Spec. No. 27.	0,150	2,7 Ext. Pump.					2,27 16.	

Spec No.	Sample Description	$t \times 10^2$ [m]	$p \times 10^{3\,a}$ [Pa]	T_H [K]	T_C [K]	Preconditioning	Calorimeter	Q/A [W.m^{-2}] $k_{eff} \times 10^6$ [W.m^{-1}.K^{-1}]	References
30	N=10 shields as for Specs. Nos. 21,22. 10 Spacers. Hand made Zeolite loaded paper. Baked at 450 K with N$_2$ purge.	≈ 0,3	37,3 Self Pump.			Paper baked		4,30 59.	
31			0,8 Ext. Pump.					2,98 41.	
32	N=10 shields as for Specs. Nos. 21,22. 10 Spacers. Machine made alumina (Actal P) loaded paper. Paper baked at 450 K with N$_2$ purge.		9,33 Self Pump.					3,14 43.	
33			0,53 Ext. Pump.					2,53 35.	
34	N=10 shields. 190x10^{-6} m thick. Polyester non-woven fabric. 50x10^{-3} kg.m^{-2}. Single aluminized t$_c$=100x10^{-9} m. No spacers.	0,37	0,5 Ext. Pump.	274	78		NBS-Cryostat Cylindrical. LN$_2$ evaporation volume flow rate measured at room temperature. Temperature distribution measured with C-Cu thermo-couples and Pt resistance sensor.	9,53 180.	Matsuda & Yoshikiyo (1980) [46]
35	N=10 shields 200x10^{-6} m thick cellulose paper 60x10^{-3} kg.m^{-2} Single aluminized t$_c$=100x10^{-9} m 50% carbon loaded. No spacers.							7,42 140.	

Spec No.	Sample Description	$t \times 10^2$ [m]	$p \times 10^{3\ a}$ [Pa]	T_H [K]	T_C [K]	Preconditioning	Calorimeter	Q/A [W.m^{-2}] $k_{eff} \times 10^6$ [W.m^{-1}.K^{-1}]	References
36	N=11 shields 10x10^{-6} m thick aluminium foil. 10 spacers glass fiber paper 26x10^{-3} kg.m^{-2} fiber diameter: 10^{-6} m to 1,5x10^{-6} m.	0,4	1.	295	90	Whole MLI system. 6h in vacuum at 600 K	Flat-plate unguarded The test MLI was surrounded by an annulus of the same MLI with an annular gap of 2x10^{-3} T_H and T_C kept constant within 5x10^{-2} K. Electric power to the measuring plate (Differential method). Calorimeter was not calibrated. Repeatibility within 2,5%-3%. T_H-T_C was measured but inner temperature was not	2,92±0,16 (4 tests) 56,9	Halaczek & Rafalowicz (1986a) [25]
37								3,25±0,25 (5 tests) 63,4	
38	N=11 shields as for Spec. No. 36. 10 spacers. 2% BAU Carbon added while in the wet state.							4,28±0,50 (3 tests) 83,5	
39	N=11 shields as for Spec. No. 36. 10 spacers. 10% BAU Carbon added as for Spec. No. 38.							4,09±0,26 (3 tests) 79,7	
40	N=11 shields as for Spec. No. 36. 10 spacers. 20% BAU Carbon added as for Spec. No. 38.							4,23±0,16 (3 tests) 82,5	
41	N=11 shields as for Spec. No. 36. 10 spacers. 30% BAU Carbon added as for Spec. No. 38.							3,90±0,17 (5 tests) 76,0	

Spec No.	Sample Description	tx10² [m]	px10³ ᵃ [Pa]	T_H [K]	T_C [K]	Preconditioning	Calorimeter	Q/A [W.m⁻²] k_{eff}x10⁶ [W.m⁻¹.K⁻¹]	References
42	N=11 shields as for Spec. No. 36. 10 spacers. 30% 5A Zeolite added as for Spec. No. 38.							4,58±0,29 (3 tests) 89,4	
43	N=11 shields as for Spec. No. 36. 10 Spacers as for Spec. No. 36.				90-150		Same as for Specs. Nos. 36 to 42. T_H is kept constant and T_C is measured while Q is monitored (Integral Method).	3,33 T_C=90 K 65,0 T_C=90 K	
44	N=11 shields as for Spec. No. 36. 10 spacers. 30% Carbon added as for Spec. No. 41.							3,91 T_C=90 K 76,3 T_C=90 K	
45		0,3						7,61 T_C=90 K 111. T_C=90 K	
46		0,4						3,90 T_C=90 K 76,1 T_C=90 K	
47		0,5						3,34 T_C=90 K 81,5 T_C=90 K	

Spec No.	Sample Description	$t \times 10^2$ [m]	$p \times 10^{3\ a}$ [Pa]	T_H [K]	T_C [K]	Preconditioning	Calorimeter	Q/A [W.m^{-2}] $k_{eff} \times 10^6$ [W.m^{-1}.K^{-1}]	References
48	N=40 shields 6,4x10^{-6} m thick Polyester foil single aluminized. t_c = 250x10^{-10} m. 39 spacers 30x10^{-6} m thick, 27x10^{-3} kg.m^{-2} Glass fiber paper.	3.	≤ 0,1	292	77		Boil-off losses of a paralellepipedic tank (2 m x 1 m x 0,15 m) LN$_2$ filled up to a level 95% within a vacuum tank. Mass flow rate measured at ambient conditions. Temperature sensors placed in the apparatus and within the MLI.	1,8 251.	Barth & Lehmann (1988) [8]
49						Whole MLI system heated at 350 K. CO$_2$ purging.		1,6 223.	
50	N=40 shields as for Specs. Nos. 48,49. 39 spacers Layers 1-18 carbon paper on total surface. Layers 19-39 carbon paper strips.	5.						0,8 186.	
51						Whole MLI system heated at 330 K		0,65 151.	
52	N=26 shields 6,4x10^{-6} m thick Polyester foil Doubled aluminized t_c= 200x10^{-10} m Crinkled by hand 25 spacers Carbon paper	3,5						1,25 203.	
53	N=40 shields 1 and 40 as for Specs. No. 52 but not crinkled. 2-39 singled	5,5			308			0,8 205.	

Spec No.	Sample Description	tx10² [m]	px10³ ᵃ [Pa]	T_H [K]	T_C [K]	Preconditioning	Calorimeter	Q/A [W.m⁻²] k_{eff}x10⁶ [W.m⁻¹.K⁻¹]	References
54	aluminized. 39 spacers 1-6 glass fiber + carbon paper total 7-20 glass fiber + carbon paper total 21-39 carbon paper total.				292	Whole MLI system heated at 330 K		0,7 179.	

ᵃ   Measured externally to the MLI.

Table 6-26: Summary of the Best and Worst Cases Reached by the Different Investigators

Reference	Shield	Spacer	Spec. [a] No.	Q/A [W.m^{-2}]	k_{eff}x10^6 [W.m^{-1}.K^{-1}]	(Q/A)$_{selfpump}$ /(Q/A)$_{convent}$	$k_{effselfpump}$ /$k_{effconvent}$
Scurlock & Saull (1976) [63]	Aluminium Foil	Glass fiber paper	11	2,14	28,1	0,31	0,33
		Same but Carbonadded. Baked.	3	0,670	9,2		
	Double aluminized Mylar	Glass fiber paper	25	3,40	41,7	0,52	0,63
		Same but Carbonadded. Baked.	23	1,76	26,3		
Matsuda & Yoshikiyo (1980) [46]	Polyester non-woven fabric. Single aluminized 0 % Carbon loaded	None	34	9,53	180	0,78	0,78 [b]
	Cellulose paper single aluminized 50 % Carbon loaded		35	7,42	140		
Halaczek & Rafalowicz (1986a,b) [25] & [26]	Aluminium foil	Glass fiber paper	36	2,92	56,9	1,34	1,34
		Same but 30 % carbon added	41	3,90	76,0		
Barth & Lehmann (1988) [8]	Polyester foil single aluminized	Glass fiber paper	48	1,8	251	0,44	0,74
		21 layers glass fiber paper 18 layers carbon paper	50	0,8	186		

[a] Refers to numbers in Table 6-25.

[b] At higher ambient pressures the carbon loaded specimen becomes worse that the non loaded.

6.17.3.1 Discussion and comments

1. MLIs with effective thermal conductivities, k_{eff}, below 10×10^{-6} W.m^{-1}.K^{-1} have been attained in a reproducible manner by Scurlock & Saull (1976) [63], see Specs. Nos. 3, 4, 9 and 10 in Table 6-25. When a conventional getter was used, further improvement in performance was achieved, $k_{eff} \approx 8 \times 10^{-6}$ W.m^{-1}.K^{-1} (Specs. Nos. 7 and 8). Pumping down during 24 h with a rotary pump resulted in $k_{eff} = 7{,}6 \times 10^{-6}$ W.m^{-1}.K^{-1} (Spec. No. 10).

No preconditioning of the MLI is needed to achieve these results.

The mentioned values of k_{eff} are one order of magnitude smaller than those usually quoted, Figure 6-1.

For the conventional (not self-pumped) insulations the results from Scurlock & Saull (1976) [63] are of the same order as those for similar systems from other sources. To see that, introduce, for example, the value $k_{eff} = 1{,}4 \times 10^{-4}$ for $N/t = 27 \times 10^2$ of Spec. No. 35 into Figure 6-55, clause 6.11.

2. Lower values of k_{eff} were generally obtained with aluminium foil than with aluminium coated plastic film. This could be one of the reasons for the more modest reductions in effective thermal conductivity reported by Barth & Lehmann (1988) [8].

3. The results from Scurlock & Saull never have been convincingly reproduced by other investigators.

Barth & Lehmann quote a reduction in Q/A down to 44 % (compare Spec. No. 50 with No. 48) but because of the lower density of layers in the MLI with carbon paper, the reduction in k_{eff} is only down to 74 %.

Results for the conventional insulation given by these authors (Specs. Nos. 48, 49) are comparable to those obtained with similar systems by other investigators, see Shu, Fast & Hart (1986) [65].

According to Matsuda & Yoshikiyo (1980) [46], no substantial gain was achieved with carbon loaded shields. Surprisingly enough just the opposite effect results when the external (to the system) pressure increases above 10^{-1} Pa. See Fig. 2 in the mentioned reference.

Halaczek & Rafalowicz (1986a,b) [25] & [26] report clear increases in the effective thermal conductivity due to carbon loading. The authors attribute this effect to the interaction between the increase due to the sorbent radiation and the decrease due to residual gas sorption. Their conventional results are also comparable to those from others.

In order to separate both effects (radiation and conduction), Halaczek & Rafalowicz (1986b) [26] considered the evolution of Q/A as a function of T_C for constant T_H. The least squares fitting to experimental data points in two typical cases, as obtained by the compiler, are (Q/A [W.m^{-2}]):

For Spec. No. 43 (no carbon)

$(Q/A) = 2{,}37 \times 10^{-10}(T_H^4 - T_C^4) + 1{,}96 \times 10^{-5}(T_H^2 - T_C^2)$.

For Spec. No. 44 (carbon-loaded)

$(Q/A) = 1{,}36 \times 10^{-10}(T_H^4 - T_C^4) + 3{,}66 \times 10^{-5}(T_H^2 - T_C^2)$.

These equations provide the unexpected result that the radiative contribution (($T_H^4 - T_C^4$) term) decreases with self-pumping, whereas the conductive one (solid plus gas) increases.

An objection to the experiments performed by Halaczek & Rafalowicz concerns the small size of the unguarded flat plate calorimeter that they use. Nevertheless any lateral heat transfer will diminish (instead of increase) the measured value of Q/A. This point will be discussed soon.

4. Barth & Lehmann (1988) [8] list several reasons to explain the more modest decreases in thermal conductivity that they achieved compared to those reported by Scurlock & Saull (1976) [63]. These reasons are:

1. Differences in system size, layer number and shield reflectance. Obviously, 10 layers instead of 40 result in more favorable vacuum conditions, but the size of the system used by Halaczek & Rafalowicz was even smaller.

2. Active carbon fraction is not always indicated and could be different in the different experiments.

3. Paper conditioning has not been considered (or reported) except by Scurlock & Saull (1976) [63]. They dried the carbon loaded paper, after manufacture, with steam-heated drums and reactivated it further by heating to 450 K with vacuum pump-out or with a dry nitrogen purge. After that, the paper was stored in air-tight containers.

5. The heat transfer along the insulation has not been considered (only Barth & Lehmann could have estimated it) and could become of concern when the heat transfer across the insulation is so effectively reduced. See clause 6.12.

Typical values of $k_{eff(lat),b}$ (in terms of the bulk cross sectional area for lateral heat transfer) can be deduced from Figure 6-89 to Figure 6-92 (where k_{eff} is $k_{eff(lat),m}$ in terms of metallic cross sectional area) as follows

For typical values $k_{eff(lat),m} = 2 \times 10^3$ W.m^{-1}.K^{-1}, $t_c = 3 \times 10^{-8}$ m, $N/t = 2 \times 10^3$ m^{-1}, $k_{eff(lat),b} = 1,2 \times 10^{-1}$ which is several orders of magnitude larger than the best values of k_{eff} across the insulation that are being considered (see Table 6-26).

In some experiments, lateral temperature gradients could be inadvertently generated, for example when a separate getter of freshly activated carbon is introduced in contact with the lower guard of the calorimeter in the set-up used by Scurlock & Saull.

The effect of lateral heat transfer is shown in the model of Figure 6-118. The MLI in a guarded flat plate calorimeter is represented by a two-dimensional anisotropic rectangular continuous medium, in lateral contact with guards of the same material but with the principal directions of anisotropy perpendicular to those of the MLI. The model is further simplified by approximating the heat flux at the $x = L$ lateral face by

$$-k_x \frac{\partial T}{\partial x} \approx k_y \frac{T - T_o}{\delta}$$

[6-45]

Note: non-si units are used in this figure

so that the problem is solved under the boundary conditions given in Figure 6-118b. In Figure 6-119 it is shown how the total heat input Q_x+Q_y separates into the part flowing through the lower face, Q_y, and through the two lateral faces, Q_x. In Figure 6-119a the parameter in abscissae is $(t/L)^2 k_x/k_y$ and the parameter for each curve is δ/L, whereas in Figure 6-119b the parameter in abscissae is $\log \delta/L$ and curves for different values of $(t/L)^2 k_x/k_y$ are presented. In a typical case $k_x/k_y \approx 10^5$, $(t/L)^2 \approx 10^{-4}$, and the heat transfer rate through the lower face, Q_y, can be drastically reduced.

Nothing more can be said without knowing the performances of the guards used in every calorimetric facility but effects such as those related to the non-uniformity of the getter distribution could be easily reproduced experimentally.
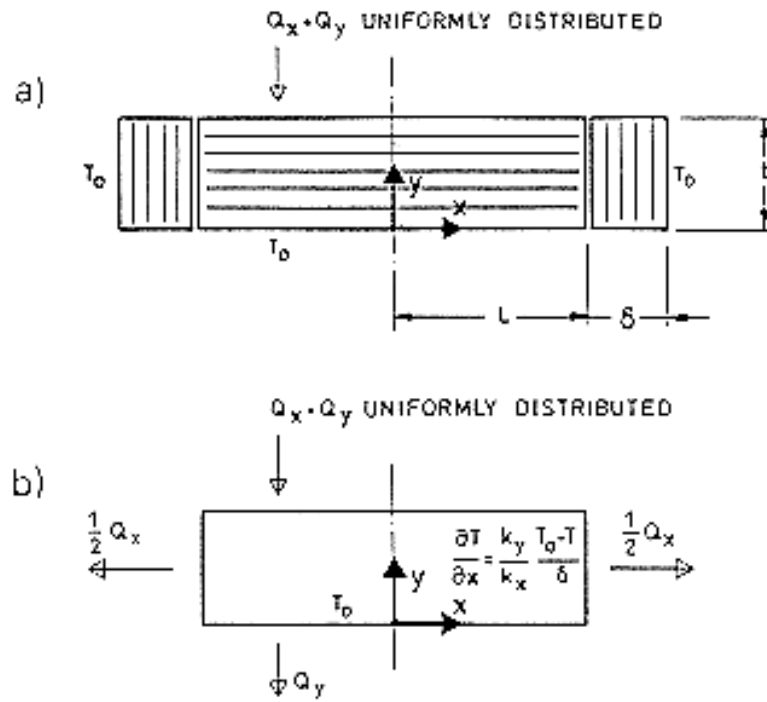
Figure 6-118: Model for a guarded two-dimensional MLI. (a) Geometry. (b) Boundary conditions for the calculations.
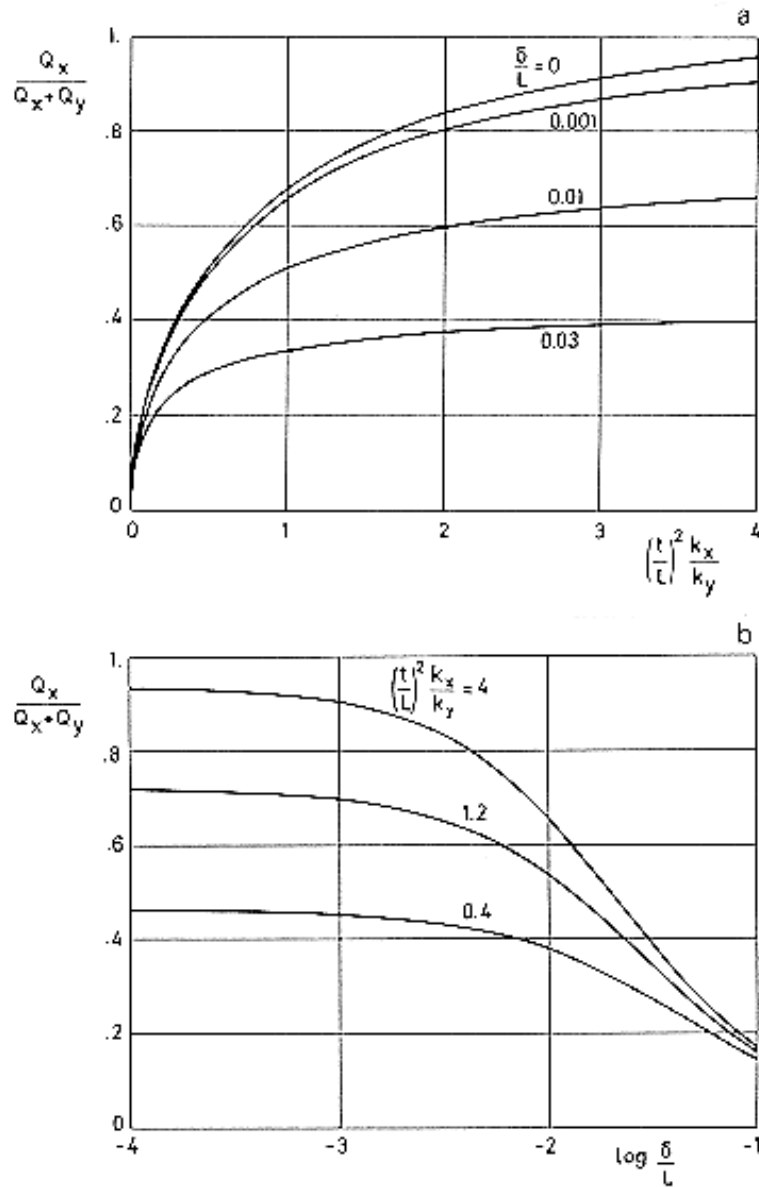
Note: non-si units are used in this figure

Figure 6-119: Ratio of lateral to total heat transfer rate, $Q_x/(Q_x+Q_y)$, in an anisotropic two-dimensional continuous medium subject to the boundary conditions indicated in Figure 6-118:

(a) as a function of $(t/L)^2 k_x/k_y$, for different values of δ/L; (b) as a function of $\log(\delta/L)$, for different values of $(t/L)^2 k_x/k_y$. Calculated by the compiler.

Bibliography

[1] ADL, "Basic Investigation of Multi-Layer Insulation Systems", NASA CR-54191, ADL 65958-00-04 (NAS3-4181), Arthur D. Little, Inc., Cambridge, Massachusetts, Oct. 30, 1964.

[2] ADL, "Advances Studies on Multi-Layer Insulation Systems", NASA CR-54929, ADL 67180-00-04 (NAS3-6283), Arthur D. Little, Inc., Cambridge, Massachusetts, June 1, 1966.

[3] Androulakis, J.G., "Effective Thermal Conductivity Parallel the Laminations of Multilayer Insulation", AIAA Paper No. 70-846, 1970.

[4] Arvidson, J.M., Durcholz, R.L., Reed, R.P., "Compressive Properties of Polyurethane and Polystyrene Foams from 76 to 300 K", in "Advances in Cryogenic Engineering", Vol. 18, K.D. Timmerhaus, Ed., Plenum Publishing Corporation, New York, 1973, pp. 194-201.

[5] ASM, "Metals Handbook", Vol. 1, "Properties and Selection of Metals", 8th Edition, T. Lyman, Ed., American Society for Metals (ASM), Metals Park, Cleveland, Ohio, 1961.

[6] BABCOCK & WILCOX, Data Sheets No. 110-1, 120-1, 5 14-4 Babcock & Wilcox, Refractories Division, Augusta, Georgia 30903 USA.

[7] Bardeen J., "Conduction: Metals and Semiconductors", in "Handbook of Physics", E.U. Condon and H. Odishaw, Eds., McGraw-Hill Book Company, Inc., New York, 1958, pp. 4-74.

[8] Barth, W., Lehmann, W., "Experimental Investigation of Superinsulation Models Equiped with Carbon Paper", Cryogenics, Vol. 28, No. 5, May 1988, pp. 317-320.

[9] Bustard, T.S., Princiotta, F.T., Barr, H.N., "Reentry Protection for Radioisotope Heat Sources", Nuclear Applications & Technology, Vol. 9, No. 10, Oct. 1970, pp. 572-583.

[10] Campbell, W.A., Marriott, R.S., Park, J.J., "A Compilation of Outgassing Data for Spacecraft Materials", NASA TN D-7362, Sept. 1973.

[11] CARBORUNDUM Co., "Fiberfrax Ceramic Fiber Technical Information", The Carborundum Company, Refractories and Electronics Division, Niagara Falls, New York 14302 USA.

[12] Chapman, J.C., Porter, H.L., "On the Physical Properties of Gold Leaf at High Temperatures", Proceedings Royal Society of London, Ser. A, Vol. 83, pp. 65-68, 1910.

[13] Coston, R.M., "Handbook of Thermal Design Data for Multilayer Insulation Systems", LMSC-A847882, Vol. II, (NAS8-20353), Lockheed Missiles & Space Company, Sunnyvale, California, June 1967.

[14] Coston, R.M., Vliet, G.C., "Thermal Energy Transport Characteristics along the Laminations of Multilayer Insulations", in "Progress in Astronautics and Aeronautics", Vol. 20, G.B. Heller, Ed., Academic Press, New York, 1967, pp. 909-923.

[15] Cravalho, E.G., Tien, C.L., Caren, R.P., "Effect of Small Spacings on Radiation Transfer between two Dielectrics". Transactions of the ASME, Journal of Heat Transfer, Vol. 89, Series C, No. 4, Nov. 1967, pp. 351-358.

[16] Crosby, J.R., "Multilayer Insulation Testing", JPL Space Programs Summary 37-64, Vol. III, 1970, pp. 79-80.

[17] Cunnington, G.R., Zierman, C.A., Funai, A.I., Lindahn, A., "Performance of Multilayer Insulation Systems for Temperatures to 700ºK", NASA CR-907 (NAS2-2441), Lockheed Aircraft Corporation, Palo Alto, California, Oct. 1967.

[18] Dixon, J.C., Musgrove, P.J., "Thermal Insulation for Electrothermal Thrusters", in "Conference on Electric Propulsion of Space Vehicles", The Institution of Electrical Engineers, I.S.B.N. 0852961197, 1973, pp. 166-170.

[19] DOW CORNING, Bulletin 61-041; Date 3/71, Dow Corning International Ltd., Chaussée de la Hulpe, 177, B-1170, Brussels, Belgium.

[20] EMERSON & CUMING INC., Technical Bulletins: 3-2-2A, 6-2-1B, 6-2-2B, 7-2-9, Emerson & Cuming Europe NV, Nijverheidsstraat 24, B-2431 Oevel, Belgium.

[21] FIBERTIL, "Ready-to-mold Fiberglass Reinforced Structural Foams", Fiberfil Division, Dart Industries Inc., 1701 N, Heidelbach Avenue, Evansville, Indiana 47717, U.S.A..

[22] Fussel, W.B., Triolo, J.J., Jerozal, F.A., "Portable Integrating Sphere for Monitoring Reflectance of Spacecraft Coatings", in "Measurement of Thermal Radiation Properties of Solids", J.C. Richmond, Ed., NASA SP-31, 1963.

[23] Glaser, P.E., Black, I.A., Lindstrom, R.S., Ruccia, F.E., Wechsler, A.E., "Thermal Insulation Systems - A Survey", NASA SP-5027, 1967.

[24] Glassford, A.P.M., "Outgassing Behavior of Multilayer Insulation Materials", Journal of Spacecraft and Rockets, Vol. 7, No. 12, dec. 1970, pp. 1464-1468.

[25] Halaczek, T.L., Rafalowicz, J., "Heat Transport in Self-Pumping Multilayer Insulation", Cryogenics, Vol. 26, No. 6, June 1986, pp. 373-376.

[26] Halaczek, T.L., Rafalowicz, J., "Temperature Variation of Thermal Conductivity of Self-Pumping Multilayer Insulation", Cryogenics, Vol. 26, No. 10, Oct. 1986, pp. 544-546.

[27] Hale, D.V., "Study of Thermal Conductivity Requirements", "High Performance Insulation Thermal Conductivity Test Program", NASA CR-61279 (NAS8-21347), Lockheed Missiles and Space Company, Huntsville, Alabama, Jan. 1969.

[28] Hammond, Jr., M.B., "An Analytical Model for Determining the Thermal Conductivity of Closed-Cell Foam Insulation", in "Advances in Cryogenic Engineering", Vol. 15, K.D. Timmerhaus, Ed., Plenum Publishing Corporation, New York, 1970, pp. 332-342.

[29] Happel, J., Brenner, H., "Low Reynolds Number Hydrodynamics with Special Applications to Particulate Media", Prentice-Hall, Inc., Englewood Cliffs, N. J., 1965, Chap. 4, pp. 153-154.

[30] Holmes, V.L., McCrary, L.E., Krause, D.R., "Measurement of Apparent Thermal Conductivity of Multilayer Insulations at Low-Compressive Loads", Journal of Spacecraft and Rockets, Vol. 9, No. 11, Nov. 1972, pp. 791-795.

[31] Jagannathan, P.S., Tien, C.L., "Experimental Investigation of Lateral Heat Transfer in Cryogenic Multilayer Insulation", in "Advances in Cryogenic Engineering", Vol. 16, K.D. Timmerhaus, Ed., Plenum Publishing Corporation, New York, 1971, pp. 138-142.

[32] JOHNS-MANVILLE, "Thermophysical Data". Data Sheets No. IN-526A, IN-554A, IN-560A, IN-563A, IN-568A, IN-569A, IN-570A, IN-571A, IN-575A, IN-576A, IN-577A, IN-578A. Johns-Manville International Corporation, Denver, Colorado 80217 USA.

[33] Kanager, M.G., "Thermal Insulation in Cryogenic Engineering", Israel Program for Scientific Translations, Jerusalem, 1969.

[34] Kazanjian, A.R., "Review of Properties of Polycarbonate Resins", in "Polymer-Plastics Technology and Engineering", L. Naturman, Ed., Marcel Dekker, Inc., New York, 1974, pp. 123-160.

[35] Keller, C.W., Cunnington, G.R., Glassford, A.P., "Thermal Performance of Multilayer Insulations", NASA CR-134477, April, 1974.

[36] Kittel, Ch., "Introduction to Solid State Physics", 3rd Edition, John Wiley & Sons, Inc., New York, 1966, pp. 208-218.

[37] Klippel, E., Langer, H., "Multilayer Superinsulation Development and Testing", UR-258-74, ESTEC/Contract 2042/73 SK, Messerschmitt-Bölkow-Blohm GmbH, Ottobrunn bei München, Nov. 30, 1974, pp. 26-28.

[38] Kneisel, K.M., Bennett, F.O., "Prediction of Interstitial Gas Pressure in Multilayer Insulation During Rapid Evacuation", Journal of Spacecraft and Rockets, Vol. 7, No. 10, Oct. 1970, pp. 1259-1261.

[39] Knopf, P.W., Murray, D.O., "Empirical Thermal Performance of Embossed/Crinkled Aluminized Film Multilayer Insulation with Joints", in "Proceedings of the Symposium in Thermodynamics and Thermophysics of Space Flight, Palo Alto, California, 1970, pp. 211-219.

[40] Krause, D.R., Private Communication. Sept. 30, 1974.

[41] Kropschot, R.H., Schrodt, J.E., Fulk, M.M., Hunter, B.J., "Multiple-Layer Insulation", in "Advances in Cryogenic Engineering", Vol. 5, K.D. Timmerhaus, Ed., Plenum Publishing Corporation, New York, 1960, pp. 189-197.

[42] Leonhard, K.E., Hyde, E.H., "Multilayer Insulation Materials for Reusable Space Vehicles", in "Space Shuttle Materials", Vol. 3, SAMPE, Azusa, California, Oct. 1971, pp. 645-658.

[43] Lin, J.T., "Analysis of Gas Flow through a Multilayer Insulation System", AIAA Journal, Vol. 11, No. 7, July 1973, pp. 995-1000.

[44] Maccalous, J.W., "Methods of Fabricating Super-Insulation Blankets", in "Advances Techniques for Material Investigation and Fabrication", Vol. 14, SAMPE, Florida Press, Inc., Orlando, Florida, Nov. 1968, II-1A-4.

[45] Maissel, L.I., "Electrical Properties of Metallic Thin Films", in "Handbook of Thin Film Technology", L.I. Maissel and R. Glang, Eds., McGraw-Hill Book Co., New York, 1970, pp. 13-7 - 13-10.

[46] Matsuda, A., Yoshikiyo, H., "Simple Structure Insulating Material Properties for Multilayer Insulation", Cryogenics, Vol. 20, No. 3, March 1980, pp. 135-138.

[47] McAdams, W.H., "Heat Transmission", 3rd Edition, McGraw-Hill Book Company, Inc., New York, 1954, p. 63.

[48] MOSITES, Data Sheets of Mosites 1062 Fluorel, Mosites Rubber Company, Inc., P.O. Box 2115, Fort Worth, Texas 76101, U.S.A..

[49]   Nies, G.E., Niendorf, L.R., "Self Evacuating Multilayer Insulation (SEMI) for Space Shuttle Obiter Cryogenic Tanks", Space Shuttle Materials, Vol. 3, SAMPE, 1971.

[50]   Perkins, P.J., Dengler, R.P., Niendorf, L.R., Nies, G.E., "Self-Evacuated Multilayer Insulation of Lightweight Prefabricated Panels for Cryogenic Storage Tanks". NASA TN D-4375, March 1968.

[51]   Petajan, J.H., Voorhees, K.J., Packham, S.C., Baldwin, R.C., Einhorn, I.N., Grunnet, M.L., Dinger, B.G., Birky, M.M., "Extreme Toxicity from Combustion Products of a Fire-Retarded Polyurethane Foam", Science, Vol. 187, No. 4178, Feb. 28, 1975, pp. 742-744.

[52]   Reed, R.P., Arvidson, J.M., Durcholz, R.L., "Tensile Properties of Polyurethane and Polystyrene Foams from 76 to 300 K", in "Advances in Cryogenic Engineering", Vol. 18, K.D. Timmerhaus, Ed., Plenum Publishing Corporation, New York, 1973, pp. 184-193.

[53]   Reid, R.L., Coon, C.W., "Hemispherical Thermal Emittance of Copper as a Function of Oxidation Conditions", in "Progress in Astronautics and Aeronautics", Vol. 24, J.W. Lucas, Ed., The MIT Press, Cambridge, Massachusetts, 1971, pp. 184-204.

[54]   Richardson, D.L., Ruccia, F.E., French, B., "Extravehicular Space Suit Thermal Insulations", in "Progress in Astronautics and Aeronautics", Vol. 24, J.W. Lucas, Ed., The MIT Press, Cambridge, Massachusetts, 1971, pp. 519-544.

[55]   Rittenhouse, J.B., Singletary, J.B., "Space Materials Handbook", 3rd Edition, NASA SP-3051, 1969, p. 647.

[56]   Rosato, D.V., "Other Properties and Characteristics (Corrosive, Thermal, Space, Biological, Ocean, Fire)", in "Environmental Effects on Polymeric Materials, Vol. I: Environments", D.V. Rosaro and R.T. Schwartz, Eds., Interscience Publishers, New York, 1968, pp. 755-991.

[57]   Ross, J.H., "Fibers", in "Environmental Effects on Polymeric Materials, Vol. II: Materials", D.V. Rosaro and R.T. Schwartz, Eds., Interscience Publishers, New York, 1968, pp. 1282-1302.

[58]   Ross, J.H., Stanton, R.M., "Relationship of Fabric Flammability to Fabric Structure", in "Applied Polymer Symposia No. 21", J. Preston and J. Economy, Eds., John Wiley & Sons, 1973, pp. 109-119.

[59]   Ruccia, F.E., Hinckley, R.B., "The Surface Emittance of Vacuum-Metallized Polyester Film", in "Advances in Cryogenic Engineering", Vol. 12, K.D. Timmerhaus, Ed., Plenum Publishing Corporation, New York, 1967, pp. 300-307.

[60]   Schroeder, C.J., "Insulation Commonality Assessment", (Phase I), Vol. 1, Clause 5.0 through 6,0, NASA CR-124471, SD72-SA-0157-1 (NAS7-200), Space Division, North American Rockwell Corp., Feb. 1, 1973, pp. 6-151.

[61]   Schroeder, C.J., "Insulation Commonality Assessment", (Phase I), Vol. 2, Clause 11.0 through 16,0, NASA CR-12447B, SD72-SA-0157-2 (NAS7-200), Space Division, North American Rockwell Corp., Feb. 1, 1973.

[62]   Scollon, T.R., Carpitella, M.J., "Long Life High Reliability Thermal Control Systems Study Data Handbook", Prepared under Contract NAS 8-26252 by Space Systems Organization, General Electric Company, Valley Forge Space Technology Center, Pennsylvania, 1970.

[63]   Scurlock, R.G., Saull, B., "Development of Multi-Layer Insulations with Thermal Conductances below 0,1 μW/cm deg K". Cryogenics, Vol. 16, No. 5, May 1976, pp. 303-311.

[64]   Shelton, J.L., Akers, W.W., "Total Hemispherical Thermal Emittance of Nickel as a Function of Oxide Thickness in the Temperature Range 400º-900°C", in "Progress in Astronautics and Aeronautics", Vol. 18, G.B. Heller, Ed., Academic Press, New York, 1966, pp. 151-165.

[65]   Shu, Q.S., Fast, R.W., Hart, H.L., "An Experimental Study of Heat Transfer in Multilayer Insulation Systems from Room Temperature to 77 K", in "Advances in Cryogenic Engineering", Vol. 31, R.W. Fast, Ed., Plenum Press, New York, 1986, pp. 455-463.

[66]   Siegel, R., Howell, J.R., "Thermal Radiation Heat Transfer", Vol. 1 NASA SP-164, 1968.

[67]   Smithells, C.J., "Metals Reference Books", Vol. II, 3rd Edition, Butterworth & Co (Publishers) Ltd., London, 1962, pp. 695-827.

[68]   Smolak, G.R., Knoll, R.H., Wallner, L.E., "Analysis of Thermal-Protection Systems for Space-Vehicle Cryogenic-Propellant Tanks", NASA TR R-130, Aug. 3, 1962.

[69]   Stimpson, L.D., Jaworski, W., "Effects or Overlaps, Stitches, and Patches on Multilayer Insulation", in "Progress in Astronautics and Aeronautics", Vol. 31, C.L. Tien, Ed., The MIT Press, Cambridge, Massachusetts, 1972, pp. 247-266.

[70]   Tien, C.L., Cunnington, G.R., "Radiation Heat Transfer in Multilayer Insulation Having Perforated Shields", AIAA Paper No. 73-718, July 1973.

[71]   Tien, C.L., Jagannathan, P.S., Chan, C.K., "Lateral Heat Transfer in Cryogenic Multilayer Insulation", in "Advances in Cryogenic Engineering", Vol. 18, K.D. Timmerhaus, Ed., Plenum Publishing Corporation, New York, 1972, pp. 118-123.

[72]   Touloukian, Y.S., "Thermophysical Properties of High Temperature Solid Materials", Vol. 4: "Oxides and Their Solutions and Mixtures", Part I: "Simple Oxygen Compounds and Their Mixtures", The MacMillan Company, New York, 1967.

[73]   Touloukian, Y.S., "Thermophysical Properties of High Temperature Solid Materials", Vol. 5: "Nonoxides and Their Solutions and Mixtures Including Miscellaneous Ceramic Materials", The MacMillan Company, New York, 1967.

[74]   Touloukian, Y.S., DeWitt, D.P., "Thermal Radiative Properties. Metallic Elements and Alloys", Thermophysical Properties of Matter, Vol. 7, IFI/Plenum, New York, 1970.

[75]   Vliet, G.C., Coston, R.M., "Thermal Energy Transport Parallel to the Laminations in Multilayer Insulation", in "Advances in Cryogenics Engineering", Vol. 13, K.D. Timmerhaus, Ed., Plenum Publishing Corporation, New York, 1968, pp. 671-679.

[76]   Wood, W.D., Deem, H.W., Lucks, C.F., "The Emittance of Iron, Nickel, and Cobalt and their Alloys", Defense Metals Information Center, DMIC Memorandum 119, Battelle Memorial Institute, Columbus 1, Ohio, July 25, 1961.

[77]   Zwaal, A., Dauphin, J., Alonso, A., "Screening of Space Materials with Micro-VCM Weight-Loss Test", ESTEC TN-110, European Research Organization, Feb. 1971.